

THE CREATION OF AN AUTONOMOUS MULTI-TERRAIN MECHATRON

A thesis
submitted in partial fulfilment
of the requirements for the degree
of
Master of Science & Technology in Physics and Electronic Engineering
at the
University of Waikato

by

Jason Craig Cordes



The
**University
of Waikato**
*Te Whare Wānanga
o Waikato*

2002

ABSTRACT

An autonomous, multi-terrain vehicle has been designed and developed for operation in general indoor, and outdoor environments. The mechatron's mobility is based around a robust caterpillar drive system, enabling powerful high torque positive drive over and through rough terrain. The platform has been designed to integrate a series of sensors and equipment to enable the unit to eventually operate autonomously. The sensory equipment includes odometry, proximity sensors, compass, and GPS. The size and scale of the vehicle allows for a large self-contained power supply, which provides adequate power for an extensive range of peripherals and systems. The unit has been primarily developed as a foundation for future research into outdoor autonomous mechatronic applications at the University of Waikato.

ACKNOWLEDGEMENTS

I would like to gratefully acknowledge the following people for their support and assistance throughout the development of the multi-terrain autonomous vehicle.

Thanks to Dr Dale Carnegie for his support and guidance throughout the project's development. I would also like to thank Bruce Rhodes, Scott Forbes, and Dave Bugden.

I would most gratefully like to thank Ricarda Townsend and my parents, Elizabeth and Jack Cordes, for their wise consultation, time, encouragement, and support throughout my academic career. A special thanks goes to my Father for the unlimited use of his equipment and resources, superb advice, and time spent in guiding and assisting myself throughout this project. To my parents, I thank you both more than I can express and dedicate this thesis to you both for all that you have done.

TABLE OF CONTENTS

ABSTRACT.....	iii
ACKNOWLEDGEMENTS	v
TABLE OF CONTENTS	vii
LIST OF FIGURES	xiii
LIST OF TABLES	xix
1. INTRODUCTION	1
1.1 INTENDED APPLICATIONS.....	1
1.2 PROJECT SPECIFICATIONS.....	2
1.3 MECHANICAL CONSIDERATIONS	3
1.4 DEVELOPMENT STRATEGY	4
2. HARDWARE SELECTION.....	7
2.1 DRIVE SYSTEMS.....	7
2.1.1 Legged Movement (Bipedal and Insects).....	7
2.1.2 Radial Wheel Drive System.....	9
2.1.3 Caterpillar/Tracked Drive System.....	14
2.1.4 Implemented Drive Method	15
2.2 MOTIVE UNIT	15
2.2.1 Motor Selection.....	16
2.2.2 Gearbox.....	18
2.3 POWER REQUIREMENTS.....	21
2.3.1 Generalised System Requirements	21
2.3.2 Battery Selection.....	22
2.4 SENSING OPTIONS.....	23
2.4.1 Ultrasonic Sensing	24
2.4.2 Infrared Sensing.....	27
2.4.3 Tactile Sensing.....	28
2.4.4 Laser Range Finding.....	28
2.4.5 Navigation.....	31

2.4.5.1	<i>Compass</i>	31
2.4.5.2	<i>Global Positioning System</i>	31
2.4.5.3	<i>Reference Transponders</i>	32
2.4.6	<i>Additional Sensing Equipment</i>	33
2.4.6.1	<i>Shaft Encoders</i>	33
2.4.6.2	<i>Yaw and Pitch Sensors</i>	33
3. MECHANICAL DESIGN AND CONSTRUCTION: TRACK MODULE		
DEVELOPMENT.....		35
3.1	CONCEPTUAL TRACK MODULE DESIGN	36
3.1.1	Drive Belts	36
3.1.2	Side Plates	39
3.1.3	Base Arc	40
3.1.4	Laser Profile Cutting	41
3.2	DYNAMIC VARIABLE TRACK TENSIONING UNIT	41
3.2.1	Construction of the Front Sliding Axle Unit	43
3.2.2	Welding	44
3.2.3	Track Tensioning Mechanism.....	45
3.2.4	Bolt Fabrication.....	45
3.2.5	Tensioning Bolt Locating Plate.....	46
3.2.6	Final Tensioning Unit Assembly.....	46
3.2.7	Threaded Tensioning Plate	47
3.2.8	Front Sliding Axle Unit Bearings	48
3.2.9	Front Sliding Axle Unit Bearing Fixings	49
3.2.10	Tensioner Springs	50
3.2.11	Front Sliding Axle Unit Pulley's and Spacers.....	51
3.2.12	Locating Tensioning Unit within the Track Modules Side Plates.....	55
3.3	DEVELOPING THE DRIVE AXLE MECHANISM.....	56
3.3.1	Self Aligning Bearing Flanges	56
3.3.2	Drive Shaft.....	58
3.3.3	Drive Pulley's	59
3.3.4	Drive Pulley Spacers	60
3.3.5	Final Drive Unit Assembly.....	60
3.3.6	Mounting the Drive Shaft Unit to the Track Module Side Plates	61
3.3.7	Drive Couplings.....	63

3.4 TRACK BOGIE UNITS	64
3.4.1 Bogie Design	65
3.4.2 Bogie Construction.....	66
3.4.3 Bogie Unit Guide Pulley's	67
3.4.4 Main Bogie Unit Pivoting Bearings	68
3.5 COMPLETE ASSEMBLY OF THE TRACK MODULES	68
4. MECHANICAL DESIGN AND ASSEMBLY: CHASSIS DEVELOPMENT ...	73
4.1 CHASSIS DESIGN	73
4.1.1 Construction of the Bottom Chassis Tray.....	74
4.1.2 Construction of the Upper Chassis Tray.....	75
4.1.3 Fitting the Chassis Trays to the Track Modules Side Plates	77
4.1.4 Motor Mounting Brackets and Packers	78
4.1.5 Battery Tray.....	79
4.1.6 ATX and Charging Unit Brackets and Packers	80
4.2 COMPUTER SUSPENSION FRAME	82
4.2.1 Computer Location.....	82
4.2.2 Design of Computer Mounts	82
4.2.3 Computer Suspension Frame Construction.....	83
4.3 UPS, MICROCONTROLLER, AND MOTOR DRIVER MOUNTING BRACKET	85
4.3.1 UPS, Microcontroller, and Motor Driver Frame Design	85
4.3.2 UPS, Microcontroller, and Motor Driver Frame Construction.....	86
4.4 EXTERIOR CASING.....	88
4.5 MECHANICAL CONCLUSION	88
5. ELECTRONIC DESIGN	91
5.1 THE CENTRAL COMPUTER.....	91
5.1.1 Communication Interfaces	91
5.1.2 Software	91
5.1.3 Installation.....	92
5.2 POWERING THE COMPUTER	93
5.2.1 Generating 230VAC at 50 Hz.....	93
5.2.2 ATX Power Supply	94
5.3 CHARGING.....	95
5.4 MOTOR DRIVERS.....	96
5.4.1 Design Criteria	96

5.4.2 Motor Driver Design.....	96
5.5 MICROCONTROLLER	99
5.5.1 AC/DC Power Supply	100
5.5.2 Internal and External Memory.....	103
5.5.3 Real Time Clock	105
5.5.4 Serial Communication.....	105
5.5.5 I/O Ports.....	106
5.5.6 Operation.....	107
5.6 RADIO CONTROL UNIT AND INTERFACE	108
5.6.1 Receiver Output Signals	110
5.6.2 Converting Receiver Signals into PWM Outputs.....	110
5.6.3 Steering Under Radio Control.....	111
5.7 DAQ CARD HUB	112
5.8 INTEGRATING SENSOR ARRAYS AND NAVIGATIONAL EQUIPMENT.....	113
5.8.1 Infrared Proximity Sensors	113
5.8.2 Tactile Sensors	117
5.8.3 Shaft Encoders	118
5.8.4 Electric Compass.....	123
5.8.5 GPS	125
6. SYSTEM INTEGRATION	129
6.1 LABVIEW	129
6.2 SPEED AND SLIPPAGE	130
6.2.1 Speed.....	130
6.2.2 Slippage.....	131
6.3 COURSE CORRECTION - UNRESTRICTED MOVEMENT IN A STRAIGHT LINE.....	133
6.3.1 Previously Used Methods	133
6.3.2 Full Integration of Sensors for course correction	134
6.4 TURNING.....	136
6.4.1 Stationary Turns	136
6.4.2 Mobile Turns.....	137
6.4.3 Steering Control.....	137
6.5 TERRAIN AND OBSTACLE AVOIDANCE	138
6.5.1 Obstacle Evasion.....	139
6.5.2 Terrain Interpretation and Evasion Parameters.....	140

6.5.3	Course Correction Due to Obstacles and Terrain	141
6.6	MOTOR CONTROL THEORY AND EVALUATION.....	142
6.6.1	PWM Control.....	142
6.6.2	Braking	144
6.6.3	DC Motor Theory and Transfer Function.....	145
6.6.4	Experimentally Determining the Motor Specifications	149
6.6.5	PID Controller	150
7.	CONCLUSION	155
7.1	RESULTS	155
7.2	FUTURE WORK.....	156
7.2.1	Laser Range Finder	156
7.2.2	Tactile Sensors	156
7.2.3	Interface DragonTalk Voice Recognition Software	156
7.2.4	Interface Pitch Sensor	157
7.2.5	System Integration Implementation.....	157
7.3	SUMMARY.....	157
	APPENDIX A: MECHATRON MECHANICAL DESIGN DRAWINGS	161
	APPENDIX B: ELECTRONIC CASE DRAWINGS	183
	APPENDIX C: ELECTRONIC SCHEMATICS	189
	APPENDIX D: DATA SHEETS	193
	GLOSSARY	207
	BIBLIOGRAPHY.....	209

LIST OF FIGURES

Figure 1-1: Flowchart of the basic project development process	5
Figure 2-1: Honda humanoid bipedal unit.....	7
Figure 2-2: Insect style, legged mechatron.....	8
Figure 2-3: Leg actuation principle	8
Figure 2-4: MARVIN – security research platform	9
Figure 2-5: Standard two-wheeled drive configuration.....	10
Figure 2-6: Standard tricycle configuration and motor attachment.....	11
Figure 2-7: Forklift steering mechanism	12
Figure 2-8: NASA’s Mars pathfinder rover	13
Figure 2-9: Conceptual design of a multi-wheeled drive configuration.....	13
Figure 2-10: Tracked drive system, sports utility vehicle snow attachment	15
Figure 2-11: Typical performance characteristics for the WMT90112 motors.....	17
Figure 2-12: Right-hand drive motor unit	18
Figure 2-13: Standard drive configuration for an electric wheelchair.....	18
Figure 2-14: Standard planetary drive configuration	19
Figure 2-15: Internal gearbox configuration	19
Figure 2-16: Standard worm drive configuration.....	20
Figure 2-17: NS70 lead acid battery.....	23
Figure 2-18: a) Ultrasonic focusing cap b) Ultrasonic attenuation cylinder	25
Figure 2-19: Dual ultrasonic transducer pair positioning to detect three zones	25
Figure 2-20: Detecting the approach angle of incidence to a wall/large obstacle	26
Figure 2-21: Incorrect detection of a secondary obstacle	27
Figure 2-22: Undesirable IR sensor configuration, due to narrow sensing window.....	28
Figure 2-23: Active triangulation ranging system.....	30
Figure 2-24: Network of 24 satellites for the GPS	32
Figure 3-1: Two point return rotation of tracks	37
Figure 3-2: Keyed $\varnothing 59\text{mm}$ H-tooth configuration polymer drive pulley.....	38

Figure 3-3: Side profile of the track.....	39
Figure 3-4: Completed internal side plate of track module	41
Figure 3-5: Customised side plate of the front sliding axle unit.....	43
Figure 3-6: Component layout of the front sliding axle unit, prior to welding	43
Figure 3-7: Completed front sliding axle unit	44
Figure 3-8: Tensioner bolt locator plate.....	46
Figure 3-9: Faced inner locating nuts for the tensioner unit.....	47
Figure 3-10: Parts layout for the tensioning unit	47
Figure 3-11: The pair of tensioning units and respective tensioning plates	48
Figure 3-12: Running bearing for the front sliding axles pulley's	49
Figure 3-13: Customised bolts for the front sliding axle and bogie units.....	50
Figure 3-14: A pair of 1/8"x4"x120 main tensioning springs	51
Figure 3-15: Guide pulley for static positions	52
Figure 3-16: Reduced guide pulley for dynamic positions	53
Figure 3-17: Aluminium spacers to separate all guide pulley units	54
Figure 3-18: Static pulley layout (left), assembled static pulley unit (right).....	54
Figure 3-19: Dynamic pulley layout (left), assembled dynamic pulley unit (right)	54
Figure 3-20: Layout of the front sliding axle unit and tensioning mechanism.....	55
Figure 3-21: Assembled front sliding axle unit and tensioning mechanism.....	55
Figure 3-22: Standard unmodified self-aligning bearing flange	56
Figure 3-23: Modified self-aligning bearing flanges	58
Figure 3-24: Track module drive shaft and corresponding keys	59
Figure 3-25: Main Drive pulley's	59
Figure 3-26: Drive pulley spacer	60
Figure 3-27: Drive shaft unit component layout.....	61
Figure 3-28: Assembled drive shaft unit.....	61
Figure 3-29: Drilled and tapped bearing flanges to suit $\text{\O}3/16''$ BSW gutter bolts	63
Figure 3-30: Cut down gutter bolt	63
Figure 3-31: Drive Coupling.....	64
Figure 3-32: Completed track bogie unit frame.....	67
Figure 3-33: Outside face of attached bearing flange	69
Figure 3-34: Inside of attached bearing flange	69
Figure 3-35: Exposed internal mechanisms of a track module.....	70

Figure 3-36: Assembled track module with tensioned belt	71
Figure 4-1: Lower chassis tray	75
Figure 4-2: Completed upper chassis tray	77
Figure 4-3: Assembled chassis trays and track modules	78
Figure 4-4: Motor mounting brackets and packers	79
Figure 4-5: Motor-mounting brackets attached to both the motors	79
Figure 4-6: Battery tray	80
Figure 4-7: ATX power supply and charging unit mounting brackets and packers	81
Figure 4-8: Ideal computer case mounting spring configuration	83
Figure 4-9: Upper corner spring attachments	84
Figure 4-10: Lower corner spring attachments	84
Figure 4-11: Completed computer suspension frame	85
Figure 4-12: UPS, microcontroller, and motor driver platform	87
Figure 4-13: UPS, microcontroller, and motor driver frame with mounted equipment	87
Figure 4-14: Front view of mechanical layout	89
Figure 4-15: Rear view of mechanical layout	89
Figure 5-1: Customised aluminium spring mounting brackets	92
Figure 5-2: Completed computer case	93
Figure 5-3: 800VA UPS	94
Figure 5-4: ATX power supply	95
Figure 5-5: Dual led acid battery charging unit	96
Figure 5-6: Front end transistor and optocoupler configurations	97
Figure 5-7: Completed motor driver circuit	98
Figure 5-8: Both motor driver circuits	98
Figure 5-9: Power supply input and battery backup	101
Figure 5-10: Crowbar circuit	101
Figure 5-11: Regulator circuit	102
Figure 5-12: Microcontroller power supply circuit	102
Figure 5-13: AND and XOR gates used to access the RAM	104
Figure 5-14: Real time clock circuitry and associated battery backup	105
Figure 5-15: Serial input interface for the '552	106
Figure 5-16: '552-microcontroller development board	108
Figure 5-17: Two-channel radio control set	109
Figure 5-18: Receiver unit	109

Figure 5-19: Receiver output signals	110
Figure 5-20: Motor control sequence for a transmitted radio signal	112
Figure 5-21: DAQ hub	113
Figure 5-22: Sharp GP2D12 IR proximity sensor module	114
Figure 5-23: GP2D12 sensor output versus distance to object (matt surfaces)	115
Figure 5-24: GP2D12 sensor output versus distance to object (gloss surfaces).....	115
Figure 5-25: GP2D12 lateral detection profile	116
Figure 5-26: IR sensor locations	117
Figure 5-27: Sensing planes and undetectable dead bands	118
Figure 5-28: HEDS-9040 shaft encoders and coded wheels	119
Figure 5-29: Additional plate mounts for the opto-sensors	120
Figure 5-30: Customised face on the inner section of the drive couplings.....	120
Figure 5-31: Completed code wheel.....	122
Figure 5-32: Assembled code wheel and drive coupling unit	122
Figure 5-33: Completed installation and assembly of the odometry units	123
Figure 5-34: V2X electronic compass	124
Figure 5-35: BCD format for 356-degree signal coming from SDO	125
Figure 5-36: M12 GPS unit and antenna	126
Figure 5-37: Active antenna gain pattern.....	126
Figure 5-38: Antenna mounting position on the outer casing of the robot	127
Figure 6-1: Shaft encoder process to compute speed and distance travelled.....	130
Figure 6-2: Speed correction pseudo code.....	131
Figure 6-3: GPS & odometry interface to reduce slippage	132
Figure 6-4: Tracking errors, and IR course correction	133
Figure 6-5: Control system for indoor unit with only SE and IR sensors	134
Figure 6-6: Course correction sequence using the compass and GPS	135
Figure 6-7: Stationary turn methods	136
Figure 6-8: Standard turning technique while in motion.....	137
Figure 6-9: Steering controller process diagram.....	138
Figure 6-10: Filtered sensor readings	139
Figure 6-11: Terrain profile that can evade IR and tactile sensor configurations	140
Figure 6-12: Obstacle Evasion Control Diagram	142
Figure 6-13: PWM signals and corresponding waveforms	143
Figure 6-14: Brake assembly	144

Figure 6-15: a) Single loop DC motor model b) Basic DC motor electric model.....	145
Figure 6-16: Block model of the DC motor transfer function.....	149
Figure 6-17: Drive motor step response for a 24VDC input	150
Figure 6-18: Process reaction curve	151
Figure 6-19: Overview of the Simulink model for the drive motors	152
Figure 6-20: Sub-system of the DC motor model within Figure 6-19	152
Figure 6-21: PID control system	153
Figure 6-22: Step response through the PID controller	153
Figure 7-1: Completed multi-terrain vehicle	158
Figure 7-2: Mechatron travelling outdoors.....	159
Figure A.1: Drive motors and half couplings	161
Figure A.2: Original pulley's.....	162
Figure A.3: Inner track module side plate	163
Figure A.4: Outer track module side plate	164
Figure A.5: Front sliding axle unit	165
Figure A.6: Track tensioning unit.....	166
Figure A.7: Main guide pulley unit's	167
Figure A.8: Guide pulley unit's for front sliding axle and bogie unit's	168
Figure A.9: Track module internals.....	169
Figure A.10: Modified bearing flanges	170
Figure A.11: Drive shaft unit.....	171
Figure A.12: Track module side plate drive end magnifications	172
Figure A.13: Drive coupling.....	173
Figure A.14: Pivoting track bogie unit	174
Figure A.15: Lower chassis tray.....	175
Figure A.16: Upper chassis tray	176
Figure A.17: Motor mounting brackets and packers	177
Figure A.18: Battery tray.....	178
Figure A.19: ATX and charging unit mounting brackets and packers	179
Figure A.20: Computer suspension frame	180
Figure A.21: Microcontroller, motor driver, and UPS mounting bracket	181
Figure A.22: Shaft encoder – code wheel.....	182
Figure B.1: Main computer case.....	183
Figure B.2: ATX power supply case	184

Figure B.3: Charging unit case	185
Figure B.4: Microcontroller development board case	186
Figure B.5: DAQ hub case.....	187
Figure B.6: Motor driver case	188
Figure C.1: Charging circuit schematic	189
Figure C.2: Motor driver circuit schematic	190
Figure C.3: Microcontroller ('552) development board circuit schematic.....	191
Figure D.1.1: Toshiba TLP620-4 GaAs IRED and photo-transistor (page1).....	193
Figure D.1.2: Toshiba TLP620-4 GaAs IRED and photo-transistor (page 2).....	194
Figure D.2.1: International Rectifier IRLZ44N power MOSFET (page 1).....	195
Figure D.2.2: International Rectifier IRLZ44N power MOSFET (page 2).....	196
Figure D.3.1: SGS-Thomson STPS1045D power Scottky rectifier (page 1)	197
Figure D.3.2: SGS-Thomson STPS1045D power Scottky rectifier (page 2)	198
Figure D.4.1: Finder type 44.62 DPDT 10A relay (page 1)	199
Figure D.4.2: Finder type 44.62 DPDT 10A relay (page 2)	200
Figure D.5.1: Philips 87C552 8-bit microcontroller (page 1).....	201
Figure D.5.2: Philips 87C552 8-bit microcontroller (page 2).....	202
Figure D.6.1: Sharp GP2D12 IR proximity sensor (page 1)	203
Figure D.6.2: Sharp GP2D12 IR proximity sensor (page 2)	204
Figure D.7.1: Honeywell HOA2001 transmissive optoschmitt sensor (page 1)	205
Figure D.7.2: Honeywell HOA2001 transmissive optoschmitt sensor (page 2)	206

LIST OF TABLES

Table 5-1: Truth table of external memory access logic	104
Table 5-2: Alternate functions for ports 1, 3, 4 and 5.....	107

1. INTRODUCTION

To date, the Mechatronics Group at the University of Waikato have developed units that are primarily based around radial drive systems. The Group has also developed a submersible Remote Operated Vehicle (ROV), a small hexapod, and are currently working on a tricycle based design.

The objective of this thesis is to design and develop a multi-terrain mechatron that is sufficiently robust to cope with the irregularities of an outdoor environment. The project is also intended to be the founding development platform for future research and development within this field at the University of Waikato.

1.1 INTENDED APPLICATIONS

As stated above, the primary objective is to provide a mechatron capable of traversing irregular outdoor terrain and environments. This requires the design and construction of a dedicated drive system and chassis. Possible applications for such a mechatron include:

- Global autonomous control systems
- Topography mapping
- Security and surveillance
- Hazardous environment applications – search and rescue support, temperature profiling of flammable areas/extinguished fires.
- 3-Dimensional mapping and interpretation
- Forestry applications – timber grading, straightness, height

Taking into account these possibilities, the mechatron must be designed to house a large volume of equipment whilst maintaining mobility and stability.

1.2 PROJECT SPECIFICATIONS

As part of the requirement for this project, the mobile unit is to have a multi-terrain locomotion system. The drive system has to be practical for outdoor operations and the entire unit is to be developed as a stand-alone system. An on-board computer will perform the majority of the system processing, providing sufficient computational capacity for future research. A self-contained rechargeable power source will provide energy for the entire system. To increase reliability, all mechanical and electric systems are to be protected as much as possible from environmental conditions. Protection methods include: zinc electroplating of all ferrous metals, sealed acrylic cases encapsulating all electronic devices, anti-shock housings for systems such as the central computer and hard drive, and external cases around the entire unit to act as a secondary shield from the elements.

It is necessary for the platform design to consider and include as many of the following attributes as possible:

- **Scope** – the drive system must have the ability to adequately house, carry and manoeuvre the volume, and associated mass of all of the necessary equipment intended for the project, while maintaining an adequate buffer for the later additions of future developments.
- **Robustness** – the unit must be of a significant design standard to not only cope with the elements associated with outdoor operation, but it must also be able to deal with any irregularities in terrain. The design should additionally incorporate measures to reduce wear, and thereby reduce the amount of required maintenance.
- **Traction** – the drive system must generate adequate traction over a wide range of surfaces including lino and carpet while indoors, ranging to pasture, gravel, and rock in outdoor applications.
- **Manoeuvrability & Controllability** - the unit must be agile enough to navigate relatively small passages such as halls and doorways, as well as being able to identify and avoid obstacles. Ideally the unit should have as tight a turning

circle as possible. In conjunction with manoeuvrability, the unit should be easily controlled in as fluid a motion as possible.

- **Stability** – due to the chaotic nature of outdoor environments, it is essential that the drive system compliments a reasonably long and wide unit. This will enable all necessary components and equipment to be fitted in as low a profile as possible so as to increase the horizontal to vertical ratio, thereby increasing stability.
- **Efficiency** – the drive method, intended geography, and scale of the robot has a great bearing on the amount of energy required to manoeuvre a unit. The drive method must therefore compliment the scale and the mass of the unit so as to reduce the energy required to drive the system.

1.3 MECHANICAL CONSIDERATIONS

The mechanical design and construction has been undertaken at a private workshop independent of the University of Waikato. As the equipment is privately owned, the majority of the tooling, including drills, taps, and dies, are from the imperial era. For this reason, throughout this thesis, measurements include a mix of imperial and metric units. This format has only been implemented to reduce the amount of additional tools that would otherwise have to be purchased for the construction phase of this project. The majority of the mixed dimensions are related to bolts, with imperial diameters, and metric depths. Wherever possible, SI units have been used for ease during design and construction.

All mechanical work is illustrated in detail in Appendix A in scale-dimensioned drawings. The drawings have been created with AutoCAD for printing on A1 and A2 paper depending on the scale. Unfortunately, when reducing the printouts to both A3 and A4, the line scale of short fine hidden detail lines have not printed. This has significantly reduced the visible detail in the included printouts and hence the AutoCAD drawing files (*.dwg) have been included on the CD-ROM in the back of this thesis.

1.4 DEVELOPMENT STRATEGY

The key objectives for this project include the evaluation, and selection of a drive system, the mechanical design and development, through to the electronic design and implementation phases.

To illustrate each step in the design and development stages, the thesis has been presented in the following manner:

- **Chapter One:** Gives a general introduction to the project requirements and objectives.
- **Chapter Two:** Discusses the conceptual designs of sensing and drive configurations in determining the best systems for the intended applications.
- **Chapter Three:** Provides a detailed outline of the mechanical construction phase of the drive modules (Mechanical Section – 1).
- **Chapter Four:** Provides the mechanical construction of the inner chassis, and additional mechanical components (Mechanical Section – 2).
- **Chapter Five:** Details the electrical and sensing systems and electronic design and construction of the control peripherals.
- **Chapter Six:** Outlines the integration and control of all systems within the project.
- **Chapter Seven:** Summarises the steps required to design and construct the mobile unit, evaluates the project and performance, and discusses future developments associated with the mechatron.

Figure 1-1 illustrates a flow diagram, which represents the intended development strategy:

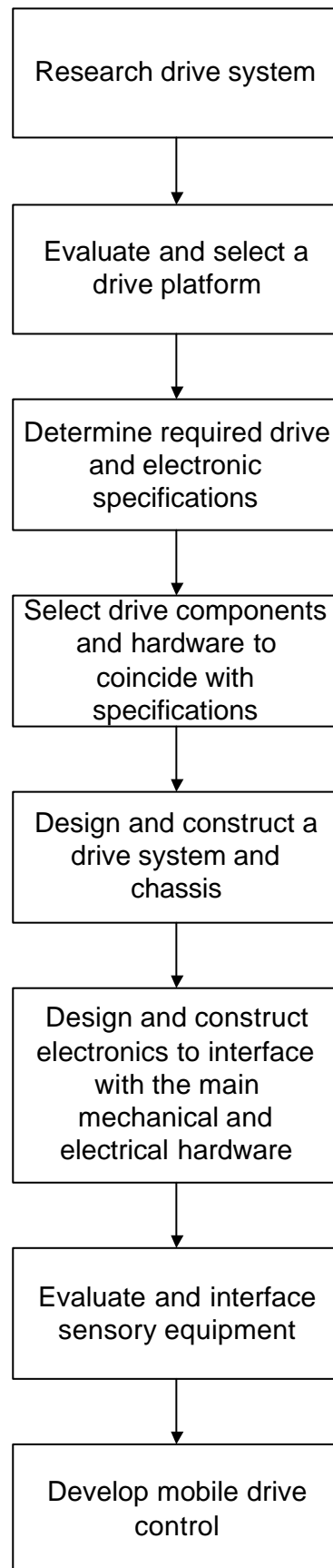


Figure 1-1: Flowchart of the basic project development process

2. HARDWARE SELECTION

2.1 DRIVE SYSTEMS

As stated in Chapter 1, the principle objective of this project is to develop the foundation for a large-scale multi-terrain indoor/outdoor robotics platform. The key consideration in choosing or developing a drive method is to ensure that the drive system suits the intended application. A discussion of different drive system options follows:

2.1.1 Legged Movement (Bipedal and Insects)

The most significant advantage associated with legged movement is its ability to manoeuvre over and around obstacles. Bipedal units (Figure 2-1) require an enormous amount of resources to develop a control system to compliment extremely advanced mechanics in order to maintain balance in rough terrain.



Figure 2-1: Honda humanoid bipedal unit

An easier option is to develop a multi-legged, insect styled unit. A small-scaled legged insect mechatron has already been developed at the University of Waikato (Lawrence, 2000, Figure 2-2). This unit employs two servo stepper units to actuate each leg forwards and backwards, as well as up and down. Figure 2-3 shows the principle movement design technique.

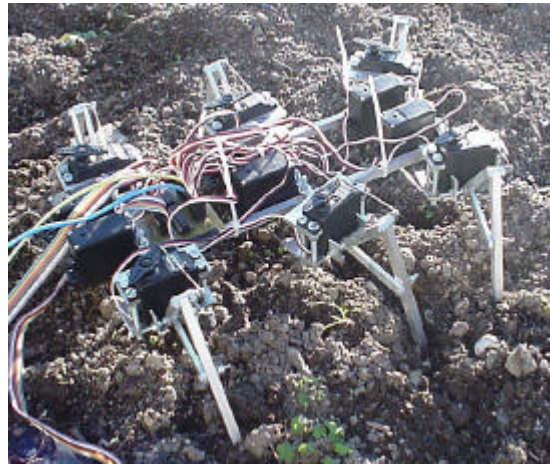


Figure 2-2: Insect style, legged mechatron

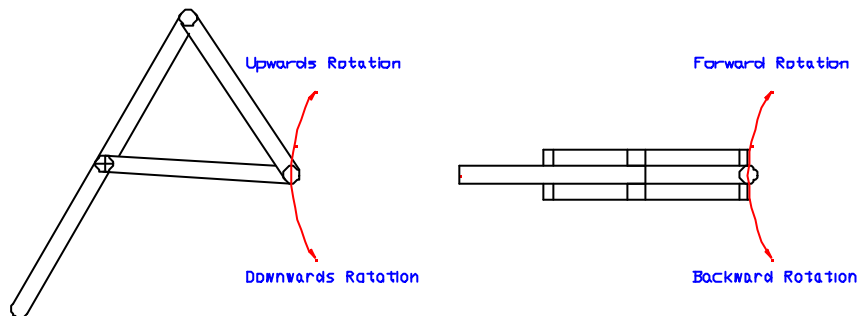


Figure 2-3: Leg actuation principle

This technique could be replicated in a larger scaled unit. Either larger, more powerful stepper motors could be used for the legs, or hydraulic/pneumatic rams could be used. For any drive method, the key considerations would be both the power consumption and weight. Due to the power required to generate three-dimensional actuation for each leg, the unit would struggle to be able transport an adequate onboard power supply.

Another disadvantage of a legged method is the speed with which the unit can manoeuvre. For these reasons, combined with the fact that the Mechatronics Group has already developed a small-scaled unit, it was decided to explore other locomotion mechanisms.

2.1.2 Radial Wheel Drive System

The easiest and most widely applied method of locomotion is to use standard radial wheels, either direct drive, or attached via a gearbox or reduction unit to an electric motor. There are many advantages in designing a drive system using a wheeled format, including a wide range of parts available, a wealth of available designs, and almost limitless possible layout configurations. However, these advantages can be offset by a number of reciprocating factors. The Mechatronics Group of the University of Waikato, has only developed one larger scale land-based mechatron in the past, christened MARVIN.

Although MARVIN was a step closer towards the style of mechatron intended for development for this project, it also was based around a standard two wheeled, wheel chair drive configuration. Figure 2-4 shows an illustration of MARVIN.

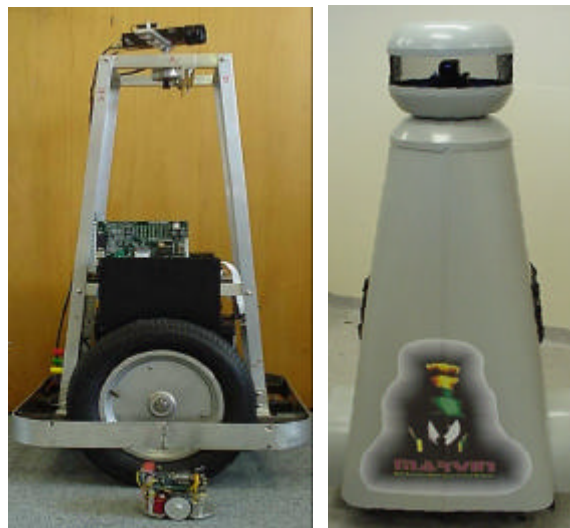


Figure 2-4: MARVIN – security research platform

Wheelchair Configuration:

As stated previously, the wheelchair configuration is based around a two-wheeled drive system, requiring no further steering mechanism. The unit is able to manoeuvre by controlling the speed and direction of both independent drive motors attached to each wheel. The greatest advantage with this configuration is the reduction in mechanical parts, and especially its ability to rotate freely in 360-degrees within its own physical perimeter. To maintain balance, this configuration requires some form of casters placed 90-degrees out of phase with the main drive wheels, to ensure the unit does not rock backwards and forwards during travel. Figure 2-5 illustrates a standard two-wheeled configuration.

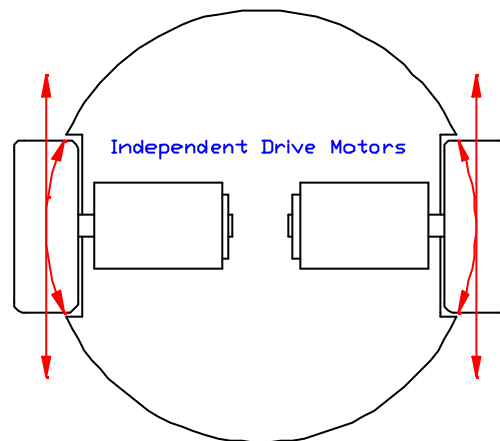


Figure 2-5: Standard two-wheeled drive configuration

The greatest disadvantage with this method is its lack of stability. To reduce the length of protrusion of the casters, the base of the chassis must be as close to the ground as possible, thereby reducing the terrain and obstacles the unit can negotiate. The greater the distance between the ground and the chassis, the longer and larger the casters have to be. As the casters get larger, they reduce their ability to free pivot easily, especially on rougher, uneven terrain. In effect, they track much like an old shopping trolley. The final disadvantage is the length, width, and height ratios. With this method, the unit is best based around a radial configuration, having an even length to width ratio. If a great deal of equipment is to be included, this can require the unit to become very tall, thereby having a large height to width ratio, reducing stability. This problem can be

seen in Figure 2-4 with MARVIN. Therefore, due to the issues previously discussed, the wheelchair configuration is not ideal for irregular outdoor conditions.

Tricycle Configuration:

As with the wheelchair configuration, the tricycle layout involves two drive wheels, with the addition of a steering wheel. It is possible to have both the main axle and the front steering wheel driving, but normally is driven solely by the two drive wheels. As with the wheelchair configuration, a drive motor can be attached to each drive wheel and controlled together, allowing the third wheel to freely pivot, or a single drive motor can drive both wheels. A single motor can be either crudely attached via a belt or chain to a main axle, or ideally attached via a limited slip differential, so as to reduce scuffing on the tyres while turning. Figure 2-6 illustrates a standard tricycle configuration and motor attachment.

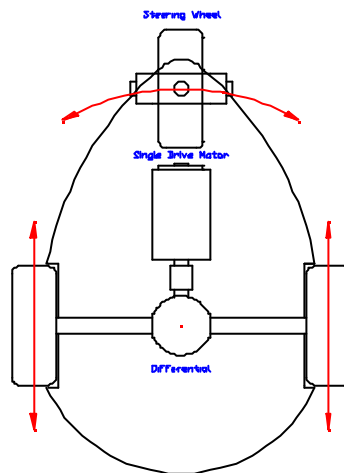


Figure 2-6: Standard tricycle configuration and motor attachment

The greatest advantages for the tricycle layout include its increased stability as compared to the wheelchair configuration, and the possible reduction in the number of drive motors required. The layout also allows for the unit to travel normally in a standard tricycle manner, or for increased manoeuvrability, travel as a forklift would, with the steering unit at the rear of the machine (forklift steering shown in Figure 2-7). As with any design, these advantages in turn have corresponding disadvantages. With the increase in stability, the configuration can have its ability to manoeuvre reduced,

especially increasing the area required to perform a 180-degree turn if a single drive motor configuration is implemented.



Figure 2-7: Forklift steering mechanism (rear wheel steering)

Further disadvantages include the increased mechanical mechanisms required to drive and steer the unit (single drive motor). With regard to the stability, the tricycle configuration is indeed more stable than the wheelchair configuration, but would still not be sufficiently stable to negotiate gradients of moderate levels, while travelling along, or across the slope. The tricycle configuration could permit the unit to topple when a line between a drive and steering wheel runs perpendicular with a gradient, causing the highest drive wheel to lift and thereby allowing the unit to roll.

Multi-Wheeled Configuration:

The final option for radial drive system is to develop a mechanism that has four or more wheels. The greatest advantages in developing a multi-wheeled drive system are the increased stability, and the ability to decrease the loading per surface area of the wheels, which would be significantly beneficial in soft, loose, and boggy terrains. When envisioning multi-wheeled robotics units, one might picture the Mars Pathfinder Rover (illustrated in Figure 2-8). This six-wheeled unit was developed to overcome unexplored terrain and conditions as a research tool for National Aeronautics and Space Administration (NASA).

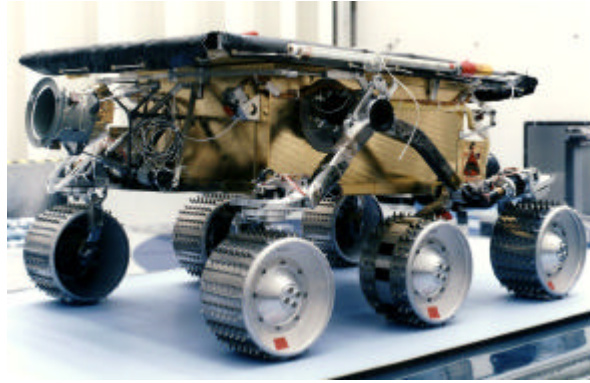


Figure 2-8: NASA's Mars pathfinder rover

An ideal multi-wheeled unit would be all-wheel drive, with a dynamically adjusting suspension system allowing the drive wheels to independently contour to the terrain while maintaining drive. To turn, the unit can control the speed and or direction of rotation of the drive motors in conjunction with an all-wheel steering mechanism, to reduce the area required to complete a 180-degree turn. Figure 2-9 shows the conceptual design of a multi-wheeled drive configuration.

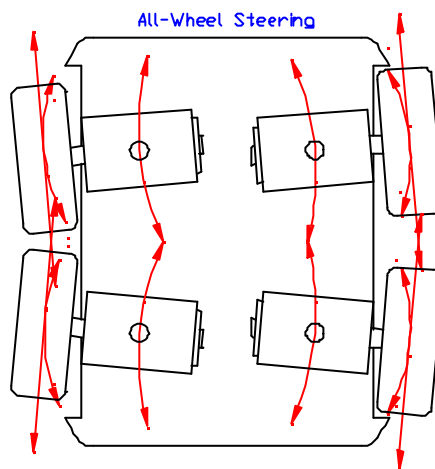


Figure 2-9: Conceptual design of a multi-wheeled drive configuration

This type of system requires complex mechanics just to implement the suspension, drive, and steering mechanisms. When a multi-wheel unit is to have more than four wheels, and they are all designed to drive, mechanisms need to be developed to reduce slippage and scuffing on the centralised tyres/wheels. Complex control systems must therefore be established to ensure that each wheel's speed and angle of steering is

independently controlled relative to the others depending on its position, type of turn, terrain, and direction to reduce slippage and wear.

2.1.3 Caterpillar/Tracked Drive System

The final option was to consider a tracked drive method, similar to that used in earth moving and military based equipment. This was one of the most appealing methods for several reasons, including its uniqueness with respect to other previously undertaken projects at the University of Waikato. Other benefits of such a system include:

- **Increased surface friction** – tracks decrease the mass loading per surface area of the device, enabling the unit's mass to be evenly distributed over a large area. Extremely beneficial in soft and boggy environments.
- **Manoeuvrability** – as with the wheelchair configuration, a tracked unit can also perform a 360-degree turn on the spot via independently driven drive belts.
- **Stability** – the length and width of the chassis can be altered to reduce the height of the unit so as to ensure the robot's centre of gravity is as low as possible, thereby increasing stability.
- **History** – for years tracked equipment has proven itself both in industrial and military applications, across a vast range of environments and conditions.

After researching small-scale (relative to industrial and military equipment) tracked robotics projects, it became very clear that very few units had been developed as compared to the other previously mentioned types. Feedback from academic institutes and research facilities indicated that the main factor for this was the lack of available parts and designs from which to manufacture a chassis and drive train. This issue would prove to be one of the most difficult and time-consuming problems to overcome. Figure 2-10 illustrates a caterpillar drive system developed for sports utility vehicles (one to be attached to each wheel hub).



Figure 2-10: Tracked drive system, developed for attachment to sports utility vehicles in snowy conditions

2.1.4 Implemented Drive Method

Taking into account all these considerations, it was decided to design and develop a caterpillar tracked drive system to allow the mechatron to optimise mobility in both indoor and outdoor environments.

2.2 MOTIVE UNIT

In order to accurately decide on the type of motive drive unit, it was first necessary to develop guidelines with regards to required specifications. Listed below is an outline of key factors considered in determining the correct drive method and unit sizing:

- As with any project at this level, expenditure must be kept to a minimum
- The motors must run off either 12 or 24 Volts DC (VDC).
- The motors must have sufficient power to drive up to 200kg while maintaining an adequate output velocity (ranging from approximately 0 – 1.2 m/s).
- The motors and any necessary gearbox units must not be of an excessive size.
- The motors and drive train must be reliable, requiring minimal maintenance.
- The motors and drive train must translate energy efficiently and smoothly, allowing for accurate acceleration and steady state travel.

2.2.1 Motor Selection

As stated in Section 2.2, the intention is to implement a DC motor drive that can run off of either 12 or 24VDC. Combined with the required load and velocities, this reduces the number of viable options. Companies such as “Maxon” manufacture a wide range of DC motors, including customised units with attached tachometers or encoders allowing for tidy motor/sensor integration. Unfortunately, these benefits come at a price, which surpassed the available budget for this project. Other drive units such as stepper motors allow great control and accuracy but simply cannot translate the required torque necessary to power the conceptual unit.

Therefore, the only viable option was to find an adequate permanent magnet DC motor. Once again, due to both expense and ease of controllability, brush type motors were chosen over brush-less units. In evaluating a series of manufacturers and motor types, a motor pair WMT90112 designed and developed by “Dynamic Controls Ltd”, a local New Zealand manufacturer of disability equipment were chosen. Two key factors aided in the decision. The first was that the motor pair was principally designed for electric wheelchairs, and secondly, the units came with an attached reduction box. Listed below are the wheelchair motor specifications:

Motor type	Permanent magnet commutator 24 VDC
Power output (maximum)	230 W @ 65 RPM
No load current	3.3 A (maximum)
Continuous current	8.0 A
Torque constant	1.1 Nm/A
Maximum torque	44 Nm (40 A controller) 55 Nm (50 A controller)
No load speed at motor shaft	3950 RPM nominal
Motor resistance	250 m Ω
Typical backlash	1.5 $^{\circ}$
Weight	5.5 kg
Bearings	Ball race
Parking brake type	Electro-mechanical 24 VDC

Parking brake hold torque < 50 Nm at output shaft

Figure A.1 illustrates scaled dimensioned drawings of the motor pair.

A further advantage with these motors is that they come equipped with concealed electro-mechanical brakes built in under the rear cowling of the motor. Although the brakes will not be required under normal operation, they could be useful when interfaced with a pitch sensor, to ensure the mechatron does not move when stationary on steep gradients.

Figure 2-11 illustrates the typical performance characteristics for the WMT90112 wheelchair motors. Figure 2-12 shows the right-hand motor.

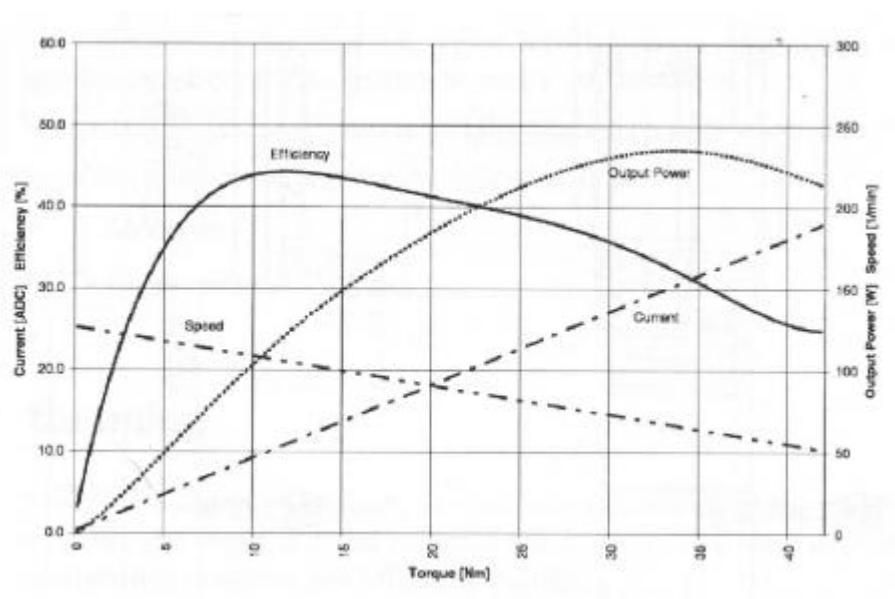


Figure 2-11: Typical performance characteristics for the WMT90112 motors



Figure 2-12: Right-hand drive motor unit

2.2.2 Gearbox

As can be seen in Figure 2-12 above, the gearbox unit has been designed to allow the motor to neatly fit into a cast sleeve, producing a single integrated unit. The gearbox attached to the wheelchair motors was designed to drive a small spur gear on the output shaft which then runs on a planetary drive surface on the inside of the wheel chair hubs. Figures 2-13 & 2-14 show a standard drive configuration for an electric wheelchair, and a planetary drive configuration respectively. This dual step drive train initially reduces the motor's output via the worm drive, and then reduces the final output again through the planetary drive ring gear.



Figure 2-13: Standard drive configuration for an electric wheelchair

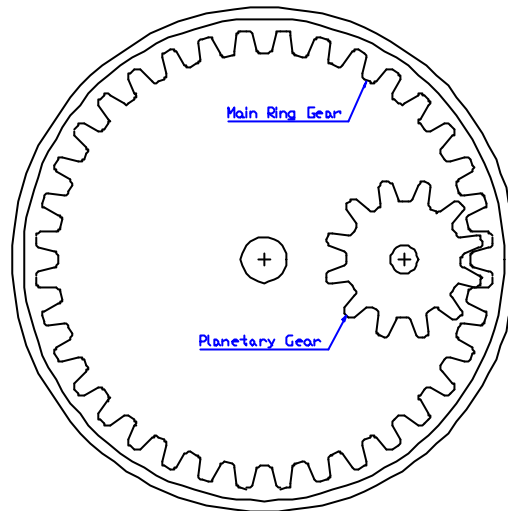


Figure 2-14: Standard planetary drive configuration

The gearbox itself consists of a worm gear pressed directly onto the motor's drive shaft, which in turn drives a helical gear. Fixed to the same axle as the helical gear is a small pinion gear that drives onto a larger pinion gear attached to the perpendicular out drive shaft from the gearbox. The second pinion gear is spring loaded, acting as a type of "dog-clutch", operated via an external lever on the top of the gearbox (illustrated in both Figure 2-12 and Figure A.1). This configuration produces a significantly geared down perpendicular output. Figures 2-15 & 2-16 show the internal configuration of the gearbox, and a worm drive configuration respectively.

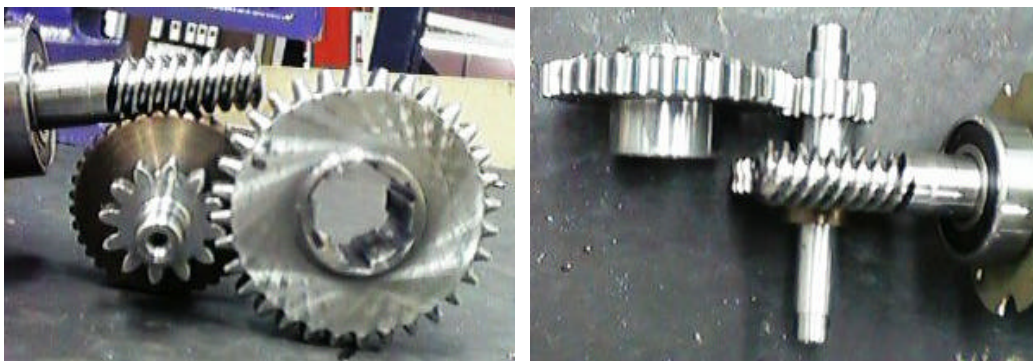


Figure 2-15: Internal gearbox configuration

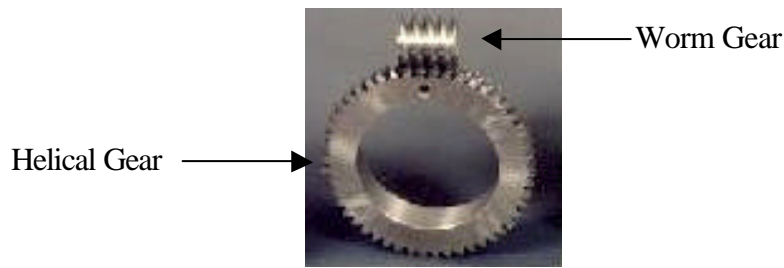


Figure 2-16: Standard worm drive configuration

The worm gear pressed onto the motor turns three teeth per revolution (has an Outer Diameter (OD) of 16mm), which then drives a 37-toothed helical gear (OD of 49mm). This configuration generates a reduction ratio of $N_{worm} = 12.33:1$. A pinion gear with 12 teeth (OD of 29mm) is attached to the helical gear, which in turn drives onto the output shaft from the gearbox via a 32-toothed pinion (OD of 67mm). This second stage gearing generates a reduction ratio of $N_{pinion} = 2.67:1$. Combining both the first and second stage outputs via Equation [2-1] calculates the overall gearbox ratio.

$$\begin{aligned}
 N_{gearbox} &= N_{worm} * N_{pinion} && \text{Eqn. [2-1]} \\
 &= 12.33:1 * 2.67:1 \\
 &= 32.89:1
 \end{aligned}$$

As per Section 3.3.3, a 15-tooth drive pulley (in effect a planetary gear), is coupled to the output shaft. This gear drives directly onto the teeth that are on the inner surface of the tracks. In effect, the tracks become a large dynamic ring gear with 180 teeth around the internal perimeter. The reduction ratio from the drive motor's output to the tracks is calculated using Equation [2-2]:

$$\begin{aligned}
 N &= \left(\frac{N_{track}}{N_{planetary}} \right) * N_{gearbox} = \left(\frac{180}{15} \right) * 32.89 && \text{Eqn. [2-2]} \\
 &= 394.33:1
 \end{aligned}$$

where: N = reduction ratio

N_{track} = gearing ratio of track

$N_{planetary}$ = gearing ratio of planetary gear head

$N_{gearbox}$ = gearing ratio of complete gearbox

For every revolution of the track, the motor must turn just over 394 revolutions.

2.3 POWER REQUIREMENTS

Once a drive system and associated motive units had been decided on, it was necessary to determine those peripherals (such as sensors) and other electronics that would produce a functional unit. Together with the drive equipment, this would allow for the unit's total power consumption to be evaluated.

2.3.1 Generalised System Requirements

This project has been developed to be the foundation for an advanced indoor/outdoor multi-terrain autonomous robot, and so allowances should be made to facilitate peripherals which may be added in the future. For this reason, all systems are to follow a modular design, allowing each component/unit to be independent from the others, and integrated with the entire system via a Central Processing Unit (CPU).

To act as the main "brain" of the unit, it was decided to include a full computer, allowing for all peripherals (including sensing equipment, instruments, and motive controls), to be controlled via a Data Acquisition (DAQ) card interface. This would also allow sub-processors such as micro-controllers to integrate with the other systems, while maintaining a certain degree of independence.

Other sub-systems for the unit could eventually include a full array of sensors so the unit would be able to detect obstacles, changes in terrain, measure distances travelled, manoeuvre with respect to reference points, correct for slippage, and many more. With future development in mind, the unit must have the ability to adequately house, interface and power this equipment.

2.3.2 Battery Selection

As stated in Section 2.2.1, the unit requires a 24 VDC power supply. This together with possible future additions implies that a large onboard power supply is required. Ideally, as with an electric wheelchair, two 12-volt deep cycle batteries would be run in series. Due to both the cost and the irregular cycling of the batteries during the prototyping stage, deep cycle batteries are not the best solution. Instead two heavy-duty lead acid batteries would be more than adequate during development. At a later stage these batteries could be swapped for deep cycle units to increase running time.

In deciding on the size of the batteries, it is desirable to have enough capacity for the unit to run for at least one hour. The continuous current drawn by each motor is listed as 8A, although this can reach as high as 10A (experimentally). The other major power user is the main computer, which draws (on average) 6A, with an efficiency rating of between 85 – 90 percent (ATX power supply rating), generating a maximum theoretical drain of approximately 7A. The remainder of the peripherals would have very little loading, being insignificant as compared to the motors and computer. Allowing 2A for additional equipment, the total current drain should not exceed 29A at any given time.

In selecting the batteries, it was important to find a unit that preferably met or exceeded a one-hour delivery time at 29A. For performance per dollar the following battery pair was chosen to power the unit during the development phase:

Manufacturer:	Marshall Batteries
Model:	NS70
Number of Plates:	13
CCA:	620 A
RC:	135 minutes

CCA = Cold Cranking Amps: This is an internationally recognised standard for accurately determining the true battery performance. It is the discharge load in amperes which a fully charged battery at -18°C can deliver for 30 seconds and maintain a minimum voltage of 1.2 volts per cell.

RC (m) = Reserve Capacity (minutes): Is the time in minutes that a new fully charged battery will supply a constant load of 25 amps at 25°C without the voltage falling below 10.5 volts for a 12 volt battery.

With the battery characteristics listed above, the robotics unit should be able to remain operational for 108 minutes at maximum power consumption rates (assuming linear RC rating per A/min). If the unit operates under normal load conditions, the power consumption rate could drop to as low as 60 percent of the maximum, increasing the operating time to up to three hours. These operating times do not deep-cycle the battery, hence these batteries could be expected to perform for many years.



Figure 2-17: Marshall Batteries – NS70 lead acid battery

2.4 SENSING OPTIONS

For any mobile robotic unit to operate autonomously it must be able to detect and interpret its surroundings. To do so it needs to be able to gain accurate information on its environment and have the means to decipher the data so that intelligent decisions can be made in its operating process. For a robot that will operate in both indoor and outdoor environments, its sensing ability becomes even more critical, as reference surfaces such as walls and doorways are not always available.

The key considerations in developing the sensor array for this project included:

- Obstacle detection
- Location
- Tracking control
- Course correction
- Terrain detection

Obstacle detection is divided into two sections, long and short range sensing. The following sub-sections outline two proximity and obstacle sensing options for both long and short range respectively.

2.4.1 Ultrasonic Sensing (long range)

Small ultrasonic sensors such as the Honeywell \varnothing 18mm Piezo-electric ultrasonic transducers can be used to detect objects up to 5 metres away. Ultrasonic sensing is generally configured using an emitter and detector pair. A known high frequency signal is produced via an oscillator through the emitter (40 ± 1 kHz). The receiver waits for a returning reflected signal, which it can measure to determine the distance to the object.

To reduce interference from external noise, band pass filters can be included after the receiver to provide a narrow window for the frequencies of interest. The emitter/detector transducers can be focussed using focussing caps and attenuation cylinders to improve the range of the signal window. This will be a compromise between imprecisely detecting more obstacles over a wide range, or precisely detecting fewer obstacles over a small field. Focussing caps cover the transmitting ultrasonic transducer and contain two small holes about the centre line at a half-wavelength ($\lambda/2$) separation. This generates an attenuated output wave from each aperture, simulating two separate emitters (Taberner, 1994). The attenuation cylinder is a tube that fits over the receiver, and extends forward. This cylinder is used to focus the receiver by only allowing returning signals within a narrow acceptance angle to pass inside the aperture of the focussing cylinder. Figure 2-18a and Figure 2-18b illustrate the focussing cap and attenuation cylinder respectively.

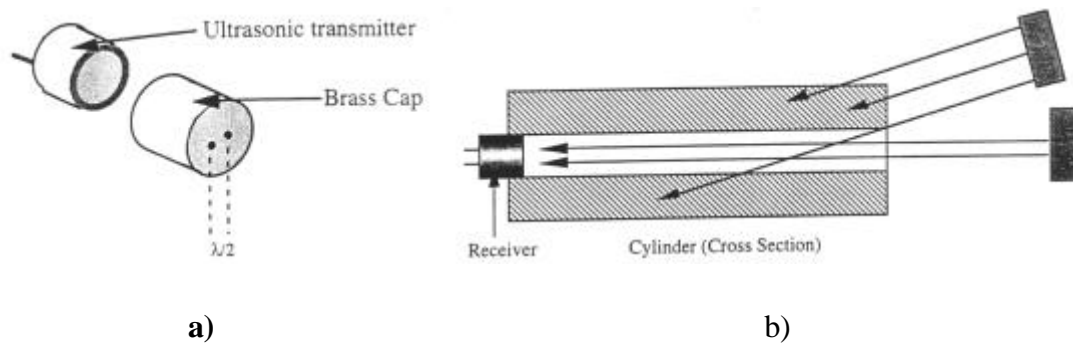


Figure 2-18: a) Ultrasonic focusing cap, b) Ultrasonic attenuation cylinder

When an object is detected, the unit can only determine the distance to that object, not the lateral position, nor necessarily the number of objects. If ultrasonic sensors are to be implemented in this project, two independent ultrasonic units would be required at both the front and rear. This would permit the sensing pairs to be able to have narrow focus windows, allowing the central computer to determine a degree of lateral position of objects. Figure 2-19 illustrates an arrangement of transducer pairs to better locate the position of an object. The three zones allow the vehicle to determine if an obstacle is to the left, right, or centre.

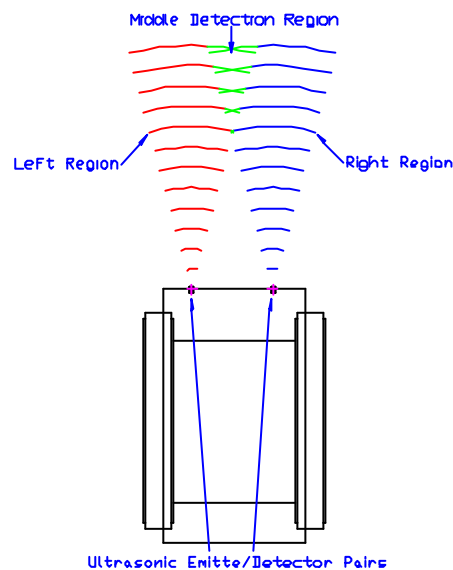


Figure 2-19: Dual ultrasonic transducer pair positioning to detect three zones

An alternative configuration would be to have a centrally positioned emitter with a series of receivers on either side. Both configuration options would produce similar

results. Two units also allow the approximate angle of incidence to a plane surface to be evaluated (illustrated in Figure 2-20).

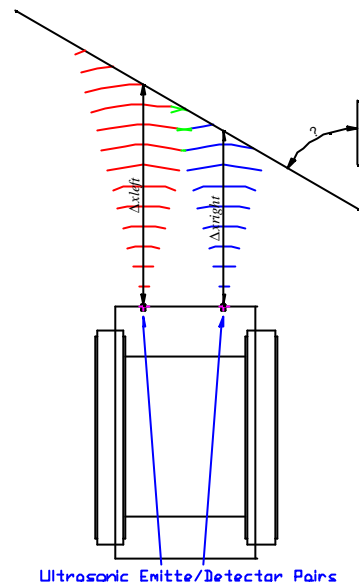


Figure 2-20: Detecting the approach angle of incidence to a wall/large obstacle

Two significant disadvantages are associated with reflected waves from ultrasonic transducers. The first is its tendency to reflect sound off of an object that exceeds the maximum acceptance angle of the receiver. Secondly, an object can cause a signal to be reflected generating a false reading. Path A in Figure 2-21 illustrates a signal being reflected off two surfaces, and consequently being prevented from returning to the detector. Path B in Figure 2-21 shows a signal originating from transducer pair 2, reflecting off two surfaces and being detected by the opposing transducer pair 1. This situation generates the illusion of an obstacle being at position 'X', implying that the wall itself is not detected.

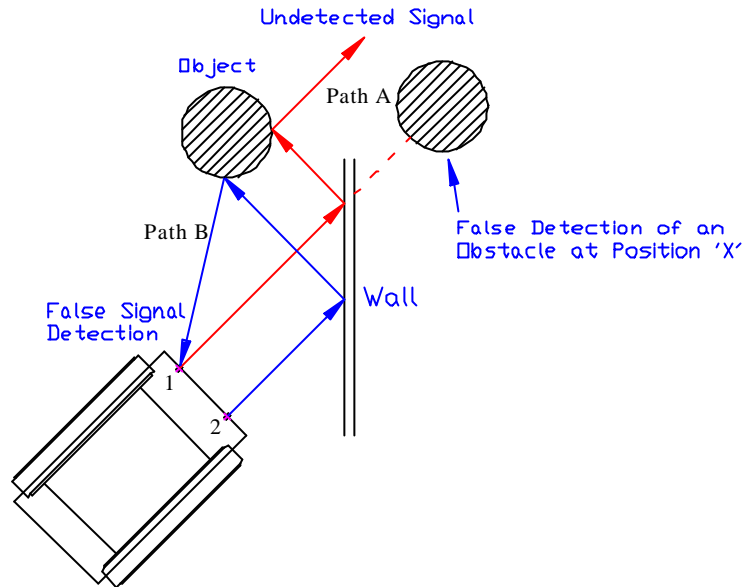


Figure 2-21: Incorrect detection of a secondary obstacle

Environmental operating conditions, such as dust, mud, and water, could significantly reduce the quality and accuracy of the ultrasonic signals. For these reasons, ultrasonic sensing is not to be implemented in this project at this stage of development.

2.4.2 Infrared Sensing (short range)

Infrared sensors operate by transmitting electromagnetic radiation in the infrared (IR) spectrum. Similar to ultrasonic transducers, the IR system comprises an emitter and detector pair.

The IR signal is transmitted from an emitter, and a matched detector scans the reflected signals to measure the difference in returning intensity. The returning signals are filtered to reduce interference from ambient and artificial light, then processed to determine the distance to an object. IR sensing has a narrower detection window than ultrasound, and hence can more accurately approximate the lateral position of an object. The major disadvantage of this is that a series of emitter/detector pairs are required to scan in front of a large face to ensure there are no ‘dead bands’ (undetectable regions). Figure 2-22 illustrates an undesirable IR sensing array, whereby obstacles can pass undetected through ‘dead bands’.

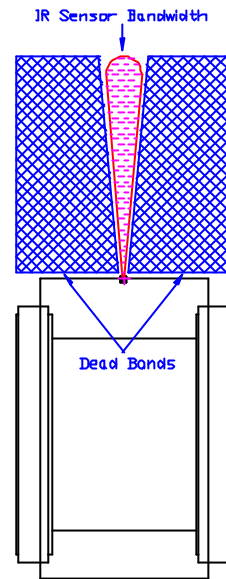


Figure 2-22: Undesirable IR sensor configuration, due to narrow sensing window

2.4.3 Tactile Sensing (extremely short range)

Tactile sensing is a method of detecting obstacles that make direct contact with a device. Instruments such as feelers and extended arms are connected to spring-loaded switches or contacts. When an obstacle makes sufficient contact to displace a connecting arm to the point where the deflection causes a short circuit on a switch, a signal is transmitted and the obstacle is detected. Increased sensing intelligence can be added to protruding feelers/arms, which can detect the changes in deflection on the feelers, and thereby the approximate location of the obstacle along the sensor. Although this is the crudest of the previously mentioned sensing methods, it is the most positive and reliable technique. Spring loaded ‘bump bars’ can be attached around the perimeter (connected to micro switches) of a mobile unit to act as a final backup-sensing device.

2.4.4 Laser Range Finding (long range)

The advantage with laser range finding is the potential for high measurement speed and accuracy over a greater distance than the IR and ultrasonic systems previously discussed (Sections 2.4.1 and 2.4.2).

A number of different laser range finding techniques can be employed including:

- Interferometry
- Frequency modulation
- Beam modulation telemetry
- Time-of flight
- Intensity measurement of reflected signal
- Triangulation

Interferometry:

Interferometry is based on the interference of two electromagnetic waves that have travelled different path lengths – a reference path and a target path. When the target path is displaced from its initial reference location, the resulting change in the number of interference fringes indicates the relative distance the target has moved. Although interferometry is one of the most accurate methods, it requires a retroreflective surface and a continuous line of sight with the target. Neither of these requirements can be guaranteed in an outdoor environment.

Frequency Modulation:

The frequency modulation method modulates an electromagnetic carrier wave using a periodic signal. When the reflected frequency is mixed with a reference frequency, a beat frequency is produced. By measuring the beat frequency, the distance to the object can be measured. This method requires precise linearity, repeatability, and control of a periodic signal, which is often difficult and requires sophisticated equipment.

Beam Modulation:

Beam modulation uses an amplitude-modulated electromagnetic wave as a source, and measures the phase difference between the source and the reflected signal. From the difference in phase, the distance to the reflective surface can be determined. If the time delay of the reflected signal is greater than the modulation wavelength, the phase measurement becomes ambiguous. Sophisticated phase-shift electronics are required to achieve reasonable accuracy.

Time-of-Flight:

A time-of-flight configuration measures the time an emitted pulse takes to travel to and from a reflective surface. As with beam modulation methods, sophisticated equipment

is necessary to obtain adequate accuracy due to the speed of light. For a range resolution of 1cm a time resolution of 67ps (67×10^{-12} s) is required.

Intensity Measurement of Reflected Signals:

This technique is based on the same principle as used for the IR sensors (Section 2.4.2).

Active Triangulation:

Active triangulation uses a Charge Coupled Device (CCD) of a camera to measure the offset of a beam (generated by a laser) from a central axis. At a known separation distance and angle, the CCD array detects the beam from the laser along its central axis. As obstacles pass in front of the line-of-sight of the emitted beam, the offset of the image within the CCD array corresponds to a change in angle relative to the central axis. This deviation can be used to determine the distance to the object. Figure 2-23 illustrates the configuration.

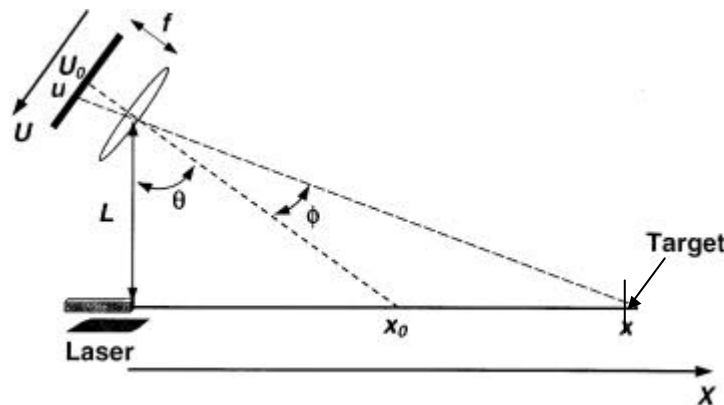


Figure 2-23: Active triangulation ranging system

As an active triangulation laser range finding unit has already been successfully developed by the Mechatronics Group (Hurd, 2001), a similar design is intended to be incorporated in the multi-terrain vehicle with a rotating stepper motor mount to allow 360-degree scans.

The advantages of a laser range finding device include:

- Self contained assembly
- Not relying on the incident angle with respect to the obstacle
- Broader scanning abilities (360-degrees)
- Additional range (up to 10m)

2.4.5 Navigation

For an autonomous mobile device to be able to operate effectively, it must be able to determine its position and have the means to navigate varying environments. This becomes even more important when a device is to operate outdoors where proximity equipment is unable to detect localised obstacles such as corridors and walls. For such environments, additional equipment must be considered.

2.4.5.1 *Compass*

A compass is an essential navigation device that uses a globally recognised coordinate system to identify direction. The compass can be used to follow a path and additionally, the steering mechanism can be interfaced to self-correct for any unwanted deviation to the course via a feedback loop. The compass therefore not only acts as a stand-alone navigation device, but also generates a means to ensure a straight heading is maintained during normal operation.

2.4.5.2 *Global Positioning System*

The Global Positioning System (GPS) is a satellite based navigation system consisting of a network of 24 satellites (illustrated in Figure 2-23) that were placed into orbit by the United States Department of Defence. In the 1980's this group of satellites (originally for military applications) were made available for civilian use.

Twice a day, each satellite orbits the earth, continually transmitting a low power UHF 1575.42 MHz signal. GPS receivers can detect these signals from multiple satellites and measure the period between the transmitted and received times. Via triangulation of three satellite signals, the receiver can determine its 2D position (latitude and

longitude) and track movement. When four or more satellites can be detected, the receiver can determine its 3D position (latitude, longitude, and altitude). Once the receiver's position has been determined, the system can calculate the heading, distance travelled, speed, and distance to and from designated positions (coordinates).

By combining coordinate waypoints into a mobile unit's navigation system, a GPS can plot a course, self-adjusting its heading and velocity to coincide with the real-time feedback from the satellites.



Figure 2-23: Network of 24 satellites for the GPS

With most modern multi-channel receivers, accuracy is maintained within 15 metres, but is generally less. A Differential GPS (DGPS) can reduce errors to between one and three metres on average (Furuno Electric Company, 2000). DGPS is operated through designated stations, which receive a signal from the GPS network, calculate the error, then transmit (via radio signal) a correction factor. The DGPS system not only requires a different GPS receiver (has an additional radio antenna integrated), but in New Zealand requires a payable annual subscription to take advantage of the service which has very few relay stations around the country.

2.4.5.3 Reference Transponders

Reference transponders are not dissimilar to the concept of DGPS except that they simply transmit a continuous signal that allows a unit to determine its location relative to the signal. Stations can be installed within an operating area to transmit reference

coordinates to a vehicle. This system has the disadvantage of requiring external equipment for accurate navigation, thereby limiting the operating range.

2.4.6 Additional Sensing Equipment

An essential part of manoeuvring a mobile device is not only avoiding obstacles, but also ensuring that the path being travelled does not exceed recommended operating parameters. Additional sensors must be installed to ensure that the motors are operating correctly, traction is being maintained, and that the surface contours and gradients will not cause the vehicle to capsize.

2.4.6.1 Shaft Encoders

This is simple method of determining the speed of a device and therefore the distance travelled. Shaft encoders generally consist of a coded wheel (a disk with a series of evenly spaced holes around the perimeter) attached to the drive shaft. As the drive shaft rotates, a photonic sensing unit detects the number of holes that pass through its aperture, which can be used to detect both the speed and direction of rotation. Although this system is prone to accumulative errors due to deviations in terrain, tyre/track diameter, and slippage/loss of traction, it is an invaluable tool. When integrated with other previously mentioned sensing systems, shaft encoders can aid in the calibration and control of the drive unit.

2.4.6.2 Yaw and Pitch Sensors

The gradient/slope of the terrain being travelled can be detected by the implementation of a Yaw and Pitch Sensor (YPS). The primary function of the YPS is to ensure that the unit does not roll due to steep or uneven terrain. Originally YPS were configured around a mercury switch design, but have recently been developed using solid-state devices to generate incremental feedback within a 3D plane.

3. MECHANICAL DESIGN AND CONSTRUCTION: TRACK MODULE DEVELOPMENT

The shift from wheels to a caterpillar drive train will allow the unit to manoeuvre over and around a greater variety of terrain. It will also increase both torque through what in effect is a large planetary drive system, and additional traction from the increased surface friction generated by the long wide dual tracks.

Taking advantage of a wide range of research facilities, including academic institutes, local industry, and the Internet, it became apparent that there were no small-scale pre-manufactured caterpillar drive units available. The units that were available on the market, were both large scale (industry related earth moving equipment), and very expensive. The few smaller scale units that were attainable, were crudely designed, manufactured from lightweight materials, and designed for specific applications.

For the reasons outlined above, it became apparent that a custom manufactured unit would be necessary to fulfil the requirements of the project. Initially the design criterion was general and limited. Key factors in the design included drive belt dimensions for the tracks, motor specifications, and required energy source to power the unit and peripherals.

A key consideration in the preliminary development stages was to develop a foundation for an autonomous modular unit, which would have the capacity to house and integrate a vast range of future research equipment. With this in mind, it was intended to develop a unit which had the presence of a large-scale robot with provision for future

peripherals, yet could manoeuvre itself through standard interior passages, enabling its range of applications to be as diverse as possible.

3.1 CONCEPTUAL TRACK MODULE DESIGN

When starting to develop the conceptual design of the track modules, five main attributes had to be implemented. The first step was to decide on a method to locate the tracks independently to the main chassis. There had to be a mechanism to tension the belts, enabling them to be installed and removed without dismantling the unit. The units had to be designed to negotiate obstacles. The tracks also had to be able to be displaced over and around obstacles while maintaining track tension. A drive mechanism had to be fitted to allow direct attachment to a gearbox and motor.

The requisite functionality listed above required six main units:

- Enclosed cavity to locate the mechanics
- Track tensioning unit
- Drive axle
- Bogie unit to adjust to terrain contours
- A unit that would dynamically adjust the track tension depending on belt displacement.

The following sections discuss and justify the design and manufacturing attributes of each of the generalised units listed above, in conjunction with parts and materials selection.

3.1.1 Drive Belts

The first consideration for the design was the availability of drive belts and pulleys to act as tracks. Available pre-manufactured caterpillar styled tracks are both too large, expensive, and not ideal for my project. Standard automotive belt's were both too narrow and had short radial lengths. The final option was to look at conveyor and super charger belts. A local Hamilton supplier had access to a vast range of belts and drive

products, and also had the ability to custom manufacture belts around standard tooth and drive configurations. With one of the largest restrictions being cost, the available belt and drive permutations were significantly reduced. To reduce both the weight and cost of the drive train, composite polymer drive pulleys were used instead of similar steel or alloy units. Furthermore to the original conceptual design, a two point return rotation for the belt was required, thereby allowing a series of smaller diameter pulleys to be used, reducing the acute angle of the belt over the pulleys and enabling the unit to more easily climb and manoeuvre over obstacles (Figure 3-1).

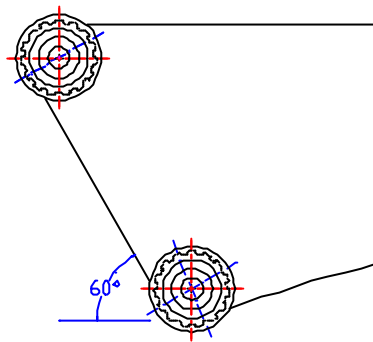


Figure 3-1: Two point return rotation of track's (60-degree leading edge differential)

Any less than a 60-degree differential between the bottom and top pulley would have reduced the robot's ability to easily climb over obstacles. If the angle were to be increased it would have amplified the acuteness of the belt on the upper pulley, restricting the thickness on the track.

The tightness of the curve around the upper pulley was a key consideration. The pulley diameter had to be as large as possible, while at the same time not increasing the vertical height between the axles too greatly. This is to ensure the vehicle's centre of gravity is as low as possible and thereby increasing its stability over rough terrain. The largest composite polymer drive pulley obtainable that would cope with the foreseen loading was a 59 mm diameter (measured from the extremities of the teeth) H configuration unit manufactured to order by Stagnoli Ltd in Italy. This pulley can cope with an axial loading of up to 500 kg, with no hollow cavities, allowing for a number of machining modifications to be carried out without affecting the integrity of the original

design (Composite Polymer Pulley illustrated in Figure A.2). The centre point came pilot bored ($\text{\O}10\text{mm}$) allowing for a customized drive shaft to be fitted and keyed. The keyed drive pulley is illustrated below in Figure 3-2.



Figure 3-2: Keyed $\text{\AE}59\text{mm}$ H-tooth configuration polymer drive pulley

Based on the pulley's H-tooth configuration, there were a number of suitable belt lengths available. This number was reduced by the belt lengths that could be obtained with varying widths. During the initial conceptual design phase, it was envisioned that the robot would be approximately 1000mm in length, and 700mm in width, standing approximately 600 – 700mm high. Ideally the tracks needed to extend along the entire length of the robot. Therefore the track's radial length would have to be between 2.1 – 2.6 metres. Unfortunately there were only two belt lengths available within the range suggested above, 2100mm and 2300mm internal radial length. To optimise the unit's length, the 2.3-metre belts were chosen. Ideally the tracks would have been more appropriate if they were manufactured to 100mm in width, but this was restricted by both the budget and the pulley dimensions. The drive pulleys have a fixed drive surface width of 28mm. Placing two pulleys face to face allowed for a 56mm belt. This distance could be safely packed out to 75mm, but a 100 mm belt could cause the track to lose drive due to only 56 percent of the belt being in contact with the drive surface. For this reason, the 2.3 metre, 75mm H-type drive belt was chosen.

The second consideration was modifying the belts to clear the guide flanges on the pulleys. In their original state, the drive belts only have a 3mm wall thickness from outer surface to tooth trough. The pulleys have a flanged guide of 7.5 mm from the

crest of the teeth to the outer edge of the guide flange. There was therefore, a deficit of 4.5mm to bring the belt surface out flush with the pulley's guide flange. To overcome this problem an additional 10mm of medium density high quality vulcanised rubber was laminated onto the outer surface of the belt's. The laminated belt profile is illustrated in Figure 3-3. This surface now clears the pulley's guide flanges by over 4mm, and also allows for a further treaded surface to be laminated over the 10mm addition, if required for further traction in outdoor environments.



Figure 3-3: Side profile of the H-Type transmission belt (black), with an additional 10mm of high quality vulcanised rubber laminated to its outer face (orange)

Once both of the tracks and pulleys had been decided upon, the horizontal and vertical distances between pulleys were adjusted to optimise both the belt length and drive capabilities of the unit. Targeting a one-metre distance between the extremities of the upper pulleys, and a 60-degree incline between upper and lower pulleys produced a vertical distance between upper and lower pulleys of 180mm (centre to centre). These general dimensions generated a foundation from which to develop the more intricate tensioning and running system to ensure constant drive and belt tension integrity.

3.1.2 Side Plates

After developing the track geometry it was necessary to decide on a method to mount and house the guide and drive pulleys. Ideally each track unit would be independent from the other, designed and built in a modular fashion. This would aid in both construction and assembly. To incorporate the characteristics listed above, two solid steel side plates were manufactured to sandwich each track. The two plates would locate and protect all of the pulleys, bearings, and internal mechanisms. The plates were designed to follow inside the profile of the ideal track geometry, so as not to foul or restrict the belt's traction. As a compromise between weight and strength, the sides

were designed using 4mm mild steel plate. This gave adequate strength and support while minimizing any ripple over the large flat surfaces. 4mm plate would also allow for a series of slots and holes to be inserted without affecting the integrity of the surfaces. The final consideration was the geometry of the base surface. This surface could not remain flat between the two bottom pulleys, as there would be no clearance when the unit was to run over an obstacle, causing the track plates to foul. Therefore it was decided to cut away the bottom surface in an arc, generated tangentially from the clearance arcs around the two bottom pulleys. The curve had to be sufficient enough so that when the track's tensioning unit was to bottom at its operating extremity, the side plate would remain inside a smooth arc generated by the track between the two bottom pulleys. It was essential that the curve was of a sufficient radius, yet enough side plate remained so as not to impinge on the integrity of the design.

3.1.3 Base Arc

The three key considerations on the size of the cutaway were the way in which the track modules were to be attached to the main chassis, the maximum arc the track could make if the front sliding axle was to bottom on the guide slots, and the centre of rotation for a bogie unit, which would run in between the two bottom guide pulleys. The first consideration was to plot the curve obtained by bottoming the front sliding axle. This gave the maximum possible theoretical cutaway, although impossible once a bogie unit was installed.

The second consideration, involving the position of the chassis attachments, was the most critical as far as the design was concerned. Ideally the height from the ground to the underside of the main chassis had to be maximised, so as to increase the height-to-width ratio in between the track modules. This would reduce the chance of the unit's chassis fouling itself on obstacles and thereby allowing the unit to travel over rougher terrain. The difficulty with having the base of the main chassis starting high on the track module's side plates, was that it reduced the distance between the lower and upper vertical fixing points on the chassis. If this distance was too small it could cause the track modules to have a spreading effect from top to bottom, especially if the loading on the chassis became high. These concerns, combined with the conceptual positioning of

the bogie unit, resulted in a compromise on the height of the arc. Therefore, the side plates were designed with a tangential arc in between the base pulleys with a radius of 954mm.

3.1.4 Laser Profile Cutting

Laser cutting was chosen over plasma, due to both the accuracy and finish. When the plates were cut they were flawless and therefore required no machining. Figure A.3 and A.4 illustrates the final drawings of the inner and outer track module side plates (TMSP). Figure 3-4 below shows the outer side plate of the finished track module.



Figure 3-4: Completed internal side plate of track module

3.2 DYNAMIC VARIABLE TRACK TENSIONING UNIT

The key component of the track's drive unit is a variable tensioning unit. After developing the intended track geometry it was necessary to develop a mechanism that would allow the drive belts to be inserted and removed with ease from the track and pulley configuration. The unit was intended to actively compensate for any displacement change in the track's shape while negotiating obstacles, so as to contour itself over and around the surface of the object to maintain a constant tension. To implement this design, a unit would only need to be fitted to one of the four main pulley extremity points. For practicality of the design, the tensioner was to be positioned on the upper pulley opposing the main drive pulley. By placing the tensioner on the upper guide pulley, it also reduces the acuteness of the belt rotation when the belt displacement is altered. The final consideration was developing the unit so that the

tension could be altered when the tracks were both on and off, in a constantly accessible fashion.

In implementing the tensioning unit, the upper pulley opposing the drive shaft was designed to run in guide slots in the side plates. Each slot was angled at 30 degrees to bisect the track's leading edge, so that equalized pressure was generated on the pulley's shaft during changes in track displacement.

The tensioning mechanism consists of two main sections. The first is the main unit, which slides along the guide slots in the track module's outer plates and holds the front axle and pulleys in position. The front sliding mechanism was originally constructed from five pieces. It consists of two slide plates (50×6mm plate), two guide rods (120×Ø12mm), and a one spacer, which also acts as a guide for the ends of the tensioning bolts (50×12mm plate). The two guide rods are centralized laterally across the side plates, and are separated longitudinally by 60mm (centre to centre). This distance is great enough to reduce the lateral force on the guide slot, allowing for a smooth slop free action. At the same time it reduces the required length for the guide slots. The guide slots needed to be positioned close enough to ensure the tracks can have adequate tension applied, and long enough so that the tensioner can be released enough to remove the tracks without disassembling the track modules.

Each of the two side plates are 240mm in length. The extended length is required so that in the unusual circumstance that the top guide rod was to bottom on the top of the running slot, there was enough length on the tensioner's side plates so that an opening would not be seen. The guide slots are 113mm long, therefore from the front of the first guide rod to the end of the side plates is 130mm giving a 17mm buffer. The extended length of the side plates also gives a greater guide distance for the adjustable tensioning plate, which runs on the two tensioning bolts.

3.2.1 Construction of the Front Sliding Axle Unit

The two side plates illustrated in Figure 3-5 below were cut to length (240mm), then the three $\text{Ø}12\text{mm}$ holes were bored for both the guide rods and front pulley shaft. The front pulley shaft hole was used to fix a temporary bearing to enable the leading edge to be ground round in the lathe. The machining was performed by mounting the temporary bearing in the tool post, and running a $\text{Ø}300\text{mm}$ grinding stone in the chuck. This allowed for an accurate controlled radial grind of the side plates about the $\text{Ø}12\text{mm}$ hole, generating a perfect 25mm radius curve. The other two-guide rod holes were counter sunk on the inner surface using a $\text{Ø}18\text{mm}$ drill. This allowed for adequate gulleeted surface to fill with weld to bond the guide rods to the side plates.



Figure 3-5: Customised side plate of the front sliding axle unit

The spacer that separates the two side plates was cut to 94mm out of $50\times 12\text{mm}$ flat bar. This spacer also acts as guide locators for the ends of the tensioning rods. The guide holes were bored to $\text{Ø}14\text{mm}$ centred axially, 15mm from each end. Figure 3-6 shows the layout of the components of the front sliding axle unit prior to welding.



Figure 3-6: Component layout of the front sliding axle unit, prior to welding

3.2.2 Welding

For ease of construction, the spacer was placed between the two guide rods, hard against the trailing edge of the front rod. In conjunction with a temporary brass spacer held in the $\varnothing 12\text{mm}$ holes of the side plates (illustrated in Figure 3-5), this enabled several spot-welds to be completed using a TIG welder while ensuring the correct separation between the plates. While welding, the guide rod overhang on either side of the plates had to be maintained. Once the spot-welds were completed, and both measurements and squareness were rechecked, full length gullet welds could be completed along all eight edges that were in contact with the side plates. Full radial gullet welds were also completed around the guide rods in the inner surface of the side plates so as to fill the counter sunk gullet.

By only welding the guide rods to the inner side plate surface, it ensured that the front axle tensioner unit would slide freely between the two side plates within the guide slots without any fouling welds. Once all welds were completed, the inner sections of the guide rods were cut off and ground flush with the inner surface of the side plates, so as not to foul the tensioning bolts that would be located in the holes in the spacer plate. By cutting the rods after welding, it was easier to ensure the side plates remained parallel, and the guide rods remained perpendicular to the side plates. Figure A.5 illustrates a scaled dimension drawing of the front sliding axle unit. Figure 3-7 below shows the completed front sliding axle unit.

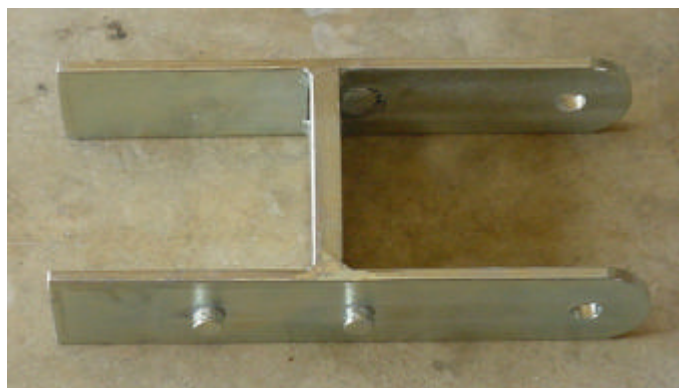


Figure 3-7: Completed front sliding axle unit

3.2.3 Track Tensioning Mechanism

The second mechanism is concealed between the TMSP. This unit consists of a fixed plate housing two tensioning bolts, which also acts as locators for the main tensioning springs. The unit has been designed to bolt between the track module's two side plates using four M10×25mm bolts. This unit runs in line with the guide slots and is designed to adjust the tension on the springs reacting against the front sliding axle unit by moving a plate that runs on the threads of the tensioning bolts, bridging across both bolts to ensure even pressure is being applied to both springs. Due to the intricacies of the unit, there were no bolts available to modify to suit the design, so customised bolts were manufactured from 5/8" United National Fine (UNF) threaded rod. It was necessary to use UNF thread to allow for extremely fine adjustment as the two bolts are interconnected via a short threaded pressure plate, reducing the independent movement that can be exerted on any one bolt prior to adjusting the other.

3.2.4 Bolt Fabrication

The 5/8" UNF threaded rod is only available in one-foot lengths. These rods were shortened to 220mm, which gave adequate length from the inside of the base curve of the TMSP to the point where the front axle unit is at its maximum tension point. Both ends of the rods were then faced in the lathe, with one end bevelled at 45 degrees down to 5mm to act as a weld gullet. The final 55mm of the other end was machined down to \varnothing 12mm, so that it could freely slide inside the 14mm diameter holes in the front axle unit (Note: 2mm was allowed for misalignment during tensioning adjustments). Prior to welding the nuts on the rod ends, both faces were chamfered off to reciprocate the rod ends so as to increase the weld gullets. The nuts were then welded to the threaded rods on both the inner and outer surfaces, building up the weld so that it finished proud of both faces. By filling the gullets proud, it enabled the welded bolts to be re-faced in the lathe, to give a smooth, flush, finished surface.

3.2.5 Tensioner Bolt Locating Plate

The bolt location plate was designed in conjunction with the tensioning mechanism, so that the tensioning bolt heads would maintain their location irrelevant of the tension on the front axle unit. This plate had to be substantial enough in depth to allow for the unit to be bolted in between the TMSP, and to reduce the lateral movement from the front to back faces. For reasons previously stated, a 50×20mm plate was used, cut to 107mm to maintain parallelism between the TMSP. To locate the plate in between the TMSP, two Ø8mm holes were bored to 25mm, centred 9mm from each end along the centreline. These holes were bottom tapped to M10×1.5 thread, enabling the unit to be located using four M10×1.5×25 bolts. Two holes were then bored in the main face to locate the large manufactured tensioning bolts. These holes were positioned 23mm from each end along the centreline, and bored to Ø18mm to allow for an overall clearance of 2.125mm. The large clearance is to allow for any misalignment that may occur during tensioning, and to give a buffer during electroplating. Figure 3-8 below shows the manufactured locating plate.



Figure 3-8: Tensioner bolt locator plate

3.2.6 Final Tensioning Unit Assembly

The final assembly involves welding a second nut on the inner face of the block to enable the tensioning bolts to maintain their location, yet rotate free in the housing. As the inner nuts will have all the pressure applied (acting as a thrust bearing on the block due to the spring's reaction), they need to be able to evenly distribute the force over as large an area as possible to ensure that the tensioner bolts maintain a free action. For this reason, large Ø1-¼"OD (Ø5/8"ID) washers have been placed against the inner

block surface prior to the inner nut. A smooth round rebated surface on the inner face of the thrust nut (inner) was machined, to ensure there is no grabbing action generated by the hexagonal corners on the nut. Figure 3-9 illustrates the modified face of the inner nut. The outer surface of the inner nut was also gullested in the same manner as the bolt head nuts, to allow for a clean weld to bond the nuts to the bolt shafts.



Figure 3-9: Faced inner locating nuts for the tensioner unit

Figure 3-10 shows the parts layout of the bolt fabrication. The final weld, which bonded the inner nut to the tensioning bolt shafts, left a 1mm clearance gap between the face of the washer and the inner surface of the fixing plate. This gap allowed enough clearance for the tensioning bolts to freely rotate in their housing after the dectroplating process.

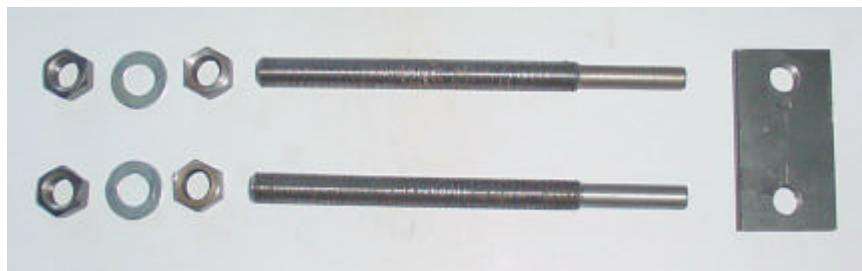


Figure 3-10: Parts layout for the tensioning unit

3.2.7 Threaded Tensioning Plate

The threaded tensioning plate is designed to neatly slide inside the two side plates of the front sliding axle unit, along the two main tensioning bolts. **Note:** All of the 50mm plates were cut and faced in the four-jaw chuck of the lathe to ensure perfect square surfaces of precise lengths. The tensioning plate is constructed from 50×12mm mild

steel plate, dressed to 92mm enabling 1mm clearance between each of the front axle's sliding units side plate. Two 9/16" holes were drilled 15mm from each dressed edge along the longitudinal centreline. The two holes were then tapped to 5/8" UNF thread to reciprocate the main tensioning bolts. Figure 3-11 shows the completed layout of the pair of tensioning units, including the tensioning plates. This unit can now be freely threaded onto the two main tensioning bolts by simultaneously rotating both bolts. Figure A.6 illustrates the scale dimensioned drawing of a completed tensioning unit.

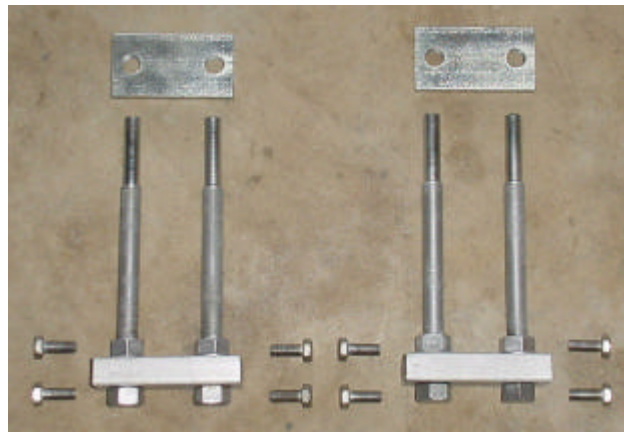


Figure 3-11: The pair of tensioning units and respective tensioning plates

3.2.8 Front Sliding Axle Unit Bearings

Phosphor bronze rod was intended to be used for all guide pulley-running bearings. Due to lack of availability this was not possible, so brass rod was used instead. This was obtained pre-gauged and dressed to a perfect 5/8" outer diameter (OD) rod. The front running axle for the front sliding unit was cut and dressed to 94mm long so as to fit neatly in between the two side plates on the unit. To hold the front axle in place, $\varnothing 8$ mm holes were bored axially along the rod's centreline to a depth of 30mm at each end. These holes were then bottom tapped to an M10 \times 1.5 metric thread. Once the holes were tapped, the leading 2mm of the threaded holes were re-bored to $\varnothing 10$ mm to allow the fixing bolt's heads to butt face-to-face with the brass bushes without fouling. **Note:** The leading 1-1.5mm of a M10 bolt is not threaded directly under the head, and protrudes to the full outer width of the thread. Figure 3-12 shows the machined axles, including the internal threads. To locate the front axle of the sliding unit, two M10 \times 1.5 \times 25mm bolts were used. First the bolts had to be modified so that they could

maintain the front shaft's position while not exceeding 106mm so as to allow the front sliding unit to completely and freely slide in between the two main side plates of the track module without fouling.



Figure 3-12: Running bearing for the front sliding axles pulley's

3.2.9 Front Sliding Axle Units Bearing Fixings

The front sliding unit's bearings required modified bolts to not only ensure the front bearing maintains its location, but to also enable them to fit inside a radial housing without fouling the TMSP when the sliding front unit passes inside the track module. Standard M10×1.5×25mm bolts have a standard head depth of approximately 8mm, therefore the first step was to reduce the depth down to 5.5mm to ensure the bolt heads did not finish proud of the 6mm side plates. The second step was to once again use the lathe to remove the hexagonal edges of the bolts, so they could snugly fit inside the Ø12mm holes in the sliding units side plates. At this stage it was critical that the bolt heads had an extremely snug fit, so there was very little movement on the brass bearing. By removing the hexagonal edges, the head of the bolts had to be modified, so that the bolts could be easily tightened in their radial housings. The easiest method was to slot the heads to suit a standard large flat screwdriver. To generate an adequate width slot, a large 300×25×1.25 power hacksaw blade was used in a hand hacksaw. This method allowed for a 1.6mm slot to be generated in a single pass. The heads were slotted to a depth of 2mm. The large slot also allowed for the sliding tensioner's side plates to be spot punched into the groove of the bolt after electroplating to stop the bolt heads and

brass bearings rotating. This forces the pulleys to run on the bearings, rather than the bolt heads running on the side plates. Figure 3-13 shows the customised locating bolts for both the front sliding axle and bogie unit pulleys.



Figure 3-13: Customised bolts for locating the running axles on the front sliding axle, and bogie units

Note: All open faces and ends have been faced in the lathe, and chamfered where required to give a clean dressed finished surface.

3.2.10 Tensioner Springs

Two compression springs were required per unit, to react against any force exerted by an obstacle trying to displace the track. The springs had to have a minimum internal diameter of 5/8" so they could freely slide over the tensioning bolts. The length and helix of the springs also had to be sufficient so that they would work over the entire operating range of the sliding front axle unit without bottoming the helix on itself. The final consideration was the gauge, as the spring had to be sufficiently strong to tension the track, ensuring it remained taut under normal operation, yet was soft enough to allow the track to contour around objects, allowing for as much track as possible to remain in contact with the surface. Although it was an option to have customised springs manufactured, it was preferable to utilise standardised springs that were commercially available. Due to the design of the tensioning mechanism, the required internal diameter and length of the springs were already determined. Due to the small selection of spring gauges available in the dimensions required, the task of selecting an adequate gauge was relatively easy. The main springs selected for the tensioning unit

were 1-1/8"×4"×120 (outer diameter, length, gauge). Figure 3-14 shows the main tensioning springs. It would have been preferable to have an extended helical length, as the springs come very close to bottoming in their most compressed state in the mechanism, but to do so they would have to have been custom made.

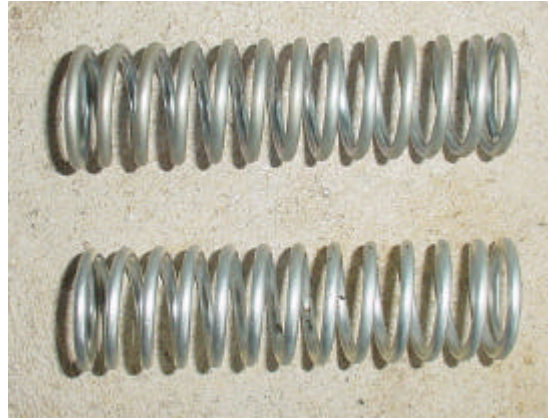


Figure 3-14: A pair of 1/8"×4"×120 main tensioning springs

3.2.11 Front Sliding Axle Unit Pulley's and Spacers

The pre-manufactured pulleys out of Italy came as per Figure A.2. In their original state, they required only minor machining for the main drive pulleys (four units). The remaining twenty units required a great deal of machining to enable them to be used as guides rather than a driving application. The guide pulleys were broken into two main groups. Those to be used in fixed positions between the two side plates of the track module (eight units), the remainder in dynamic positions, such as the sliding tensioner front axle, and bogie unit (twelve units). For the guide pulleys in both applications, the first step was to bore the pulleys out to 5/8". All pulleys were independently bored in the lathe, to a precise 5/8".

After all final machining was completed, the pulleys were reamed to ensure a smooth running surface on the brass bearings. The next step was to remove the drive teeth in the lathe so as to ensure they would not catch or foul on the teeth of the track. This would ensure a smooth free running surface, thereby reducing the risk of the guide pulleys causing the track to jump teeth on the main drive pulleys. A parting tool was used in the lathe to remove the teeth. This allowed the tool to run perpendicular to the

radial pulley surface, allowing the cutting face to take a clean cut right up to the outer flange of the pulley. For ease and accuracy, two pulleys were bolted inner face to inner face using a $\text{Ø}5/8'' \times 4''$ UNF bolt. This bolt had been centre bored in its head to allow the fastened nut to be fixed in the three-jaw chuck, thereby allowing the head to freely rotate while attached to a live centre. Over a series of passes, the teeth were removed from each pair of pulleys so that a radial running diameter of 53.5mm remained.

The third and final step was only necessary for the pulleys to be used in the dynamic positions. The pulleys in the static positions required no further machining, and were ready for use after they had been reamed to suit the brass bearing. Figure 3-15 below shows the full size pulleys used in static positions. Figure A.7 illustrates the scale dimensioned drawing of the main guide pulleys.



Figure 3-15: Guide pulley for static positions

The remaining pulleys had to have their outer running face reduced in width to accommodate the additional thickness of steel from the side plates of the units that run and pivot inside the main side plates of the track modules. The original distance from the outer edge of the track flange of the pulley, to the outer extremity of the pulley was 12mm. This was reduced to 6mm as per Figure A.8, to allow for a 6mm steel plate either side, plus 1mm of clearance between the inner face of the TMSP, and the outer edge of the plate attached to the pulley. Figure 3-16 shows the reduced guide pulleys for both the front sliding axle, and bogie units.



Figure 3-16: Reduced guide pulley for dynamic positions

The final stage in the preparation of all the guide pulley units was the manufacturing of spacers, which would be sandwiched in between each pair of pulleys. The spacers are necessary to prevent the guide pulleys from running inside the outer edge of the tracks, onto the toothed surface. This could not only cause the track's movement to be restricted and at worst derail, but it could also prevent the tensioning and bogie mechanisms from working correctly. The spacers were manufactured from $\text{Ø}40\text{mm}$ high quality machining grade aluminium rod. The rod was then centrally bored out using a $\text{Ø}5/8''$ drill in the lathe. The outer face was shaved down to a $\text{Ø}38\text{mm}$ so that the spacer would sit neatly inside the outer edge of the inner radial lip of the pulleys. After drilling and facing, the rod was cut into approximately 20mm wafers using a cut-off saw. The wafers were faced on both sides in the lathe, bringing the overall width down to 17mm. This brought the overall distance from inner flange to flange of the pulleys out to 76mm, giving 1mm of clearance for the 75mm track. Once the width was gauged, both the interior and exterior radial corners were chamfered to remove any sharp edges. As with the pulleys, the interior diameter was reamed to generate a gauged running surface for the brass bearings. The finished spacer is shown below in Figure 3-17. A total of ten of these spacers were made for all of the guide pulleys.



Figure 3-17: Aluminium spacers to separate all guide pulley units

The complete static and dynamic guide pulley unit layouts and assemblies can be seen respectively in Figures 3-18 and 3-19 below.

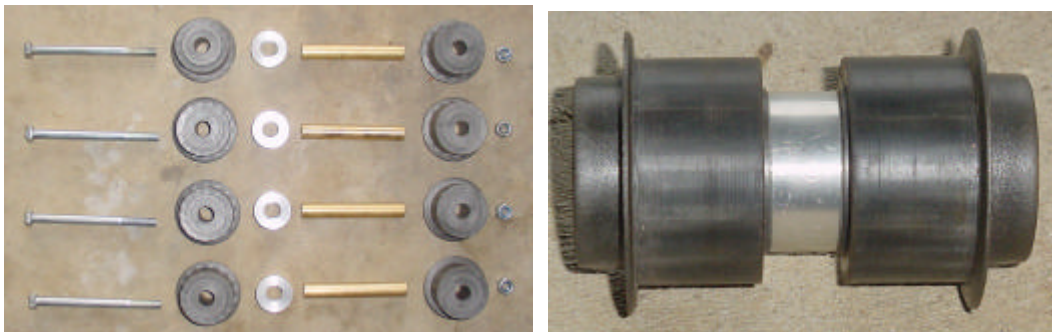


Figure 3-18: Static pulley layout (left), Assembled static Pulley unit (right)

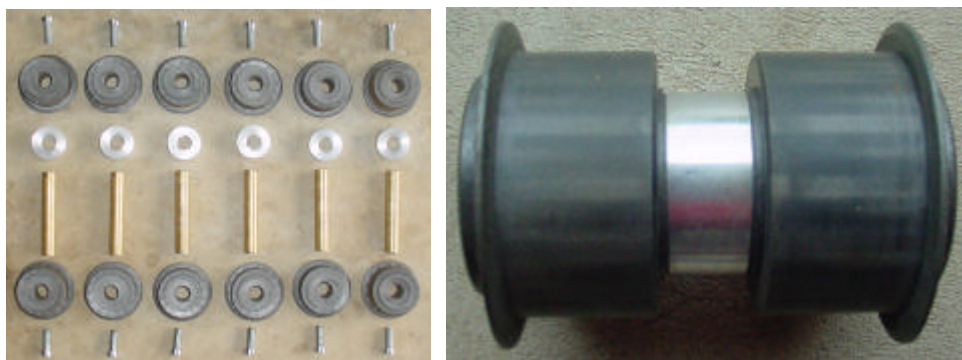


Figure 3-19: Dynamic pulley layout (left), assembled dynamic pulley unit (right)

Below are a series of figures, illustrating the completed front sliding axle, pulleys, plates, springs, and tensioner.

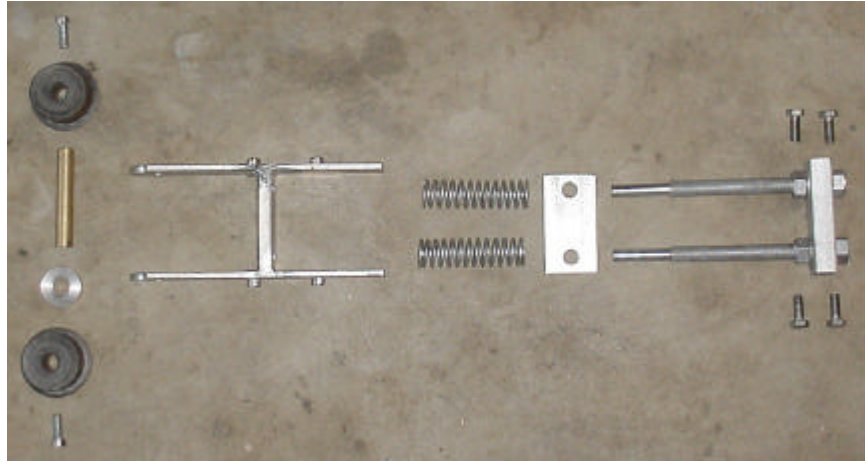


Figure 3-20: Layout of the complete front sliding axle unit and tensioning mechanism

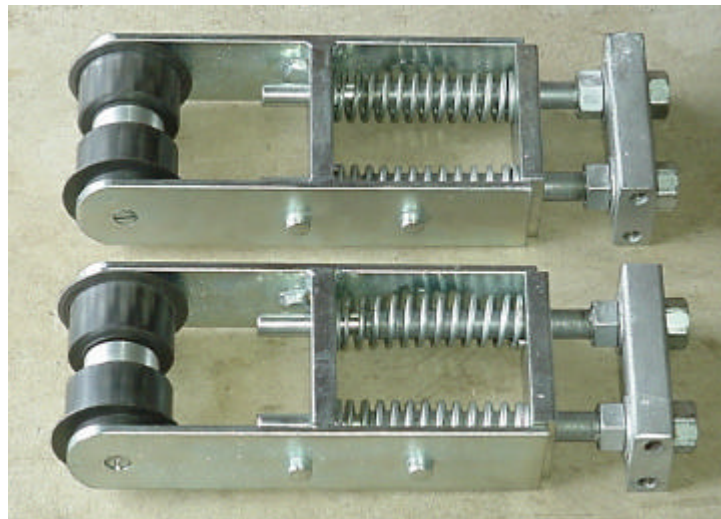


Figure 3-21: Assembled view of the complete front sliding axle unit and tensioning mechanism (ready to be installed in between TMSP)

3.2.12 Locating Tensioning Unit within the Track Modules Side Plates

The tensioning unit had to be located in between the TMSP using four M10×1.5×25mm bolts, directly inline with the sliding front axle units guide slots. It also had to be positioned far enough inside the TMSP so that the heads of the units tensioning bolts would not foul on the tracks when an obstacle was being negotiated. For this reason it was decided to position the tensioning block unit so that the heads on the tensioning bolts would remain a minimum distance of 10mm inside the edge of the side plates. This positioned the tensioning unit's main block 43.4mm from its outer edge to the edge

of the side plates, along the guide slots centreline. Figure A.9 illustrates the overlaying of the complete front axle sliding and tensioning unit. Therefore points were marked 53.4mm out from the edge of the side plates (along the guide slot's centreline), at a perpendicular distance of 16mm either side of the guide slot's centreline. Once the two points were centre punched (one side plate only), all four plates were stacked and cramped together so that all plates could be simultaneously pilot bored to $\text{Ø}3\text{mm}$ to reduce inaccuracies. The plates could then be separated and independently bored out to $\text{Ø}10\text{mm}$.

3.3 DEVELOPING THE DRIVE AXLE MECHANISM

It was necessary to design a method to adequately hold an axle and corresponding bearings in place in a streamlined configuration. The unit had to follow the flow of the side plates to remain discrete.

3.3.1 Self Aligning Bearings Flanges

An easy and streamlined method was to use self-aligning bearings and flanges, which could be bolted on the outside of each side plate. Unfortunately standard bearing flanges come in either quad, or two point mounting configurations. Figure 3-22 shows a standard two node self-aligning bearing flange.



Figure 3-22: Standard unmodified self-aligning bearing flange

To follow the flow of the side plates, a mounting method was, which radially contours with the upper corner of the side plate. To overcome this problem, the standard two-point mounting of the bearing flanges had to be modified to better follow the contours of the side plates. Due to customised manufactured sizes of the flanges to suit common bearing sizes, a perfect outer radial match could not be obtained to suit the 25mm radius of the upper corner of the side plates. The closest match was a bearing flange with a main body radius of 30.8mm. This flange would suit a 16 - 20mm bearing, which allowed for an adequate drive shaft range.

The next step was to modify the bearing flanges so that they did not protrude past the edges of the side plates by removing one of the fixing nodes. In removing a node an additional method to fix the bearing flanges in place was required. The bearing flanges are manufactured from cast iron, which allowed for the integrity of the flange to be maintained during and after the machining off of one of its fixing limbs. The majority of one of the flange's nodes was removed using a cut-off saw. The remaining metal was removed using the same method as that used to round the leading edges of the side plates on the front sliding axle unit. The remaining node on the flange was fixed in the tool post of the lathe via a bolted pin. This gave a point of rotation to grind off the excess metal to give a smooth finished surface that followed the radial contour of the flange. Figure 3-23 shows the bearing flange after one of its fixing nodes was removed.

Due to the removal of one node, further mounting points are required for the flange. As the complete project will be relatively lightweight as compared to bearing flanges, it was only necessary to restrict the rotation of the bearing flanges about the bolt through the remaining fixing node. Unfortunately the bearing flanges had only 6mm of wall thickness around the bearing on the underside where it made contact with the surface.



Figure 3-23: Modified self-aligning bearing flanges

The other consideration was that any method used to fix the bearing from the inside of the plates into the flange, could not impinge on the rotation of the drive pulleys. This reduced the options significantly, but allowed for two $\text{Ø}3/16''$ British Standard Whitworth (BSW) gutter bolts to be used to fix the bearing flange from the inside along the centreline 90 degrees out of phase with the original fixing node's centreline. By using $\text{Ø}3/16''$ BSW gutter bolts, it maximized the bolt strength relative to the wall thickness, and also reduced the bolt head profile in the inside, so as to reduce the modifications necessary to the drive pulleys, to stop them from fouling on the bolt heads. The procedure for boring and tapping the flanges is covered below in Section 3.3.6. Figure A.10 illustrates the scale dimensioned drawing of the modified self-aligning bearing flange overlaid on the original flange.

3.3.2 Drive Shaft

Due to the size of the bearing flanges, the drive shaft could be between 16 – 20mm. It was decided to manufacture the drive shafts to suit a 17mm bearing, as this reduced the amount of material that would have to be removed from the inside of both the drive pulleys and couplings, increasing their strength. The other factor was the current stock of $\text{Ø}18\text{mm}$ silver steel rod in the author's workshop. Two pieces of 210mm rod were cut, faced, and centre bored in the lathe. Both pieces were then independently shaved down to exactly 17.005mm, so as to have a snug fit in the self-aligning bearings. The drive shaft was sent to an engineering company to be slotted and to make the corresponding keys, where it had two inline slots rebated. Both slots were to be 6mm in

width, and 3mm deep, from the apex of the shaft's round. The first slot was to start 2mm from one end, and extend 16mm in length. The second was to start 69mm from the same end as the first, and extend towards the other end for 104mm. Figure 3-24 shows a completed drive shaft and corresponding keys. The first slot was to attach the drive coupling to the shaft; the second was for the drive pulleys. Figure A.11 illustrates the completed drive shaft unit.



Figure 3-24: Track module drive shaft and corresponding keys

3.3.3 Drive Pulley's

As stated previously, the back facing surface of the drive pulleys, had to have a small chamfer taken off of the outer radial edge. This would allow the heads of the gutter bolts to clear the pulleys. The chamfer was taken 4mm in from the outer edge, at an angle of 30 degrees. The pilot holes through the centre of the drive pulleys were bored out to $\varnothing 17\text{mm}$ in the lathe, and reamed to suit the drive shaft. At this stage the drive pulleys were ready to be sent with the drive shaft to be keyed. Figure 3-25 shows the completed drive pulleys.

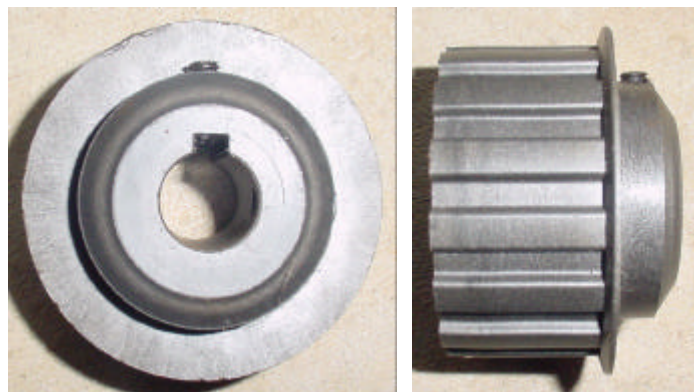


Figure 3-25: Main Drive pulley's

3.3.4 Drive Pulley Spacers

The drive pulley spacers were manufactured in the same manner as those used for the guide pulleys. The only differences were the resize of the bearing orifice, and the addition of a key way. To suit the drive shaft, the centre hole was bored out to $\text{Ø}17\text{mm}$ and reamed to suit the shaft. The key ways were manually installed by cutting an undersized slot using the power hacksaw blade, and finishing the slots with a file. Figure 3-26 shows the drive pulley spacer.



Figure 3-26: Drive pulley spacer

3.3.5 Final Drive Unit Assembly

Once the drive shafts and pulleys had been keyed, the pulleys had to be drilled and tapped to house grub screws to retain the location of the bearings and pulleys on the shaft. Each pulley had to have two grub screws fitted. One grub screw was positioned directly over the key. The pulleys had the second grub screws positioned 90 degrees out of phase with the first. The bearings had the second screw positioned 120 degrees out of phase. The pulleys were marked and centre punched 5mm out from the back of the track flange. All four pulleys were then mounted on a dummy shaft within a vice on the drill press and had each of their two holes bored using a $\text{Ø}5\text{mm}$ drill bit (ensuring the holes were bored perpendicular to the radial surfaces). Each of the eight holes were then threaded using an M6 \times 1.5 metric tapered tap. The pulleys and bearings were now ready to be fixed to the drive shaft using M6 \times 1.5 \times 10mm grub screws. Figures 3-27 and 3-28 show the layout of the drive unit components and completed drive shaft assembly, ready for insertion into the running bearings respectively.



Figure 3-27: Drive shaft unit component layout

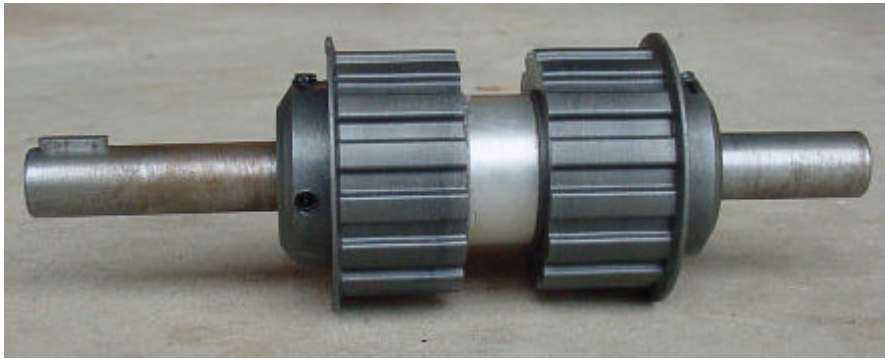


Figure 3-28: Assembled drive shaft unit

3.3.6 Mounting the Drive Shaft Unit to the Track Module Side Plates

The position of the drive shaft relative to the TMSP was determined by the diameter of the bearing flange. Ideally the drive shaft would have been centred about the 25mm radius curve at the top of the side plate. Due to the 61.6mm outer diameter of the flange, the drive shaft centre had to be brought down away from the ideal position by 9mm along the line that bisected the angle between the top and trailing edges of the side plate. This ensured that the edges of the flange would sit flush with the outer edges of the side plates. As the bearing flange was modified to have only one mounting node, the flange was rotated so that the centre of the fixing node would lay along the line that bisected the angle at the upper ear corner. Although not critical to the design, it generated a balanced effect as it complimented the tensioner's guide slot at the front. A single side plate then had both the drive shaft and bearing flange fixing points marked and centre punched. The remaining two-guide pulley axle centres were also marked and punched at the centre of each 25mm radius located at both ends of the bottom of the side plates.

Once again all four side plates were cramped together to ensure alignment whilst pilot boring. Each plate could then be independently bored, with $\text{Ø}10\text{mm}$ holes for both the

remaining guide pulley positions, $\text{Ø}11\text{mm}$ for the bearing flange mounting node, and $\text{Ø}20\text{mm}$ for adequate clearance around the drive shaft location. Figure A.12 illustrates a magnified view of the track side plate drive end.

The final task was to locate the position of the gutter bolts within the exterior radial band around the bearing flange. Due to the bearing flanges being made via a casting method, there was a certain amount of variance between each unit. Therefore it was necessary to locate the position of the fixing bolts independently for each flange. Each flange was fixed to each matched side plate via a M12 \times 2 \times 30mm United National Coarse (UNC) bolt and respective nylon-locking nut (nylock). The radial section was then cramped flush with the edges of the side plate. This allowed for the exterior of the flange to be scribed around so as to generate an outline that was visible after the unit was removed. The flange was then unbolted, and re-bolted and cramped on the opposite face of the plate to the scribed silhouette. This generated a template from which the intended positions of the gutter bolts could be marked 3mm in from the radial edges, along the lines outlined above. Any deviation could cause the bolt housings to come through the sides of the flange. This method ensured that gutter bolts were located directly in the centre of the each flanges exterior rim.

Once the gutter bolt locations were accurately located, marked, and punched, the fixed side plates and flanges were bored together in the drill press to a total depth of 12mm (4mm for the side plates, and 8mm into the bearing flanges) using a $\text{Ø}9/64$ " drill bit. Finally the holes were threaded while the flanged maintained fixed to the side plate using a $\text{Ø}3/16$ " BSW bottoming tap. By threading both the flange and side plate, it was felt that this would reduce any movement that may occur if there was any over sizing of the clearance hole through the side plate. It would also reduce the risk of the bolts working free through vibration. Figure 3-29 shows the drilled and tapped bearing flanges.

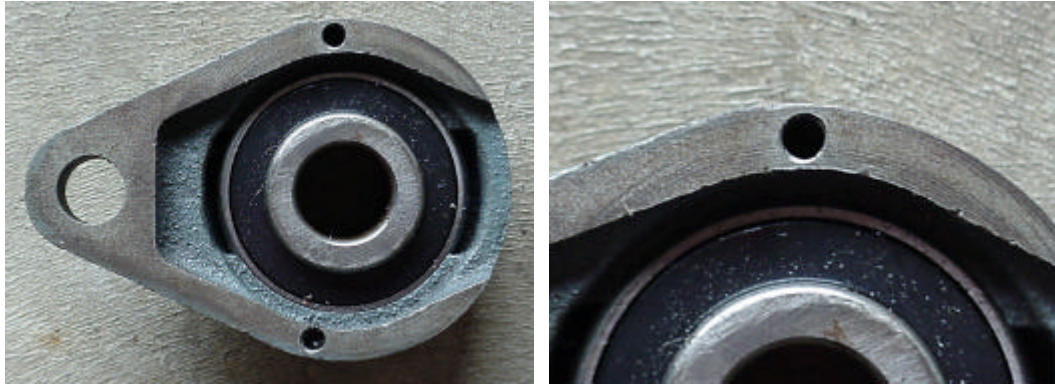


Figure 3-29: Drilled and tapped bearing flanges to suit $\text{Æ}3/16''$ BSW gutter bolts

This procedure was carried out independently for all four side plates and bearing flanges. Due to the reduction of wall thickness in the bearing flanges, the thread for the gutter bolts could go no further in than 8mm. Therefore, the standard $\text{Ø}3/16'' \times 1/2''$ BSW gutter bolts had to be cut down to $\text{Ø}3/16'' \times 3/8''$ BSW so that the heads would bind on the side plates. Figure 3-30 shows one of the cut down $\text{Ø}3/16'' \times 3/8''$ BSW gutter bolts.



Figure 3-30: Cut down gutter bolt ($\text{Æ}3/16'' \times 3/8''$ BSW)

3.3.7 Drive Couplings

To connect the drive shafts on the track modules to the drive motors, a unit was required that could adequately transfer the power from the motor in a two piece package that could fit in the area available. The Unit also had to be constructed robust enough for modifications to be made for envisioned sensing equipment such as shaft encoders.

For the $\text{Ø}17\text{mm}$ drive shafts on both the track modules and motors, two adequate coupling units were available locally. Both units' specifications exceeded the power output levels required, so a unit was selected which had a reduced overall length (slightly larger diameter). As with the drive pulleys, the unit was slotted for a keyway, and drilled and tapped in both sections (two locations per section, 90-degrees out of phase with one another, with one directly over the keyway) to suit $\text{M6}\times 1.5\times 8\text{mm}$ grub screws. The selected coupling also came with a rubber sleeve so as not to have metal on metal drive, reducing translated vibration, noise, and generally improving the interface. Figure A.13 illustrates the scale dimensioned drawing of the final modified drive couplings. Figure 3-31 below shows a drive coupling.



Figure 3-31: Drive Coupling

3.4 TRACK BOGIE UNITS

The track bogie units were designed to work dynamically in conjunction with the track-tensioning unit, so as to alter the displacement of the tracks while negotiating obstacles. The bogie units were designed to free pivot in between the TMSP. The concept behind the bogie was to displace the track while it freely contoured around and over an obstacle. The unit consists of two sets of pulley guides, able to rotate in an isosceles triangular configuration. This layout allows the guide pulley initially being displaced by an obstacle to pivot upwards, allowing the track to follow the contour, while the rear guide pulley is being forced to the ground. This guarantees contact with the surface, and thereby ensures drive traction is maintained, which is critical to overcome rough terrain.

3.4.1 Bogie Design

As with the sliding front axle unit, the bogies were designed to pivot freely in between the TMSP. As stated above, the bogie was based around an isosceles three-point configuration. In order to reduce the different gauges of materials required, 50×6mm plate was used to manufacture the side plates of the bogie unit, which would provide a means to locate the guide pulleys and pivoting bearing. The design of bogies were greatly determined by the curve at the base of the TMSP. This was a boundary arc for the tracks, therefore the bogie unit should be able to allow the tracks to infringe up to, but not cross inside the arc. The second consideration was the position of the pivot point. Thirdly, was deciding on the distances between the pulleys on the bogie, and the relative gaps between the fixed pulleys at the base of the TMSP. The only restriction was ensuring that the leading pulley unit of the bogie cleared the heads of the tensioning bolts when it rotated in between the side plates.

The key consideration in determining the design of the bogie unit included; the point of rotation, the angle of the pulley arms with respect to the ground, the length of the pulley arms, and the separation between all of the base pulleys. Ideally the point of rotation of the bogie unit had to lie along the vertical centreline of the TMSP. It was intended to use an M10×1.5×130mm as a method to locate the bogie units bearing in between the TMSP, therefore the pivot position had to ensure that the nut was free of the internal chassis unit. The next step was to decide on both the angle between the two pulley units of the bogie, and the length of the arms. To ensure that both guide pulley units of the bogie unit were in contact with the track while travelling along a flat surface, the centre of the pulleys axles had to be in line with those of the fixed pulleys located in between the TMSP.

An integrated decision was finally made on the entire bogie unit. It was decided to locate the centre point of rotation 112mm down from the top of the TMSP. In doing so, it would allow the bearing-locating bolt to also fix the base of the chassis to the track modules. To aid in the negotiating of obstacles, a slightly larger gap between the bogie unit's pulleys (rather than even displacement between the fixed pulleys and those attached to the bogie unit) would be beneficial. For this reason the pulleys were

separated by 120 degrees, relative to the pivot point. For the bogie's pulleys axles to be in line with the fixed pulleys, the side plates of the bogie units had to be 180mm from centre to centre of the pivot points. As with the front sliding axle unit, the side plate ends were to be ground round for both cosmetic and practical reasons. The final consideration was developing a means to fix the side plates together whilst including a running surface for a bearing.

3.4.2 Bogie Construction

Four side plates were cut from 50×6mm mild steel plate. The plates were cut at 60 degrees at one end, and 90 degrees at the other, with a total length of 227mm on the long side. The 90 degree ends of all the plates were roughly ground proud of round. This enabled only a small amount of work to be performed in the lathe to produce perfectly round ends on the plates, using the same method as outlined in Section 3.2.1. Each pair of side plates were then butt-welded together, using a jig to ensure the plate's flatness and angle, along the 60-degree faces using an arc welder. After welding, the seams were ground smooth, and the plates were marked along their centrelines to determine the pivot point at the welded seam. The centre for the pulleys were also marked 180mm from the pivot point. After being centre punched, the side plates were pilot bored together in the drill press while being held in the jig used to weld the units. This ensured accurate identical alignment for all the plates. The pulley centres when bored to a $\text{Ø}12\text{mm}$, and the pivot point was bored to $\text{Ø}9/16''$.

As with the other pulley bearings, $\text{Ø}5/8''$ brass rod was used for the bogie. To act as a running surface for the bearing, and to join a pair of side plates, steam pipe was used. Standard water pipe could not be used, as its wall thickness was not sufficient to accommodate a $\text{Ø}5/8''$ internal diameter. The steam pipe had an external diameter of $\text{Ø}7/8''$ with a $3/16''$ wall thickness, which enabled a further $1/16''$ to be reamed out to accommodate the $\text{Ø}5/8''$ bearing. To enable a clean weld between the steam pipe and bogie plates, the inside of the plates were gulleed around the $\text{Ø}9/16''$ pivot hole using a $\text{Ø}7/8''$ drill bit. The gullees were taken down to a depth of 3mm. The steam pipe was cut and faced in the lathe to 98mm in length. The radial edges were then bevelled, and the internal diameter was bored out to $\text{Ø}9/16''$. This allowed for a bevelled radial edge

on the steam pipe to increase the surface area to which the heat from a welder would be applied, reducing the risk of burning away the metal.

The steam line was welded to the side plates, using the same jig used originally to weld the plates. A dummy pin was placed through both the plates and pipe to ensure a perpendicular finish. Additionally, each end of the side plates were fixed together via spaced rods through the $\text{Ø}12\text{mm}$ holes. An arc weld was run around the pipe in the gullet on the inside only, so as to give a clean hidden weld and to also prevent the weld from obscuring the inner surface of the pipe. Once both welds were independently completed to bond both ends of the pipe to each plate, the entire unit was re-bored out to $\text{Ø}5/8"$. This allowed for any misalignment that may have occurred during the welding process (due to pulling and warping under the heat), to be corrected. The inner surface of the pipe was reamed to give a smooth snug contact face for the bearing. The completed unit finished with a total width of 104mm, which enabled it to comfortably pass inside the TMSP. Figure 3-32 below shows the completed bogie unit frame. Figure A.14 illustrates a scale dimensioned drawing of the completed bogie unit.



Figure 3-32: Completed track bogie unit frame

3.4.3 Bogie Units Guide Pulley's

The bogie units guide pulleys, brass bearings, and fixing bolts were manufactured identical to those for the front sliding axle unit. Refer Section 3.2.8, and Figure A.8 for the procedures and specifications.

3.4.4 Main Bogie Unit Pivoting Bearings

The bogie unit's main pivoting bearing was manufactured in a similar way to those used for the bearings in the front sliding axle (refer Section 3.2.8). The brass rod was cut and faced to 94mm in length. Each bearing was centre-bored using a $\varnothing 10$ mm drill bit in the lathe to suit the M10 \times 1.5 \times 130mm through bolts. **Note:** identical running bearings were manufactured for the fixed guide pulleys at the base of the track module illustrated in Figure 3-18. The specifications can be referred to in Figure A.8.

3.5 COMPLETE ASSEMBLY OF THE TRACK MODULES

The most intricate part of the track module assembly was the tensioning mechanism. Prior to bolting the tensioning unit in place, it was necessary to position the threaded plate that runs on the tensioning bolts at least 30mm down from the nuts on the inside of the unit. This allowed for the tension on the main springs to be reduced sufficiently to allow the track to be placed over the assembled track module prior to tensioning. The next step was to bolt the bearing flanges onto each side plate using the M12 \times 2 \times 30mm UNC bolts and nylocks, and the cut down gutter bolts (ensuring that the correct flange is fixed to its matching side plate). Figures 3-33 and 3-34 show the attached bearing flanges to the side plates. The front sliding axle units, and bogie units then had the guide pulleys fitted and held in position with the customized slotted radial head bolts. For the final assembly the side plates were punched to bur the metal into the bolt head slots, preventing the heads on the bolts from turning.



Figure 3-33: Outside face of attached bearing flange



Figure 3-34: Inside of attached bearing flange

Prior to inserting the key for the drive pulleys, the drive pulleys, and spacers are placed onto the drive shafts, with the retaining grub screws done up loosely. The tensioning unit is assembled by sliding the two tensioning springs over the tensioning bolt shafts, then placing the turned ends on the tensioning unit through the holes in the front sliding axle unit, as per Figure 3-21. The components are located between the TMSP. The first step is to fit the two guides on the front sliding unit, into the slot on one side plate. One side of the tensioning bolt block is bolted to the side plate using two M10×1.5×25mm bolts. The drive shaft and pulleys are placed through one bearing and the bogies, and base guide pulleys are retained in position using the holding bolts as pins. Figure 3-35 shows the internals of the track module mounted on a single side plate. The track modules can now have the top reciprocal side plate placed over the assembly fixing the

remaining two bolts into the other side of the tensioning block, and doing up the nuts on the bottom guide pulley bolts.



Figure 3-35: Exposed internal mechanisms of a track module

Note: The bogie unit cannot have its nut done up until the lower chassis tray is fitted. The drive shaft and pulleys must be adjusted so that the shaft on the outside finishes flush with the outer edge of the bearing, the pulleys position can also be aligned so that they sit perfectly in the centre of the two side plates. Once the shaft and pulleys locations are corrected, the grub screws can be done up on both pulleys and bearings (a total of eight grub screws).

The tracks are placed over each track module. This is best performed by placing the belt over the front sliding axle first, and compressing the unit to allow the track to pass over the other pulleys, and drive shaft. The track is now ready to be tensioned. This is the most tedious step, which takes several minutes per module. The easiest method is to turn the track modules upside down, so that the heads of the tensioning bolts face upwards. In this position it is easy to place a socket and ratchet on each bolt either side of the track. The ratchet's handles can be held in one hand, so as to generate an even actuation action on both heads at once. This ensures that one bolt gets no more movement than the other, preventing out-of-alignment binding on the threads between the two units. Figure 3-36 below shows the completed track module with tensioned belt.



Figure 3-36: Assembled track module with tensioned belt

4. MECHANICAL DESIGN AND CONSTRUCTION: CHASSIS DEVELOPMENT

The key initial consideration for the chassis was the width. Ideally the entire robot needed to be able to go through a standard 700mm wide household door. Unfortunately due to the dimensions of the motors intended for use, this was not possible. Therefore the minimum chassis size was limited to the clearance width of two motors, gearboxes, drive shafts, and drive couplings. For the previously stated reasons it was necessary to make the overall width of the chassis unit 440mm wide. This would give an overall width of the robot, from distance between the self-aligning bearing flanges on each track module of 734mm, not including a sheet metal cover. Fortunately this would still enable the units to pass through commercial and industry standard doorways.

4.1 CHASSIS DESIGN

For ease of construction and assembly, the chassis was designed around two separate trays. The two trays could be independently fixed between TMSP, and would allow for peripherals and components to be easily mounted on and in between the cavity generated by the two trays. As stated in Section 3.1.3, it was necessary to maximize the height in between the base of the chassis and the ground, so as to increase the clearance for negotiating rough terrain. At the same time there also needed to be an adequate distance between the two trays so as not to get a spreading effect in between the two track modules. The bottom tray's location had already been decided upon due to the bogies bearing tie-in bolt (outlined in Section 3.4.1). The position of the upper chassis tray was critical, as this would be the surface on which the drive motors, and other peripherals would be attached. The most critical of these was the alignment of the drive

motors, relative to the drive shafts from the track modules. The drive shaft out of the reduction gearbox on the drive motors was centred exactly 47.5mm down from the top of the motors fixing plates.

For ease of construction and assembly, 30mm mild steel angle iron was used to manufacture the two chassis trays. The angle iron would allow a shallow wall thickness of 4mm to easily bolt the trays to the track modules, and provide an adequate 30mm flat surface to fix motor and peripheral mounts.

4.1.1 Construction of the Bottom Chassis Tray

If possible, both chassis trays would span the entire length of the track modules. Due to the track-tensioning unit, housed inside the front end of the track modules, the lower chassis tray had to be substantially reduced in length so that its fixing bolts would not foul the mechanism. The lower chassis tray was therefore designed to start 50mm in from the rear of the side plate, and span 658mm towards the tensioning mechanism.

The lower tray consists of two longitudinal angle iron sections 650mm in length, and two lateral sections 432mm long. The ends of all the joints were initially cut off square. The lower tray was designed to bear the weight of the lead acid batteries used as the robot's power supply. Due to the intended loading on the tray, an additional three M8×1.5×20mm bolts were used to fix the tray to the track modules in conjunction with the main M10×1.5×130mm bolt to locate the bogie unit. The top surface of the tray was fixed 100mm down from the top of the TMSP, so that the nylock nut for the bogie pin would not require holding when doing up the bolt. To allow the nut to be tightened hard against the flat surface of the angle iron, the round was ground away in the internal corner. A $\varnothing 11$ mm hole was bored 18mm up from the bottom of the angle iron, and 255mm from the front to suit the bogie pin. The remainder of the bolt holes were bored 12mm up from the bottom, with one positioned 35mm out from each end, and the third bisecting the greater distance between the end bolt and the bogie pin. A scale dimensioned mechanical drawing of the lower chassis tray is shown in Figure A.15. The two 440mm ends were pilot bored using a $\varnothing 1/8$ " drill along the longitudinal centreline, 35mm from each end, and the centre, to allow for any future fixings.

Prior to welding the chassis tray components together, the ends of all four pieces were mitred in the cut off saw, removing only the metal from the top surface. The ends maintained their original lengths and square along the 4mm width of the metal. The 4mm square ends would allow the joints to be cramped 4mm proud of the ends, generating 4mm² trench to fill with weld. If the ends were cut in a standard mitred joint, the sharp exterior leading edges would be burnt away by an arc welder. Each joint was independently welded on both sides of the seam, ensuring they maintained flat and square. After welding all four joints, the welds were ground flush and smooth so as to ensure a clean pit free surface for future electroplating. Figure 4.1 below shows the completed lower chassis tray.

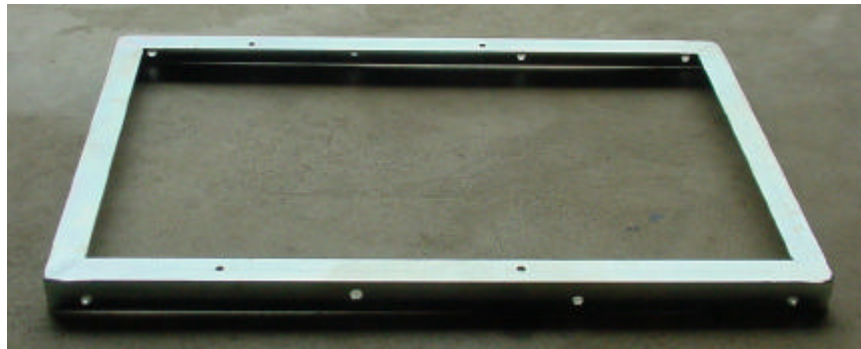


Figure 4-1: Lower chassis tray

4.1.2 Construction of the Upper Chassis Tray

Ideally, uneven angle iron would be preferred for the upper tray so as to allow it to stand 8mm above the TMSP, requiring no further packing to enable both the drive shaft out of the gearbox, and the shaft from the drive pulleys to line up. Unfortunately there was no 30×40mm uneven angle iron available, so instead the top tray was mounted so that 30×5mm flat plate could be used to pack the motor mounts out to the required height of 13mm above the top of the side plates.

The top chassis tray was based around a similar configuration to the lower tray using 30mm angle iron. To accommodate the drive motor units, the upper chassis tray had to be open at the rear, so that it would not foul the gearboxes and couplings. The critical aspect of the upper tray was positioning the mounting holes correctly so that there was

enough material to adequately fix the tray to the side plates, and ensuring the tray sat at the correct level. The upper tray was designed to fit closely to the bearing flange, and almost the entire length of the unit, stopping just prior to fouling on the front tensioning mechanism.

The upper tray consisted of two 856mm longitudinal bearers, and two 432mm cross members. The two main bearers were all bored along a base line 10mm up from the bottom of the angle iron using a $\varnothing 7$ mm drill. The first hole was bored 35mm from the front, and each of the remaining three holes were separated by 257mm, centre to centre. The two cross members were pilot bored identical to those in the lower chassis tray. One of the two cross members, and the front edges of the longitudinal members were mitred in the same fashion as used for the lower tray. The other member was modified, as it was positioned down from the end, so as not to foul on the motors. The rear cross member had to have 26mm of the flat cut away, leaving a 26mm recess which finished flush with the underside of the remaining flat section. The end corners were rounded to suit the extruded interior curve of the angle iron.

These modifications allowed the rear cross member to neatly fit between the longitudinal members. To allow the longitudinal members to run closer to the bearing flanges the ends were cut back by 45 degrees. The chassis tray pieces were then welded together in the same manner as stated for the lower chassis tray in Section 4.1.1. The rear cross member was welded with the vertical flat facing outwards so that it was 600mm from the front face. Figure A.16 illustrates a scale-dimensioned mechanical drawing of the upper chassis tray. Figure 4.2 below shows the completed upper chassis tray.

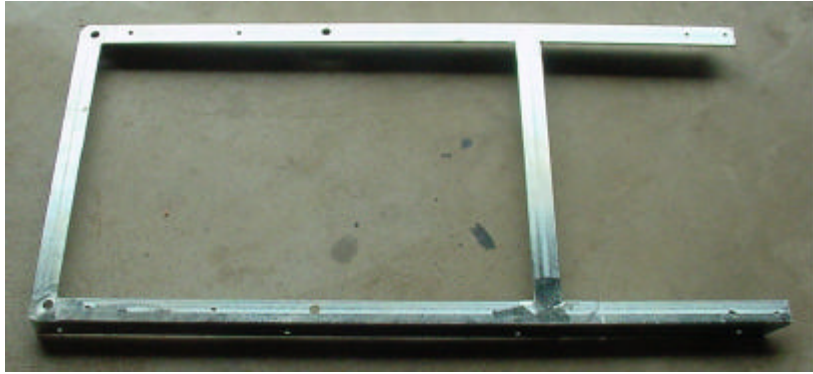


Figure 4-2: Completed upper chassis tray

4.1.3 Fitting the Chassis Trays to the Track Modules Side Plates

Both the upper and lower chassis trays were now ready to be fitted to the track modules.

Note: To allow for any misalignment both the holes in the chassis trays and the corresponding holes in the track modules were bored 1mm over size. The lower chassis tray was the easiest to position due to the bogie pin acting as a reference point. A tri-mitre square was used to locate the tray parallel with the upper flat edge of the track module. Once the tray was positioned correctly, it was cramped and drilled with a portable electric drill, using the holes in the tray as guides. The lower tray was bolted in place with six M8×1.5×20mm bolts and the two M10×1.5×130mm through bolts for the bogie units.

The upper tray was far more difficult to locate accurately. The most difficult aspect was maintaining the tray the correct distance from the ends. Once the tray was lightly cramped correctly out from the ends, a tri-mitre square was used to ensure the top of the upper tray was adjusted so that it was exactly 8mm from the top of the TMSP over the entire length of both sides. When positioned correctly, the cramps were tightened, and the measurements were rechecked to ensure there was no movement prior to drilling. The upper tray was drilled as per the method used for the lower tray. The upper tray was bolted in place using eight M6×1.5×20mm bolts and nylocks, prior to undoing the cramps. Figure 4.3 shows both the upper and lower chassis trays attached to both track modules.



Figure 4-3: Assembled chassis trays and track modules

4.1.4 Motor Mounting Brackets and Packers

The motor mounts were designed to span across the sides of the upper chassis tray. This gave a clean flat unrestricted surface at the rear of the unit. The intention was to replace four out of the six 25mm cap screws that held the top cover plate on with 30mm equivalents. This would allow for no further modifications to the motor units to be made to attach the mounting brackets. Through the design of the motor and gearbox, there was limited width for the mounting brackets due to some of the protrusions coming out from the top of the mounting plane. Only 40mm of clearance was available between restrictions, therefore excess 30mm angle iron was used. In doing so there would be adequate clearance, and it would produce far more rigid braces than if flat plate was used.

As stated earlier, 30×5mm plate was required under the angle iron braces, to lift the motor unit so that the drive shafts aligned. Figure A.17 illustrates a scale dimensioned drawing of the mounting brackets and packers. To finish flush with the edge of the chassis tray, both mounts were cut to 440mm. The ends were drilled with the chassis 15mm in from each end to allow two M6×1.5×20mm bolts to hold each of the two mounting brackets in place. Four holes in each bracket were bored oversize to Ø8mm for the Ø7mm mounting cap screws. The holes were intentionally over bored so that

there was plenty of movement to allow the drive shafts to line up perfectly. If required, the configuration allowed for shims to be easily inserted to ensure alignment. The packing brackets were made to bridge both motor mount cross members, finishing flush with the accurate separation distance. Figures 4-4 and 4-5 show the motor packers and brackets, and the attached motors and brackets respectively.

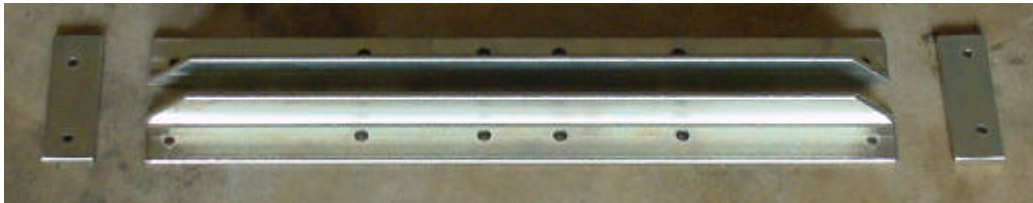


Figure 4-4: Motor mounting brackets and packers

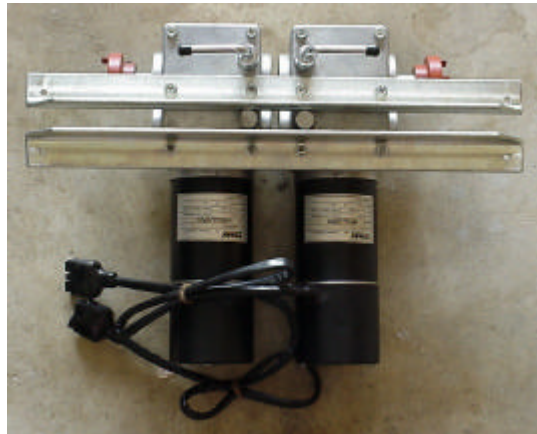


Figure 4-5: Motor-mounting brackets attached via four of the six gearbox cover plate cap screws

4.1.5 Battery Tray

The battery tray was designed to locate the batteries directly behind the back of the drive motors. As stated earlier, the weight of the batteries was intended to sit on the lower chassis tray, so as to keep the centre of gravity of the robot as low as possible, and hence increase stability. The battery tray was designed to be semi-generic with respect to battery dimensions. To increase running time, the robot would require large batteries. Due to weight and expense, it was necessary to compromise on the size of the batteries. When evaluating batteries (covered in Section 2.3.2) the physical dimensions varied little between manufacturers. Therefore in manufacturing a battery tray, a unit

that would accept batteries from over six manufacturers was constructed. Once again, due to availability and strength, the battery tray was manufactured from 30mm angle iron. The angle iron's profile would enable the batteries to be both supported from underneath and restrict movement in the horizontal plane.

The tray was manufactured from four sections. Two were standard 440mm runs, the other two were cut to 272mm. The shorter lengths were customized in the same manner as the rear cross members of the upper chassis tray outlined in Section 4.1.2. This enabled the four sections to generate a tidy rectangular support, which held each battery at both ends and along one side. Figure A.18 shows a scale dimensioned drawing of the battery tray design. The battery tray was held in place by four M6×1.5×20mm bolts and nylocks, positioned 15mm in from each end. Figure 4-6 shows the completed unit.



Figure 4-6: Battery tray

4.1.6 ATX and Charging Unit Brackets and Packers

The ATX power supply and charging unit cases were designed to fit neatly in between the chassis frame. This layout allowed the two units to be fixed together in a similar format to that used for the motor mounting brackets in Section 4.1.4. The only difference from the motor brackets was that 30×5mm plate was used instead of angle iron, and the separation distance between cross members. Angle iron was not necessary as the combined weight of the two electronic units was not significant, and would not generate enough load to distort the mounts. The plate also reduced the overall profile allowing a further unit to be placed on top.

The fixing brackets were designed to use four of the six bolts that attach the top plates to the cases, thereby requiring no further modifications to the unit's cases. As the ATX unit has a different width compared to the charging unit, the fixing cross members could not be positioned evenly at either end. For appearance only, both unit's front edges were aligned flush with the internal front edge of the upper chassis tray, this left the charging unit rear edge 3mm behind that of the ATX case. The fixing plates were bored to suit the alignment of the fixing points for the lid of the cases. Figure A.19 shows a dimensioned drawing of ATX and charging unit mounting brackets, illustrating the necessary offset in alignment.

Packers were required to lift the base of the ATX case up a fraction to allow for access underneath, for when a protection tray is installed. The packers followed the identical format to those made in Section 4.1.4. The ends of the brackets and packers were then bored 15mm out from the ends, to correlate with the mounting holes in the chassis tray. To aid in assembly, the chassis tray was drilled and tapped to suit a $\text{Ø}1/4''$ BSW thread, so that $\text{Ø}1/4'' \times 3/4''$ BSW bolts could be used to attach the mounting brackets to the chassis. Figure 4-7 shows the finished mounting brackets and packers for the ATX power supply and charging units.

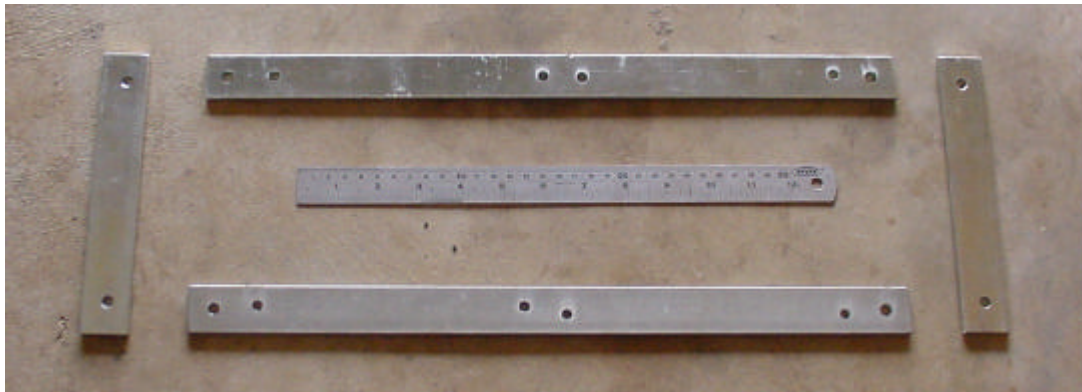


Figure 4-7: ATX power supply and charging unit mounting brackets and packers

4.2 COMPUTER SUSPENSION FRAME

To locate the main computer, there was a need to develop a method to ensure that any and all vibration that would be translated through the robot, as it manoeuvred over and around rough terrain would be minimised through the main computer, and especially the hard drive. The other consideration was to reduce the area that the unit took as it was already significantly large.

4.2.1 Computer Location

Two key considerations were considered when locating the unit. The first was ensuring that the ports on the computer would not be restricted, and ideally accessible via a hatch in the casing. The second was its location with respect to the ATX power supply. Due to both these reasons the best location would be at the front of the robot. This would allow for all ports to be accessible from the front, unrestricted from other equipment (including mouse, monitor, keyboard, network, serial, parallel, and DAQ card). This location also allowed the unit to sit directly on top of its power supply, reducing cabling length, and optimise available space within the robot.

4.2.2 Design of Computer Mounts

The key criteria for the mounting unit, was to reduce the amount of shock exerted through the computer during general operation. To overcome this problem it was necessary to have the computer suspended on reacting extension springs, similar to the format used in automotive, stacked compact disc stereo units. Therefore the mounts needed to locate eight springs, for each corner of the case. Ideally if space was not a concern, it would have been preferable to have had each spring mounted under half extension, 45-degrees vertically and 45-degrees radially with respect to the mounting bracket and case (as per Figure 4-8).

Due to the restriction of chassis width, and the distance between the front of the unit and the batteries, a compromise was found to position the springs as close to the ideal locations as possible. The final consideration was the general format of the design.

Ideally the unit should be made as a single piece, able to have to computer suspended prior to attaching the frame to the chassis. The frame should therefore be significantly solid enough so as not to distort under the force exerted by the springs. The springs should be easily attached to allow them to be removed or attached while the unit is attached to the chassis. The frame should not restrict the access to the computer ports, and should not foul cables.

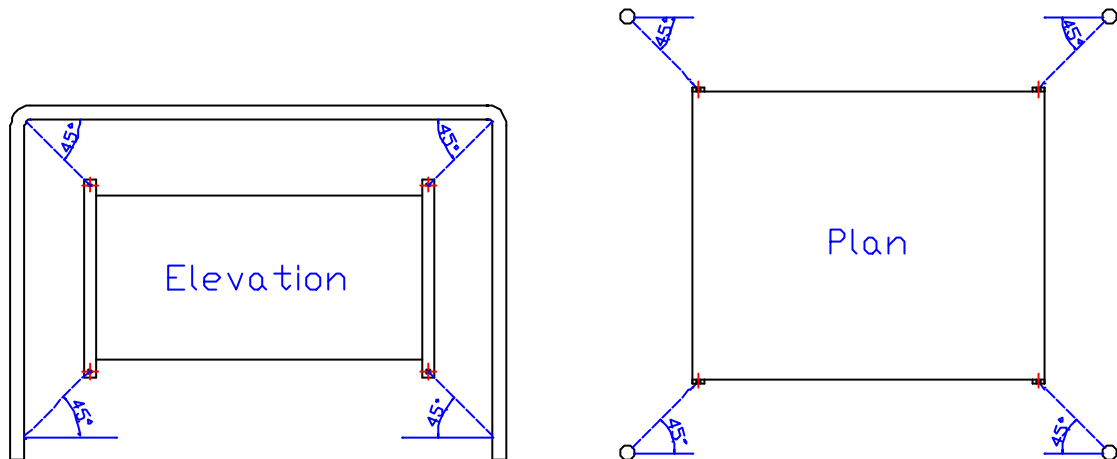


Figure 4-8: Ideal computer case mounting spring configuration

4.2.3 Computer Suspension Frame Construction

The basis of the suspension frame was made from $\varnothing\frac{1}{2}$ " mild steel rod, for two reasons. The first was it allowed the ends to be threaded to suit $\varnothing\frac{1}{2}$ " United National Coarse (UNC) nuts, which could be used to locate and fix the unit to the chassis tray. The second was that it allowed the frame to be easily bent in a "U" shape cradle, which could span the two sides of the chassis tray.

Two "U" shaped cradles were bent up, with vertical uprights of 365mm, and a span of 420mm. The ends were then threaded 33mm up the legs. This was to allow a locating nut to be permanently fixed at the extremity of the thread, to ensure the suspension frame was always the correct height from the upper chassis tray. This allowed enough clearance for the remaining thread to fit through the chassis tray, and be fixed in place with another nut on the underside.

To locate the springs in the upper corners of the suspension frame, holes were drilled in the internal corners of the frame at 45-degrees to suit cut down cotter pins. The cotter pins could then be brazed in place as per Figure 4-9 below.



Figure 4-9: Upper corner spring attachments

To attach the springs at the lower four corners, the fixed base nuts were drilled at 45-degrees on one of their flat faces. The nuts could then be slightly rotated so that the cotter pin angled towards the centre of the frame. The cotter pins were brazed into position as per the top units with the fixed nuts. Figure 4-10 shows the base nuts with the spring mounts.



Figure 4-10: Lower Corner Spring Attachments

Finally to fix both “U” frame pieces together, a 305mm piece of $\varnothing 1/2$ ” rod was welded in between the two pieces at the centre of the top sections. This ensured the correct separation distance between pieces and allowed the computer to be fitted prior to installation on the chassis.

To mount the suspension frame, corresponding $\text{Ø}13\text{mm}$ holes were bored in the upper chassis tray. Figure A.16 illustrates the scale dimensioned drawing of the upper chassis tray illustrating the location of the $\text{Ø}13\text{mm}$ mounting holes for the suspension frame. Figure 4-11 below shows the completed computer suspension frame. Figure A.20 illustrates the scaled dimensioned drawing of the completed computer suspension frame.



Figure 4-11: Completed computer suspension frame

4.3 UPS, MICROCONTROLLER, AND MOTOR DRIVER MOUNTING BRACKET

To locate the UPS, microcontroller, and motor drivers, a single frame was designed to be fixed to the top of the upper chassis tray. To utilise the space available in the rear section of the vehicle, it was necessary to design the frame to fit around the motors and batteries.

4.3.1 UPS, Microcontroller, and Motor Driver Frame Design

As the lead acid batteries emit both hydrogen and oxygen gas during high drain applications and charging, all electronic equipment is encapsulated to reduce the risk of exposed arcing in an enriched oxygen and hydrogen atmosphere.

The frame has been designed to allow the UPS to sit directly over the drive motors, reducing the distance to the AC inlet port, and allowing for adequate ventilation for the transformer. To keep in close proximity to the motors, the motor drivers will sit above the UPS on the upper tier of the platform. To optimise space, the microcontroller board is mounted on the upper tier over the batteries. The entire frame has been constructed as one piece, allowing for easy removal and access to the drive motors and batteries.

4.3.2 UPS, Microcontroller, and Motor Driver Frame Construction

To follow the format of the other electronic equipment mounts, 30×5mm flat bar has been used to construct the entire frame for the UPS, microcontroller, and motor drivers. To optimise the available space in between the drive motor mounting brackets and the computer suspension frame, the additional platform extends 445mm in length. The platform consists of two longitudinal flat bar sections spanning 445mm, which sit on the upper chassis tray (380mm apart). Two cradles have been bent up to bridge the two longitudinal fixing bearers, and extend 175mm high. To ensure sharp 90-degree bends, a jig was set up in the vice, ensuring that all corners were identical. The two cradles have been welded at each end of the longitudinal bearers, with the inner face flush with the edge of the horizontal bearers. All welds for this platform have been performed with an arc welder.

To provide an adequate surface to mount both the microcontroller and motor driver cases, two further 385mm sections of flat bar have been fitted to the upper horizontal surface of the cradles, generating the upper tier. The two plates have been centred 100mm from the centreline. This separation distance allows both the microcontroller and motor driver cases to be mounted using their existing locating bolt holes for the bottom surface of their cases. The final components consist of two 380mm sections of flat bar, which laterally span between the longitudinal base sections. These sections of plate provide a flat surface on which to mount the UPS. One section is welded flush with the rear outer surface, and the other is centred 100mm from the rear edge. The external sheet metal case of the UPS is drilled to suit the platform, allowing the external case to be mounted using M6×1.5×20mm bolts prior to attaching the UPS to the case, which conceals the fixing bolts.

The entire platform is held in position with four M6×1.5×20mm bolts. Both the upper chassis tray and the platform for the UPS have been drilled to Ø5mm then tapped to M6×1.5 so that nuts are not required (it would be too difficult to locate nuts due to the position of the bolts). Figures 4-12 and 4-13 show the completed platform frame, and the completed platform with mounted UPS, microcontroller, and motor driver cases respectively. Figure A.21 illustrates the dimensioned scale drawing of the completed platform.

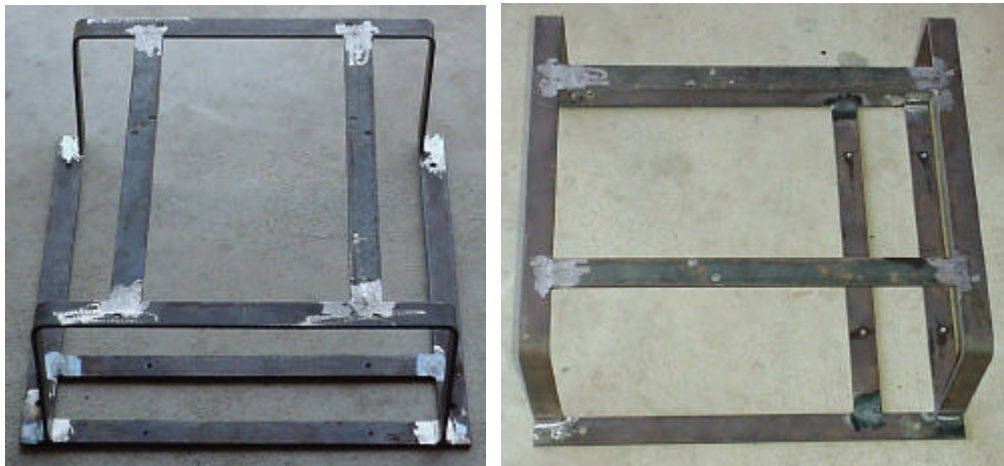


Figure 4-12: UPS, microcontroller, and motor driver platform frame

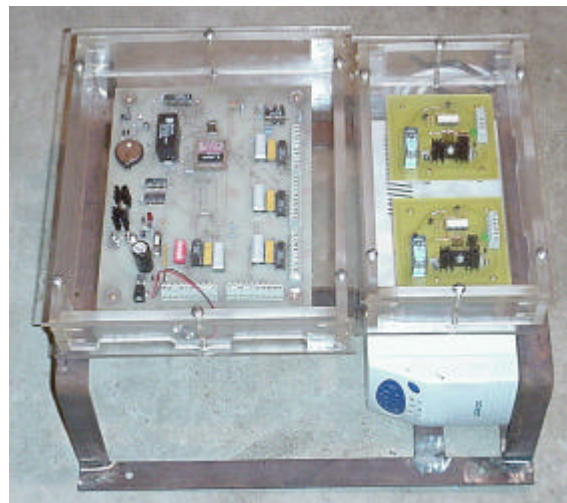


Figure 4-13: UPS, microcontroller, and motor driver frame with mounted equipment

4.4 EXTERIOR CASING

The external case is the primary defence against the elements in outdoor environments. It has been designed to prevent as much water and debris as possible from finding its way into the internal cavity. It is not necessary to be 100-percent water tight as all electronic and vital equipment has secondary protection via encapsulating acrylic cases.

The casing has been designed around four main sections; the under tray, sides, ends, and overhead cover. The under tray has been designed to be attached to the front and rear of the upper chassis platform, and extends underneath the bottom of the lower chassis tray. The sides attach to the upper chassis platform and extend vertically to help prevent debris coming off the tracks and entering the inner cavity. The overhead cover is the largest section, and overlaps the side extensions to help prevent elements such as rain and hail damaging internal components.

So as not to affect internal components such as the electronic compass and receiver, the outer case is manufactured from aluminium sheet metal. Figure 5-37 illustrates the basic design of the aluminium cover.

The completed casing has not been received back from the sheet metal folders at the time of submission for this thesis.

4.5 MECHANICAL CONCLUSION

The entire mechanical component of this project consists of over 46 main sections, which are made up of over 600 subcomponents. All of the sub components have been machined and customised for this project by the Author. Figures 4-14 and 4-15 illustrate exploded layouts of the completed components excluding the 'UPS, microcontroller and motor driver platform, tactile bump bars, and external casing.

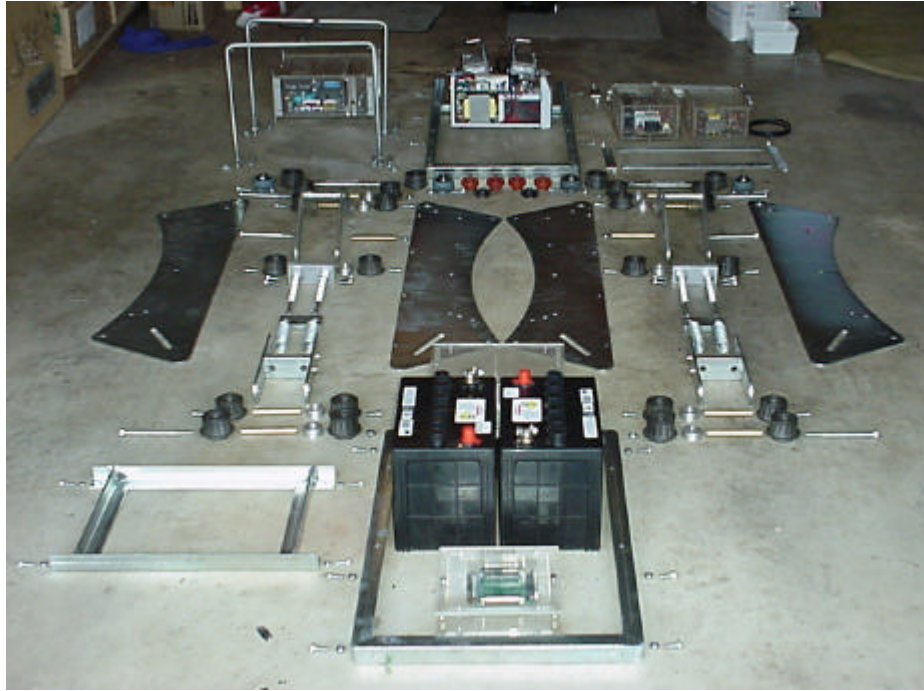


Figure 4-14: Front view of mechanical layout

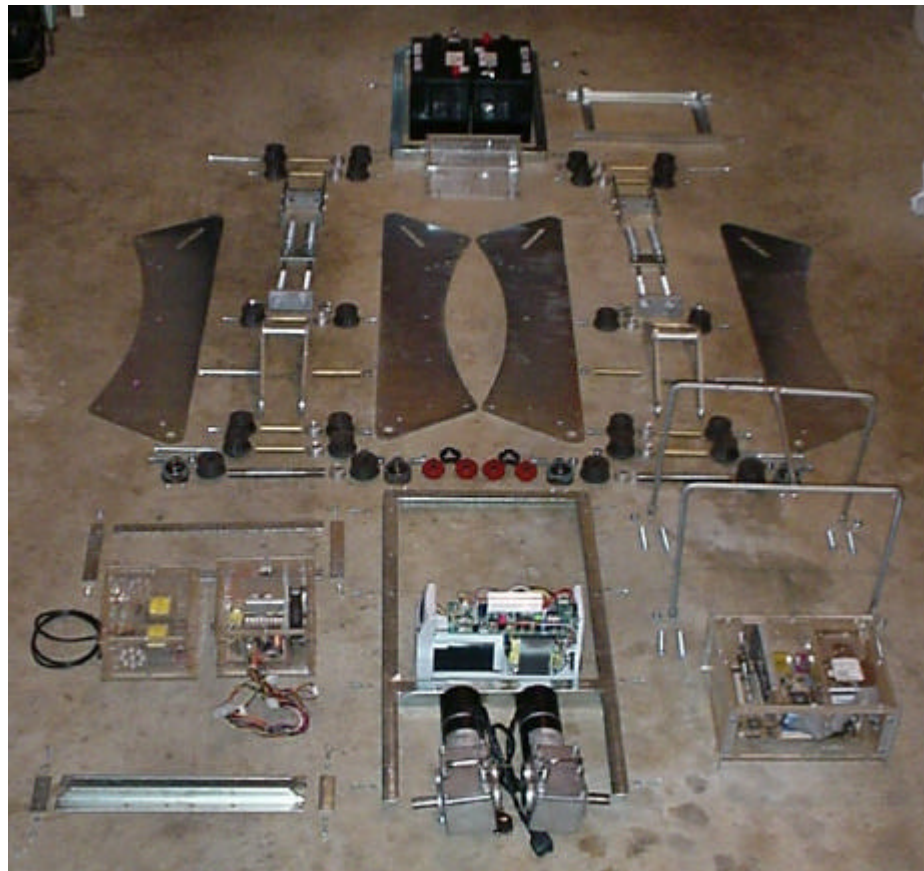


Figure 4-15: Rear view of mechanical layout

5. ELECTRONIC DESIGN

Several electronic subsystems need to be developed to integrate with the central computer. These sub-systems provide the interface to the drive motors, sensors, and additional peripherals. As stated in Chapter Two, it is intended to develop each section independently. This will allow a generic modular interface between each unit, and facilitate the addition of future components.

5.1 THE CENTRAL COMPUTER

At the heart of the electronics is a central processor. The computer is an AMD K6 500 MHz central processor housed on a Gigabyte GA-5VMM cut down motherboard, with onboard sound and graphics, 128 MB of SDRAM and a 20Gb hard drive.

5.1.1 Communication Interfaces

The central computer contains two serial (RS232) ports, two Universal Serial Bus (USB) ports, and a parallel (ECP) port. A PCI 100 Mbps Ethernet card was inserted for a universal interface with other computers. An IOTECH data acquisition card (DAQ) is included to provide an interface with additional electronic components, including the motors and sensors. This card was chosen primarily as it is significantly cheaper than similar units manufactured by National Instruments. However, due to limitations with LabVIEW interfacing with the IOTECH hardware, the DAQ interface is intended to be replaced in the future with a National Instrument card.

5.1.2 Software

The operating system used for the computer is Microsoft Windows Millennium (ME). Other software installed includes: LabVIEW, to provide the graphical programming

interface between the DAQ card and the electronic sensors and motor drivers; Hi-Tech C to communicate with sub-system micro-controllers via the onboard serial ports; DragonTalk Naturally speaking software to enable human speech interface with the unit; Microsoft Office and Matlab to allow for sensor output to be dumped into interpretable file formats via macros to allow for calculations and simulations to correlate the data.

5.1.3 Installation

As discussed in Sections 5.2.2 and 5.2.3, a mechanism was developed to ensure the computer was safely housed within a unit that would protect the hard drive, especially from impact and shock damage. In conjunction with minimizing vibration, the housing had to be fully insulated to protect from short circuits and static damage. For the reasons previously stated, custom-made clear acrylic cases have been made for all electronic units. This generated a trouble free method for inspecting each unit, and allowed for customised wiring and attachment. Figure B.1 illustrates a scaled dimensioned drawing of the final computer case including routed port access for all accessories. Figure 5-1 shows the customized aluminium brackets manufactured to attach both the lower and upper extension springs onto the computer case. Figure 5-2 shows the completed computer case with all four aluminium-mounting brackets.



Figure 5-1: Customised aluminium spring mounting brackets

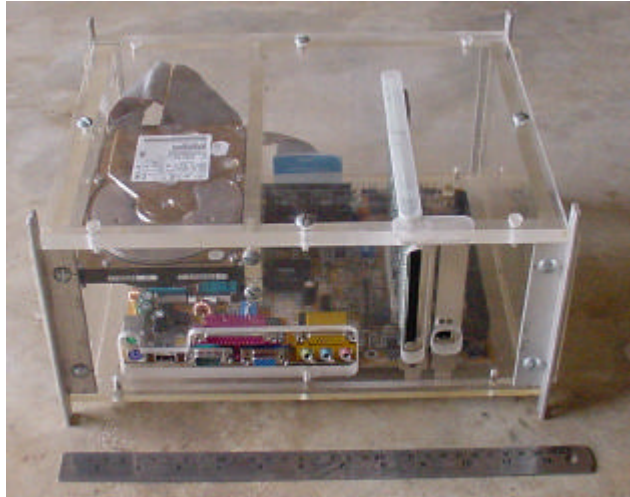


Figure 5-2: Completed computer case

5.2 POWERING THE COMPUTER

The AMD based computer requires an 8A 3.3V, 12A 5V, and 6A 12V power supply. This power supply requirement could be provided in three ways: develop a customised power supply; purchase a pre-made DC-to-DC converter; or invert the DC output from the batteries and feed the output into a mains (230VAC) ATX power supply. Options one and two require considerable time and financial expenditure. With the pre-made converters, there was nothing available within one unit that would generate all of the required output voltages, so two separate converters would be required. The third option was by far the most cost effective and simple, but due to the losses through each stage of converting DC to AC through an inverter, then AC to DC through the ATX power supply, it was not the most efficient. However, due to budget and time constraints, option three was selected.

5.2.1 Generating 230VAC at 50 Hz

To generate a 230V output at 50 Hz, the 24VDC supply had to be inverted. To generate the AC output, an Uninterruptible Power Supply (UPS) was used instead of a stand-alone inverter. The UPS provides a cheap option of generating an AC signal, and allows the onboard battery to run in series with a lead acid battery. This mechanism also allows for easy automatic switching to a direct AC signal when the mains are attached to the unit. For both expense and functionality, an 800VA UPS was selected,

illustrated in Figure 5-3. **Note:** the 800VA rating of the UPS selected is meaningless as this relates to the capacity of the sealed lead acid battery included in the unit. Within the mechatron, the self-contained battery within the UPS will run in parallel with one of the main lead-acid batteries.

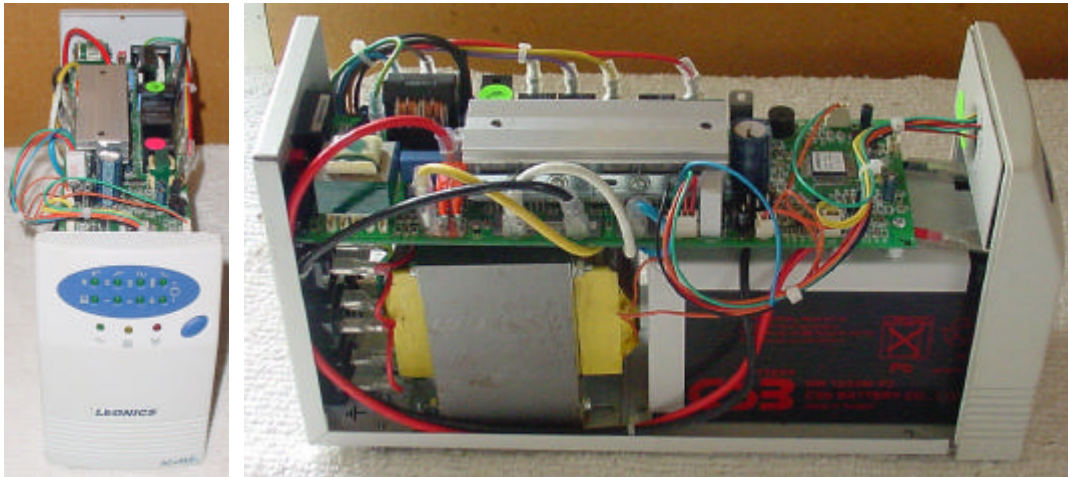


Figure 5-3: 800VA UPS

5.2.2 ATX Power Supply

The ATX power supply used is a standard unit taken out of an ATX certifi file mini-tower case. The power supply provides the following outputs:

- +3.3V at 14A
- +5V at 20A
- +12V at 8A,
- +5VSB at 1A
- -5V at 0.5A
- -12V at 0.5A

As can be seen in Figure 5-4, the power supply was removed from its sheet metal case and placed in an acrylic case so as to follow the same format outlined in Section 5.1.3. Figure B.2 illustrates a scale dimensioned drawing of the ATX power supply case.

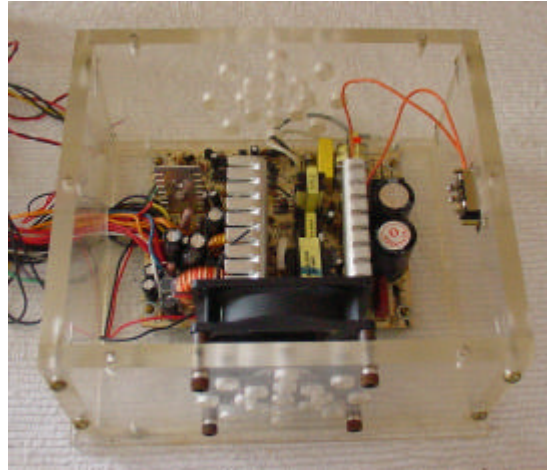


Figure 5-4: ATX power supply

By using a pre-manufactured power supply, it allowed for easy attachment to the motherboard via the standard socketed plug, and allowed the unit to be hard wired into the UPS to ensure fault free connection.

5.3 CHARGING

To reduce both the quantity of external equipment to accompany the vehicle, and the level of human intervention required to maintain and operate the mechatron, much of the unit's equipment needs to be self-contained. For these reasons, an onboard charging unit for the lead acid batteries have been included. These units, as with all other mains powered devices, have been connected to a single power point, thereby requiring only one lead to be connected. To continue with the modular design, the charging unit is based around two independent circuits, allowing each battery to be charged simultaneously. Figure C.1 shows the schematic of the two chargers and associated circuitry. Thermal cut outs have been included to ensure the transformers do not get damaged. To show when the batteries are connected, charging, or charged, a series of coloured LED's have been included.

Figure 5-5 shows the internals of the completed charging unit. Figure B.3 illustrates a scaled dimensioned drawing of the charging unit's acrylic case.

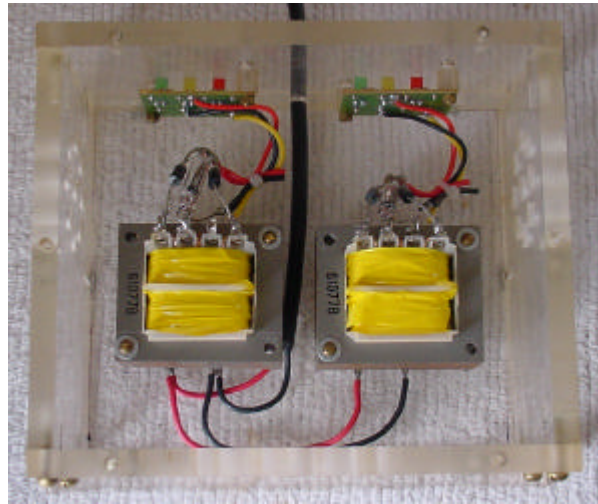


Figure 5-5: Dual lead acid battery charging unit

5.4 MOTOR DRIVERS

The motor drivers have been designed to supply the drive motors with a high current 24VDC PWM input.

5.4.1 Design Criteria

As stated above, the motor drivers have to be able to pass a high current (10A) 24VDC supply directly from the two lead acid batteries. The switching components for relaying the PWM signal have to be sufficiently fast to switch at a minimum of $34.6\mu\text{s}$ (Section 7.6.1), while passing the input voltage and current. A mechanism must also be incorporated to switch polarity to the motors, to alter the mechatron's direction.

5.4.2 Motor Driver Design

To increase reliability, and to allow for easy replacement and repair, each motor has its own independent driver circuit. The motor driver circuit is split into two sections, a low voltage signal input front end, and a high voltage high current output back end. To isolate the front and back ends, TLP620-4 (Figure D.1) Darlington configuration optocouplers have been implemented. The TLP620-4 is a quad package, though only two of the four optocouplers are utilised in this project.

To minimise the connections into the motor drivers and to increase independence, a separate 5V power supply has been included within each motor driver circuit.

At the front end, the PWM signal originating from the microcontroller is used to switch both a NPN (BC550) and a PNP (BC557) transistor. When on, each transistor supplies 5V to independent optocoupler diodes. With the configuration of the circuit illustrated in Figure 5-6, the two transistors ensure that during switching the output from the optocouplers is not floating. This configuration guarantees a positive switching and also prevents any irregularities that may have occurred on start up.

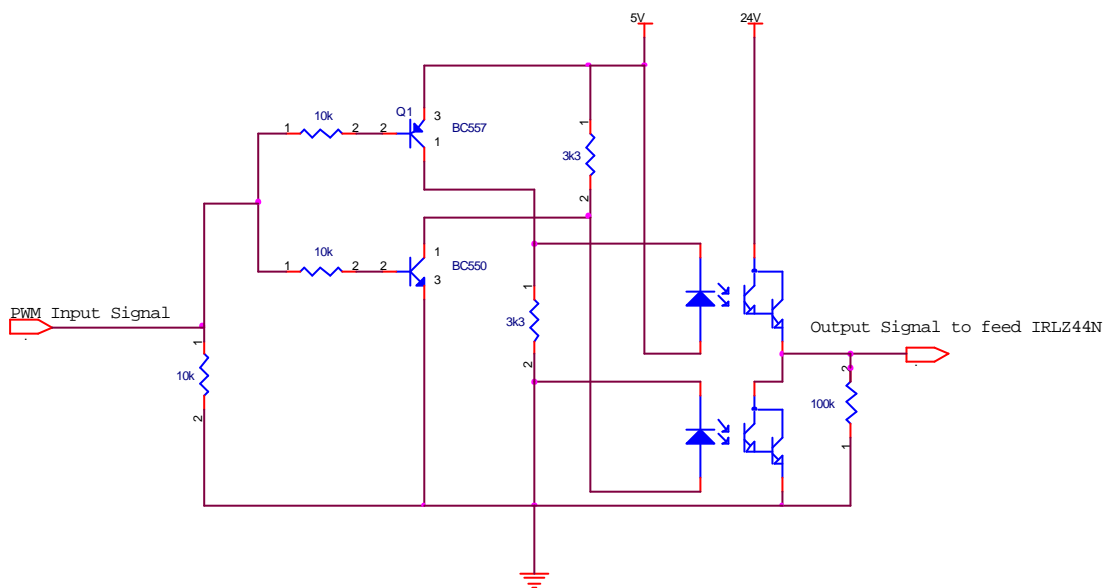


Figure 5-6: Front end transistor and optocoupler configurations

The detector side of the optocouplers has a 24V supply attached to the collector of the Darlington configuration. When a pulse from the PWM signal causes the leading optocoupler to activate, a signal is supplied to the main power MOSFET. A IRLZ44N (Figure D.2) has been used for the main switch device. A large STPS1045 45A diode (Figure D.3) has been placed on the output side of the IRLZ44N to prevent any back emf from the motor damaging components. To provide the physical switching for forward and reverse, a finder 44.62S double pole double throw (DPDT) 10A (Figure D.4) relay has been included. To drive the solenoid with the relay, a BST704A transistor receives a signal from either the microcontroller or central computer. Under forward movement, the solenoid is isolated. When the BST704A receives a signal, it

switches, allowing the 5V supply to the solenoid to pass through to ground, energising the relay and causing the mechanical switches to swap poles. To prevent the BST704A from damage, a small IN4007 diode has been inserted to stop the collapsing field on the solenoid feeding back to the transistor. Figure 5-7 shows a completed motor driver circuit, and Figure 5-8 illustrates the motor driver circuits. Figure C.2 shows the complete schematic for each motor driver.

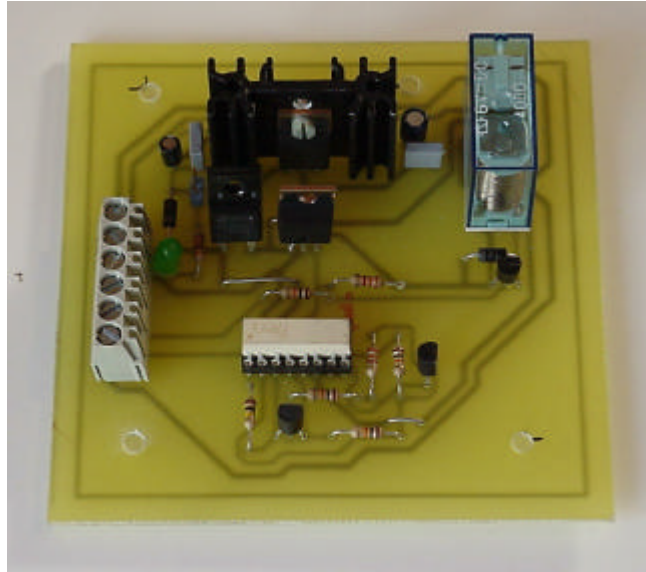


Figure 5-7: Completed motor driver circuit

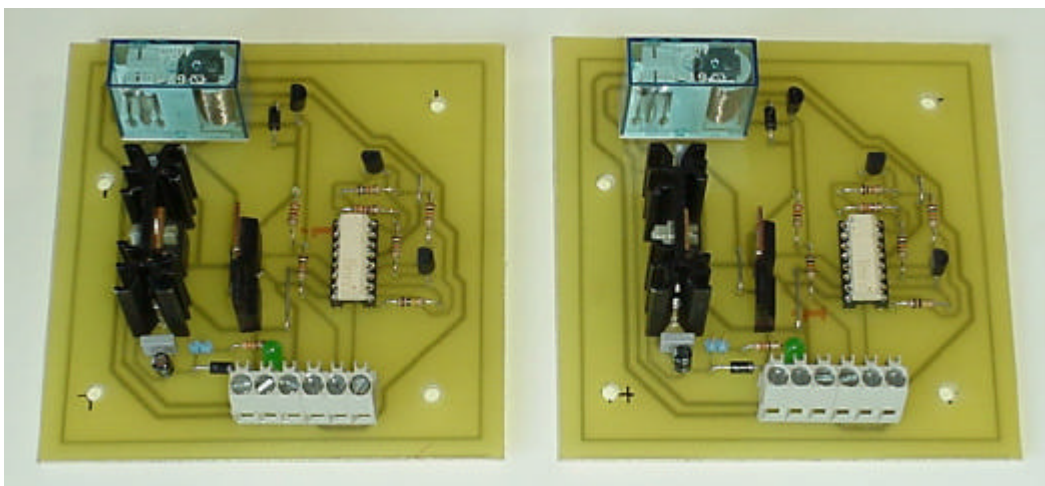


Figure 5-8: Both motor driver circuits

5.5 MICROCONTROLLER

Due to complications in timing issues when sending PWM signals from LabVIEW (using the operating system's internal clock) through the DAQ card to the motor drivers, an independent micro controller board was developed to ensure synchronisation of the signals. The primary application for the microcontroller is to accept a signal from the DAQ card (sent from within LabVIEW's motor control code) and generate an independent PWM signal for each motor.

This was implemented using the Philips 8-bit S87C552-4A68 ('552) (Figure D.5) microcontroller. Listed below are the features associated with the '552:

- 80C51 central processing unit
- 8k bytes EPROM
- Additional 16-bit timer/counter coupled to four capture registers and three compare registers
- Two 16-bit timer/counters
- 256 bytes of internal RAM
- 10-bit ADC
- Dual 8-bit resolution DAC PWM interface
- Five 8-bit I/O ports
- One 8-bit input ADC port
- 15-source, two-priority-level, nested input structure
- Two serial interfaces (I²C-bus and full duplex UART)
- Watchdog timer

An extensive development board was produced to allow for possible future expansion.

Although the primary function for this microcontroller is to generate PWM signals for the motor drivers, the design does not need to be limited to this task. Added functions and components include:

- Additional 128 kB of external memory (64 kB data, 64 kB program memory)
- Real Time Clock (independent batter backup)
- RS232 or 0 to 5 volt serial communications
- Digital input on port 5
- LED array indication of port status on ports 1, 3, 4, and 5
- Watchdog timer
- Dual battery connections to allow hot swapping of batteries
- AC/DC 9-19 volt power input

5.5.1 AC/DC Power Supply

The power supply for the development board has been designed to take a wide range of inputs including AC. The primary power source will be one of the two lead acid batteries, but an additional small 9V battery is installed in case of a power failure. Two further ports are included to allow an external mains power supply unit to interface with the board, and for another 9V battery. The secondary 9V battery port enables the onboard battery to be replaced while the unit is running under battery power without disrupting operations. As can be seen in Figure 5-9, the main input and battery power supplies are connected to the circuit via two diodes. Each source connects to the anode of each of the diodes, while the diodes' cathodes are connected to each other and the on/off switch. This allows for dynamic switching between the two supplies. When the main input voltage from either an external power supply or the lead acid battery drops below the supply voltage provided by the backup source (9V battery), the unit will automatically switch to the reserve supply.

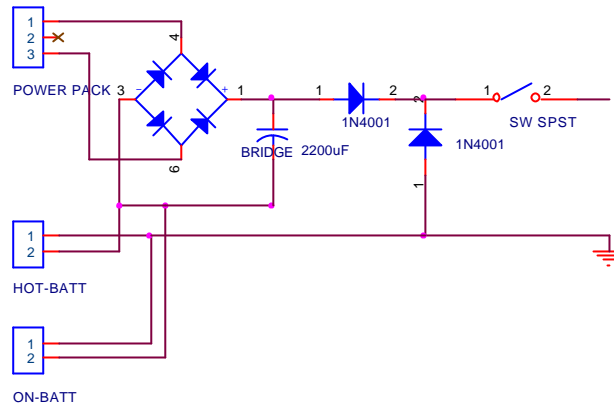


Figure 5-9: Power supply input and battery backup

To allow for both AC and DC inputs, a small 1A bridge rectifier has been included at the front end, as well as smoothing capacitors. To protect the power supply from excess input voltages, a crow bar circuit has been implemented. A 20-volt zener diode (BZX79C20) in series with a 4.7 k Ω resistor is connected between ground and V_{in} . The node between the zener and the resistor is connected to the gate of a DIAC (2N5061), which is also connected to ground and V_{in} . A 100nF capacitor is placed between the gate of the DIAC and ground to smooth any spikes in the supply. In the event that the DIAC is activated, a short circuit will be created between V_{in} and ground. The passing high current will blow the 2A fuse, preventing the power supply from being damaged. Figure 5-10 shows the implemented crowbar circuit.

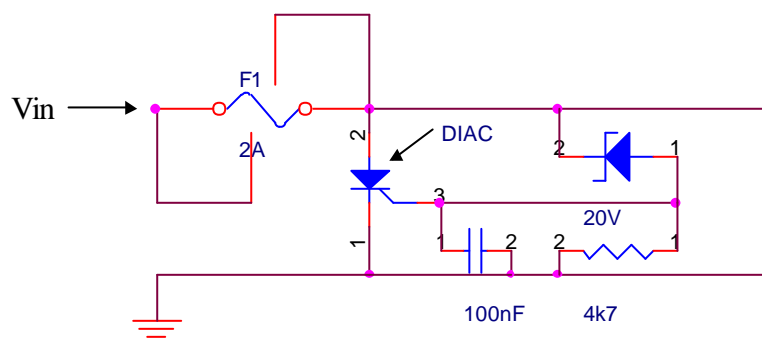


Figure 5-10: Crowbar circuit

A MC7805CT voltage regulator is used to supply a constant +5V to the micro board. A diode is included between V_{out} and V_{in} to protect the regulator in the unlikely event that its input is shorted to ground. Two capacitors are also included on either side of the

regulator to smooth and remove high frequency noise from the supply. Figure 5-11 shows the regulator circuit.

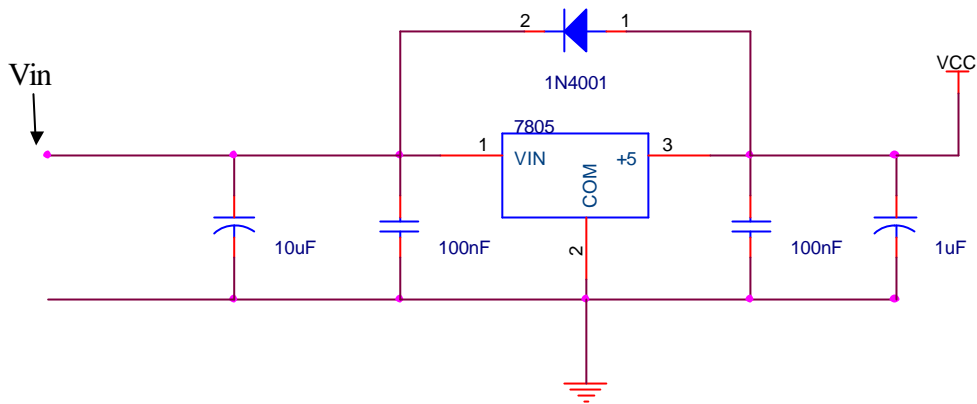


Figure 5-11: Regulator circuit

The final addition to the circuit is a 330Ω resistor in series with an LED between Vout and ground to indicate that the micro board is being supplied with power. Figure 5-12 shows the complete power supply circuit.

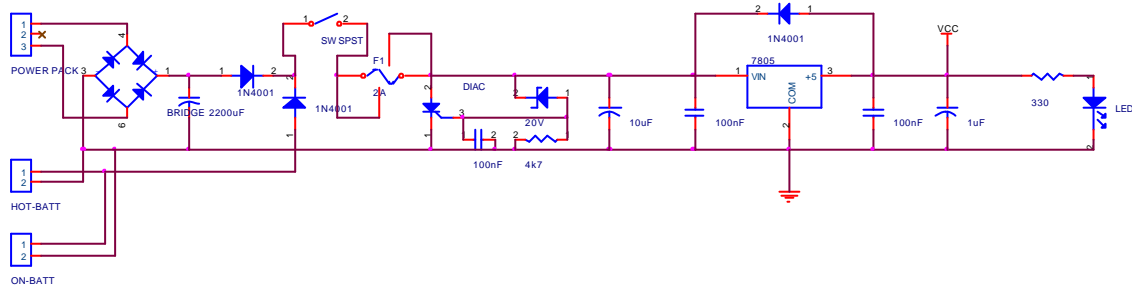


Figure 5-12: Microcontroller power supply circuit

To smooth and reduce noise being transmitted through the 5V lines feeding the integrated circuits (IC), 100nF capacitors have been included between Vcc and ground for most of the IC's.

5.5.2 Internal and External Memory

Internal Memory:

The 8k bytes of the '552's internal memory is used to store code that instructs the micro how to store data being downloaded from a computer.

External Memory:

The '552 can address 64kB of external memory. However, a single 64kB SRAM was not available, and so rather than employ two 32kB SRAM, the decision was made to implement a 128 * 8-bit CMOS SRAM chip (TC551001-BPL70L). The RAM has an ultra low power consumption rate with an access time of 70ns, which was more than adequate given the slow access time of the '552 (238ns).

In order to use a single RAM chip over 64k * 8 bit, care must be taken to ensure the correct addressing of the data and program sections. The NPSEN (Not Program Strobe ENable) and the NRD (Not ReaD) are ANDed and fed into the NOE (Not Output Enable) of the memory chip.

The 128kB RAM chip must be split into two 64kB blocks. This is achieved by using the most significant bit of the address bus to select between the upper and lower memory blocks. When the program code is downloaded, the micro is 'tricked' into writing to the program memory area. This is achieved by inverting the most significant memory bit, thus when the micro tries to write to the data (upper memory block) it is in fact writing to the program memory block. When the code is downloaded, NEA (not External Access) is held high indicating that the micro is running off of the internal memory. A low on NPSEN indicates the micro is reading from program memory. These two signals can then be used to control the most significant bit of the address bus, as shown in Table 5.1.

NEA	NPSEN	Output
0	0	0
0	1	1
1	0	X
1	1	0

Table 5.1: Truth table of external memory access logic

The 'X' in Table 5.1 indicates an impossible logic state, as when NEA is high, NPSEN should never be low (as NPSEN is not active during internal fetches). If the 'X' was changed to a '1', the truth table in Table 5.1 becomes an Exclusive OR (XOR) gate. To implement both the AND and XOR logic, 74VHC08 and HCF4070BEY independent discrete packages were used respectively. Figure 5-13 illustrates the hardware connections implemented to perform these operations.

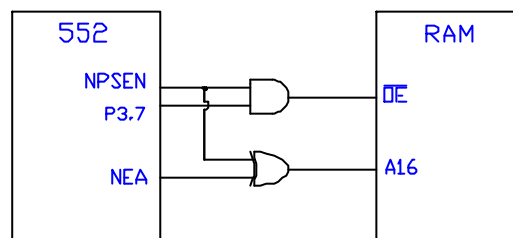


Figure 5-13: Hardware Implementation of both the AND and XOR gates used to access the RAM memory

To ensure that the RAM does not lose its stored data if the power to the board fails, a 'smart socket' was installed to provide continuous independent battery backup.

As the '552 shares the external memory data bus with the lower 8-bits of the external memory address bus, a 74HC573 latch was used to allow the RAM to be addressed and accessed simultaneously, where the Address Latch Enable (ALE) controls the latching.

5.5.3 Real Time Clock

A real time clock (RTC) with an I²C bus interface has been included on the board, so that future development can access an independent timing mechanism. This chip requires its own 32.768 kHz crystal to provide the correct clock frequency. To allow for the clock period to be fine-tuned, a 5-25 pF capacitor is placed between the oscillator input and Vdd. To ensure that the RTC continues to operate in the event of a power failure to the development board, an independent battery backup circuit has been included (3V coin cell-implemented in the same manner as the 9V battery backup used in Section 5.5.1). Figure 5-14 shows the RTC unit and associated battery backup.

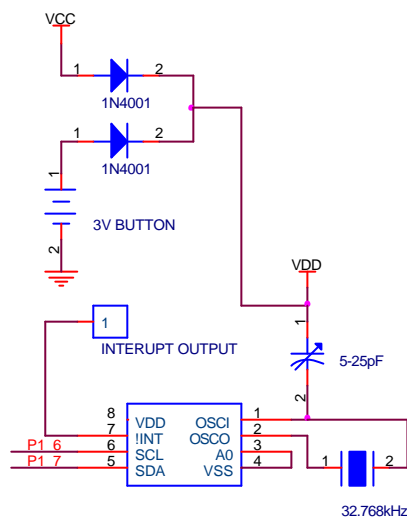


Figure 5-14: Real time clock circuitry and associated battery backup

5.5.4 Serial Communication

To allow code to be uploaded to the microcontroller, a serial interface was developed to allow a computer to transmit data via its serial port to the '552. As the output from a computer's RS232 port is $\pm 10V$, this signal has to be converted to the same 5V logic level as the '552. This is implemented using a MAX232 chip. Figure 5-15 shows the implementation of the MAX232 chip with the serial interface.

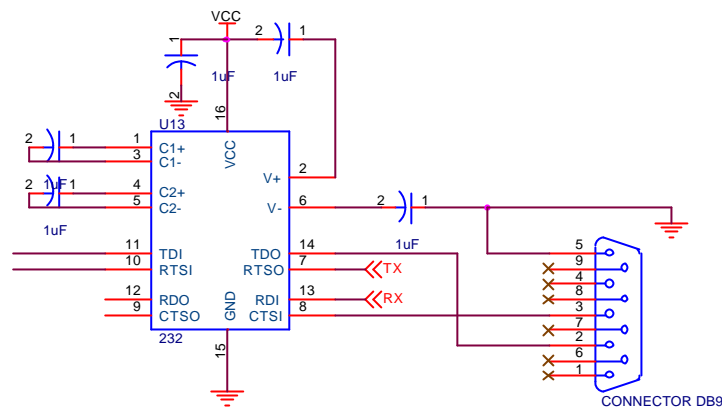


Figure 5-15: Serial input interface for the '552

5.5.5 I/O Ports

The '552 microcontroller has six onboard 8-bit ports. Ports 0 and 2 are used to address the RAM. Ports 1, 3, 4, and 5 are multifunctional, the alternate functions of which are shown in Table 5.2. Ports 1, 3, 4, and 5 also include a buffered bank of LED arrays to indicate the status of each bit on the port. The ports are buffered so as not to adversely affect the I/O port's logic levels. In the event that the unit is required to run under minimal power, the LED's can be disabled via the removal of the LED Enable jumper. Port 5 also has a series of eight switches attached to each of its 8-bits. This allows for a digital signal to be loaded onto the port via the switches. This input can be isolated from port 5 by disabling the tri-state buffer. All ports except 0 and 2 allow for external connection via PCB mount wire clamps around the perimeter of the board. The clamps allow for easy access and connection to the board by external circuits and peripherals. Each independent clamp has ten connectors for each of the 8-bits as well as +5V and Ground.

Port	Additional Function
P1.0, P1.1, P1.2, P1.3	Capture Timer input for Timer 2
P1.4	Timer 2 event input
P1.5	Timer 2 reset
P1.6	Serial clock line (I ² C bus)
P1.7	Serial port (I ² C bus)
P3.0	Serial input Port (UART)
P3.1	Serial output port (UART)
P3.2	External Interrupt 0
P3.3	External Interrupt 1
P3.4	Timer 0 external input
P3.5	Timer 1 external input
P3.6	External data memory write strobe
P3.7	External memory read strobe
P4.0 – P4.5	Timer 2 compare and set/reset outputs
P4.6, P4.7	Timer 2 compare and toggle outputs
P5.0 – P5.7	Analogue ADC inputs

Table 5.2: Alternate functions for ports 1, 3, 4 and 5

5.5.6 Operation

Power:

The main power isolation to the board is controlled via a single pole, single throw (SPST) switch.

Run/Download:

A DPDT toggle switch is used to switch between the run and download modes for the '552. This switch selects the read and write access modes between the '552 and the RAM.

Reset:

A momentary push-button switch resets the '552, allowing the installed program to start from its initial conditions. A capacitor and a resistor could have been installed to

control the period that the switch must be depressed to reset the '552, but as an instant reset was ideal, the resistor was omitted.

Figure 5-16 shows the completed '552-microcontroller development board. Figure C.3 and B.4 shows the complete schematic for the '552-microcontroller development board, and the scale dimensioned drawing of the acrylic case respectively.

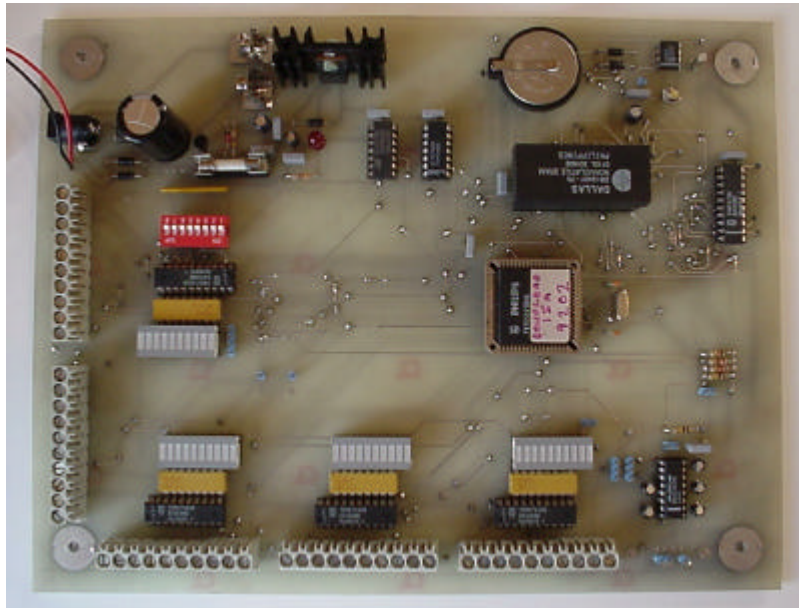


Figure 5-16: '552-microcontroller development board

5.6 RADIO CONTROL UNIT AND INTERFACE

To aid in the transportation of the unit, a radio control unit has been interlinked into the '552 microcontroller. This interface permits an operator to manoeuvre the unit around, including driving it up onto a trainer for transportation without requiring at least two people to lift the unit. Once the unit has reached its destination, the radio control can be disengaged allowing for an internal control system (autonomy control) to take over. A pre-manufactured 2-channel radio control unit was purchased for the radio interface. The two-channel receiver is integrated into the development board allowing the '552 to interpret the received signal from the hand controller, and process the signal into a suitable input for the motor drivers. Figures 5-17 and 5-18 shows the two-channel radio control set, and receiver unit respectively.



Figure 5-17: Two-channel radio control set



Figure 5-18: Receiver unit

The receiver is interfaced with the '552 rather than the DAQ card to allow the unit to be controlled via the radio transmitter without the main computer having to be powered up, allowing easy mobility and less power consumption during transit.

Eight AA batteries power the hand radio transmitter, accepting a normal supply voltage between 9.6 – 12VDC (Nickel Cadmium or Alkaline). The transmitter will continue to transmit with an input voltage as low as 7.8VDC, although the output signal power is substantially reduced. The receiver is intended to be powered by 4 AA batteries, allowing for a normal input voltage between 4.8 – 6VDC. As the robot's systems have a multitude of regulated 5V power supplies, the receiver does not require an additional battery pack. The transmitter and receiver have matched crystals to operate at 26.995 MHz in the AM band.

5.6.1 Receiver Output Signals

When viewing the output signals from the receiver, a pulsed square wave is observed with a period of 19.22ms and a pulse width of 1.53ms. This generates a continuous operating frequency of 52.03Hz. When the controls are altered on the transmitter, the pulse width alters (period remains constant). The minimum pulse width produced is 1.14ms, and the maximum pulse width is 1.89ms. In the default position on the transmitter, the 1.14ms pulse width represents full throttle forward, although the reversing switches on the transmitter can select the state. Figure 5-19 illustrates the initial receiver state (stationary), full throttle forward (default), and full throttle in reverse respectively. The signals in Figure 5-19 have been measured with a 6VDC input into the receiver.

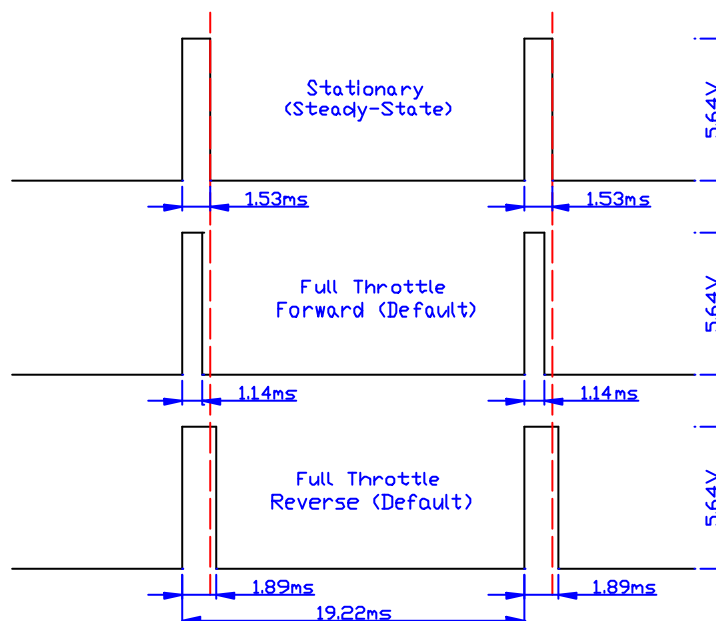


Figure 5-19: Receiver output signals; a) initial receiver signal (stationary), b) full throttle forward, c) full throttle reverse

5.6.2 Converting Receiver Signals into PWM Outputs

In order to control the PWM signal through the radio control unit, the microcontroller has to be able to interpret the steady state (stationary), 1.14ms pulse width for full throttle forward, and the 1.89ms pulse width for full throttle in reverse.

As with electric model aircraft speed controllers, on start up, a calibration sequence initiates. During this stage the microcontroller scans the incoming signal from the receiver for a set period to determine the steady state pulse width. The signal is scanned using an external interrupt (INT0 – IE0) on the '552. When the interrupt is triggered (by the leading edge of the first pulse) a timer starts to count until the falling edge of the pulse is detected.

Once a predefined period has passed (1 - 2s), a signal is relayed to the operator (via LED output), to indicate that the steady state has been determined, and to request full throttle forward. This sequence repeats for reverse also. Once all three values have been determined, the respective counter values can be used to generate PWM signals based on incoming pulse widths from the receiver.

For the receiver speed controller interface, only five incremental PWM outputs will be implemented in both the forward and backward directions (*pwm_{50,100,150,200,250}*). This is due to both the track configuration and the resolution of the output from the receiver. To ensure that interference fluctuations from the receiver do not affect the stationary position, the first PWM output will not initiate until a 0.08ms differential is detected from the steady state position.

When a large pulse width (greater than 1.60ms) is detected by the micro, a signal is sent to the direction control transistor BST704A (Section 5.4.2) prior to sending the PWM signal. This ensures the motor is travelling in the correct direction prior to the PWM input.

5.6.3 Steering Under Radio Control

As the receiver has two channels, it is possible to control each motor independently using each lever of the control. Each channel on the receiver controls an independent PWM signal, and is scanned with a separate external interrupt and timer. Figure 5-20 illustrates the sequence of generating a motor response from a transmitted radio signal.

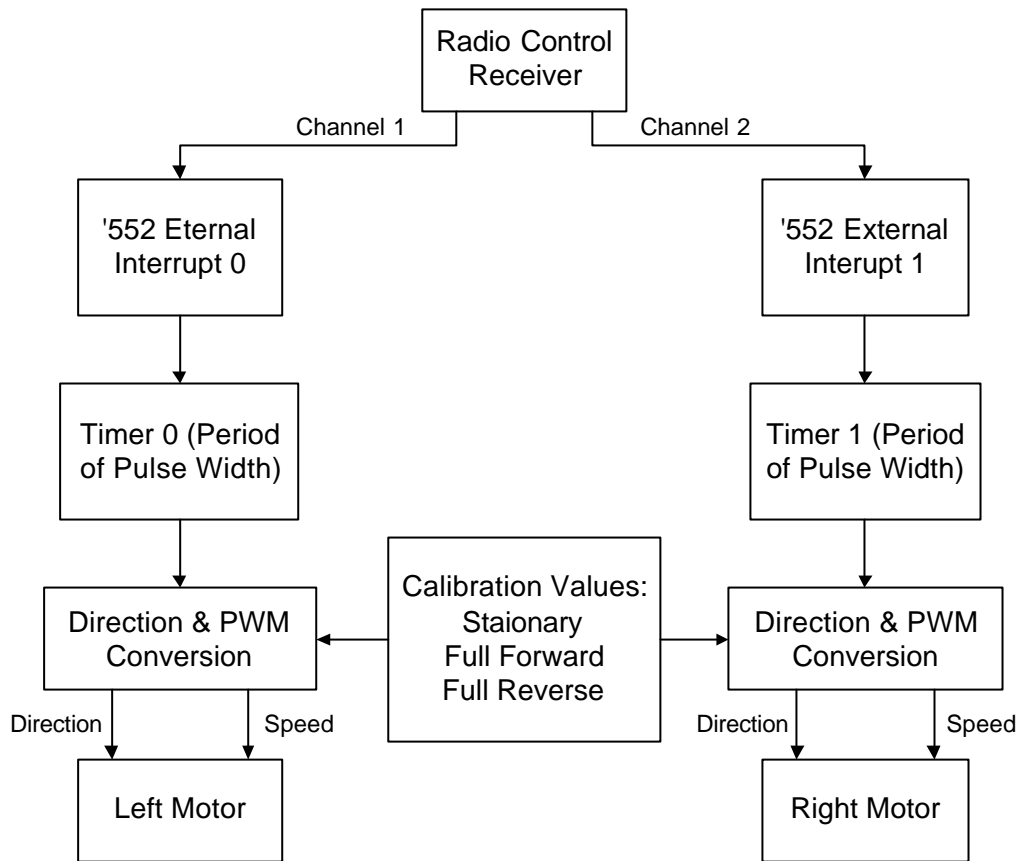


Figure 5-20: Motor control sequence from a transmitter radio signal

5.7 DAQ CARD HUB

The DAQ card hub has three 25 pin D-sub (ECP) ports, which allow peripherals to be directly connected to the DAQ card. The hub provides a means to connect components in a less congested format, away from the central computer. A large ribbon cable simply interconnects between the DAQ card and the hub, allowing for easy separation. Figure 5-21 shows the DAQ card in its customised acrylic case. Figure B.5 shows a scale dimensioned drawing of the DAQ hub case.

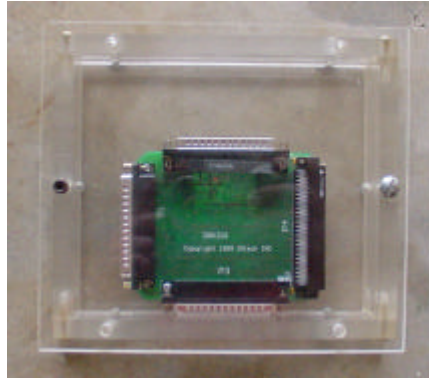


Figure 5-21: DAQ hub

5.8 INTEGRATING SENSOR ARRAYS AND NAVIGATIONAL EQUIPMENT

This project implemented many of the sensors and navigational equipment discussed in Section 2.4. All equipment was designed, manufactured, and purchased to suit both indoor and outdoor conditions, which could include poor weather and rough terrain.

5.8.1 Infrared Proximity Sensors

Prior to the implementation of a laser range finding device, IR sensors are to act as the primary obstacle detection mechanism. They are chosen for their performance, compactness, ability to operate in poor weather (as compared to ultrasonic transducers), and because they are easily mounted (pre-manufactured units).

In reviewing development work on IR detection undertaken at the University of Waikato in the past for the micro-mouse projects, IR detection units were operated reliably up to distances of 50cm (Taberner, 1994). Data sheets for current pre-manufactured IR proximity detection units indicate that sensors with an 80cm range are available for relatively low expense. As a result, Sharp GP2D12 IR proximity sensors (shown in Figures 5-22 and D.6) have been installed around the perimeter of the chassis.

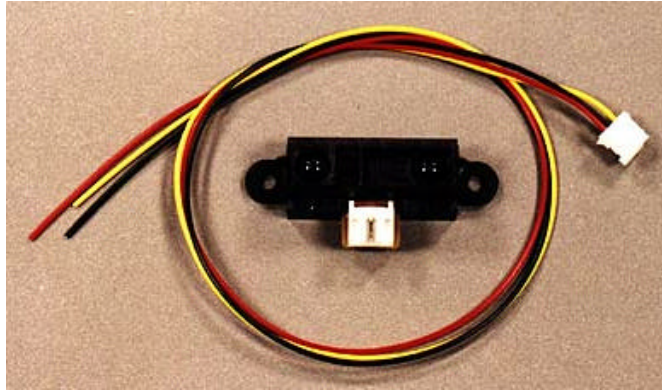


Figure 5-22: Sharp GP2D12 IR proximity sensor module

The emitter and detector are positioned 20mm apart in an enclosed sealed unit. All associated circuitry is self-contained within the module, generating an analogue voltage output corresponding to distance. The GP2D12 is configured to reduce the influence of the colour of reflected objects as well as ambient light with a series of onboard filters and signal amplifiers. This additional signal processing extends both the range and accuracy. The operating range of the sensor is between 10 to 80cm, which generates a corresponding average output of between 5 and 0.2V respectively ($V_{cc} = 5V$). Figure 5-23 shows the experimentally determined output voltage versus distance to object ($V_{cc}=5V$) for both shiny and textured white and black surfaces. From Figure 5-23, very little deviation can be seen between the matt black and white textured surfaces. Figure 5-24 shows the sensor output for both gloss black and white surfaces. Figure 5-25 shows the average experimentally determined lateral detection profile of the sensors using a 100mm matt white block as a reflective surface. Each set of angular readings was taken at 5cm incremental steps from the sensor.

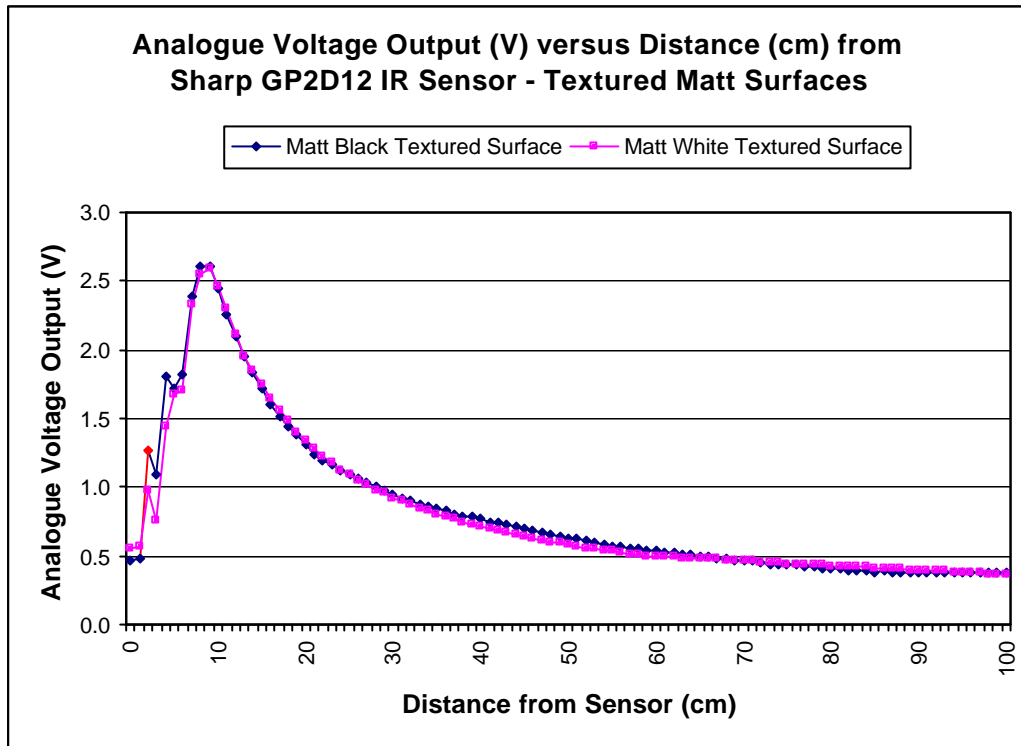


Figure 5-23: GP2D12 sensor output versus distance to object (experimentally determined) for matt surfaces

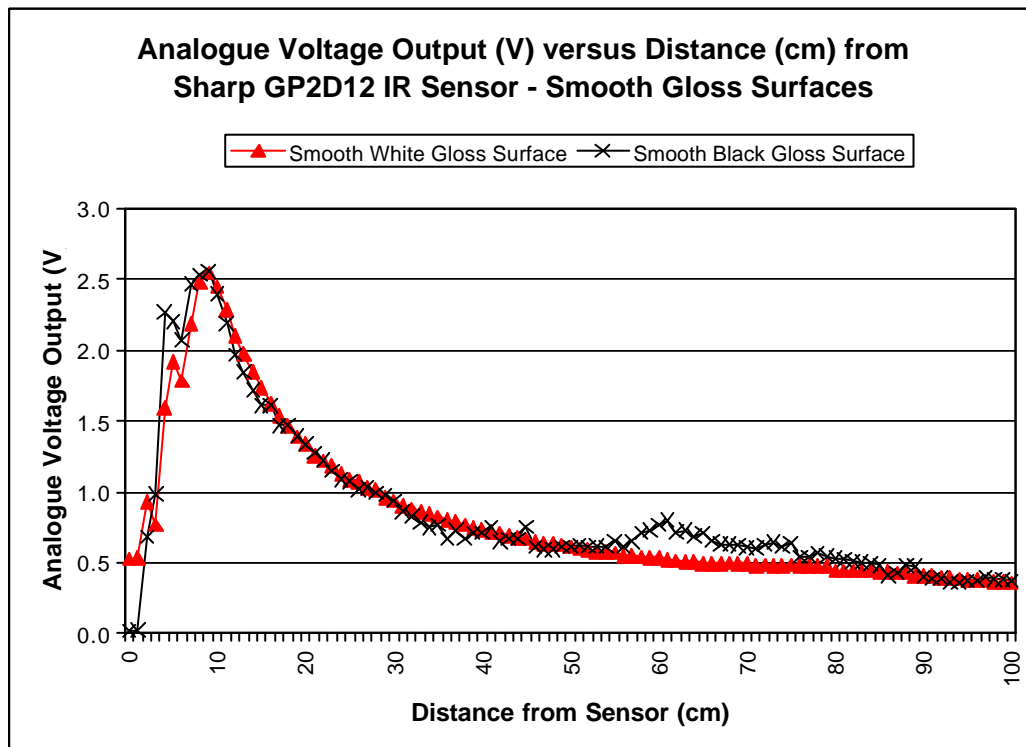


Figure 5-24: GP2D12 sensor output versus distance to object (experimentally determined) for gloss surfaces

With no reflective surfaces in the path of the sensor, the output voltage fluctuated between 0.27 and 0.30V.

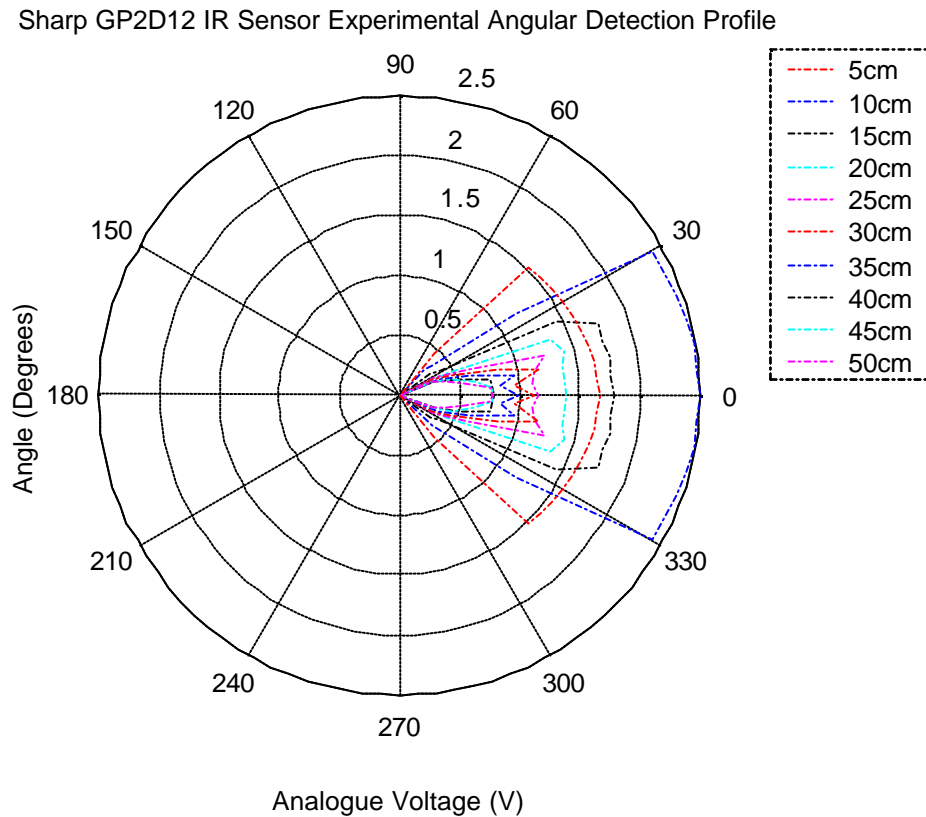


Figure 5-25: GP2D12 lateral detection profile (experimentally determined)

The outputs from the sensors are fed directly into the DAQ card as part of the integrated sensor array (processed by LabVIEW).

Due to the physical size of the tracked drive platform, a series of IR sensor packages have been placed around the entire perimeter to reduce the risk of not detecting an obstacle. Figure 5-26 shows the layout of all eight of the IR sensors around the perimeter of the drive chassis.

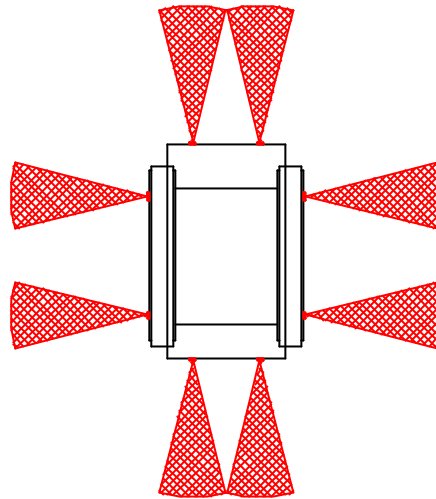


Figure 5-26: IR sensor locations

The front sensors provide the most important information during normal travel, enabling course correction upon detection of an obstacle. The side sensors can be used in conjunction with the compass, GPS, and shaft encoders, when a continuous obstacle such as a wall is detected in order to maintain a constant separation distance. The side sensors can also be used to ensure that an obstacle will not make contact with the unit during a turn (especially a stationary turn).

Due to the configuration of the drive system, objects that are lower than 10cm from the ground do not need to be detected as they will safely pass under the central chassis or be negotiated over by the track modules. Therefore, the front and back IR sensors have been positioned on the upper chassis tray, 22.5cm from the ground, and 8cm from each end. The side IR sensors have been placed 22cm from the ground (due to the limited height of the side plates), and 10cm from each end of the track modules (measured from the edge of the side plates along the horizontal plane).

5.8.2 Tactile Sensors

Although not implemented at the completion of this project, the design and development for the addition of tactile sensors has been completed. To perform this operation, eight NTE-5A micro-switches have been purchased. Each micro-switch is to be located in similar positions to the IR sensors. Four independent spring loaded ‘bump

bars' are to be fixed in position along each face of the chassis. When contact is made with the bars (the bars only require a 6mm deviation from their equilibrium position), the corresponding micro switch(es) sends a signal to the DAQ card. Although relatively crude, the device can determine where the initial contact was made (relative to each switch on each face). Figure 5-27 illustrates the location of the tactile sensing equipment. Both the IR and tactile sensing methods minimise the chance of an obstacle being undetected, but do not guarantee against an obstacle that comes in over or under the sensing zones.

It is the intention that the additional sensors (GPS, compass, shaft encoders) in conjunction with software would be able to distinguish when the unit is stationary, yet should be moving.

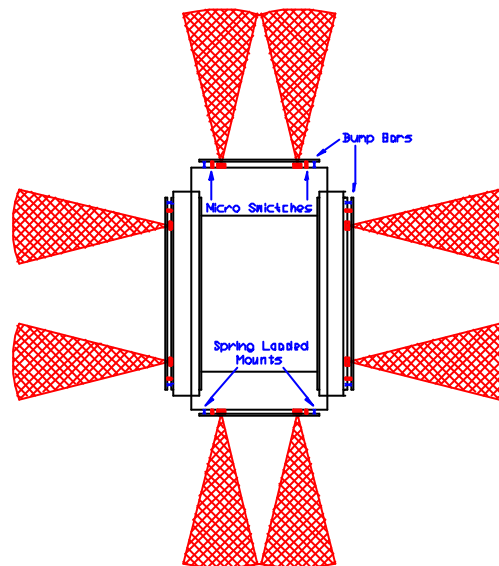


Figure 5-27: Sensing planes and undetectable dead bands

5.8.3 Shaft Encoders

The Mechatronics Group has experience with the Hewlett Packard HEDS-9040 two-channel pre-manufactured optical shaft encoders and HEDM-5120 metal code wheels (illustrated in Figure 5-28). These units allow for very precise measurement of angular displacement with 512 Counts Per Revolution (CPR).

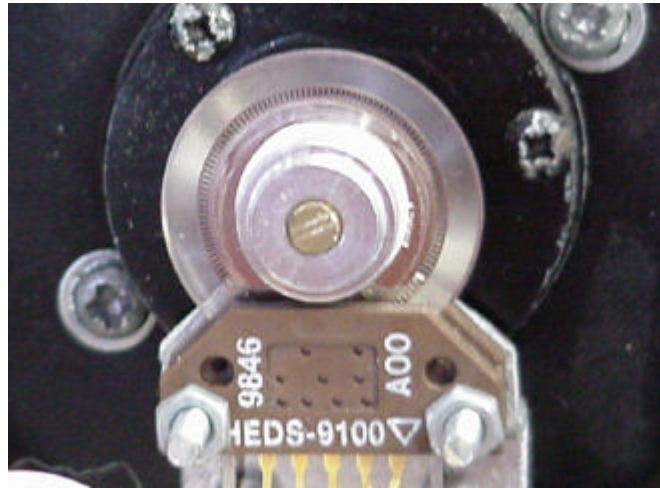


Figure 5-28: HEDS-9040 shaft encoders and coded wheels

The HED series units are ideal for precise enclosed applications that are free from foreign matter, but are prone to both damage and signal corruption in this project's operating environments. The other disadvantage is that an accumulative counter would have to increment 201900 times per revolution of the belt, as shown by Equation [5-1] (assuming the encoder disk is attached to drive shaft out of the gearbox).

$$\begin{aligned}
 C_{encoder} &= cw_{cpr} * \left(\frac{N_{track}}{N_{planetary}} \right) * N_{gearbox} && \text{Eqn. [5-1]} \\
 &= 512 * 394.33 \\
 &\approx 201900
 \end{aligned}$$

where: $C_{encoder}$ = total number of counts after one revolution
 cw_{cpr} = code wheel (CW) CPR (constant)

To both reduce the counts an accumulator has to make, and to increase the operating tolerance, a customised shaft encoder unit is required. Such a unit requires a solid method of attachment to the output shaft in the area available without fouling the chassis, motors, or track modules. Also required is a robust optical sensor that can be easily mounted to suit a customised CW. The HOA2001 transmissive optoschmitt sensor (shown in Figure D.7) is a fully integrated sensor in a package that allows for easy attachment (through bolt holes) and can accept a CW up to 3mm in width. With the configuration of the motor mounts (illustrated in Figure 3-40), additional plates have

been mounted to allow the HOA2001 sensors to align themselves with the central axis of the drive shaft. Figure 5-29 shows the plate mounts for the opto-sensors.

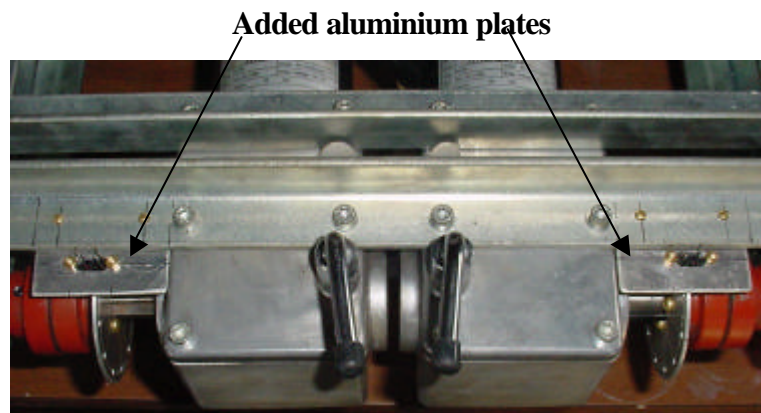


Figure 5-29: Additional plate mounts for the opto-sensors

There is only one available location to mount the CW's on the gearbox's output shaft. The CW must be fixed in between the motor and the inside of the drive coupling, as there is only 0.5mm clearance on the other side of the coupling. To generate an adequate surface to mount the CW, the inside outer surface of the drive couplings were faced in the lathe. The face was then tri-sectorised, marked half the distance in from the inner and outer edges, and drilled using a $\text{Ø}5/32$ " bit. The three holes were then tapped to suit a $\text{Ø}3/16$ " BSW thread. Figure 5-30 shows the completed face of the inner section of the drive coupling.

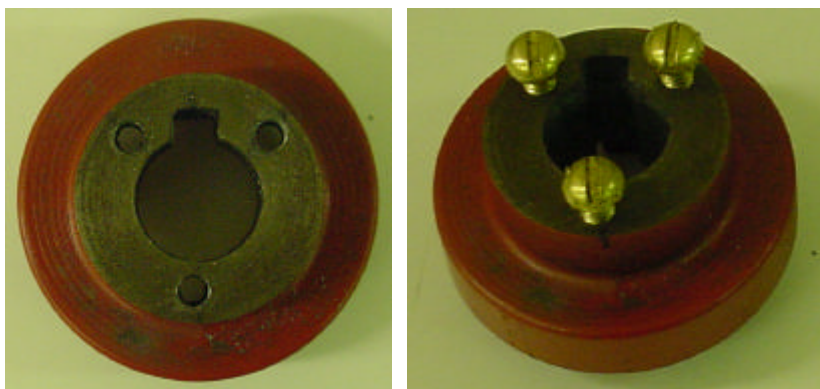


Figure 5-30: Customised face on the inner section of the drive couplings

With both the CW surfaces completed and the optical sensors mounted on the added mounting plates, accurate measurements could be taken to determine the precise

required diameter for the CW ($\varnothing 79\text{mm}$). To ensure a perfectly round CW relative to each drive coupling, 3mm aluminium plate was cut oversize, and mounted to each drive coupling using $\varnothing 3/16'' \times 3/4''$ BSW brass bolts (shown in Figure 5-32). This allowed for each drive coupling to be mounted in the lathe, and have the aluminium plate precisely turned down to size. After the outer face was reduced to size, the inner diameter could be machined out (using a fine boring tool in the lathe) to suit the 17mm drive shaft. The thickness of the plate was reduced to 2.5mm, 10mm in from the outer edge, to ensure there was adequate clearance for the sensor (3.05mm sensor opening). The keyway was then drilled out and filed square.

The number of holes to be bored around the perimeter then had to be calculated. Ideally, due to the gear ratio between the drive pulley and the track, fewer holes would be preferable providing resolution was not severely reduced. With the gear ratio from the drive pulley to the belt being 12:1 (refer Section 2.3.2), the belts travel 0.19m per revolution from the gearbox (2.3m belt length). Hence, twelve, 30 degree incremental steps would produce a linear travelling distance of just under 16mm, which is more than adequate for the terrain and drive system.

Each aluminium disk was scribed at 30-degree incremental steps over its surface, and marked 5mm in from the outer edge (using the lathe). A series of twelve $\varnothing 1/8''$ holes were then bored at the intersection of the scribed lines. Figures 5-31 and 5-32 show a completed aluminium CW and assembled CW and drive coupling respectively. Figure A.22 illustrates a scale dimensioned drawing of the CW.

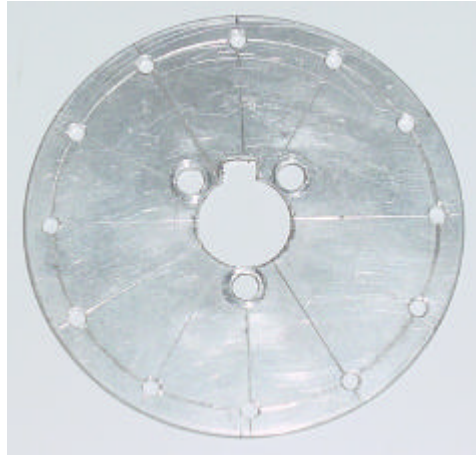


Figure 5-31: Completed code wheel



Figure 5-32: Assembled code wheel and drive coupling unit

Figure 5-33 below shows the completed units assembled on both the drive shaft and motor mounts, illustrating the final configuration of the odometry unit.

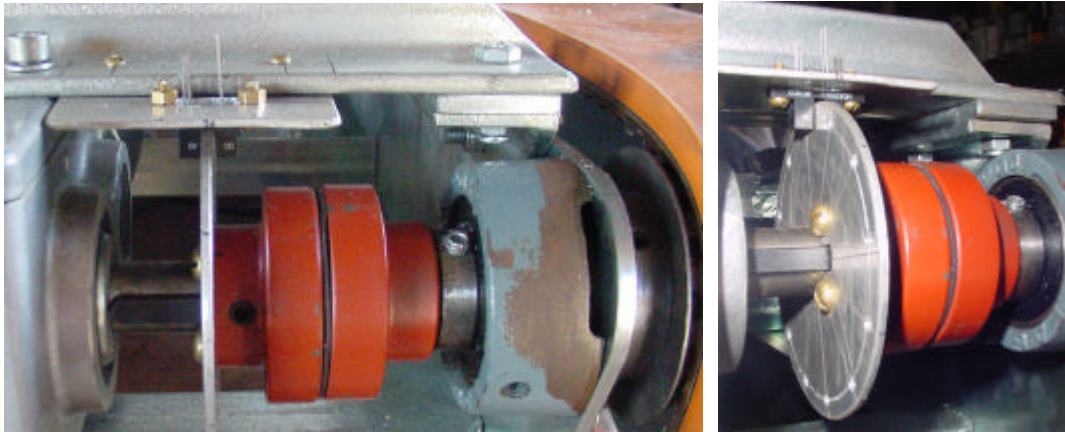


Figure 5-33: Completed installation and assembly of the odometry units

The HOA2001 has five terminals, two from the emitter and three from the detector. The anode on the emitter is connected to the universal 5V supply of the robot, and the cathode is connected to ground (negative earthing plane). 5V and earth are also connected to the detector circuit, with the remaining output terminal connecting directly into the hub for the DAQ card.

5.8.4 Electronic Compass

The electronic compass chosen for this project is the Vector V2X. As with most of the other components, the VX2 was chosen for its functionality per dollar, with a significantly lower price than most of the other available units on the market. The VX2 is a 2-axis magnetometer that measures the electric field in a single plane. The measurement plane is created between two perpendicular sensors. The sensors measure the Earth's magnetic field to determine the heading. The major disadvantage with the VX2 is its lack of gyroscopic ability to ensure that the sensors remain parallel with the water line on the surface of the earth. If the sensors are not parallel, error factors occur. Although a compass with a built in gyroscope would reduce the heading errors, it would not give any indication of the differential gradient. Therefore, a yaw and pitch sensor is ideal to correct heading errors using gradient correction conversions, as well as generating feedback to other systems. The addition of mechanical gimbals could be used to generate a natural gravitational level.

Under normal (level) conditions, the V2X has an operating resolution of 2°. In calculating the adequacy of the resolution, it can be seen via Equation [5.2] that this produces a lateral offset of 35mm over one metre.

$$\begin{aligned}\Delta L &= d * \sin(2) && \text{Eqn. [5.2]} \\ &= 1 * 0.035 \\ &= 35\text{mm}\end{aligned}$$

In conjunction with the odometry and GPS, the resolution calculated from Equation 5-2 provides adequate feedback to allow the drive system to track accurately. Figure 5-34 shows the V2X compass.

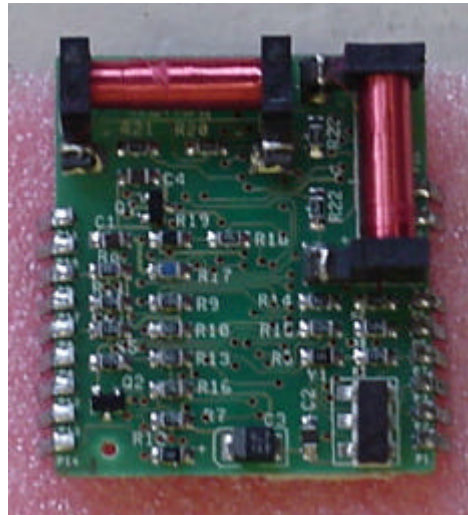


Figure 5-34: V2X electronic compass

The V2X produces a binary coded decimal (BCD) or binary output format, which relates to the heading in degrees. For this project, the BCD format has been implemented. The signal coming from pin 2 of the device is the serial data output (SDO) which when pin 9 is low, sends a BCD output relative to the bearing. Figure 5-34 illustrates a 356-degree signal coming from SDO in BCD format.

```
SDO = 1101010110;
```

```
BCD bits:  1    1    0    1    0    1    0    1    1    0
Values:    200  100  80   40   20   10   8    4    2    1
```

SDO output is equivalent to:

```
SDO ≡ 200 + 100 + 40 + 10 + 4 + 2
      ≡ 356
```

Figure 5-35: BCD format for 356-degrees coming from SDO

The SDO is fed into LabVIEW where a BCD conversion is carried out to convert the signal into a relative angular coordinate system, to integrate with the information from the other systems.

5.8.5 GPS

The Motorola M12 Oncore GPS unit provides a cost effective solution in an extremely small package. In addition to its size, the M12 has enhanced foliage and urban canyon performance, with an extremely fast Time To First Fix (TTFF), and requisition time rating. An additional benefit of the M12, is its inbuilt inverse differential GPS, which allows for improved positioning between a central base station and other GPS units with the same functionality. Including latitude, longitude, and altitude, the M12 also relays information on velocity, heading and time, which it can transfer via a software selectable output rate through communication ports. Figure 5-36 shows the complete M12 GPS unit.



Figure 5-36: M12 GPS unit and antenna

In order for the M12 to receive signals from satellites, an associated antenna must be connected. Included within the antenna module are a microstrip patch antenna, ceramic radio frequency (RF) filter, and a signal preamplifier. The module is designed to receive L1 band signals at a nominal frequency of 1575.42 MHz from the GPS satellites. Figure 5-37 shows a cross-sectional view of the antenna gain pattern along a fixed azimuth (vertical cut).

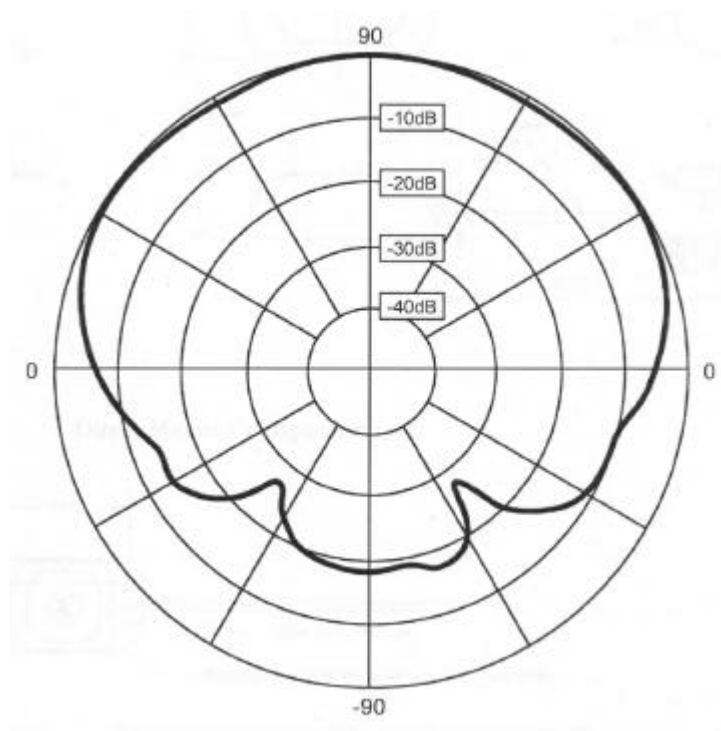


Figure 5-37: Active antenna gain pattern

Although the antenna will operate within the aluminium case encapsulating the robot, it will be mounted on the highest vertical horizontal plane to reduce the risk of any possible signal degradation caused by being concealed within the outer case (illustrated in Figure 5-38).

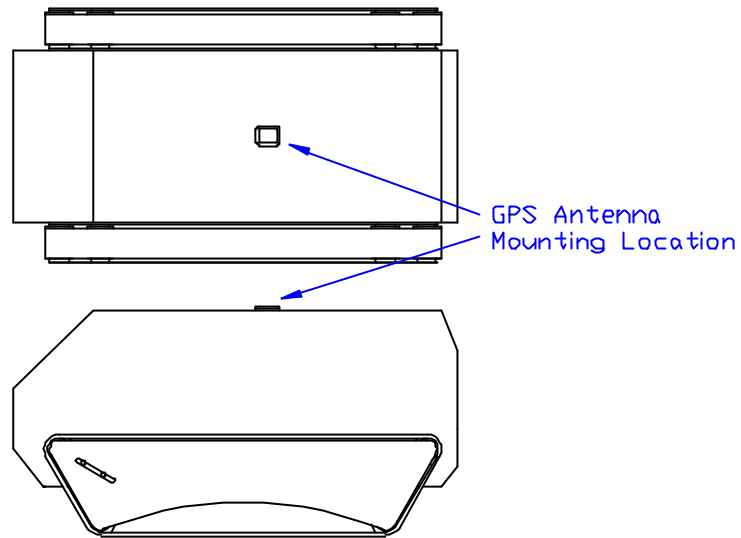


Figure 5-38: Antenna mounting position with respect to the outer casing of the robot

6. SYSTEM INTEGRATION

The robot's control system is based around the central computer, which transmits and receives signals to and from the onboard electric systems via the DAQ card. As discussed in Chapter Two, these signals are intended to be interpreted by a real-time software package (LabVIEW), to provide an intelligent, integrated method of control. By developing software to complement the array of sensory equipment, the unit can obtain a certain degree of autonomy in its mobility. Due to limitations with the interface of LabVIEW with the IOTECH DAQ cards and time constraints, the programming of the control theory within this section is conceptual, and has not yet been implemented.

6.1 LABVIEW

LabVIEW is a programming development application which uses a graphical programming language, G, rather than being text-based such as C and Pascal. G code is developed around interconnected block diagrams to build up a program. Each block can be built up of a series of more complex modules, to create a layered high-level application. As with other programming languages and applications, LabVIEW has extensive libraries of functions and subroutines for most programming tasks. LabVIEW also contains application specific libraries for data acquisition, allowing equipment such as sensors, instruments, and controls, to communicate bi-directionally through a DAQ card directly with LabVIEW. Programs developed in LabVIEW are defined as Virtual Instruments (VI). LabVIEW is the primary programming language used in for this project to control all equipment connected to the DAQ card.

6.2 SPEED & SLIPPAGE

6.2.1 Speed

The odometry units illustrated in Section 5.4.3 are the primary sensory devices used to establish and thereby control the speed of each track module. For each hole on the code wheel that passes the optical sensor, the unit recognises a linear distance travelled of 16mm. The speed is determined via a software counter for each Shaft Encoder (SE), which multiplies the number of counts by 16mm and divides by the time passed to generate a relative speed in metres per second (m/s). Figure 6-1 shows the basic flow diagram for each SE's signal processes.

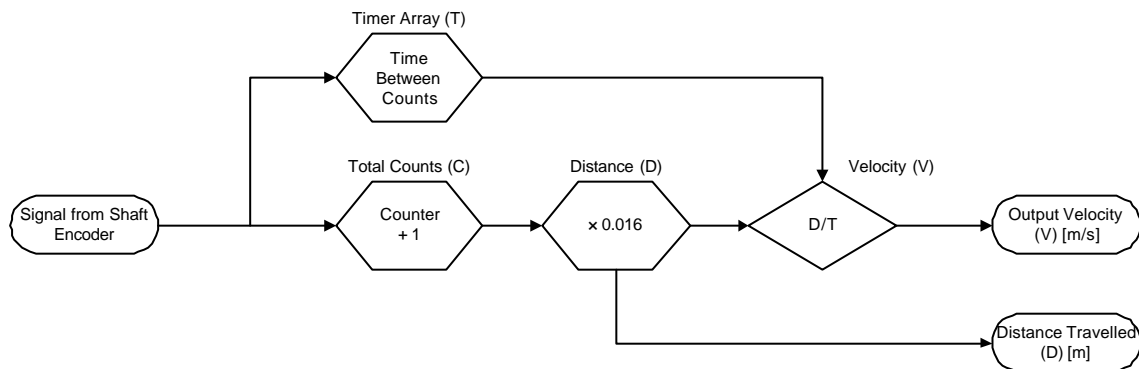


Figure 6-1: Shaft Encoder's signal process to compute speed and distance travelled

The timer array in Figure 6-1 consists of a series of cells that has its indexing incremented in conjunction with the counter to enable the time of each count to be stored in the indexed location. The time between each count is the previously stored value minus the current reading. The indexing system is a rolling array with three cells, overwriting the initial value on the preceding signal. The system indexes the memory array as illustrated in Figure's 6-2 pseudo code.

```

Continuous Loop: % Assuming all array cells have been set to 0
for i = 0, i ≤ 2, i++;
    {% Wait for a pulse signal from the SE
    Signal: ti = time of signal (via software clock);
    if(t(1-i) = 0)
        break % initial condition when array does not have values
        stored
    else if(ti = 0)
        Time between counts = t2 - ti
        break
    else
        Time between counts = t(1-i) - ti
        Break
    i++}

```

Figure 6-2: Speed correction pseudo code

In conjunction with the SE method of tracking speed and distance travelled, the GPS also transmits a real-time signal on the current velocity and course. The integration of the GPS as a tool for determining slippage is discussed in Section 6.2.2.

6.2.2 Slippage

By itself, the SE have no way of determining the loss of traction that occurs during normal travel. As terrain and conditions alter over a path, the amount of lost drive can significantly vary, not only across the drive system as a whole, but between independent track modules. The GPS is one of the best instruments to aid in determining the amount of lost traction, and thereby helping the control system to make corrections to the drive controllers. Due to moderate errors that can cloud the accuracy of the GPS, other instruments such as the SE and compass must also be incorporated into the motor control to reduce inaccuracies.

Two factors cause the majority of lost traction, the rate of acceleration, and the environment. Under the normal operation of the motors, the control system ideally wants to maximise the rate of acceleration up to the required velocity, while reducing

the amount of overshoot and oscillation (discussed in Section 6.6.5). In conjunction with both the type and gradient of the surface, the rate of acceleration, and final velocity may have to be substantially lowered to reduce slippage in order to maintain positive control. If a significant amount of slippage occurs, it not only affects the efficiency of the drive system, but also substantially reduces the controllability. Without positive control, the robot can not only become dangerous; it could also incur serious damage. In order to detect the amount slippage, the GPS signals for speed and distance travelled must be compared to the speed of rotation of the CW. If the detected speed/distance travelled by the GPS does not coincide with the output from the odometry units (exceeds an allowable standard deviation error), then slippage is occurring, and the velocity of the motor should be dropped until the speed/distance is within adequate boundaries. Figure 6-3 illustrates the generic process flow diagram for the interface of the GPS and odometry units with the motor's control system.

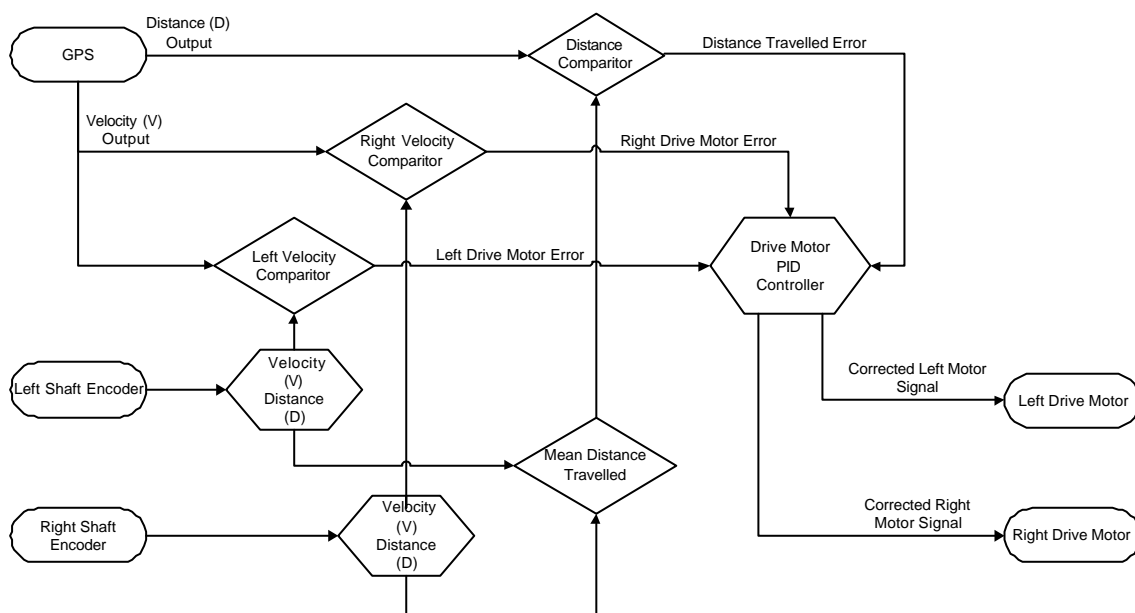


Figure 6-3: GPS & odometry interface to reduce slippage due to over acceleration and speed

As can be seen from Figure 6-3, comparative computations are performed to find the differential errors between the SE and the GPS. This information is fed into the drive motor's Proportional, Integral, and Differential (PID) controller (discussed in Section 6.6.5). Adjustments are then performed by the control system, relaying the corrections

back to the motor drivers. This system allows for continual real-time feedback to reduce slippage caused by excessive speed and acceleration.

6.3 COURSE CORRECTION DURING UNRESTRICTED MOVEMENT IN A STRAIGHT LINE

6.3.1 Previously Used Methods

Other indoor projects developed at the University of Waikato have used only SE and IR sensors to correct for heading errors while moving in a straight line. This is performed by using the IR sensors to continually transmit feedback to the motor driver control system on any differential fluctuation between the sensor pairs on each side of the device. A continual feedback system ensures the device runs parallel with the walls. Using the IR system also allows for an auto calibration to be performed to generate a correction factor to be multiplied with a SE counter to reduce tracking errors. Figure 6-4 illustrates a general tracking error due to fractionally different tyre diameters. When walls/obstacles are outside of the IR sensor's range, there is no way of correcting for any deviation in course until an obstacle is detected. As per the dashed line in Figure 6-4, in an open environment this tracking error could result in the unit losing orientation, though it still believes it is travelling in a straight line.

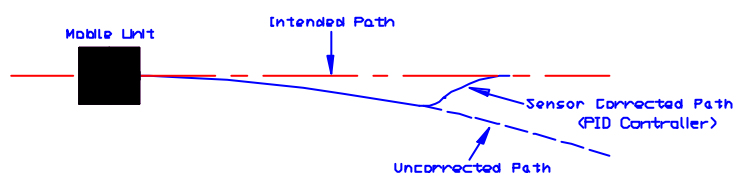


Figure 6-4: Tracking errors, and IR course correction

The corresponding indoor course correction control flow diagram is illustrated below in Figure 6-5.

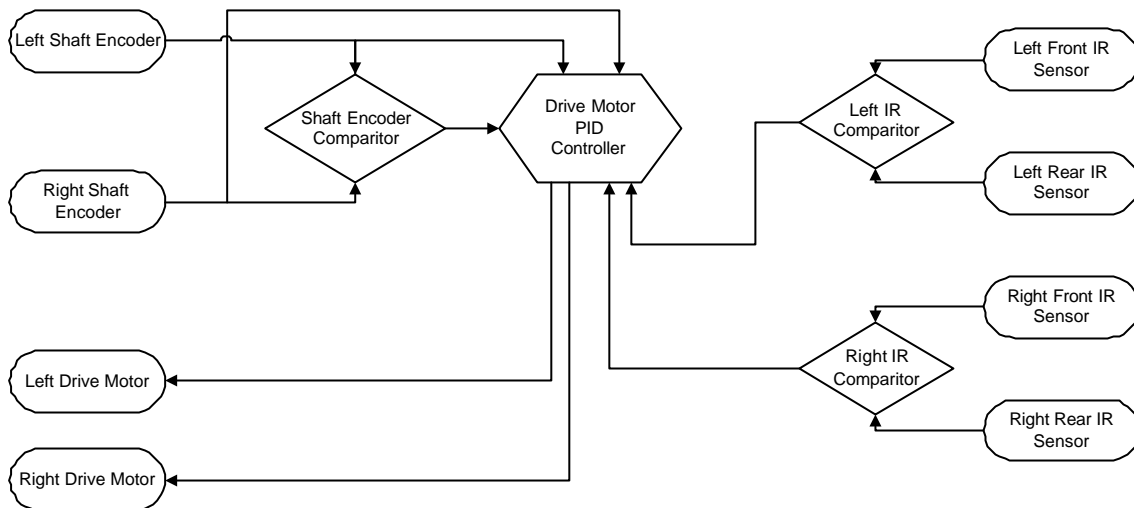


Figure 6-5: Control system for indoor unit with only SE and IR sensors

6.3.2 Full Integration of Sensors for Course Correction

The SE's provide the primary feedback for the correction in motor speeds to maintain course. The course itself is checked against both the outputs from the compass and the GPS. Both the compass and GPS not only provide a secondary backup for the course correction operation if one device was to fail, but it also allows for any incorporated errors in the output to be averaged prior to adjustment. If a tilt sensor could have been purchased, this would have been interfaced with the compass to correct for any error factors due to incline. Although the GPS has recognised global errors in position, its heading output is not affected by the gradient of the device.

The first stage of the sensor integration is to convert both the compass and GPS output bearings into the same format for analysis. Once in the same format, the two readings can be combined to minimise errors in the readings. For more accuracy, an output on the number of satellites acquired by the GPS can be fed into a controller to weight the precedence of the GPS versus the compass. The minimum would be four satellites (enabling 3D bearings: latitude, longitude, and altitude) prior to the GPS heading having a greater weighting than the compass heading. As more satellites are acquired by the GPS, the relayed heading from the combined signal of the GPS and compass contains a higher percentage of the value from the GPS.

As the M12 GPS can track up to 12 satellites at any one time, experimentally the readings from the GPS versus the compass would have to be established over varying terrains to determine the weighting factors. The combined output from both the compass and GPS can then be compared with the heading required. The difference in values would then be fed into a PID controller to smoothly adjust the motor speeds to track the unit back on course. By having a well-tuned controller, the device should quickly reacquire an accurate course without significantly overshooting the bearing. As with the method in Section 6.3.1, if the heading adjustments are continually the same, an auto-calibration sequence can be included to allow for any natural deviation in course due to slight variances in the CW and track modules. Figure 6-6 shows the control flow diagram for the course correction sequences using the compass, GPS, and SE's.

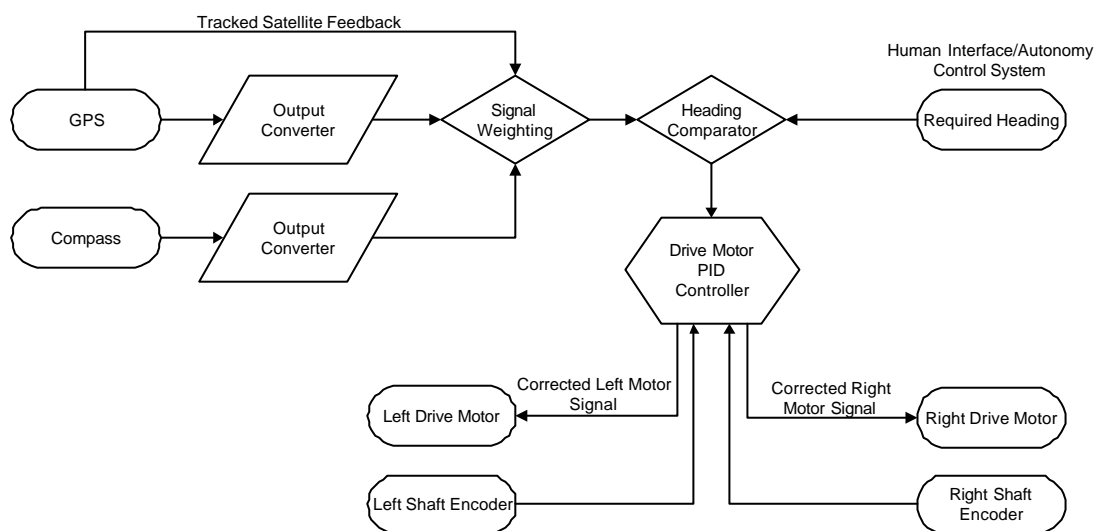


Figure 6-6: Course correction sequence using the compass and GPS

The IR sensors are not included for course corrections that have not been prompted by the detection of an obstacle. The integration of the IR sensors are discussed in Section 6.5.

6.4 TURNING

Due to the tracked drive configuration, steering can only be performed by either altering the speed of each TM or counter-driving the direction of the tracks to induce a pinpoint turn.

6.4.1 Stationary Turns

To perform a stationary turn, the track configuration requires both drive belts to be driven in opposing directions at the same rates. This creates a pivot point in the centre of the unit, allowing the robot to turn within the arc swept out by its extremities. Due to the nature of the turn and drive system, a certain amount of scuffing/drag will occur, but is significantly less than if one belt was to remain stationary and the other was used to drag the unit in the direction of rotation. Figure 6-7 illustrates the two methods and required areas to perform a stationary turn.

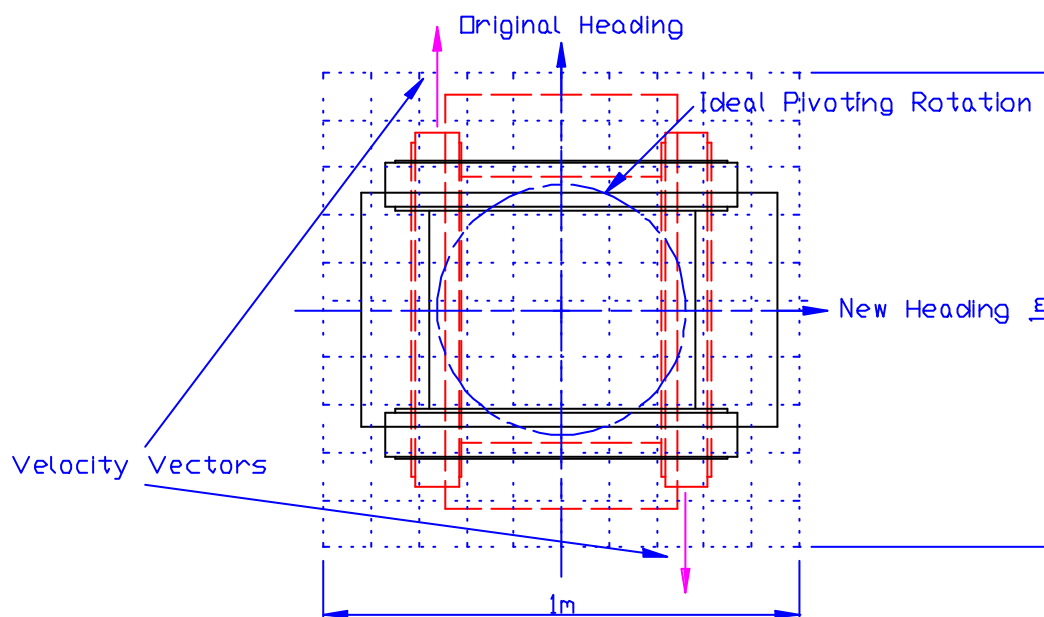


Figure 6-7: Stationary turn methods

6.4.2 Mobile Turns

If the distance and area required to make a turn is not critical, a different technique can be used to produce a smoother flowing turn. To control both the radius and speed of the turn, the drive motors are controlled by either increasing or maintaining constant speed on the outer track of the arc, while decreasing the speed on the inner track. This technique is used for the majority of turns while the unit is in motion. To perform a turn outlined in Section 6.4.1 while in motion, it would require one drive motor to decelerate to a stop, and then accelerate in the opposite direction. This would decrease efficiency, and increase the amount of drag and slippage. Figure 6-8 illustrates the standard technique used to turn a tracked vehicle while in motion.

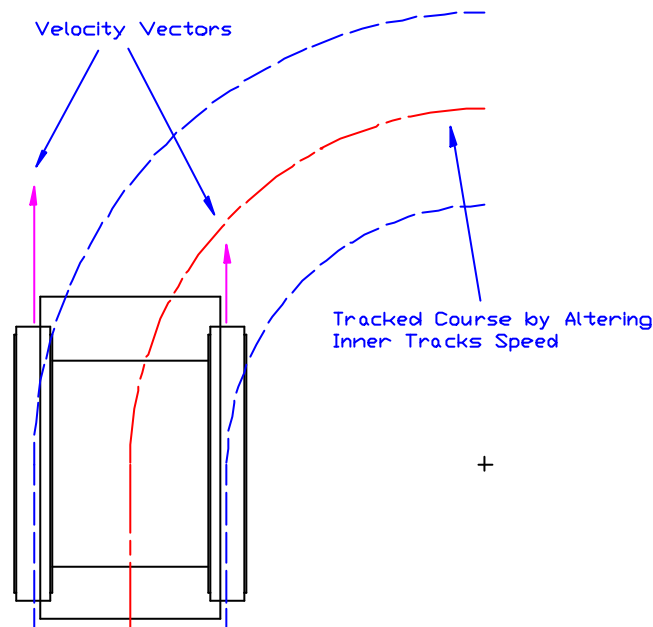


Figure 6-8: Standard turning technique while in motion

6.4.3 Steering Control

In order for the unit to make an informed decision on the type and rate of the turn, it requires the integration of all of the sensor systems and techniques outlined in Section 6.2. Figure 6-9 illustrates the control input and output into a turning control module.

Both the required change in heading and the current speed are fed into the steering module to determine the method and speed of a turn. Within the module, the current speed determines if either a stationary or mobile turning method should be implemented. If the unit was already in motion, the turning module selects the rate at which a mobile turn should commence. The speed of a track during a turn should not exceed the maximum velocity set point determined by the traction controller (discussed in Section 6.2.2). The more significant the change in required heading, the slower the internal track (with respect to the arc generated by the turn) will travel, to reduce both the distance and time it takes to complete the manoeuvre. After the steering controller determines the most efficient method, the relative PWM and directional signals are sent to the motor drivers.

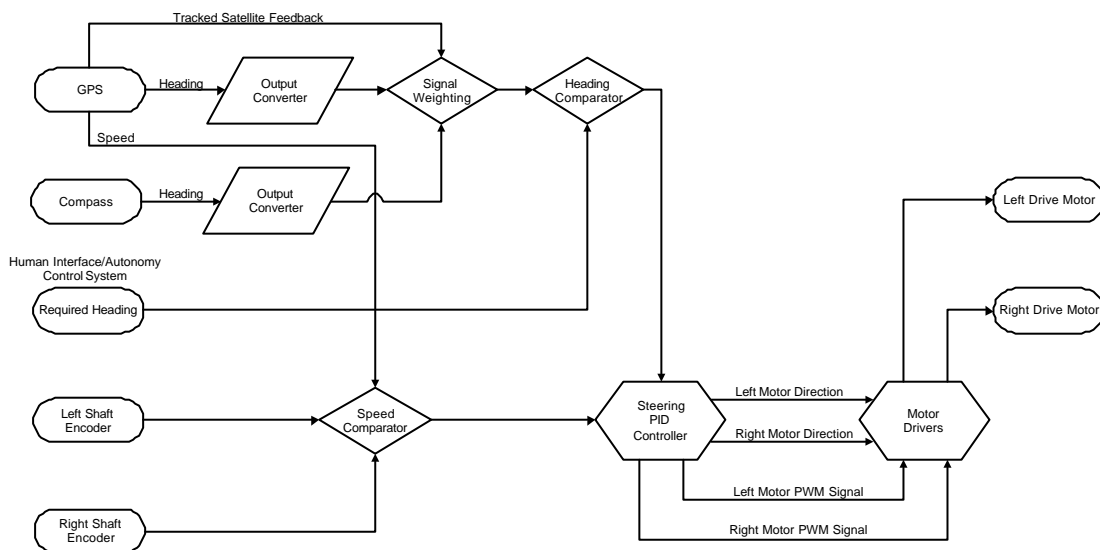


Figure 6-9: Steering controller process diagram

6.5 TERRAIN & OBSTACLE AVOIDANCE

The obstacle detection interface uses all of the pre-existing control systems developed through Sections 6.2 to 6.4, with the addition of the IR sensors to detect and locate obstacles.

6.5.1 Obstacle Evasion

The only sensory means of detecting an obstacle not in direct contact with the unit is through the IR sensors around the perimeter of the chassis. The IR sensors on the plane facing the direction being travelled are the most important. All IR sensors are continually scanning. When an obstacle is detected, the sensory control receives information on the location and distance to the obstacle. In order to differentiate between each sensor and its location around the perimeter, each sensor is independently attached to the DAQ hub, and numbered clockwise in software, starting at the front left (illustrated in Figure 6-10). The course correction sequence for detected obstacles is only initiated if an obstacle is detected in the sensors facing the direction, or intended direction of travel. During normal operation, the side IR sensors will regularly detect obstacles. These signals are generally filtered and ignored, as they have no bearing on the current course (illustrated in Figure 6-10). The side sensors become significant when the unit has to change direction (especially for stationary turns), allowing for the intended heading to be scanned prior to commencing with a change in course.

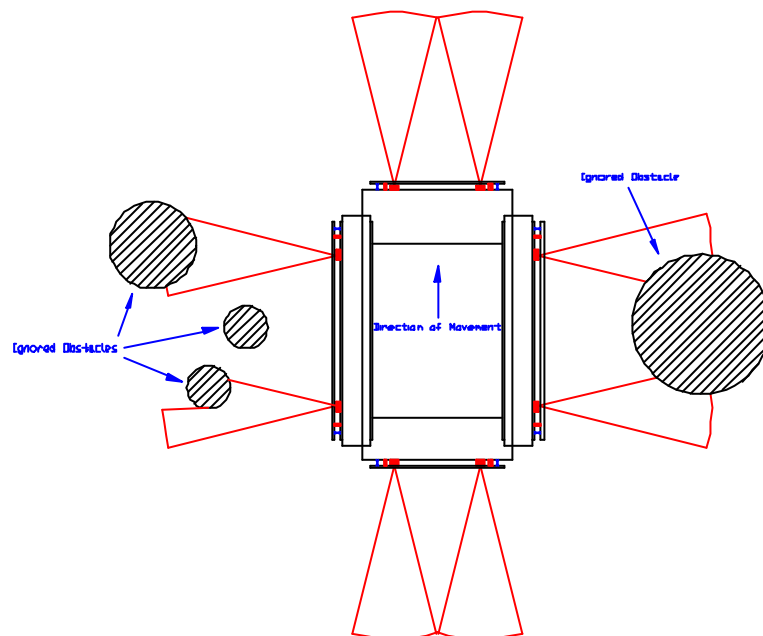


Figure 6-10: Filtered sensor readings

If an object avoids detection by the IR sensors, and comes in contact with the unit, the tactile sensors should activate once direct contact has been made. When activated the tactile sensor(s) will relay a signal back to the main controller.

The final method for detection is in case both the IR and tactile sensors fail to detect an obstacle. Figure 6-11 illustrates an example of the type of terrain that could allow both the IR and tactile sensors to fail in detection process. If the undetected obstacle is sufficiently large or solid to restrict movement, the GPS will detect, in conjunction with the SE's, no (or little) movement for the motor output. In these circumstances the traction controller will initiate. When this fails, the secondary mechanism will engage, notifying that an undetected obstacle is restricting movement, requiring a course change.

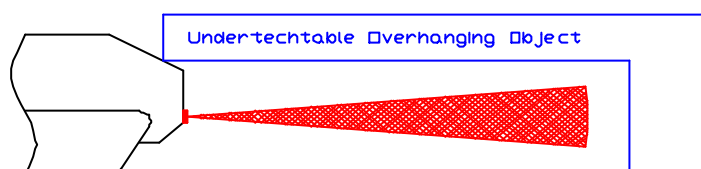


Figure 6-11: Possible terrain profile that can evade current IR and tactile sensor configurations

6.5.2 Terrain Interpretation and Evasion Parameters

With the introduction of a yaw and pitch sensor, the slope of the terrain can be determined and used as a method to reduce the risk of losing traction and perhaps even rolling. This would only require a single interface to the course controller for signalling the contour of the terrain. The sensor signal could then be compared to predefined set points. As the signal from the sensor encroaches on the set points, a change of direction could be implemented by the control system. If the signal equals or exceeds the limits, the unit would track backwards along the path taken until the terrain was sufficiently level to continue on a different heading.

6.5.3 Course Correction Due to Obstacles and Terrain

When an obstacle is detected in the mechatron's path, the sensory control evaluates both sensors on that plane to determine the location and size of the obstacle. Both side sensor pairs are then scanned for obstacles on the left and right. If an obstacle is detected on only one side, the course can be altered using a mobile turn (Section 6.4.2) towards the other side. As the turn is commencing, both the front and side sensors on the inside of the turn are used to detect further obstacles that may be in the way through the turn. If no obstacles are detected, the movement would proceed away from the side that detected the obstacle at the front, otherwise a clockwise rotation is taken as a default heading. Once the obstacle is cleared by the sensors on the outside of the arc, the course can be re-corrected parallel with the original bearing. This cycle continues until the unit is back on its original course (using the GPS).

During mobile course correction turns, if obstacles continue to get closer to the unit, the overall speed will decrease proportionally to the detected distances to the obstacles. When obstacles are detected at 40cm, all forward movement is stopped. This allows the unit to perform a stationary turn (Section 6.4.1) to scan the terrain for obstacles. After the scan has been completed, the unit can continue on an unrestricted course, correcting its bearings to eventually continue on its original path.

If the sensors detect obstacles that will make contact during a stationary turn, the unit will follow a reverse heading until it has sufficient room to proceed with a turn. Figure 6-12 illustrates the control logic to be implemented to avoid obstacles.

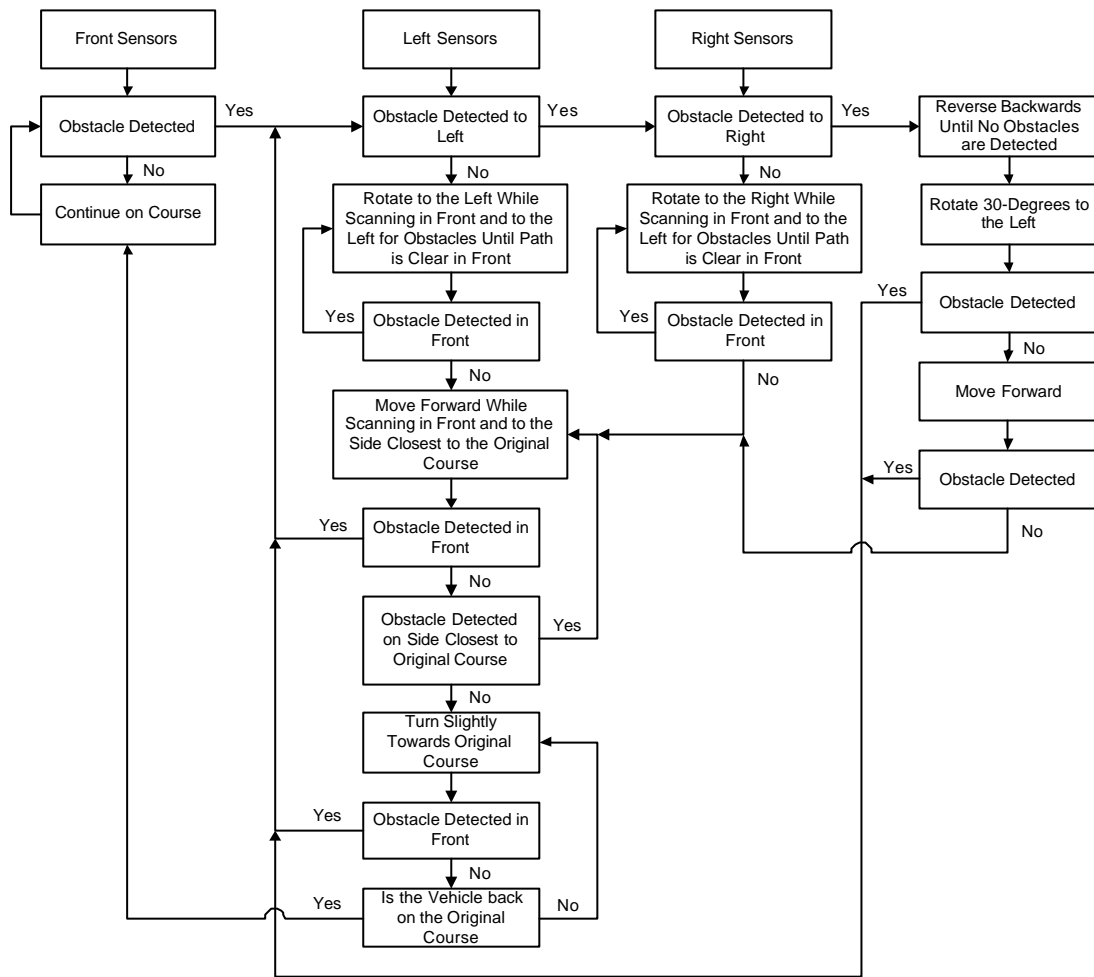


Figure 6-12: Obstacle Evasion Control Diagram

6.6 MOTOR CONTROL THEORY & EVALUATION

To control the wheelchair motors, it is necessary to develop a variable speed drive system. In order for this to be done efficiently, it is necessary to determine the motor's transfer functions.

6.6.1 PWM Control

Pulse width modulation (PWM) is a technique of using a square wave of constant mark to space ratio as an approximation to a DC supply voltage. The DC voltage is approximately given by the amplitude of the square wave multiplied by the duty cycle. The PWM signal is defined by three properties: a period T , duty cycle t/T , and amplitude V_o . If the PWM is passed through a low pass filter, the (co)sinusoidal

components from the PWM waveform can be largely removed, leaving only the DC term of:

$$u(t) = \frac{V_o t}{T} \quad \text{Eqn. [6-1]}$$

An advantage of the PWM system is that by pulsing the supply voltage, the amount of continuous current being supplied to the motors via the motor driver circuits is reduced, hence simplifying the motor driver design. The drive motors for this project are driven from a 24VDC power supply. The speed at which the motors are driven is controlled by the duty cycle of the PWM wave.

Due to the timing inaccuracies caused by the software and DAQ system on the main computer, the '552 (Section 5.5) is used to generate the PWM signal to feed the motor driver circuits (Section 5.4). As the '552 is an 8-bit microcontroller, the PWM signal has a maximum resolution of 256 (2^8). In this implementation, the lower the value sent to the PWM, the greater the time the output remains at 24V. Figure 6-13 illustrates corresponding PWM values to signal waves.

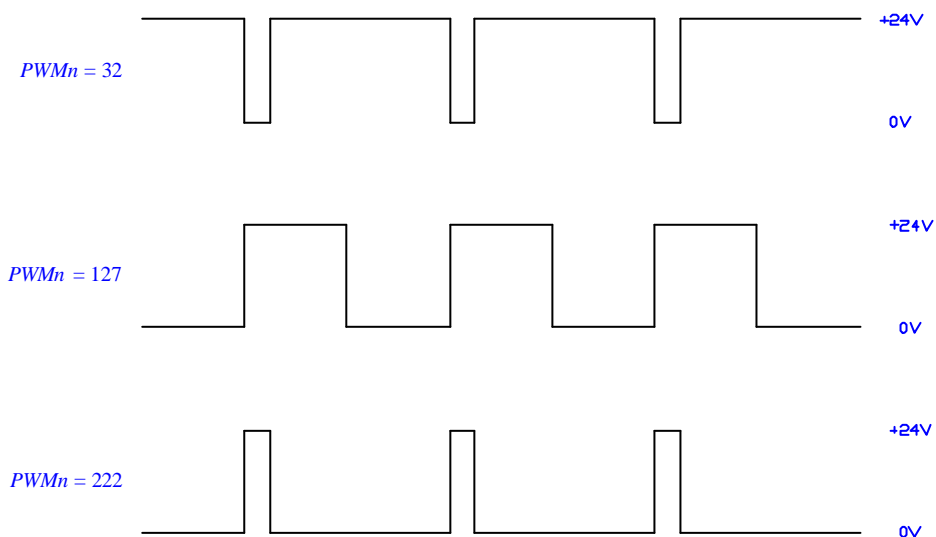


Figure 6-13: PWM signals and corresponding waveforms

As the '552 has two independent PWM ports (PWM0 & PWM1), isolated control for each motor is possible. The '552 uses an 8-bit pulse width modulation prescaler (PWMP) to generate the repetition frequency, which supplies the clock signal for the counter. The repetition frequency f_{PWM} at the PWM_n outputs is generated by Equation [6-2] below:

$$f_{PWM} = \frac{f_{OSC}}{2 * (1 + PWMP) * 255} \quad \text{Eqn. [6-2]}$$

where f_{OSC} is the operating frequency of the '552, which is set to 14.75 MHz. Therefore, for this example $f_{PWM} = 28.9$ kHz. The generated PWM signal is sent from the '552 into motor driver circuit to control the speed of the motors.

6.6.2 Braking

Contained in the back of the drive motor units is a braking friction element. This element can be engaged by sending an 8 – 16 VDC signal to the actuating solenoid. Figure 6-14 illustrates the system configuration at the rear of each motor.

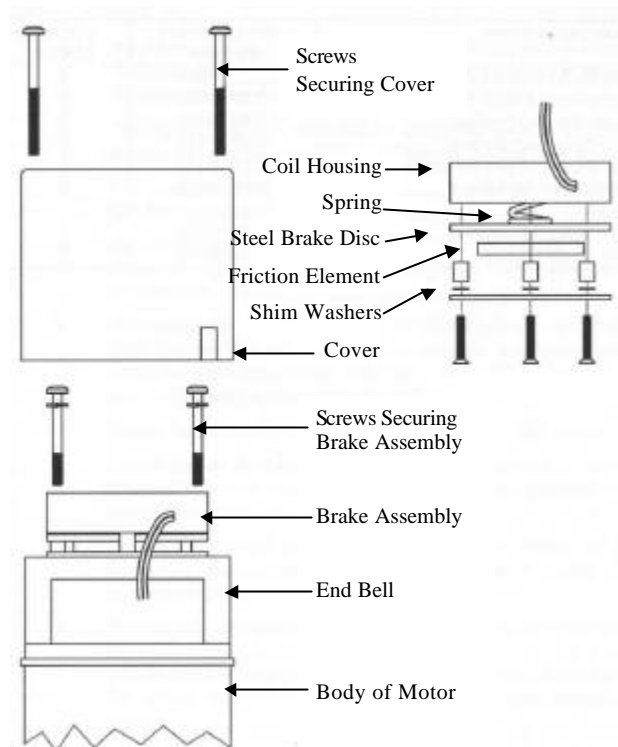


Figure 6-14: Brake assembly

Although this mechanism has little influence with regard to resistance applied to the end of the motor shaft, it is extremely useful as a park brake. While the tracked configuration requires an excessive gradient to induce a natural roll (experimentally determined to be 32-34 degrees on a smooth timber surface) the braking mechanism can ensure the tracks do not freely rotate.

Due to the configuration of the drive system, once the PWM signal ceases, the unit will halt almost instantaneously on a flat surface. As discussed above, if the unit is travelling on a gradient in excess of 30-degrees, the park brakes may have to be engaged.

6.6.3 DC Motor Theory Transfer Function

A DC motor consists of an inductor with a large number of windings in between a magnetic field generated by permanent magnet. Considering a simple inductor with a single coil as shown in Figure 6-15a, the current passing through the inductor in the presence of a magnetic field induces the opposing forces F_1 and F_2 . In accordance with Lorentz Law:

$$F(t) = I(t)l \times B \quad \text{Eqn. [6-3]}$$

where:

B = magnetic field flux density

l = length of the inductor within the magnetic field

$I(t)$ = Current flow through the inductor

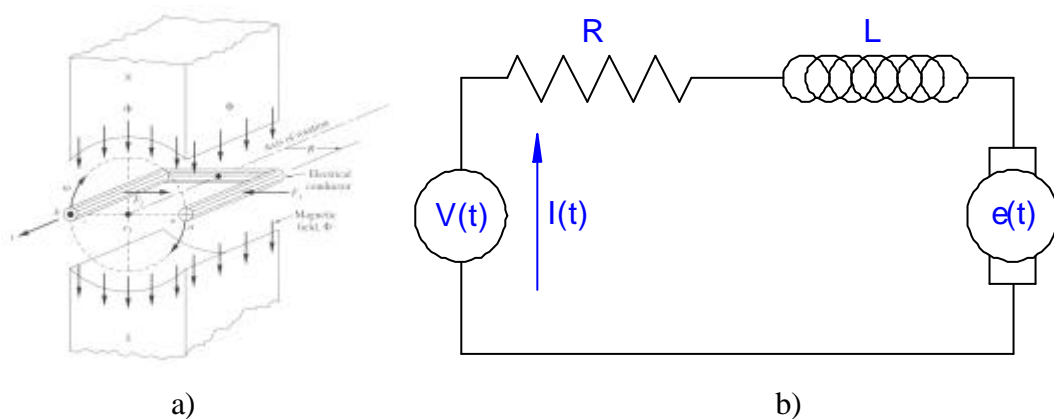


Figure 6-15: a) Single loop DC motor model b) Basic DC electrical model

The torque on the motor shaft is given by:

$$T(t) = K_t i(t) \quad \text{Eqn. [6-4]}$$

where: T = induced torque
 $K_t = Brl$ = torque constant

When the armature (rotating inductor) starts to rotate in the magnetic field, it generates a voltage which opposes the motor current, called the back emf (e) such that:

$$e(t) = K_e w(t) \quad \text{Eqn. [6-5]}$$

where: K_e = back emf constant; $K_e = K_t = K$
 w = angular frequency of the armature

Rearranging the circuit illustrated in Figure 6-15b, and applying Kirchhoffs Law gives:

$$V(t) = i(t)R + L \frac{di(t)}{dt} + e(t) \quad \text{Eqn. [6-6]}$$

where: i = the motor current
 R = armature resistance
 L = armature inductance

Evaluating the mechanical model, Newton's second law (Equation [6-7]) illustrates that the applied torque is equal to the inertia of the armature multiplied by the angular acceleration of the motor. To simulate the model as accurately as possible, it is necessary to make allowances for subsidiary forces such as viscous friction generated by the armature bearings.

$$T(t) = J \frac{d\omega_m}{dt} + B_v \omega_s(t) \quad \text{Eqn. [6-7]}$$

where: T = motor torque
 J = motor inertia

ω_m = rotational speed of the shaft

B_v = viscous friction

To control the drive motors as efficiently as possible, it is necessary to calculate the transfer function for the system. To do so it is useful to apply Laplacian transforms to convert from the time domain (t), to the frequency domain (s).

Converting Equation [6-6] to the frequency domain yields:

$$V(s) = I(s)(sL + R) + E(s) \quad \text{Eqn. [6-8]}$$

where: $E(s) = K_e \Omega_m(s)$

Rearranging Equation [6-8] gives:

$$I(s) = (V(s) - K_e \Omega_m(s)) \frac{1}{sL + R} \quad \text{Eqn. [6-9]}$$

Now evaluating the mechanical model, Equation [6-10] yields:

$$T(s) = Js\Omega_m(s) + B_v \Omega_m(s) \quad \text{Eqn. [6-10]}$$

Rearranging Equation [6-10] gives:

$$T(s) = \Omega_m(s)(Js + B_v) \quad \text{Eqn. [6-11]}$$

Equation [6-11] (mechanical system) and Equation [6-9] (electrical system) can be combined to obtain the transfer function between the applied voltage and the resultant angular velocity of the motor, shown in Equation [6-12]:

$$\frac{\Omega_m(s)}{V(s)} = \frac{K_t}{K_t K_e + B_v R + s(B_v L + JR) + JLs^2} \quad \text{Eqn. [6-12]}$$

As the output from the motor is configured to drive directly onto the attached gearbox, the output speed is reduced and the torque is increased. A secondary step further

reduces the speed as the output shaft from the pulley drives onto the track (acting as a secondary planetary gearbox). This series of reductions alters the mechanical system of the motor, slowing the response and thereby increasing the mechanical time constant, τ_m . As per Equation [2-2], the speed on the track can be related to the speed of the motor by the following:

$$\omega_t = \left(\left(\frac{N_{track}}{N_{planetary}} \right) * N_{gearbox} \right) * \omega_{ms} \quad \text{Eqn. [6-13]}$$

And the torque generated at the track is:

$$T_t = \left(\left(\frac{N_{track}}{N_{planetary}} \right) * N_{gearbox} \right) * T_m \quad \text{Eqn. [6-14]}$$

where:

$$\begin{aligned} \omega_t &= \text{track speed} \\ \omega_{ms} &= \text{motor speed} \\ T_t &= \text{track torque} \\ T_m &= \text{motor torque} \end{aligned}$$

The total torque for the system (τ_{total}) can be shown as:

$$\tau_{total} = \frac{J + \left(\left(\frac{N_{track}}{N_{planetary}} \right) * N_{gearbox} \right)^2 J_L}{B_m + \left(\left(\frac{N_{track}}{N_{planetary}} \right) * N_{gearbox} \right)^2 B_L} \quad \text{Eqn. [6-15]}$$

Simplified:

$$\tau_{total} = \frac{J_T}{B_T} \quad \text{Eqn. [6-16]}$$

where:

$$\begin{aligned} J_T &= \text{total inertia} \\ B_T &= \text{total friction} \\ J_L &= \text{load inertia} \\ B_L &= \text{load friction} \end{aligned}$$

The block diagram of the transfer function, including the gearbox, and planetary track configuration is shown below in Figure 6-16.

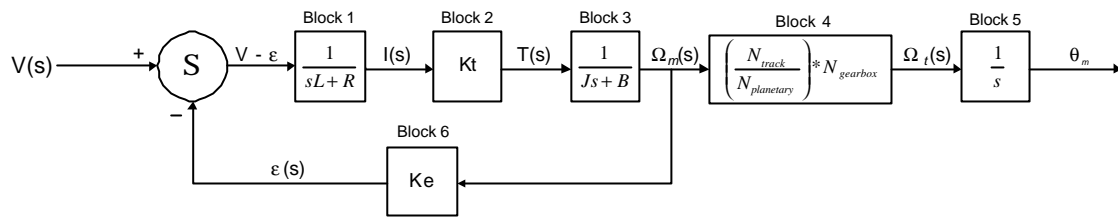


Figure 6-16: Block model of the DC motor transfer function

Block 1 in Figure 6-16 represents the electric pole and acts as a low pass filter. Block 2 converts the electrical current into torque for the armature. Block 3 acts as the mechanical pole, and block 4 represents the gearing mechanism, producing the final output speed (Ω_r). Block 5 represents the motor's position (θ_m). Block 6 converts the angular velocity into back emf.

6.6.4 Experimentally Determining the Motor Specifications

Due to the integrated configuration of the motors, the New Zealand manufacturer could not supply the data sheets on the motors with all the required specifications. As per Section 2.3.1, the maximum power output, no load current, torque constant, and internal resistance of the motors have been supplied. The remaining information to be determined included the inductance, back emf constant, and the mechanical time constant. The inductance of the motor was measured at 0.40 mH. To determine the back emf constant required the motor to be run as a generator, measuring the induced voltage across the input terminals, generating a relationship between the output voltage and the input speed. The experimentally determined value was 4.0 V/krpm (± 0.2 V/krpm).

To determine the mechanical time constant, a 24V-stepped pulse was used to drive the motor while a data logger tracked the motor output (rpm) over time. The mechanical time constant (τ_m) is then taken at the point where the motor output reaches 63.2% of the

maximum output. Figure 6-17 shows the drive motor's step response for a 24VDC input.

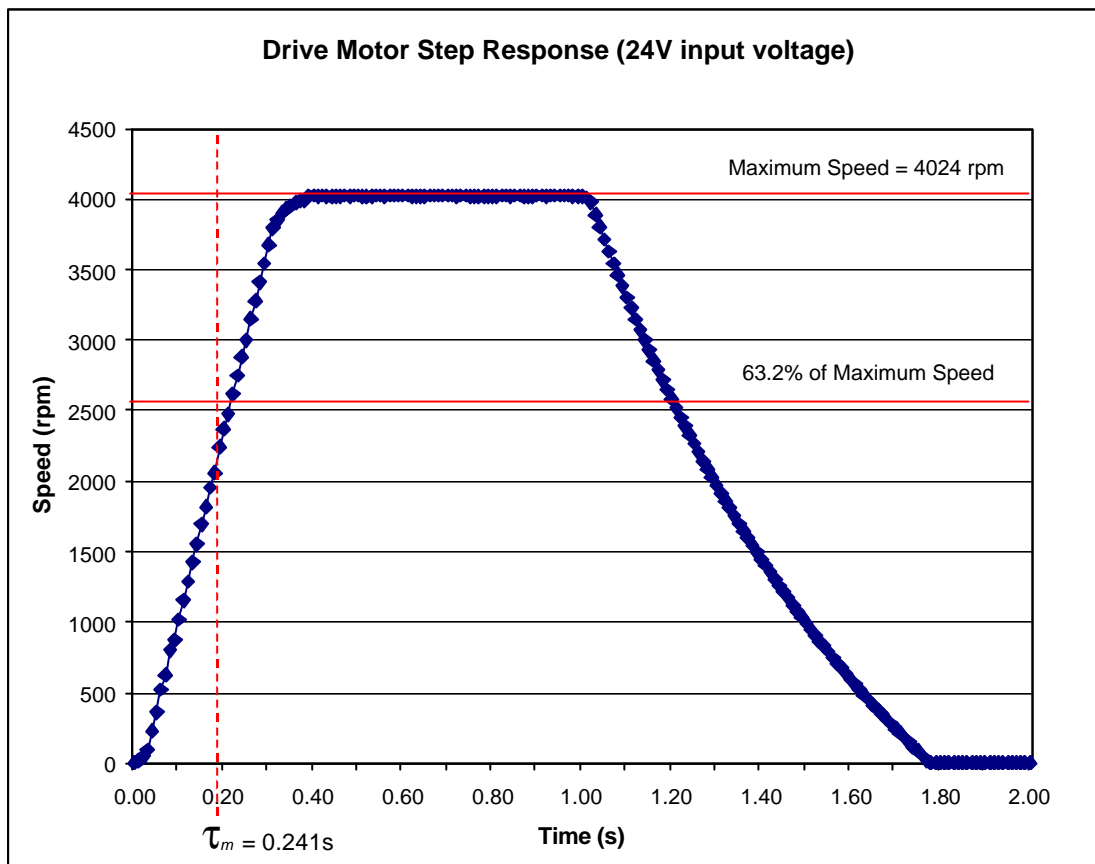


Figure 6-17: Drive motor step response for a 24VDC input

From Figure 6-17 above, it can be seen that τ_m is 0.241s as it takes 0.381s to reach the maximum velocity of 4024 rpm.

6.6.5 PID Controller

Using the motor specifications supplied in Section 2.3.1 and the constants determined in Section 6.6.4, the step response was modelled using Simulink, a dynamic system simulation for Matlab. Simulink has been used to evaluate and tune the PID controllers for adjusting the PWM signal for optimal control over steady state and transient errors. The advantage with a PID controller is its ability to provide an satisfactory degree of error reduction with suitable stability and damping. The general form of a PID controller is given by:

$$D(s) = K\left(1 + \frac{1}{T_I s} + T_D s\right) \quad \text{Eqn. [6-17]}$$

where: $D(s)$ = controller transfer function
 K = gain
 T_I = integral time
 T_D = derivative time

To obtain acceptable performance for the system, the constants K , T_I , and T_D in Equation [6-17] must be carefully calculated. This is referred to as “tuning the controller”. To perform the tuning of the motor system, the Ziegler-Nichols method was applied for a decay ratio of 0.25, so that the dominant transient decays to a quarter of its value after one period of oscillation. Listed below are the Ziegler-Nichols tuning rules applied for the PID controller:

$$K = 1.2/RL$$

$$T_I = 2L$$

$$T_D = 0.5L$$

where K , R , and L are determined from the unloaded step response (Figure 6-17), as illustrated in Figure 6-17.

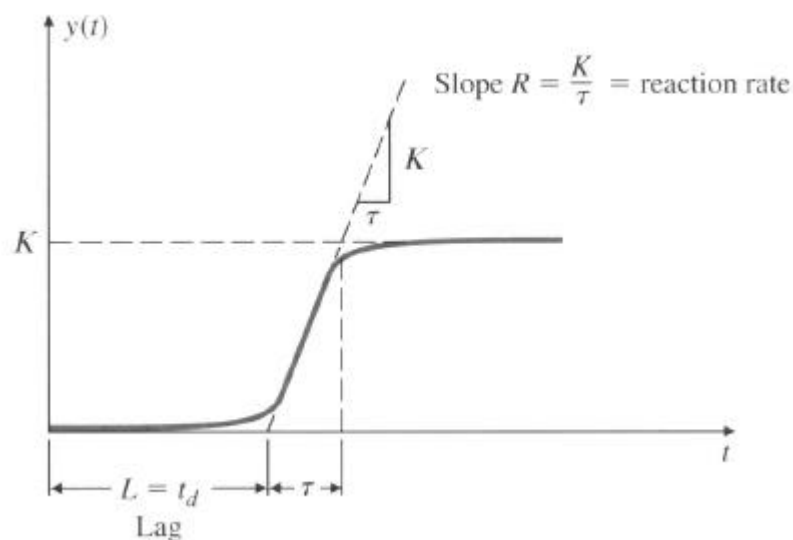


Figure 6-18: Process reaction curve

From the step response illustrated in Figure 6-17, the following constants have been determined:

$$L = 0.028$$

$$R = 12550$$

$$K = 1255$$

$$T_I = 0.056$$

$$T_D = 0.014$$

Figures 6-19, 6-20, and 6-21 illustrate the Simulink model with a PWM input source of initially 50 percent, wheelchair motor transfer function, and PID controller respectively. Figure 6-22 shows the step response through the PID control system to obtain the nominal motor speed of 3950 rpm.

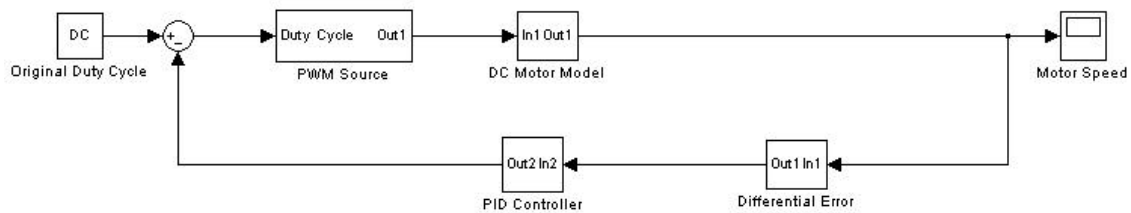


Figure 6-19: Overview of Simulink model of the drive motors

where the DC motor model consists of:

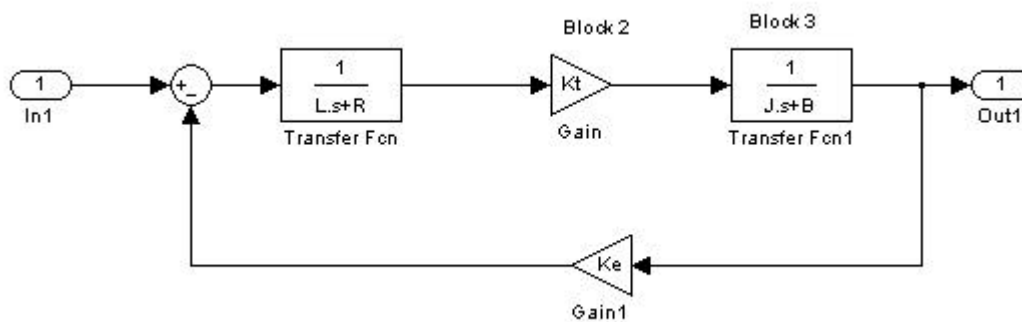


Figure 6-20: Sub-system of the DC motor model within Figure 6-19

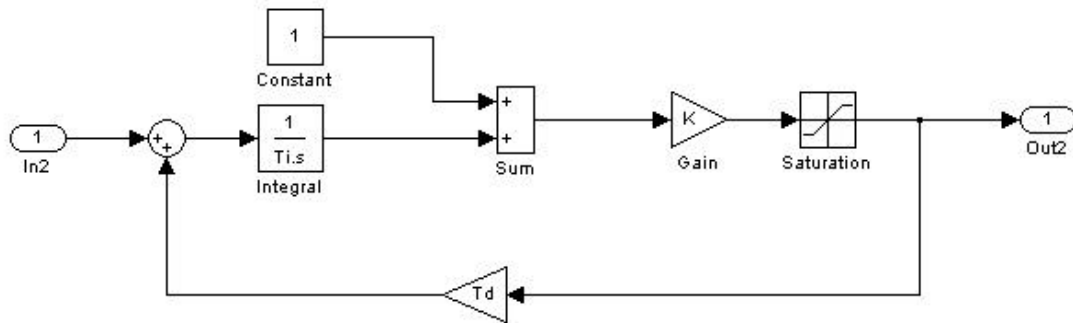


Figure 6-21: PID control system

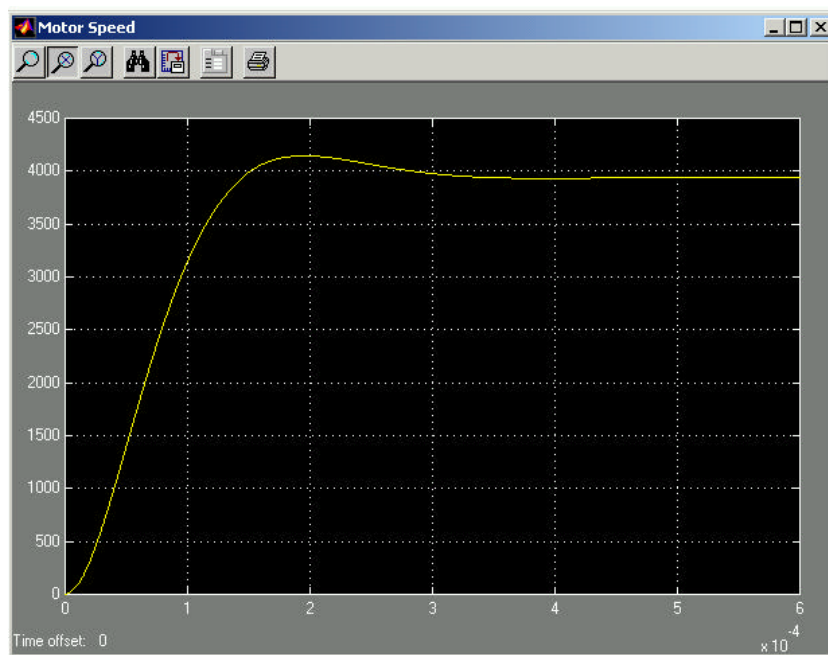


Figure 6-22: Step response through the PID controller to obtain a nominal output speed of 3950rpm

The PID controller developed within Simulink has been designed specifically for the mechatron's wheelchair motors. The controller adjusts the duty cycle of the PWM input to compensate for fluctuations in motor response. Due to time constraints, the PID controller has not been installed, but as Matlab is compatible with LabVIEW such an implementation should be straight forward.

7. CONCLUSION

7.1 RESULTS

As outlined in the objectives in Section 1.2, a large-scale vehicle has been designed and constructed specifically for coping with the chaotic nature of an outdoor environment. The design allows for rough terrain to be traversed through a powerful drive and gearing system. The track design incorporates a dynamic tensioning and bogie mechanism that allows the tracks to contour to the terrain without derailing or jumping teeth on the belt.

The scale of the vehicle allows for a wide range of electronic equipment to be carried onboard, with a large battery reserve. The dimensions of the vehicle allow for a stable chassis design, reducing the risk of capsizing while travelling across rough terrain. Many measures have been taken to reduce the effects of environmental hazards, such as: zinc electroplating of all ferrous metals, the use of non-ferrous metals where applicable, and encapsulating electronic components in acrylic cases.

The electronics are based around a central computer, and another microcontroller has been interfaced to correct for timing delays in PWM signals generated by LabVIEW. As well as PWM signals, the microcontroller board includes additional peripherals such as a RTC, digital input switch panel, and LED arrays for port signals.

In addition to the construction of a functioning drive interface, sensors have been incorporated within the vehicle, including IR proximity sensors, Shaft Encoders, Electronic Compass, and GPS. Battery chargers have been installed to allow direct charging of the lead acid batteries through a single 230VAC connection.

Due to the physical size of the vehicle, a radio control unit has also been interfaced with the microcontroller, enabling the mechatron to be easily transported without powering up the entire system.

Appropriate high current motor drivers have been developed to accept a PWM signal and supply 24V at up to 10A to the drive motors.

7.2 FUTURE WORK

The following extensions could be made to further develop the autonomy and functionality of the vehicle.

7.2.1 Laser Range Finder

A laser range finding device (discussed in Section 2.4.4) would enable the vehicle to detect obstacles potentially up to ten metres away. This long-range detection instrument would be able to scan (up to 360-degrees) the terrain to locate the most efficient course correction to avoid obstacles. A laser range finder has already been developed for the Mechatronics Group (Hurd, 2001). As the interface equipment is included onboard the vehicle, few modifications would be required to implement such a device.

7.2.2 Tactile Sensors

Due to time constraints, the attachment of the tactile sensors was not completed. Once the aluminium case is finished, the tactile sensors and bump bars are to provide secondary protection from contact with obstacles. The interface and configuration is outlined in Section 5.8.2.

7.2.3 Interface DragonTalk Voice Recognition Software

DragonTalk software has been installed on the onboard computer to provide a human speech interface for recognising and carrying out voice commands. As DragonTalk is designed to covert recognisable audio into text based documents, it was intended to

interface the designated text commands into LabVIEW as stored string arrays. LabVIEW has the ability to open and close documents and interface bi-directionally with documents. This sequence would allow DragonTalk to convert audible speech into text, then allow LabVIEW to scan text documents for recognised commands (comparing to stored text strings) and use the commands to activate vehicle systems.

7.2.4 Interface Pitch Sensor

As stated in Section 6.5.2, a yaw and pitch sensor is required to both reduce the risk of system failure due to steep hazardous terrain, and to correct the electronic compass signal for heading errors associated with varying inclines. As the commercial sensors are expensive, this could be implemented using either a series of mercury switches or IR sensors. Mercury switches orientated at different angles could approximate pitch and yaw in incremental steps. Comparing four IR sensors measuring the distance to the ground could also approximate the pitch and yaw of the terrain it is currently traversing.

7.2.5 System Integration Implementation

The system integration discussed in Chapter Six should be implemented as per the flow diagrams using LabVIEW. Due to the limitations with the IOTECH DAQ board, the mechatron first requires a (more LabVIEW compatible) National Instruments DAQ card. By using LabVIEW in conjunction with such a DAQ card, all peripherals can be interfaced to the central computer, in an intuitive, modular, graphical format.

7.3 SUMMARY

This project has successfully developed a functioning multi-terrain vehicle. Emphasis has been placed on the design and construction of the track configuration and chassis design. The developed dynamic drive system is capable of traversing a range of outdoor terrains. All mechanical components have been designed for both practicality and operability, and are easily assembled. The track module design reduces operating wear, requiring little to no maintenance.

To control and drive the motors, electronics have been developed to interface both with a central computer and additional microcontrollers. All onboard electronics are powered by a self-contained battery source. The central computer is powered through a UPS and ATX power supply, and incorporates a DAQ card for interfacing system peripherals. The microcontroller board has been over-designed to increase functionality both for development work, and future research. Human interfaces include a radio control system and the potential for speech recognition. Onboard charging units are included to re-energise the batteries.

A range of sensing and navigation equipment has been interfaced to aid in intelligent autonomous control for the future. Interfaced electronics include an array of eight IR proximity sensors, shaft encoders, compass, and GPS. Consideration has been given to the interfacing of the control system to the sensing and navigation electronics.

Extensive measures have been taken to reduce environmental effects (such as weather conditions and static electricity) on the vehicle, including the encapsulation of sensitive electronic equipment. Independent acrylic cases have been made for each set of circuits. This allows each circuit to be accessed separately and enabled a compact utilisation of space within the internal cavity of the vehicle. The acrylic casing allows for all components to be clearly visible during development.

Figure 7-1 shows the completed multi-terrain vehicle (excluding case). Figure 7-2 shows the completed mechatron travelling outdoors.

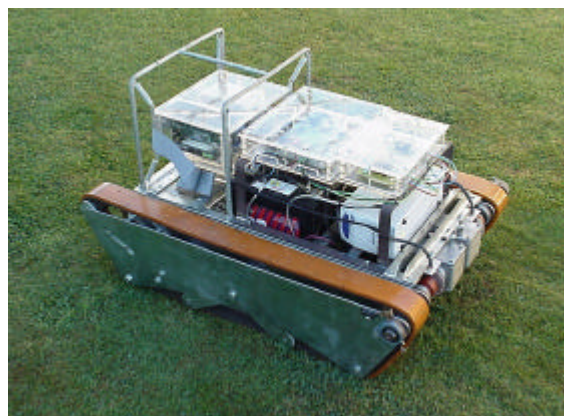


Figure 7-1: Completed multi-terrain vehicle

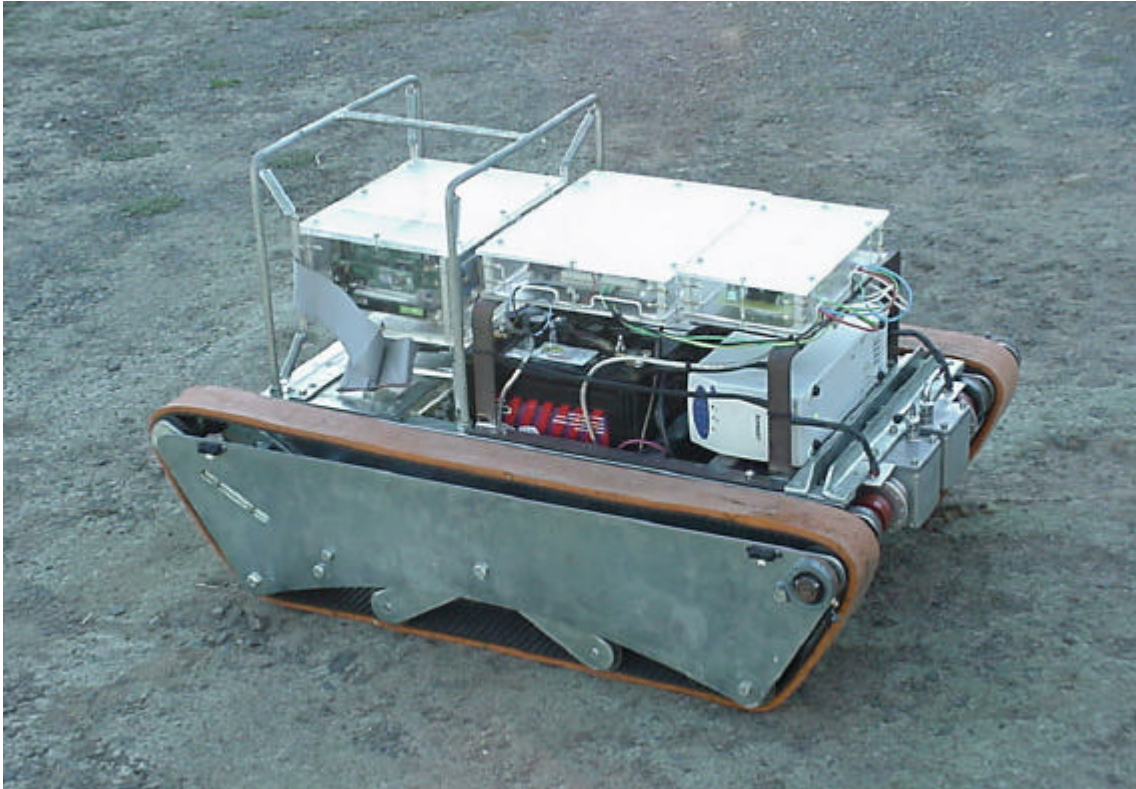
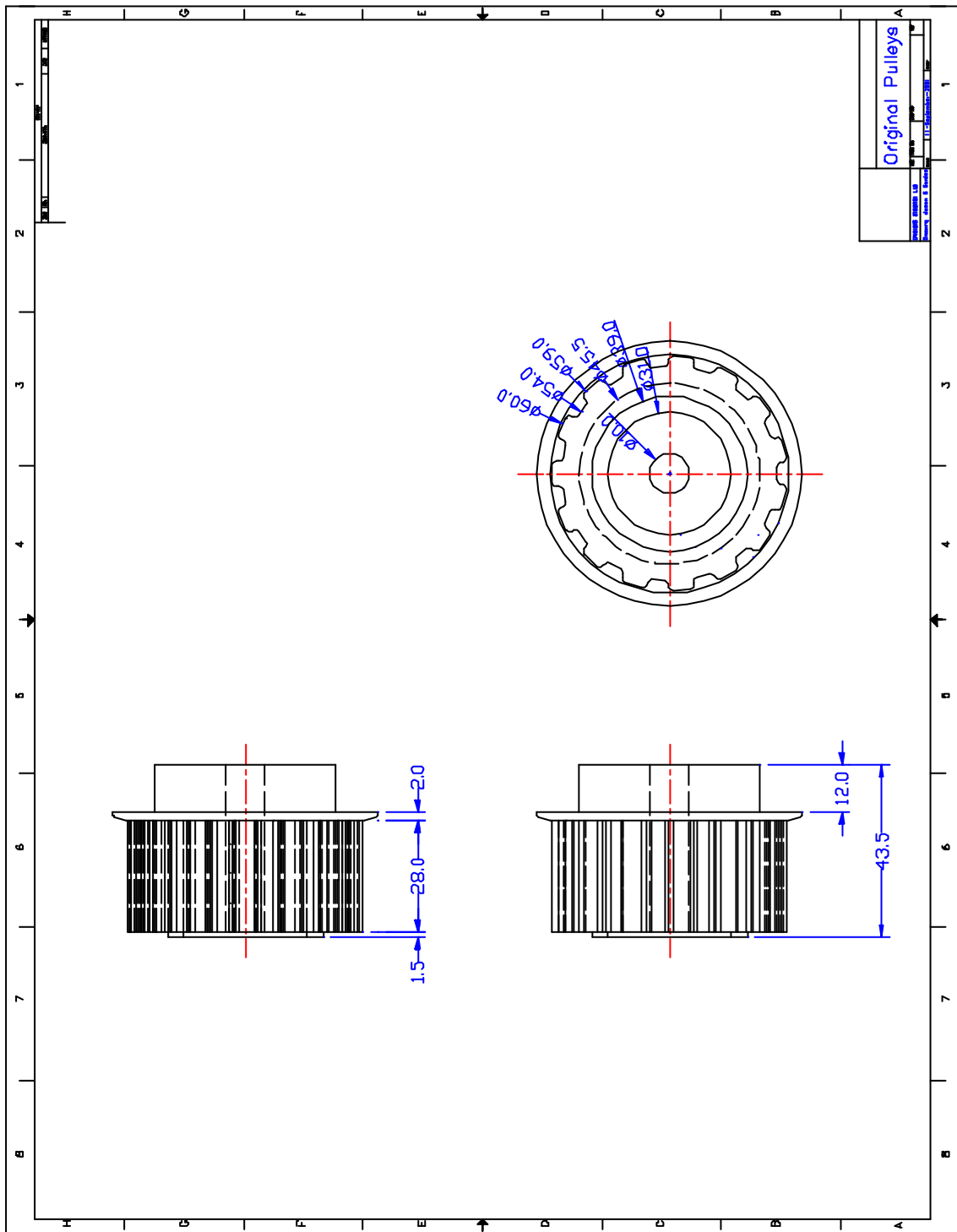
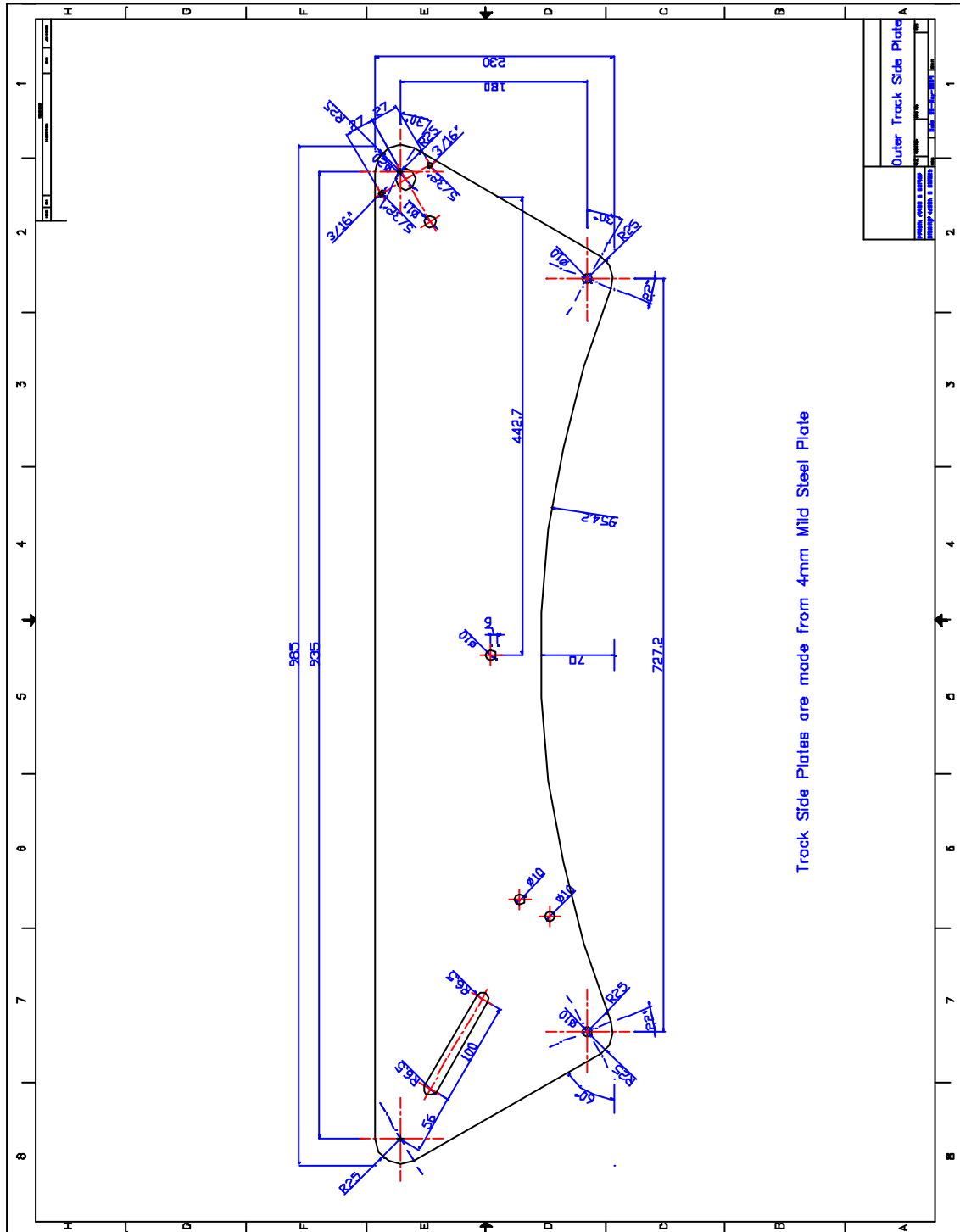


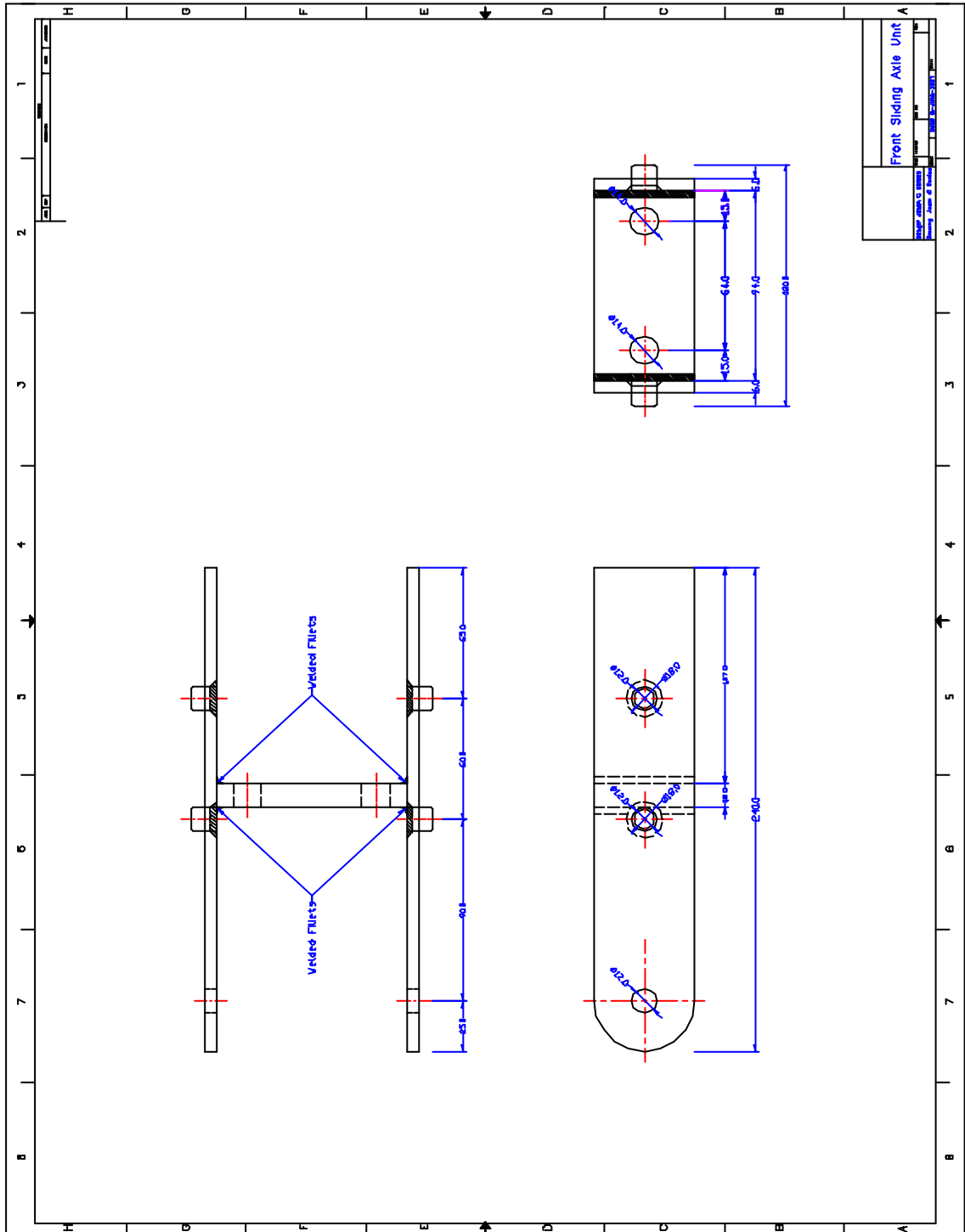
Figure 7-2: Mechatron travelling outdoors

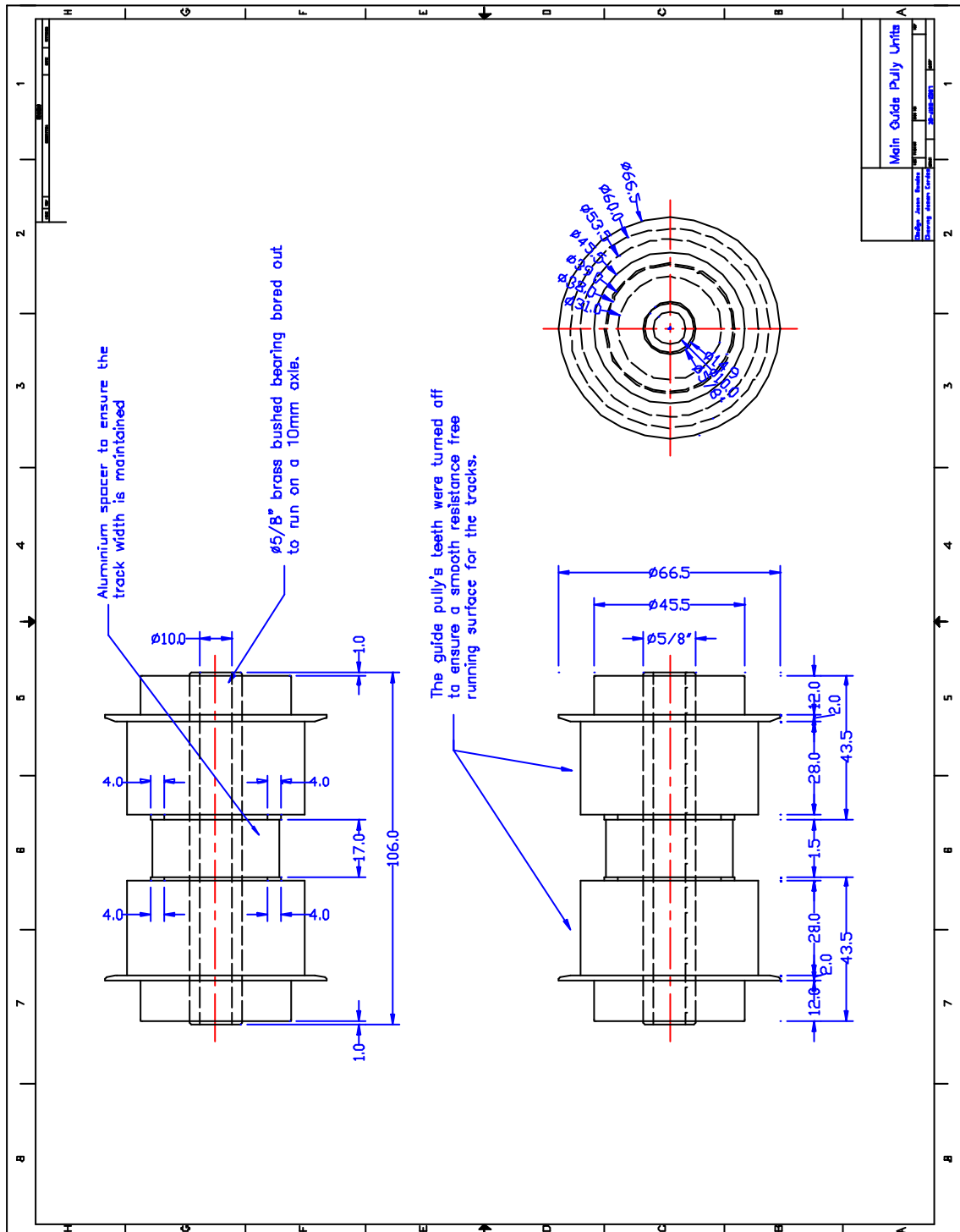
Included on the CD-ROM at the back of this thesis are videos of the mobile vehicle in operation.

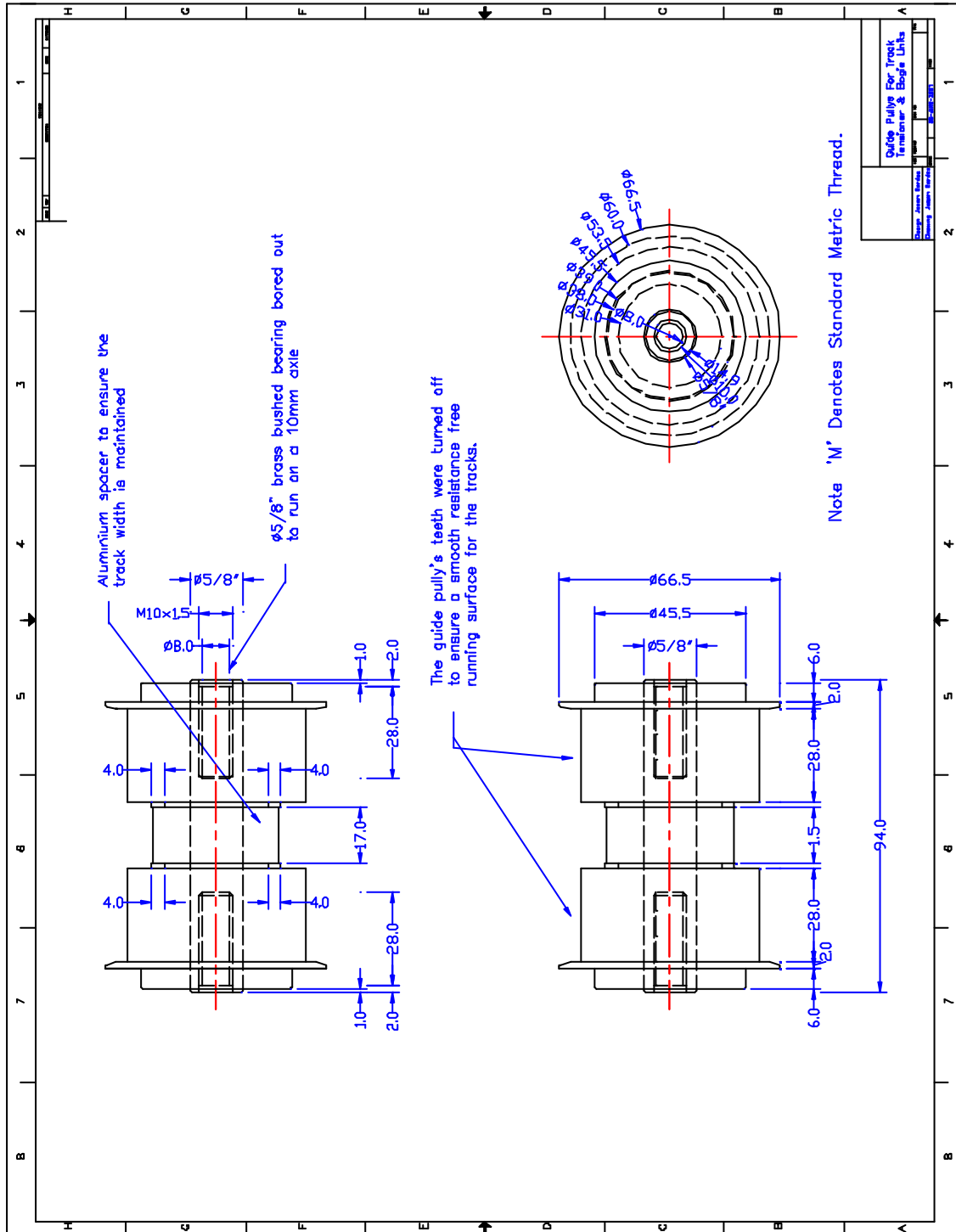
This project has exceeded the original objectives. In addition to completing a mobile multi-terrain device, the unit developed is physically larger than that expected, and therefore has the ability to carry a far greater payload. The mechanical component of this project required more resources, and was far more complex than the original proposal predicted. This was mainly due to the unavailability of pre-manufactured components and designs. At the completion of this project, a suitable foundation has been developed to continue research using multi-terrain vehicles at the University of Waikato.

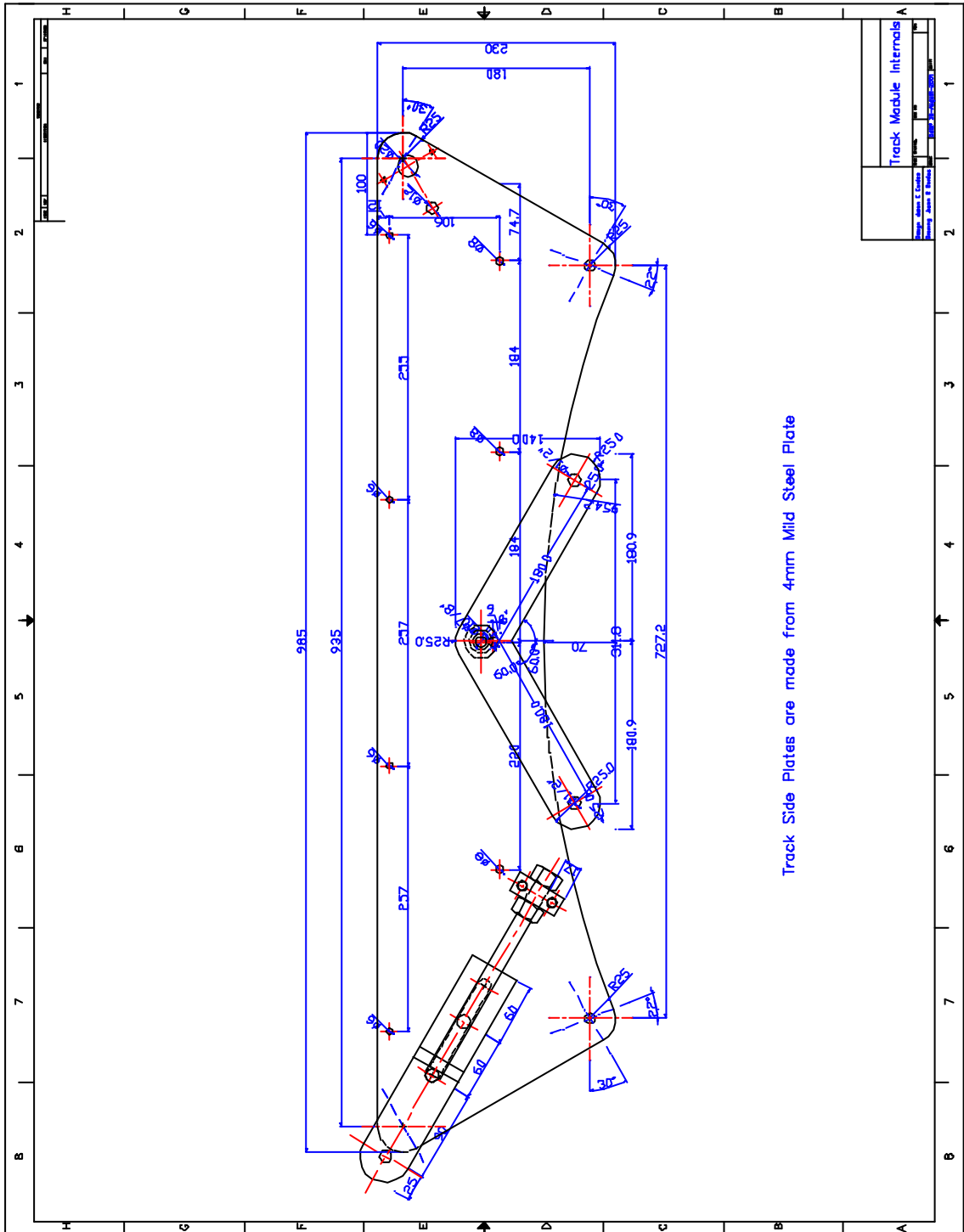




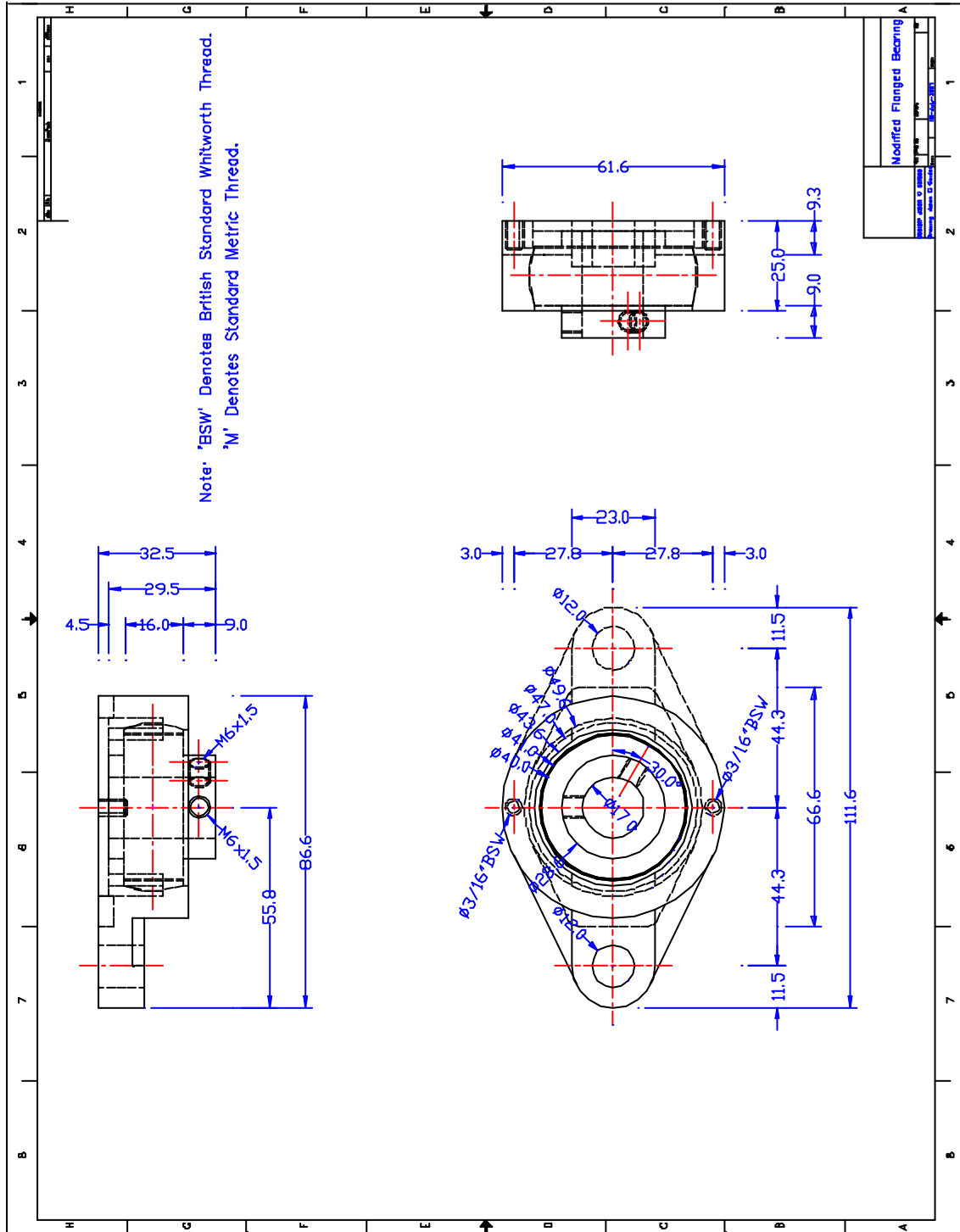


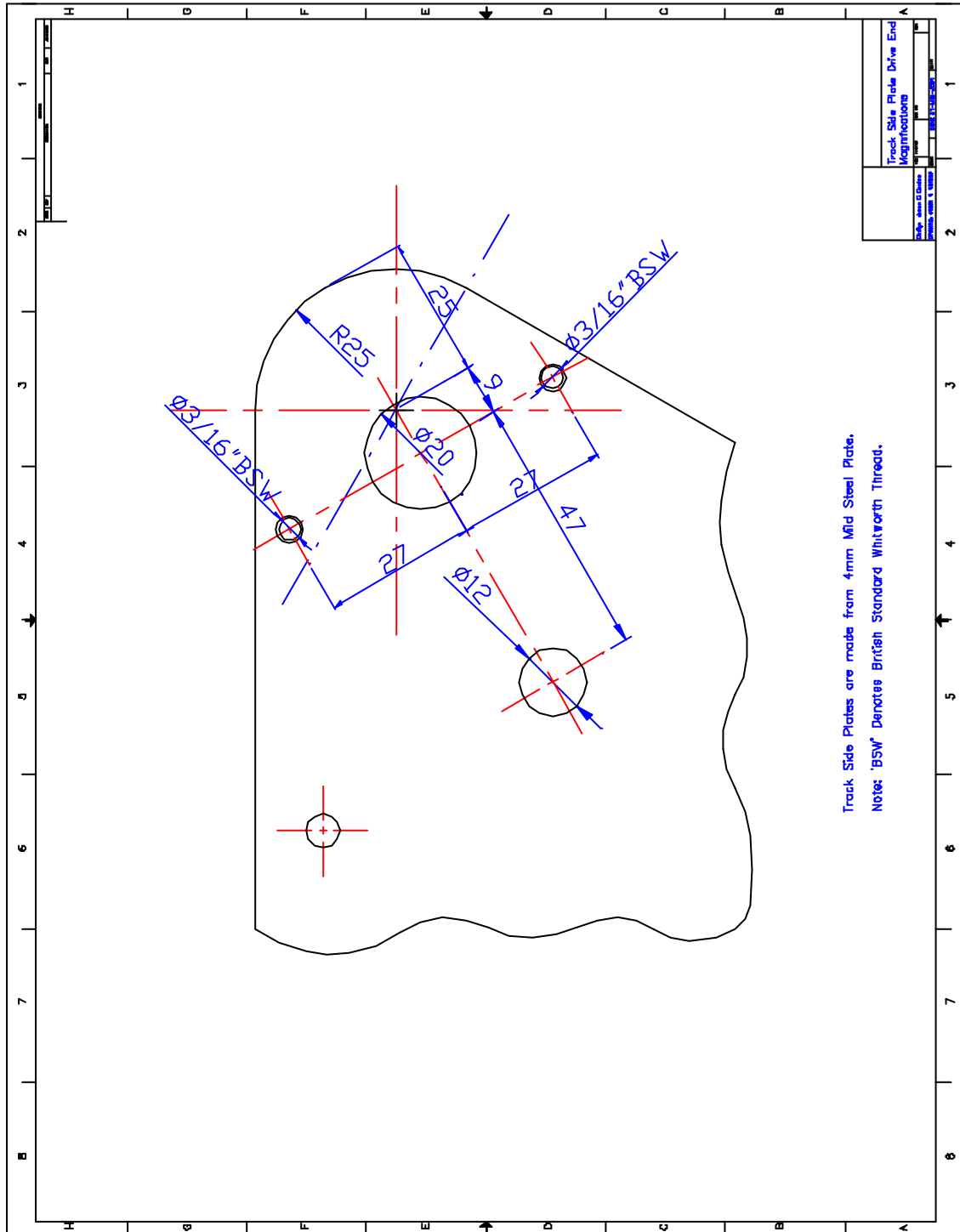


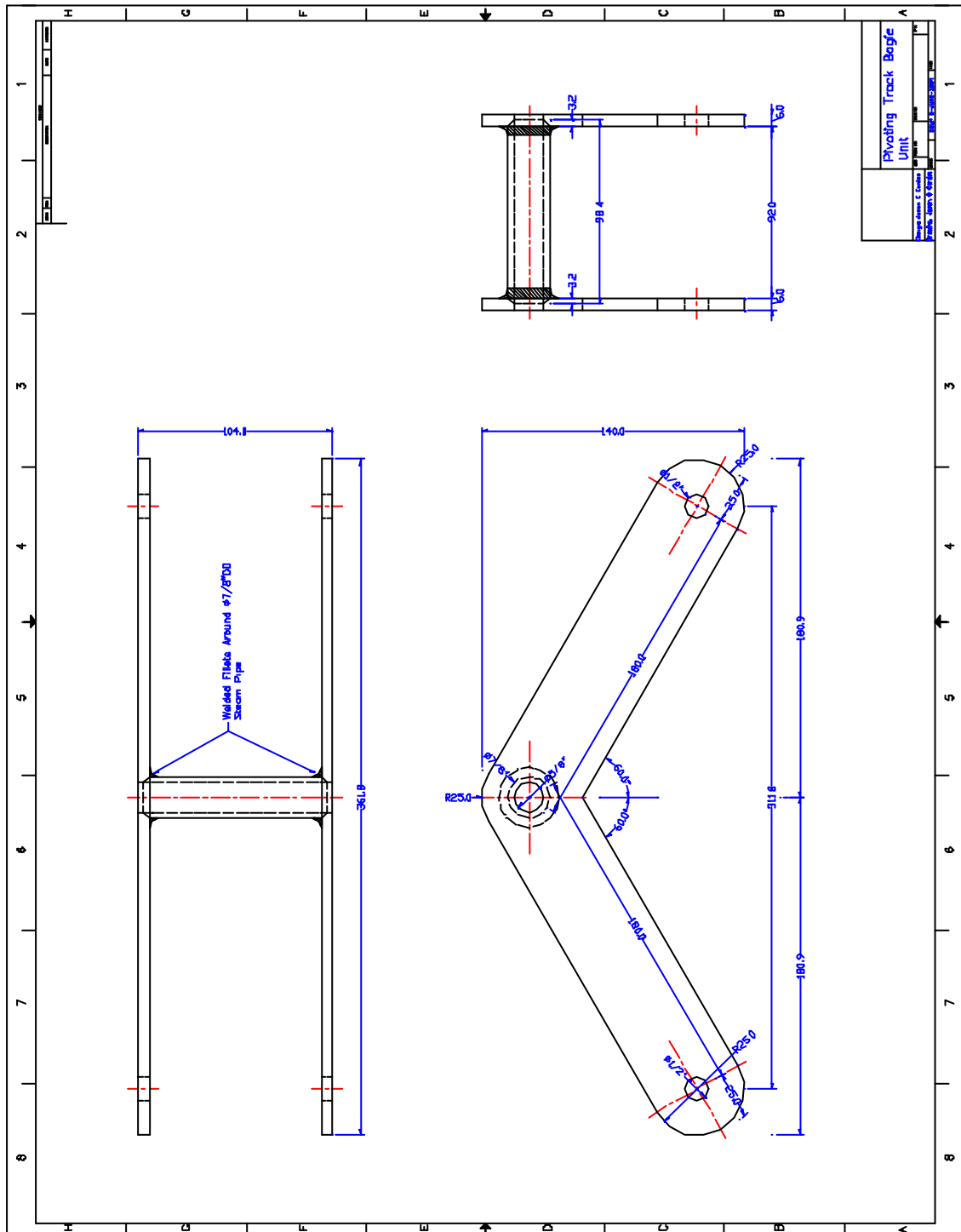


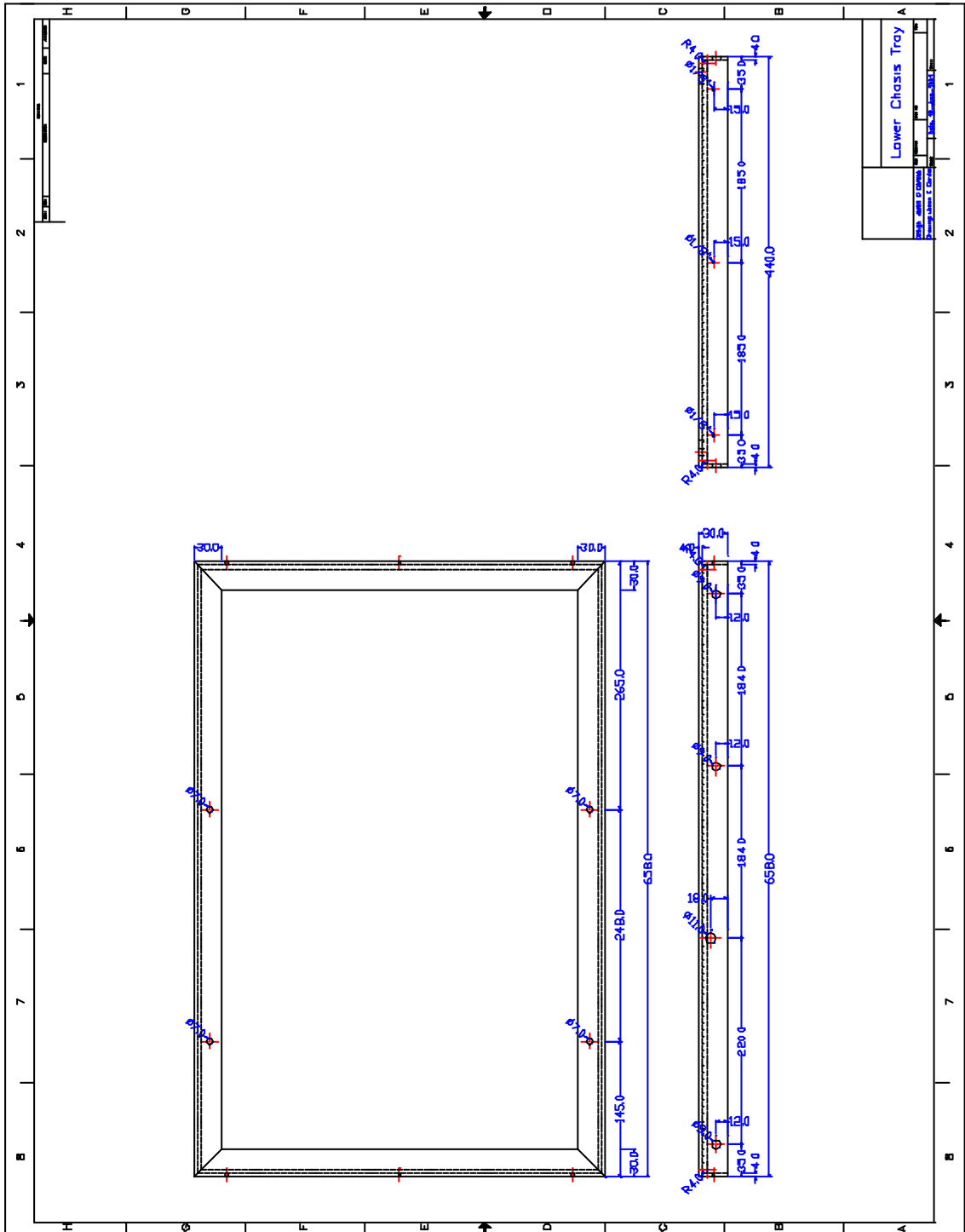


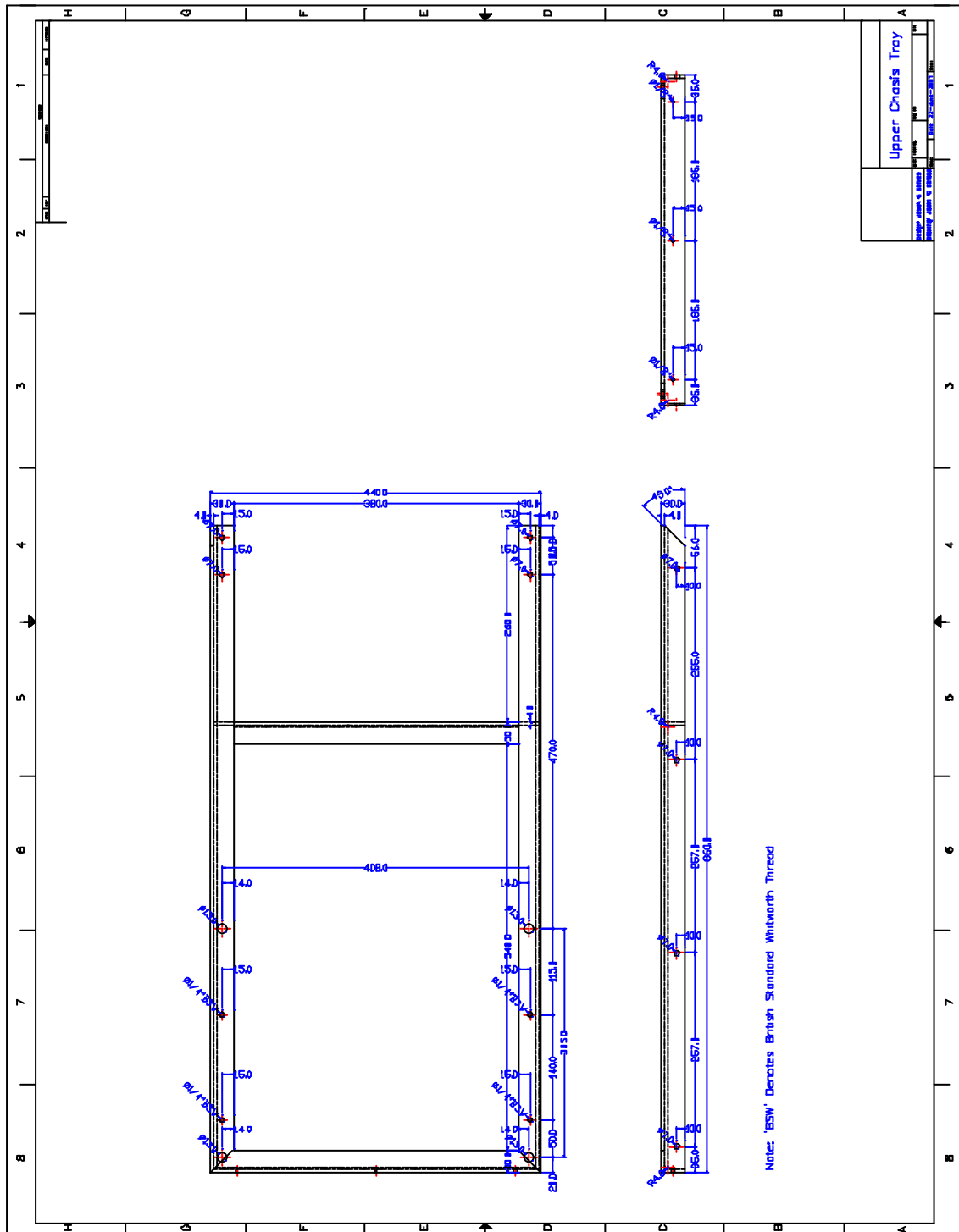
Track Side Plates are made from 4mm Mild Steel Plate

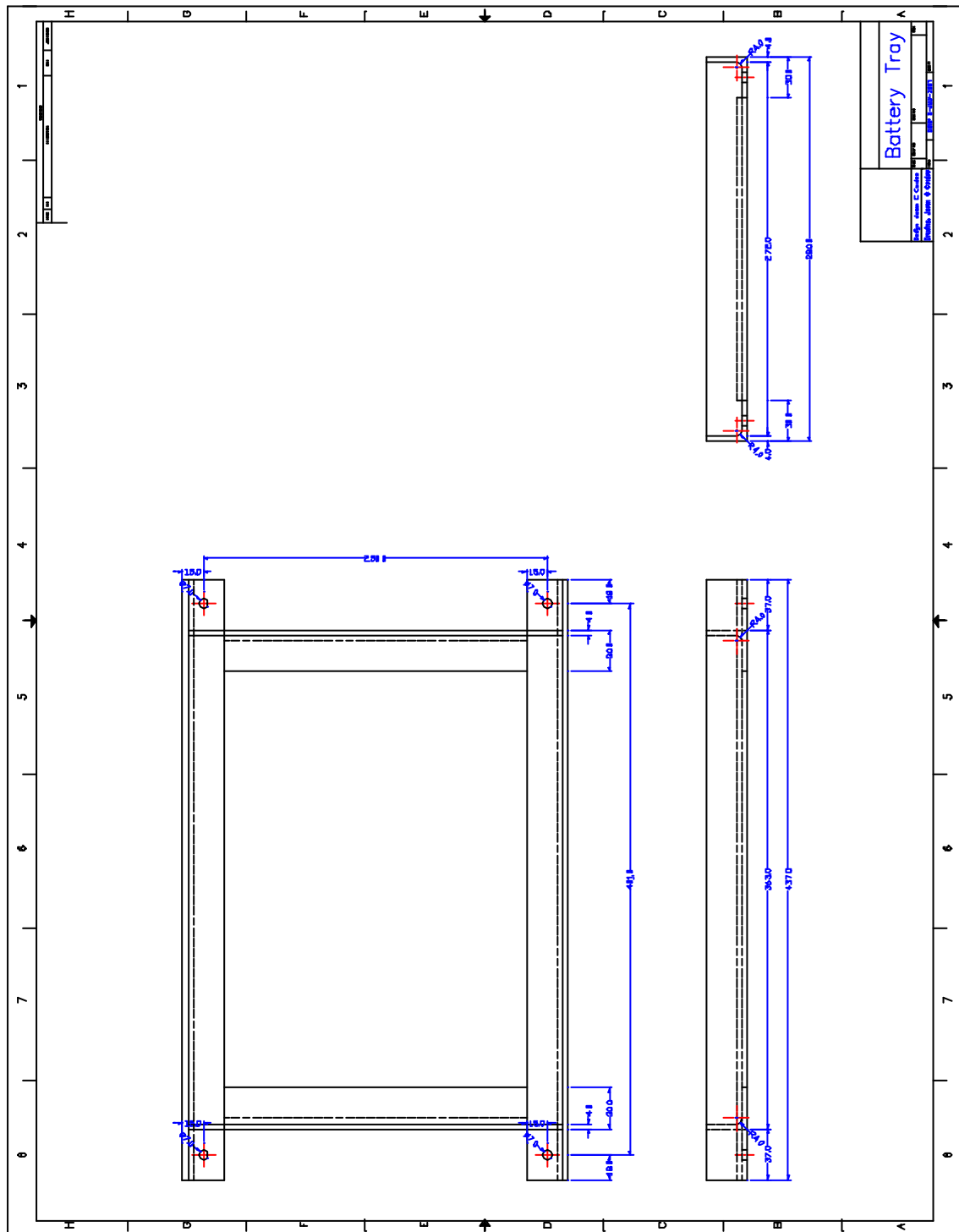


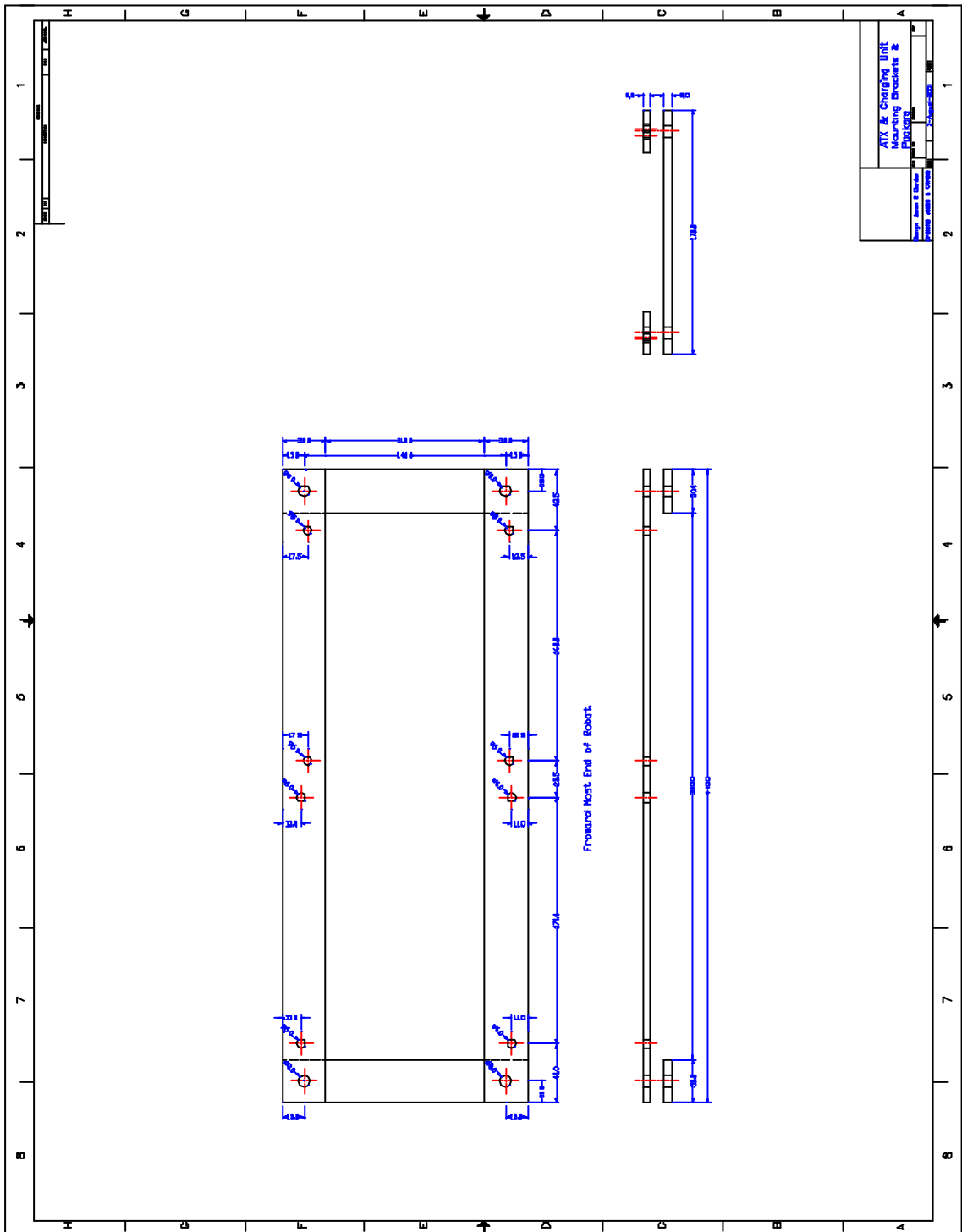


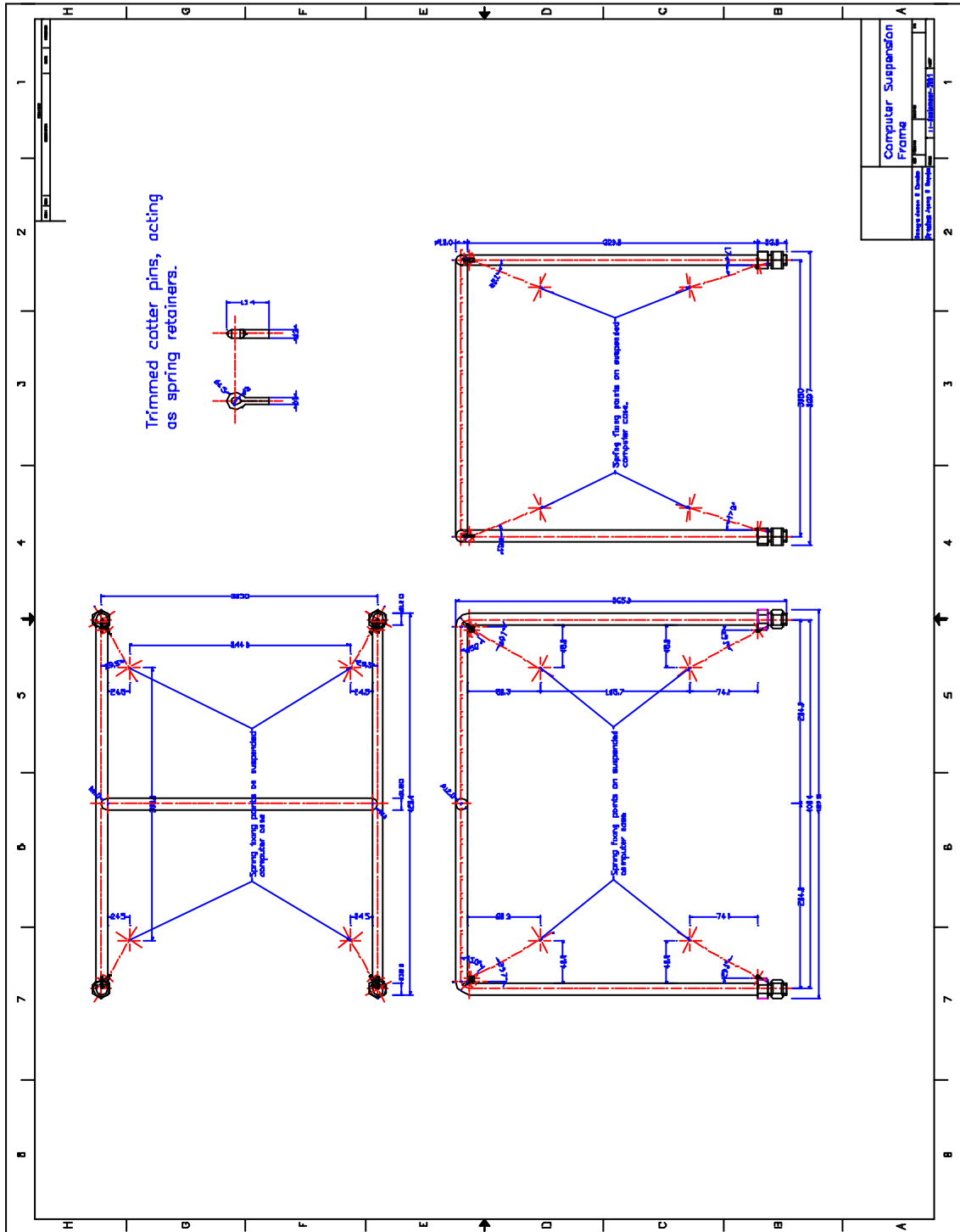


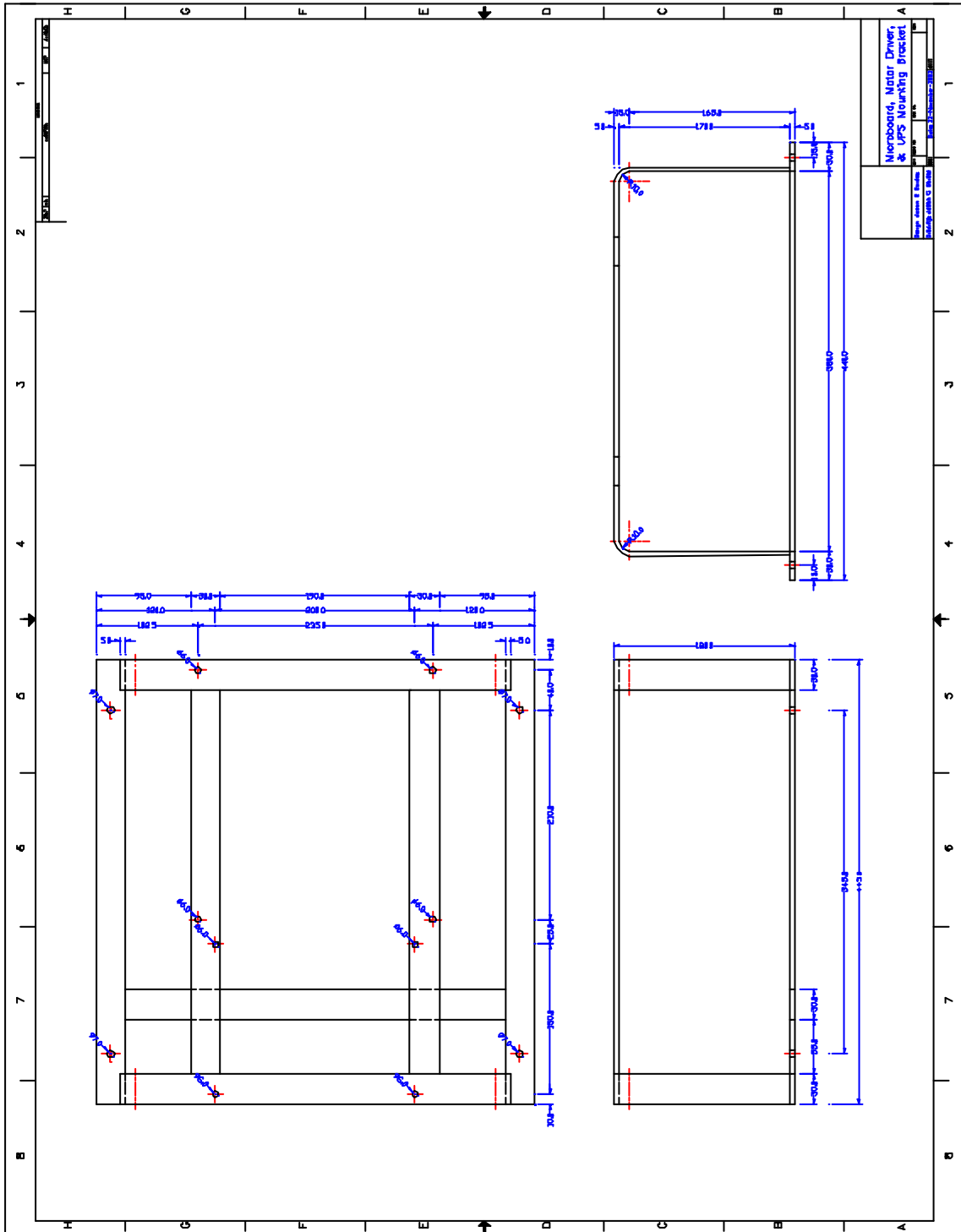


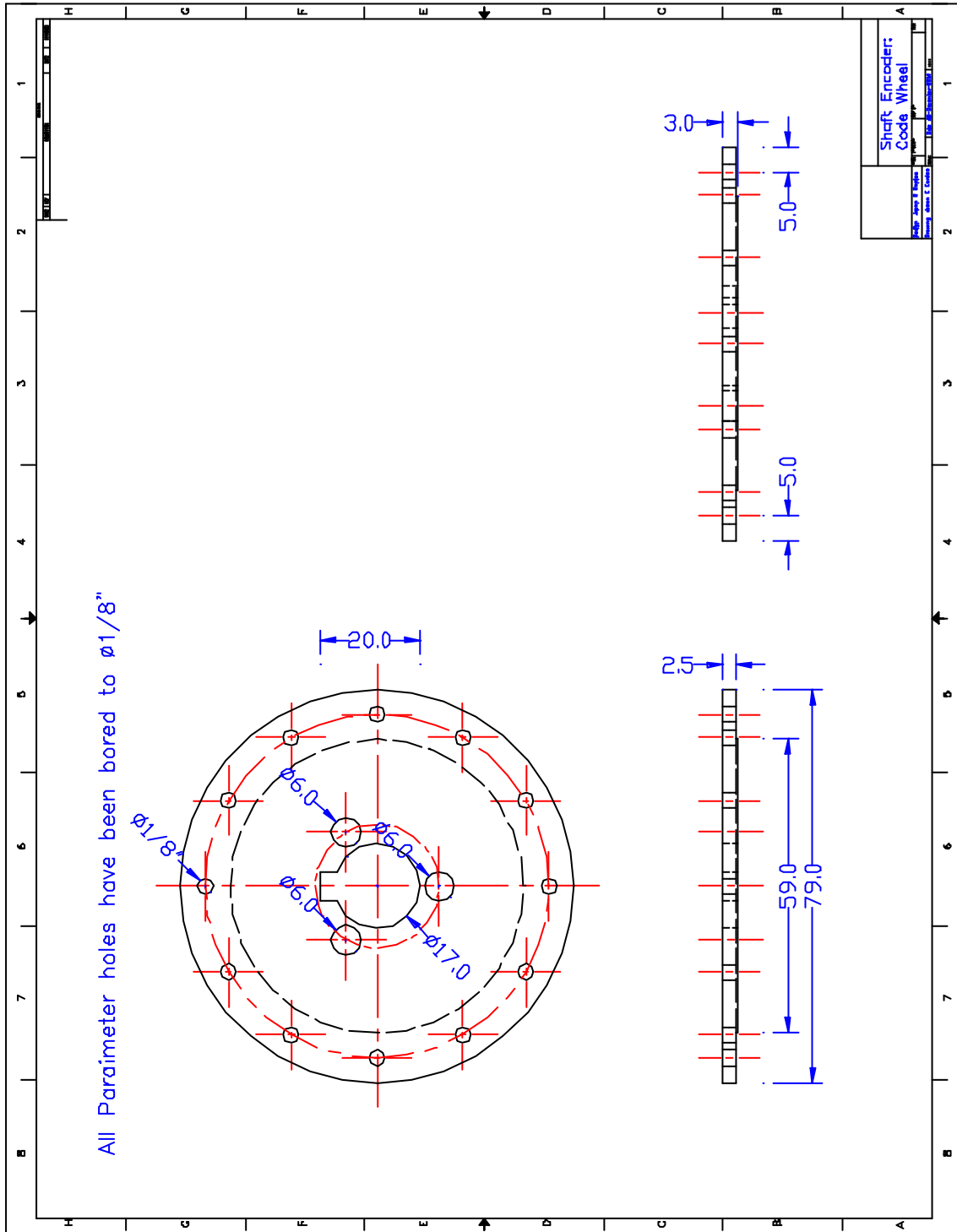


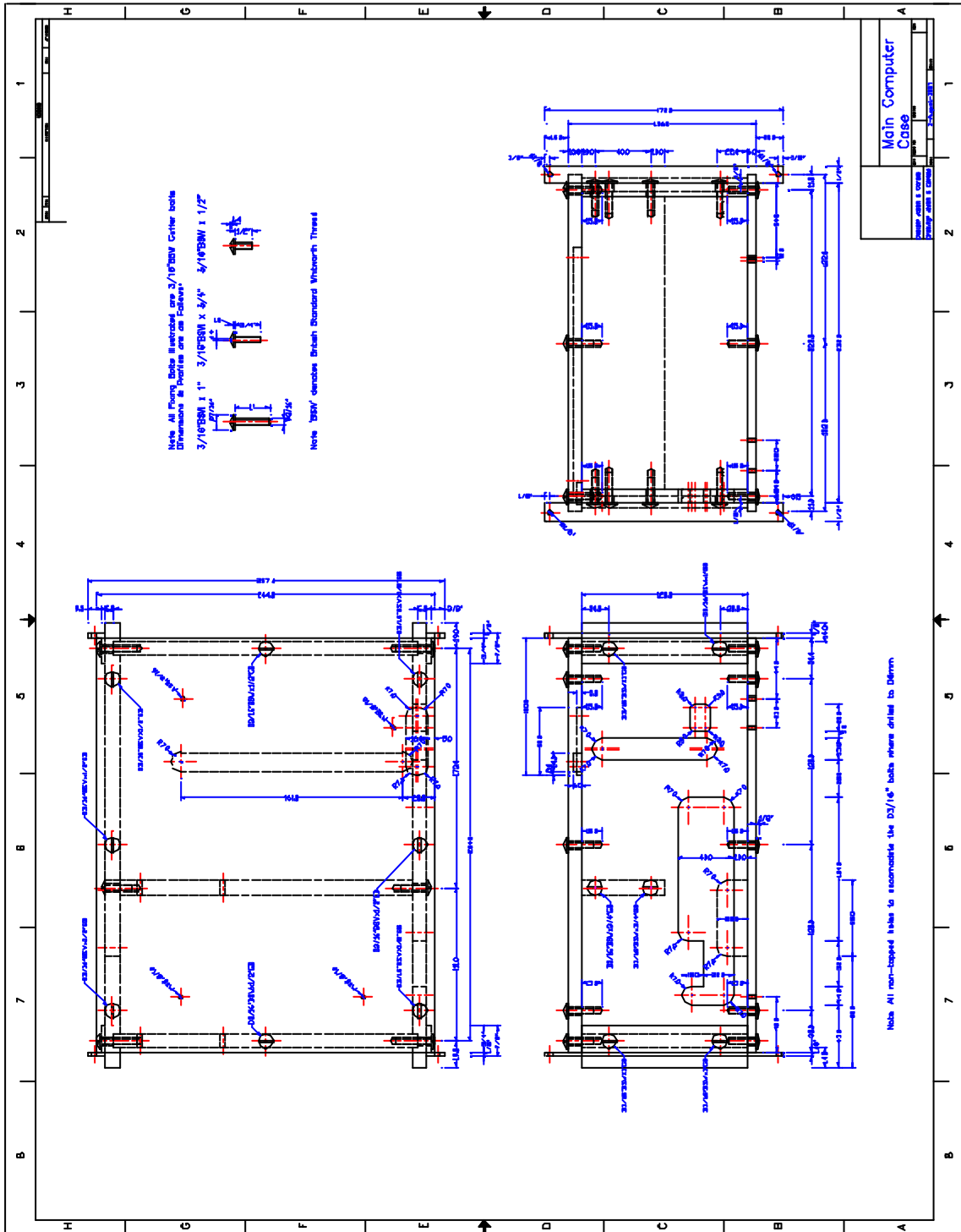


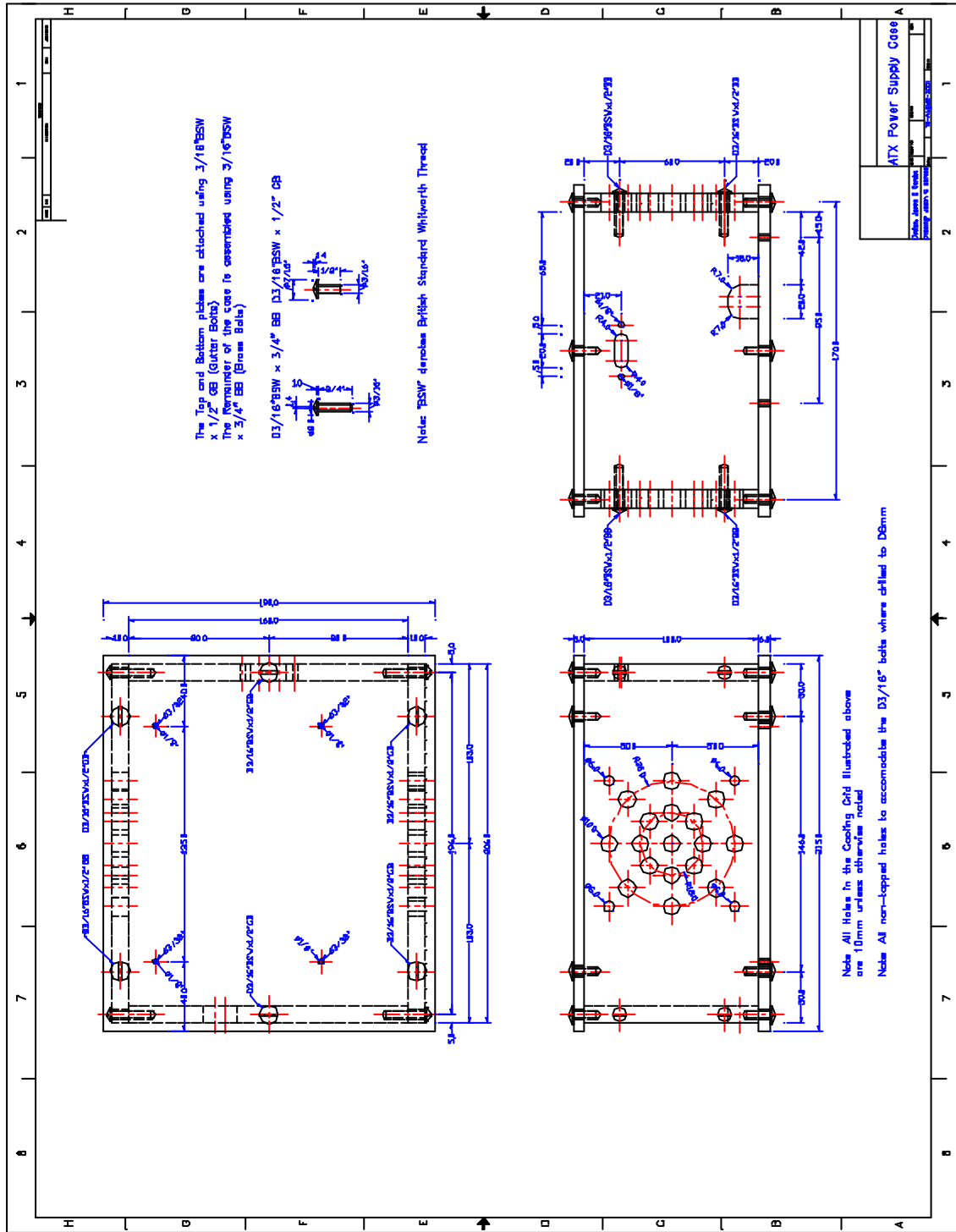


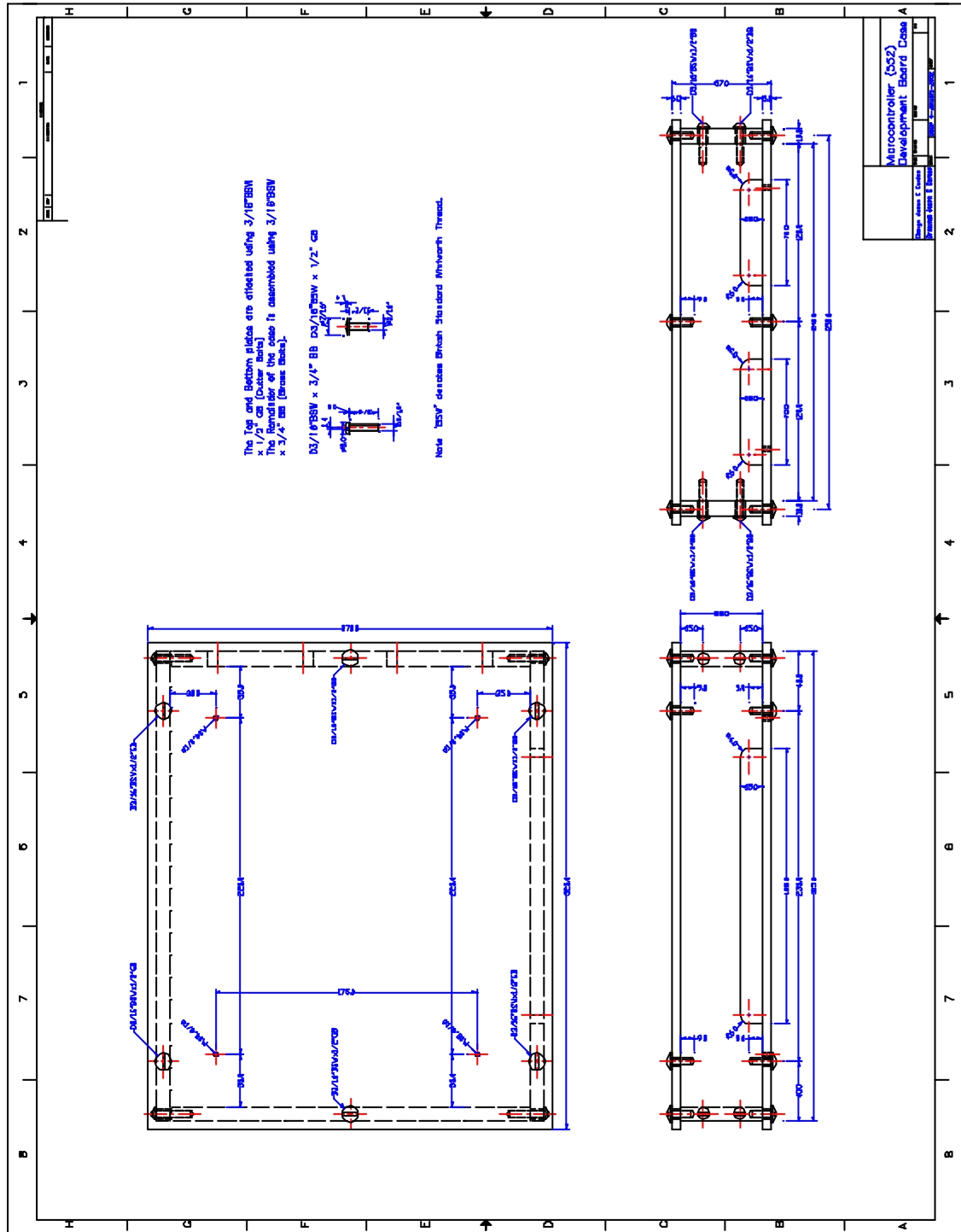


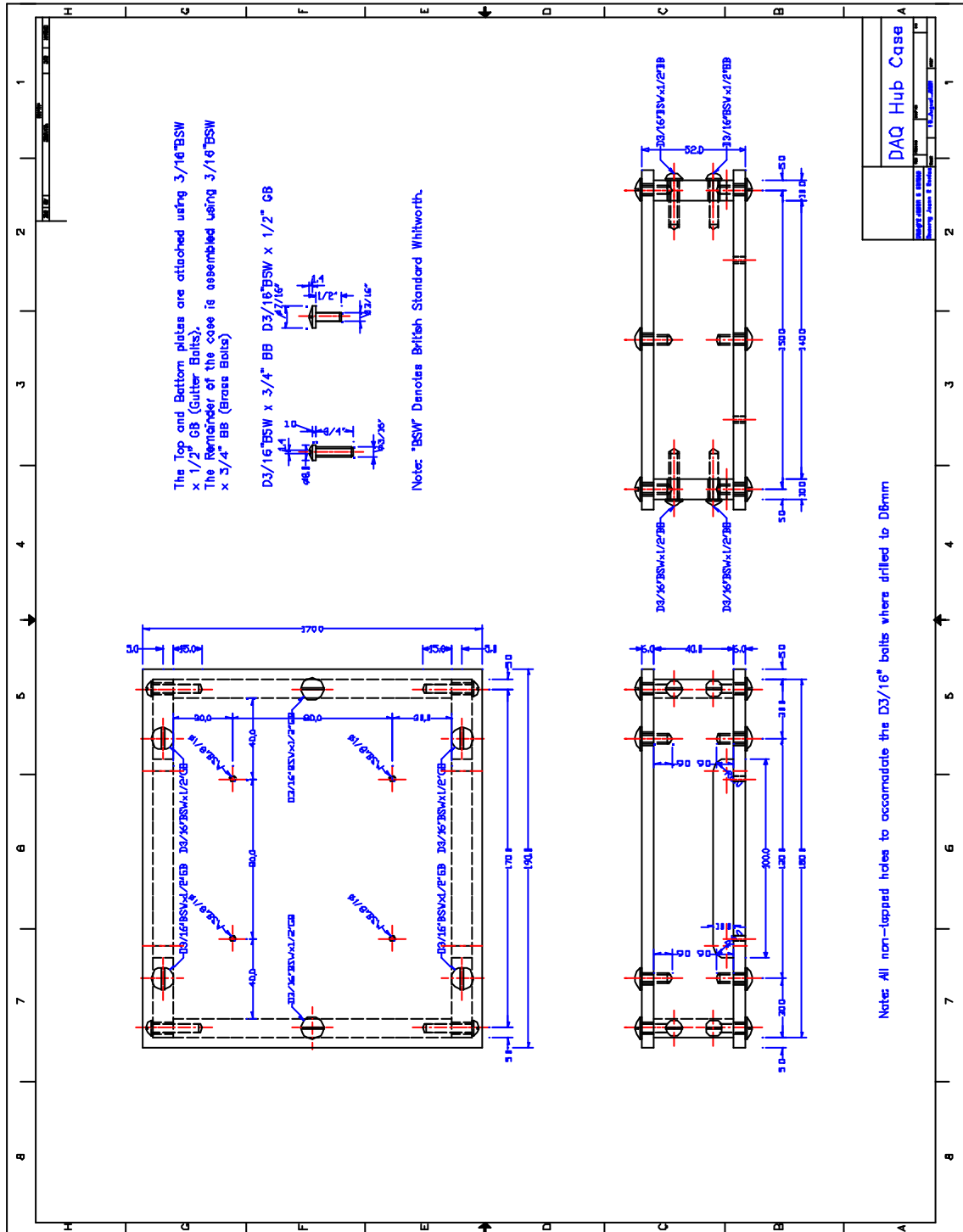


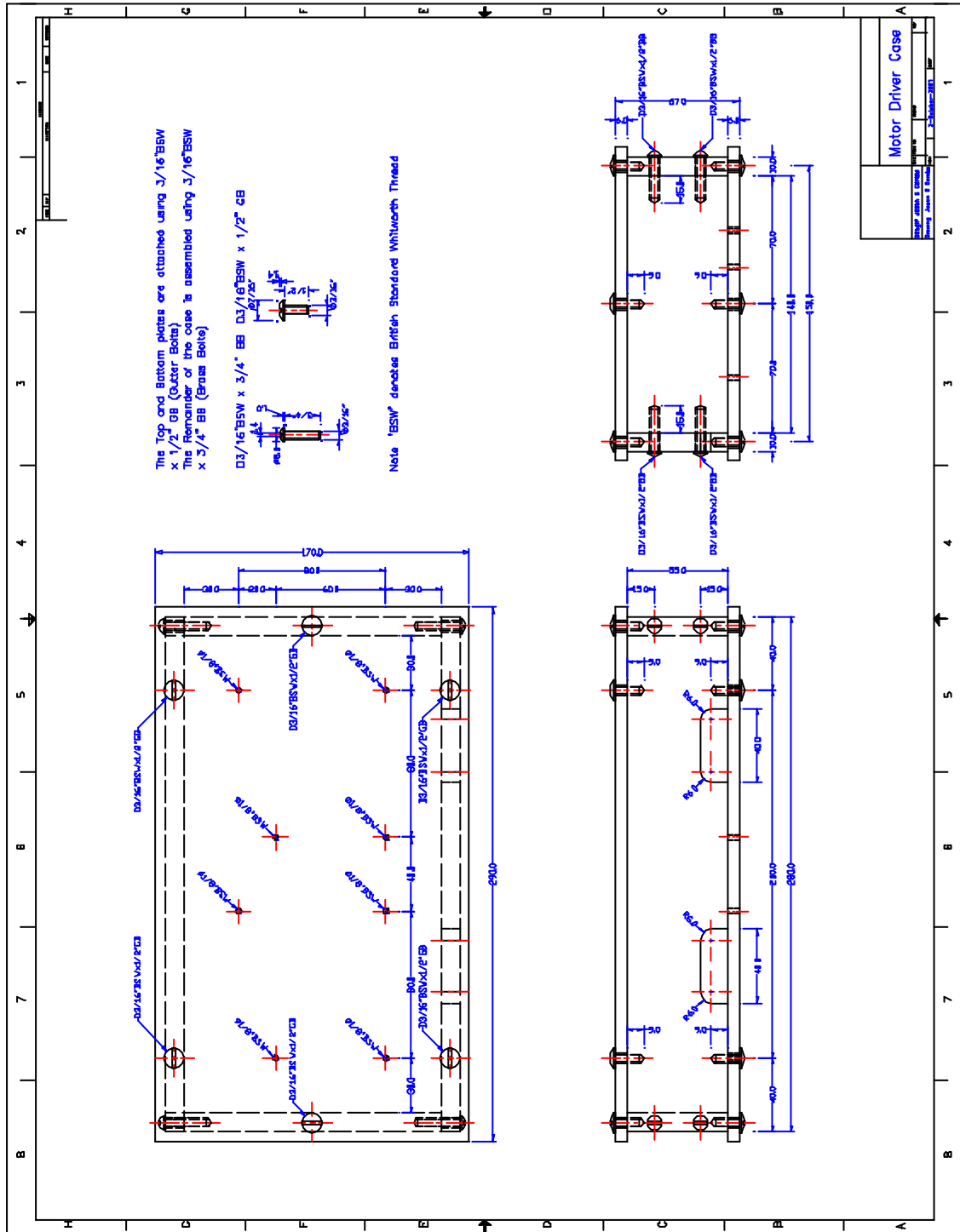


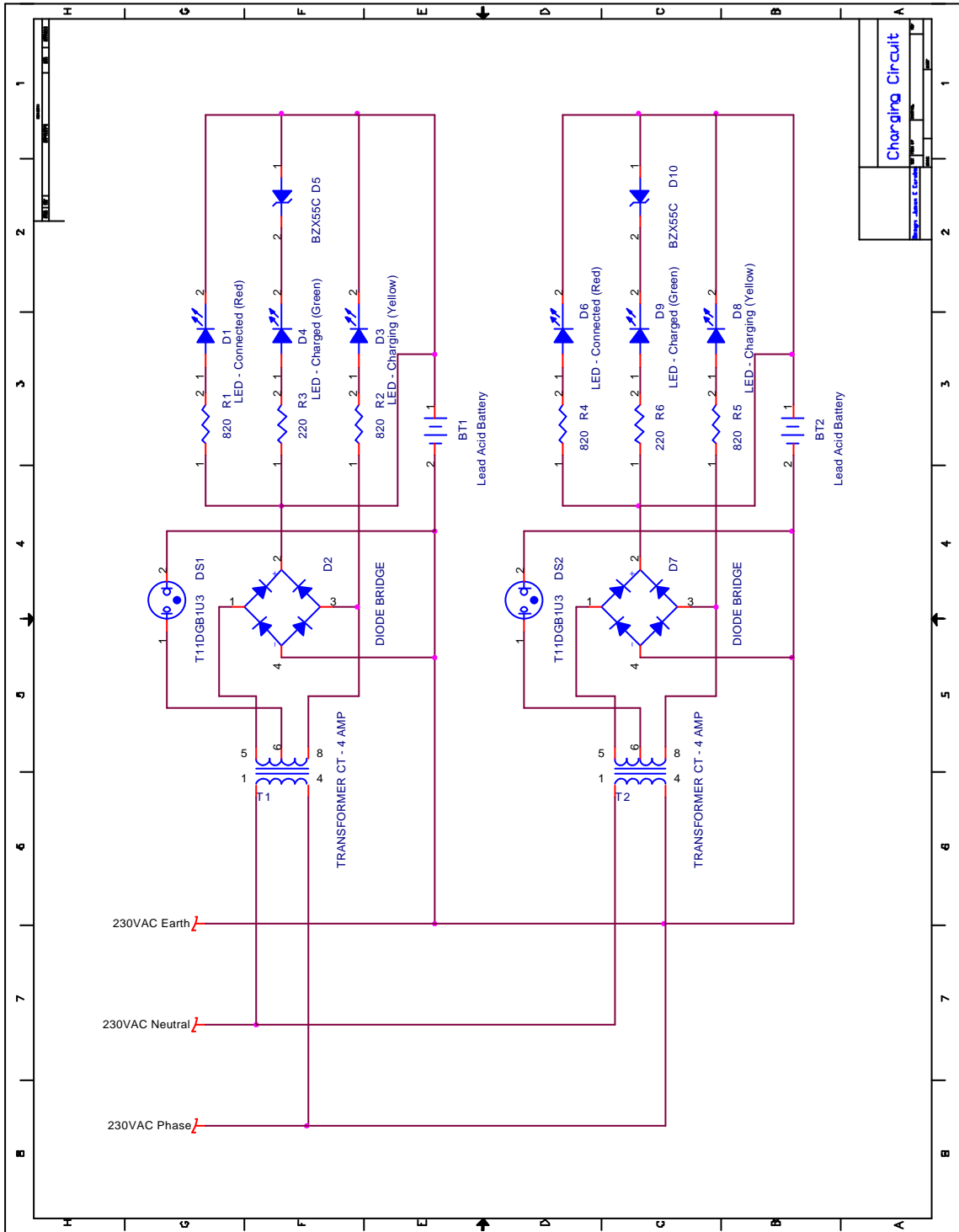


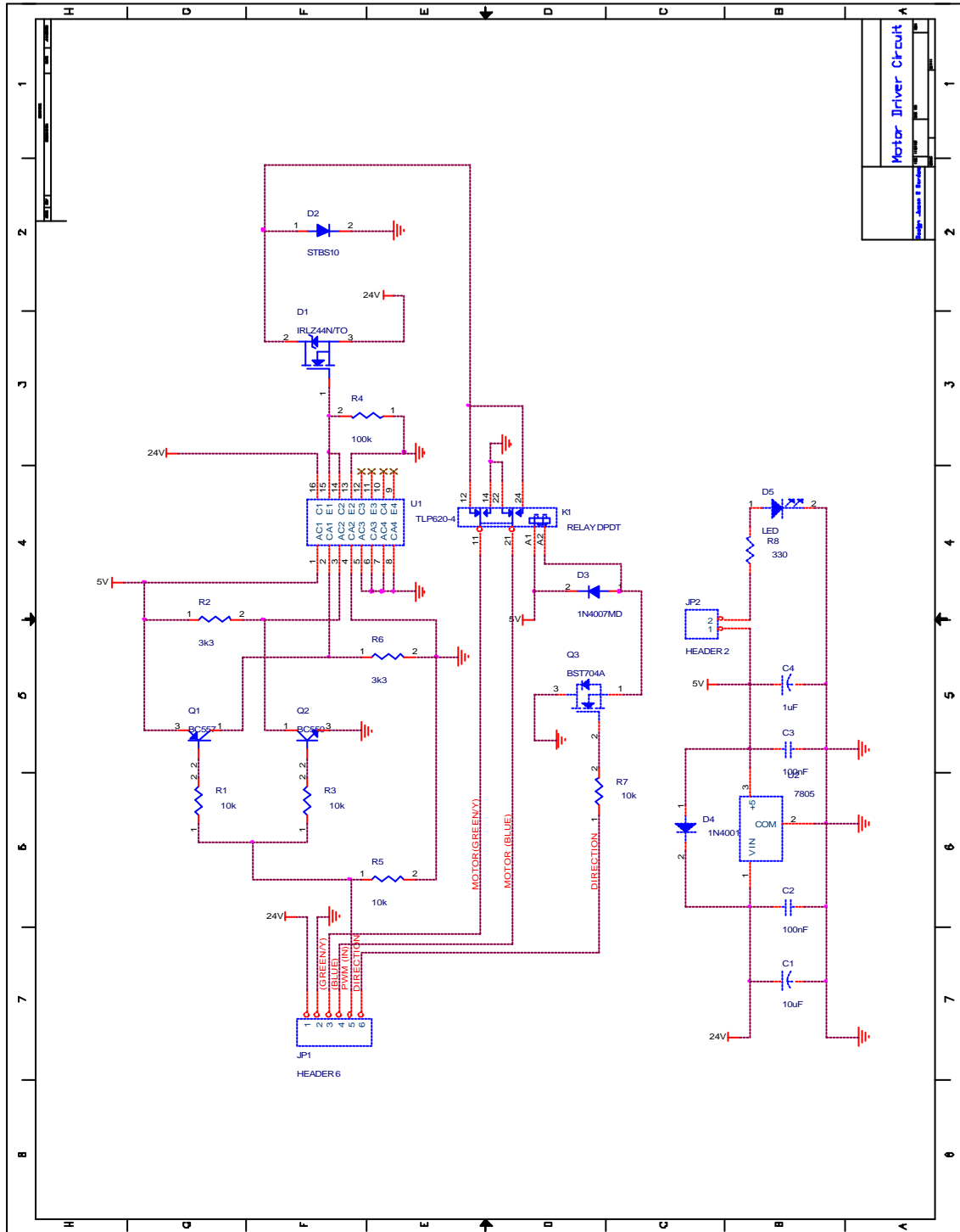


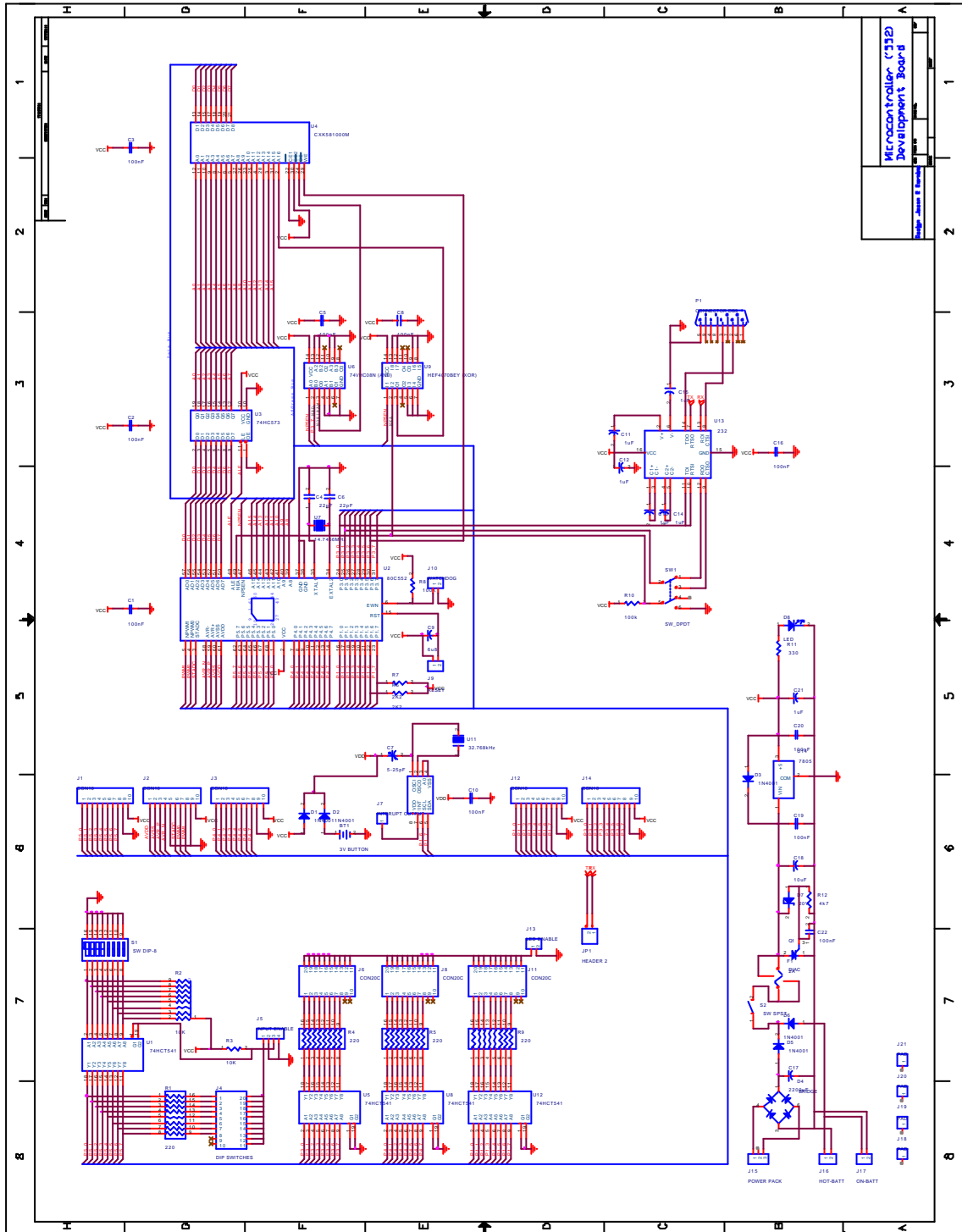












SEMICONDUCTOR
TOSHIBA TECHNICAL DATA

TOSHIBA PHOTOCOUPLER
TLP620, TLP620-2, TLP620-4
 GaAs IRED & PHOTO-TRANSISTOR

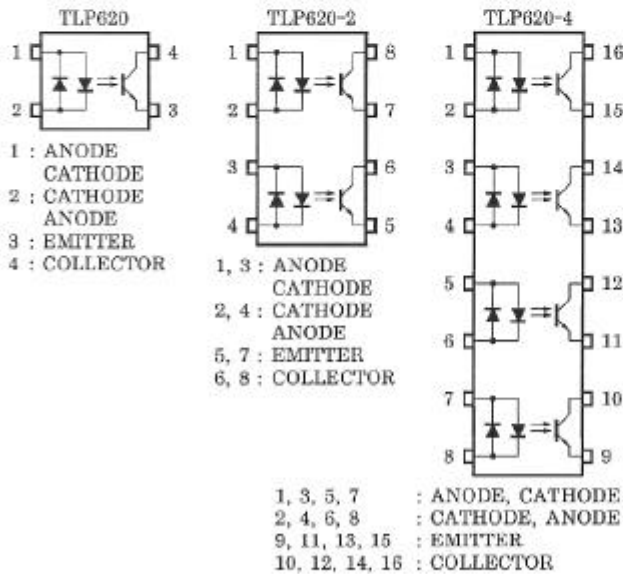
(TLP620)
 PROGRAMMABLE CONTROLLERS
 AC/DC-INPUT MODULE
 TELECOMMUNICATION

The TOSHIBA TLP620, -2 and -4 consists of a photo-transistor optically coupled to two gallium arsenide infrared emitting diode connected in inverse parallel.

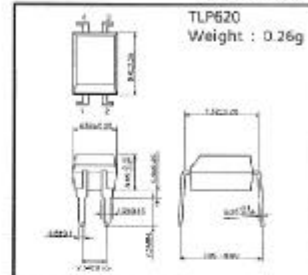
The TLP620-2 offers two isolated channels in an eight lead plastic DIP package, while the TLP620-4 provides four isolated channels in a sixteen plastic DIP package.

- Collector-Emitter Voltage : 55V (Min.)
 - Current Transfer Ratio : 50% (Min.)
- Rank GB : 100% (Min.)

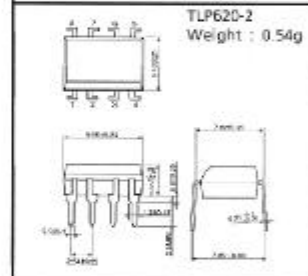
PIN CONFIGURATIONS (TOP VIEW)



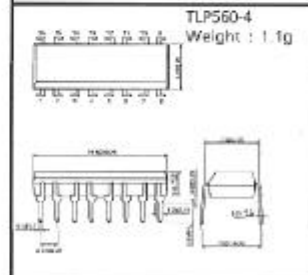
Unit in mm



JEDEC	—
EIAJ	—
TOSHIBA	11-5B2



JEDEC	—
EIAJ	—
TOSHIBA	11-10C4



JEDEC	—
EIAJ	—
TOSHIBA	11-20A3

① The information contained herein is provided only as a guide for the applications of our products. No responsibility is assumed by TOSHIBA CORPORATION for any infringement of intellectual property or other rights of the third parties which may result from its use. No license is granted by implication or otherwise under any intellectual property or other rights of TOSHIBA CORPORATION or others.
 ② These TOSHIBA products are intended for use in general commercial applications (office equipment, communication equipment, measuring equipment, domestic appliances, etc.). Please make sure that you consult with us before you use these TOSHIBA products in connection with equipment which requires extraordinarily high quality and/or reliability, and in equipment which may involve life-threatening or critical applications, including but not limited to such uses as atomic energy control, airplane or spacecraft instrumentation, traffic signals, medical instrumentation, combustion control, all types of safety devices, etc. TOSHIBA cannot accept and hereby declines liability for any damage which may occur in case the TOSHIBA products are used in such equipment or applications without prior consultation with TOSHIBA.

TLP620 - 1
1996 - 4 - 8
TOSHIBA CORPORATION

SEMICONDUCTOR
TOSHIBA
 TECHNICAL DATA

TLP620, TLP620-2, TLP620-4

(TLP620)

- UL Recognized : UL1577, File No. E67349
- Isolation Voltage : 5000V_{rms} (Min.)
- Option (D4) type
 VDE Approved : DIN VDE0884/08.87, Certificate No. 68384
 Maximum Operating Insulation Voltage : 630V_{PK}
 Highest Permissible Over Voltage : 6000V_{PK}

(Note) When a VDE0884 approved type is needed,
 please designate the "Option (D4)".

- Creepage Distance : 6.4mm (Min.)
 Clearance : 6.4mm (Min.)
 Insulation Thickness : 0.4mm (Min.)

MAXIMUM RATINGS (Ta = 25°C)

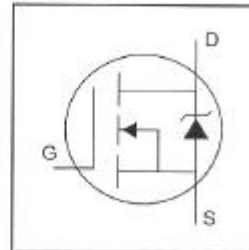
CHARACTERISTIC	SYMBOL	RATING		UNIT	
		TLP620	TLP620-2 TLP620-4		
LED	Forward Current	I _F (RMS)	60	50	mA
	Forward Current Derating	ΔI _F / °C	-0.7 (Ta ≥ 39°C)	-0.5 (Ta ≥ 25°C)	mA / °C
	Pulse Forward Current	I _{FP}	1 (100μs pulse, 100pps)		A
	Power Dissipation (1 Circuit)	P _D	100	70	mW
	Power Dissipation Derating	ΔP _D / °C	-1.0	-0.7	mW / °C
	Junction Temperature	T _J	125		°C
DETECTOR	Collector-Emitter Voltage	V _{CEO}	55		V
	Emitter-Collector Voltage	V _{ECO}	7		V
	Collector Current	I _C	50		mA
	Collector Power Dissipation (1 Circuit)	P _C	150	100	mW
	Collector Power Dissipation Derating (1 Circuit) (Ta ≥ 25°C)	ΔP _C / °C	-1.5	-1.0	mW / °C
	Junction Temperature	T _J	125		°C
Storage Temperature Range	T _{stg}	-55~150		°C	
Operating Temperature Range	T _{opr}	-55~100		°C	
Lead Soldering Temperature	T _{sold}	260 (10s)		°C	
Total Package Power Dissipation	P _T	250	150	mW	
Total Package Power Dissipation Derating (Ta ≥ 25°C, 1 Circuit)	ΔP _T / °C	-2.5	-1.5	mW / °C	
Isolation Voltage	BV _S	5000 (AC, 1 min., RH ≤ 60%)		V _{rms}	

TLP620-2

1996-4-8

TOSHIBA CORPORATION

- Logic-Level Gate Drive
- Advanced Process Technology
- Dynamic dv/dt Rating
- 175°C Operating Temperature
- Fast Switching
- Fully Avalanche Rated



$$V_{DSS} = 55V$$

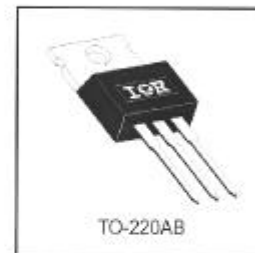
$$R_{DS(on)} = 0.022\Omega$$

$$I_D = 41A$$

Description

Fifth Generation HEXFETs from International Rectifier utilize advanced processing techniques to achieve the lowest possible on-resistance per silicon area. This benefit, combined with the fast switching speed and ruggedized device design that HEXFET Power MOSFETs are well known for, provides the designer with an extremely efficient device for use in a wide variety of applications.

The TO-220 package is universally preferred for all commercial-industrial applications at power dissipation levels to approximately 50 watts. The low thermal resistance and low package cost of the TO-220 contribute to its wide acceptance throughout the industry.



Absolute Maximum Ratings

	Parameter	Max.	Units
I_D @ $T_C = 25^\circ\text{C}$	Continuous Drain Current, V_{GS} @ 10V	41	A
I_D @ $T_C = 100^\circ\text{C}$	Continuous Drain Current, V_{GS} @ 10V	29	
I_{DM}	Pulsed Drain Current ①	160	
P_D @ $T_C = 25^\circ\text{C}$	Power Dissipation	83	W
	Linear Derating Factor	0.56	W/°C
V_{GS}	Gate-to-Source Voltage	±16	V
E_{AS}	Single Pulse Avalanche Energy ②	210	mJ
I_{AR}	Avalanche Current ③	25	A
E_{AR}	Repetitive Avalanche Energy ④	8.3	mJ
dv/dt	Peak Diode Recovery dv/dt ⑤	11	V/ns
T_J	Operating Junction and	-55 to +175	°C
T_{STG}	Storage Temperature Range		
	Soldering Temperature, for 10 seconds	300 (1.6mm from case)	
	Mounting torque, 6-32 or M3 screw.	10 lbf·in (1.1N·m)	

Thermal Resistance

	Parameter	Min.	Typ.	Max.	Units
$R_{\theta JC}$	Junction-to-Case	—	—	1.8	°C/W
$R_{\theta CS}$	Case-to-Sink, Flat, Greased Surface	—	0.50	—	
$R_{\theta JA}$	Junction-to-Ambient	—	—	62	

11/6/96

IRLZ44N

International
RectifierElectrical Characteristics @ $T_J = 25^\circ\text{C}$ (unless otherwise specified)

	Parameter	Min.	Typ.	Max.	Units	Conditions
$V_{(BR)DSS}$	Drain-to-Source Breakdown Voltage	55	—	—	V	$V_{GS} = 0V, I_D = 250\mu A$
$\Delta V_{(BR)DSS}/\Delta T_J$	Breakdown Voltage Temp. Coefficient	—	0.070	—	V/°C	Reference to $25^\circ\text{C}, I_D = 1mA$
$R_{DS(on)}$	Static Drain-to-Source On-Resistance	—	—	0.022	Ω	$V_{GS} = 10V, I_D = 25A$ ④
		—	—	0.025		$V_{GS} = 5.0V, I_D = 25A$ ④
		—	—	0.035		$V_{GS} = 4.0V, I_D = 21A$ ④
$V_{GS(th)}$	Gate Threshold Voltage	1.0	—	2.0	V	$V_{DS} = V_{GS}, I_D = 250\mu A$
g_{fs}	Forward Transconductance	21	—	—	S	$V_{DS} = 25V, I_D = 25A$
I_{DSS}	Drain-to-Source Leakage Current	—	—	25	μA	$V_{DS} = 55V, V_{GS} = 0V$
		—	—	250		$V_{DS} = 44V, V_{GS} = 0V, T_J = 150^\circ\text{C}$
I_{GSS}	Gate-to-Source Forward Leakage	—	—	100	nA	$V_{GS} = 16V$
	Gate-to-Source Reverse Leakage	—	—	-100		$V_{GS} = -16V$
Q_g	Total Gate Charge	—	—	48	nC	$I_D = 25A$
Q_{gs}	Gate-to-Source Charge	—	—	8.6		$V_{DS} = 44V$
Q_{gd}	Gate-to-Drain ("Miller") Charge	—	—	25		$V_{GS} = 5.0V$, See Fig. 6 and 13 ④
$t_{d(on)}$	Turn-On Delay Time	—	11	—	ns	$V_{DD} = 28V$
t_r	Rise Time	—	84	—		$I_D = 25A$
$t_{d(off)}$	Turn-Off Delay Time	—	26	—		$R_G = 3.4\Omega, V_{GS} = 5.0V$
t_f	Fall Time	—	15	—		$R_D = 1.1\Omega$, See Fig. 10 ④
L_D	Internal Drain Inductance	—	4.5	—	nH	Between lead, 6mm (0.25in.) from package and center of die contact
L_S	Internal Source Inductance	—	7.5	—		
C_{iss}	Input Capacitance	—	1700	—	pF	$V_{GS} = 0V$
C_{oss}	Output Capacitance	—	400	—		$V_{DS} = 25V$
C_{rss}	Reverse Transfer Capacitance	—	150	—		$f = 1.0MHz$, See Fig. 5

Source-Drain Ratings and Characteristics

	Parameter	Min.	Typ.	Max.	Units	Conditions
I_S	Continuous Source Current (Body Diode)	—	—	41	A	MOSFET symbol showing the integral reverse p-n junction diode.
I_{SM}	Pulsed Source Current (Body Diode) ①	—	—	160		
V_{SD}	Diode Forward Voltage	—	—	1.3	V	$T_J = 25^\circ\text{C}, I_S = 25A, V_{GS} = 0V$ ②
t_{rr}	Reverse Recovery Time	—	80	120	ns	$T_J = 25^\circ\text{C}, I_F = 25A$
Q_{rr}	Reverse Recovery Charge	—	210	320	nC	$di/dt = 100A/\mu s$ ③
t_{on}	Forward Turn-On Time	Intrinsic turn-on time is negligible (turn-on is dominated by L_S+L_D)				

Specification changes

Rev. #	Parameters	Old spec.	New spec.	Comments	Revision Date
1	V_{GS} (Max.)	± 20	± 16	Decrease V_{GS} (Max). Specification	4/30/96

Notes:

- ① Repetitive rating; pulse width limited by max. junction temperature. (See fig. 11)
 ② $V_{DD} = 25V$, starting $T_J = 25^\circ\text{C}$, $L = 470\mu H$
 $R_C = 25\Omega$, $I_{AS} = 25A$. (See Figure 12)

③ $I_{SD} \leq 25A$, $di/dt \leq 270A/\mu s$, $V_{DD} \leq V_{(BR)DSS}$,
 $T_J \leq 175^\circ\text{C}$

④ Pulse width $\leq 300\mu s$; duty cycle $\leq 2\%$.

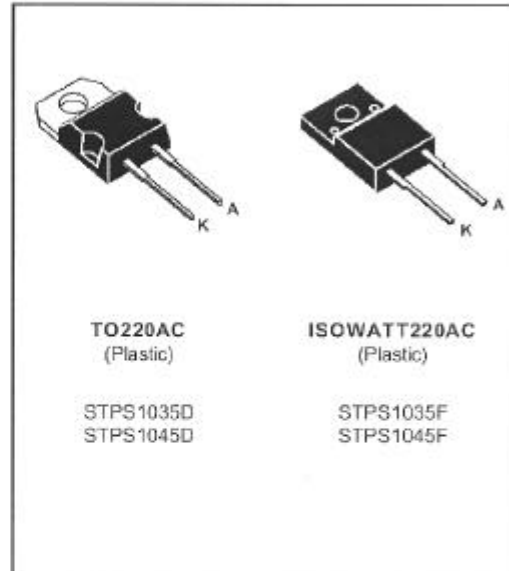
POWER SCHOTTKY RECTIFIER

- VERY SMALL CONDUCTION LOSSES
- NEGLIGIBLE SWITCHING LOSSES
- EXTREMELY FAST SWITCHING
- LOW FORWARD VOLTAGE DROP
- HIGH AVALANCHE CAPABILITY
- LOW THERMAL RESISTANCE
- INSULATED PACKAGE :
 Insulating voltage = 2000V DC
 Capacitance = 12pF

DESCRIPTION

Single chip schottky rectifier suited for switchmode power supply and high frequency DC to DC converters.

Packaged in TO220AC and ISOWATT220AC, this device is intended for use in low voltage, high frequency inverters, free wheeling and polarity protection applications.


ABSOLUTE RATINGS (limiting values)

Symbol	Parameter		Value	Unit	
$I_{F(RMS)}$	RMS Forward Current		30	A	
$I_{F(AV)}$	Average Forward Current $\delta = 0.5$	TO220AC	$T_c = 135^\circ\text{C}$	10	A
		ISOWATT220AC	$T_c = 120^\circ\text{C}$		
I_{FSM}	Surge Non Repetitive Forward Current		$T_p = 10 \text{ ms}$ Sinusoidal	180	A
I_{RRM}	Peak Repetitive Reverse Current		$T_p = 2 \mu\text{s}$ $F = 1\text{KHz}$	1	A
T_{stg} T_j	Storage and Junction Temperature Range		- 65 to + 150 - 65 to + 150		$^\circ\text{C}$
dV/dt	Critical Rate of Rise of Reverse Voltage		1000		V/ μs

Symbol	Parameter	STPS		Unit
		1035D 1035F	1045D 1045F	
V_{RRM}	Repetitive Peak Reverse Voltage	35	45	V

STPS1035D/F / STPS1045D/F

THERMAL RESISTANCE

Symbol	Parameter	Value	Unit
R _{TH(j-c)}	Junction-case	TO220AC	2.2
		ISOWATT220AC	4.5

ELECTRICAL CHARACTERISTICS

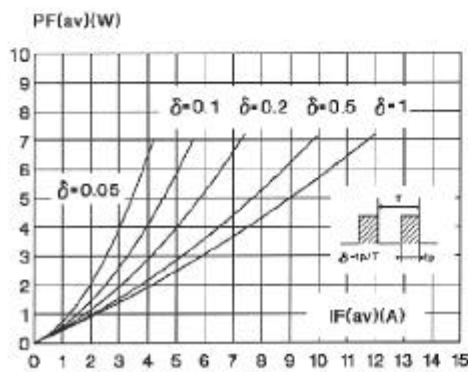
STATIC CHARACTERISTICS

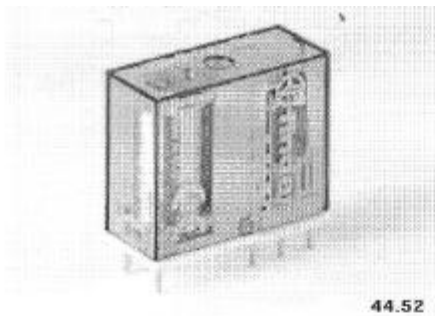
Symbol	Tests Conditions		Min.	Typ.	Max.	Unit
I _R *	T _j = 25°C	V _R = V _{RRM}			100	μA
	T _j = 125°C				15	mA
V _F **	T _j = 125°C	I _F = 20 A			0.72	V
	T _j = 125°C	I _F = 10 A			0.57	
	T _j = 25°C	I _F = 20 A			0.64	

Pulse test : * t_p = 5 ms, duty cycle < 2 %
 ** t_p = 360 μs, duty cycle < 2%

To evaluate the conduction losses use the following equation :
 $P = 0.42 \times I_{F(AV)} + 0.015 I_{F(RMS)}^2$

Fig. 1 : Average forward power dissipation versus average forward current.



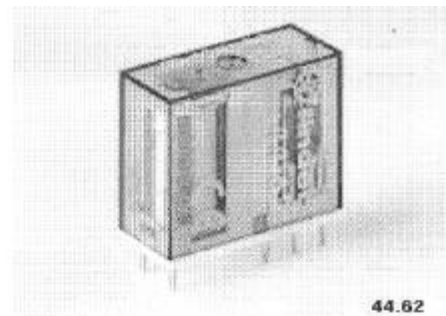
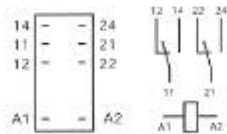
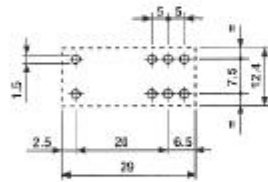
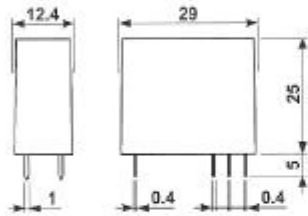


44.52



MINIATURE P.C.B. RELAY

- TYPE 44.52** 2 CO (DPDT) 6 A - 5 mm pinning
 - tin plated pins for P.C.B.
 - standard contact material: Ag Ni
 - ordering information: see page 20

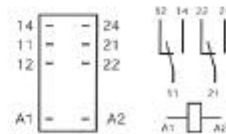
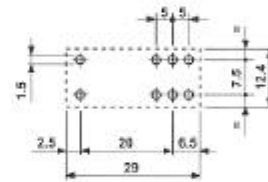
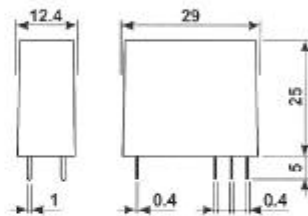


44.62




MINIATURE P.C.B. RELAY

- TYPE 44.62** 2 CO (DPDT) 10 A - 5 mm pinning
 - tin plated pins for P.C.B.
 - standard contact material: Ag Ni
 - option: see coding table page 20
 - ordering information: see page 20



TECHNICAL DATA

DIELECTRIC STRENGTH tested at leakage current ≤ 10 mA for 1 min at 50 Hz	between coil and contacts	4000 V
	between open contacts	1000V
	between adjacent contacts	2000 V
	between frame and live parts	relay without external ground
SURGE TEST (1.2/50 μs) voltage between coil and contacts	6000 V	
INSULATION RESISTANCE	≥ 20 · 10 ⁹ MΩ	
INSULATION GROUP	C 250	
INSULATION DISTANCES	≥ 8 mm between coil and contacts according to VDE 0700	
MECHANICAL LIFE	20 · 10 ⁶ cycles	
MAXIMUM SWITCHING FREQUENCY	36000 cycles/h	
- without load	900 cycles/h	
- at rated load		
AMBIENT TEMPERATURE	- 40 to + 85° C	
PROTECTION CATEGORY OF ENCLOSURES	IP 40	
OPERATE AND RELEASE TIME:		
- pick-up time (from 0 to U _n)	≤ 15 ms (including contact bounce)	
- drop-out time (from U _n to 0)	≤ 20 ms (including contact bounce)	
TYPE OF DUTY	continuous	
PICK-UP CLASS	C (according to IEC 255)	
DIELECTRIC TEST		
TYPE OF RELAY	all - or - nothing	

Single-chip 8-bit EPROM microcontroller with 10-bit A/D, capture compare timer, high-speed outputs, PWM

87C552

FEATURES

- 80C51 central processing unit
- 8k x 8 EPROM expandable externally to 64k bytes
- An additional 16-bit timer/counter coupled to four capture registers and three compare registers
- Two standard 16-bit timer/counters
- 256 x 8 RAM, expandable externally to 64k bytes
- Capable of producing eight synchronized, timed outputs
- A 10-bit ADC with eight multiplexed analog inputs
- Two 8-bit resolution, pulse width modulation outputs
- Five 8-bit I/O ports plus one 8-bit input port shared with analog inputs
- I²C-bus serial I/O port with byte oriented master and slave functions
- Full-duplex UART compatible with the standard 80C51
- On-chip watchdog timer
- Extended temperature ranges
- OTP package available

DESCRIPTION

The 87C552 Single-Chip 8-Bit Microcontroller is manufactured in an advanced CMOS process and is a derivative of the 80C51 microcontroller family. The 87C552 has the same instruction set as the 80C51. The 87C552 is an EPROM version of the 83C552.

The 87C552 contains an 8k x 8 EPROM program memory, a volatile 256 x 8 read/write data memory, five 8-bit I/O ports, one 8-bit input port, two 16-bit timer/event counters (identical to the timers of the 80C51), an additional 16-bit timer coupled to capture and compare latches, a 15-source, two-priority-level, nested interrupt structure, an 8-input ADC, a dual DAC pulse width modulated interface, two serial interfaces (UART and I²C-bus), a "watchdog" timer and on-chip oscillator and timing circuits. For systems that require extra capability, the 87C552 can be expanded using standard TTL compatible memories and logic.

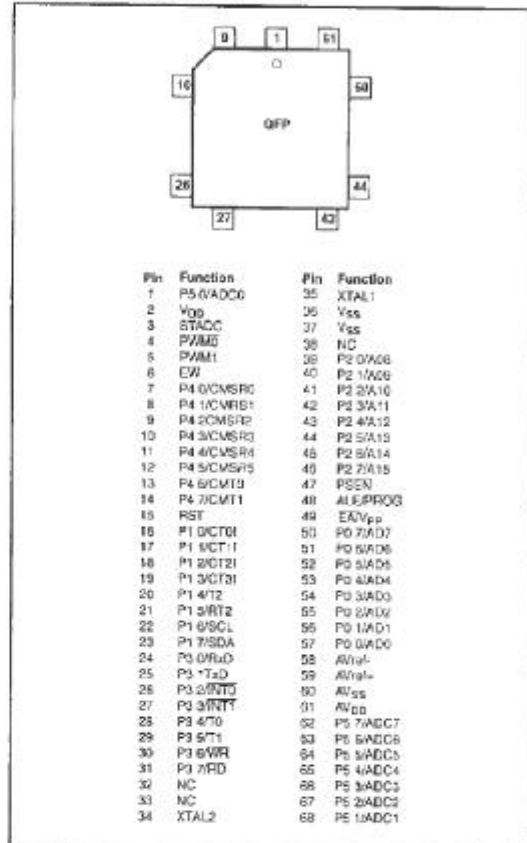
In addition, the 87C552 has two software selectable modes of power reduction — idle mode and power-down mode. The idle mode freezes the CPU while allowing the RAM, timers, serial ports, and interrupt system to continue functioning. The power-down mode saves the RAM contents but freezes the oscillator, causing all other chip functions to be inoperative.

ORDERING INFORMATION

DESCRIPTION	ORDER CODE	FREQUENCY	PKG DESIGNATOR*
Ceramic Quad Flat Pack with J Bend Leads	87C552/θMA	3.5 - 12MHz	QGCC1-J68

* MIL-STD 1835 or Appendix A of 1995 Military Data Handbook

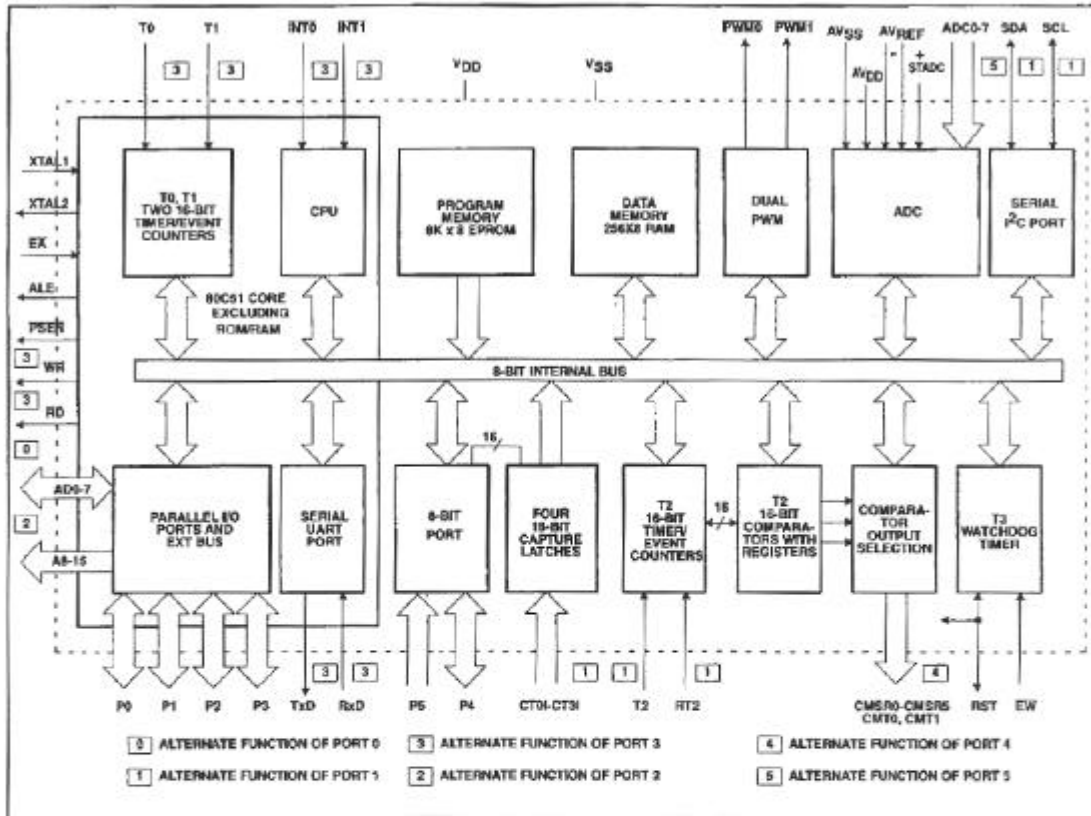
PIN CONFIGURATION



Single-chip 8-bit EPROM microcontroller with 10-bit A/D, capture compare timer, high-speed outputs, PWM

87C552

BLOCK DIAGRAM



PIN DESCRIPTION

MNEMONIC	PIN NO.	TYPE	NAME AND FUNCTION
V _{DD}	2	I	Digital Power Supply: +5V power supply pin during normal operation, idle and power-down mode.
STADC	3	I	Start ADC Operation: Input starting analog to digital conversion (ADC operation can also be started by software).
PWM0	4	O	Pulse Width Modulation: Output 0.
PWM1	5	O	Pulse Width Modulation: Output 1.
EW	6	I	Enable Watchdog Timer: Enable for T3 watchdog timer and disable power-down mode.
P0.0-P0.7	57-50	I/O	Port 0: Port 0 is an 8-bit open-drain bidirectional I/O port. Port 0 pins that have 1s written to them float and can be used as high-impedance inputs. Port 0 is also the multiplexed low-order address and data bus during accesses to external program and data memory. In this application it uses strong internal pull-ups when emitting 1s. Port 0 is also used to input the code byte during programming and to output the code byte during verification.
P1.0-P1.7	16-23	I/O	Port 1: 8-bit I/O port. Alternate functions include:
	16-21	I/O	(P1.0-P1.5): Quasi-bidirectional port pins.
	22-23	I/O	(P1.6, P1.7): Open drain port pins.
	16-19	I	CT0-CT3 (P1.0-P1.3): Capture timer input signals for timer T2.
	20	I	T2 (P1.4): T2 event input
	21	I	RT2 (P1.5): T2 timer reset signal. Rising edge triggered.
	22	I/O	SCL (P1.6): Serial port clock line I ² C-bus.
	23	I/O	SDA (P1.7): Serial port data line I ² C-bus. Port 1 is also used to input the lower order address byte during EPROM programming and verification. AD is on P1.0, etc.



GP2D12/GP2D15

General Purpose Type Distance Measuring Sensors

■ Features

1. Less influence on the color of reflective objects, reflectivity
2. Line-up of distance output/distance judgement type
 Distance output type (analog voltage) : **GP2D12**
 Detecting distance : 10 to 80cm
 Distance judgement type : **GP2D15**
 Judgement distance : 24cm
 (Adjustable within the range of 10 to 80cm)
3. External control circuit is unnecessary
4. Low cost

■ Applications

1. TVs
2. Personal computers
3. Cars
4. Copiers

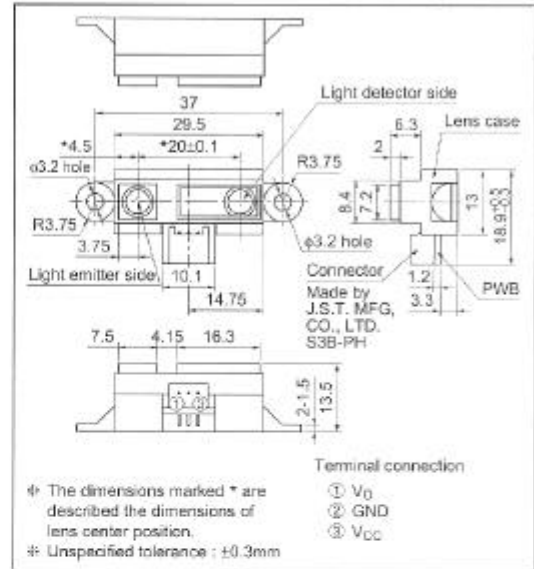
■ Absolute Maximum Ratings

(Ta=25°C, Vcc=5V)

Parameter	Symbol	Rating	Unit
Supply voltage	V _{CC}	-0.3 to +7	V
Output terminal voltage	V _O	-0.3 to V _{CC} +0.3	V
Operating temperature	T _{OPR}	-10 to +60	°C
Storage temperature	T _{STG}	-40 to +70	°C

■ Outline Dimensions

(Unit : mm)



Notice: In the absence of confirmation by device specification sheets, SHARP takes no responsibility for any defects that may occur in equipment using any SHARP devices shown in catalogs, data books, etc. Contact SHARP in order to obtain the latest device specification sheets before using any SHARP devices.
 Internet: Internet address for Electronic Components Group <http://www.sharp.co.jp/elec/>

SHARP

GP2D12/GP2D15

Recommended Operating Conditions

Parameter	Symbol	Rating	Unit
Operating supply voltage	V _{CC}	4.5 to +5.5	V

Electro-optical Characteristics

(T_a=25°C, V_{CC}=5V)

Parameter	Symbol	Conditions	MIN.	TYP.	MAX.	Unit	
Distance measuring range	ΔL	*1 *2	10	-	80	cm	
Output terminal voltage	GP2D12	V _O	L=80cm *1	0.25	0.4	0.55	V
	GP2D15	V _{OH}	Output voltage at High *1	V _{CC} -0.3	-	-	V
		V _{OL}	Output voltage at Low *1	-	-	0.6	V
Difference of output voltage	GP2D12	ΔV _O	Output change at L=80cm to 10cm *1	1.75	2.0	2.25	V
Distance characteristics of output	GP2D15	V _O	*1 *2 *4	21	24	27	cm
Average Dissipation current	I _{CC}	L=80cm *1	-	33	50	mA	

Note) L : Distance to reflective object.

*1 Using reflective object : White paper (Made by Kodak Co. Ltd. gray cards R-27 - white face, reflective ratio ; 90%).

*2 We ship the device after the following adjustment : Output switching distance L=24cm±5mm must be measured by the sensor.

*3 Distance measuring range of the optical sensor system.

*4 Output switching has a hysteresis width. The distance specified by V_O should be the one with which the output L switches to the output H.

Fig.1 Internal Block Diagram

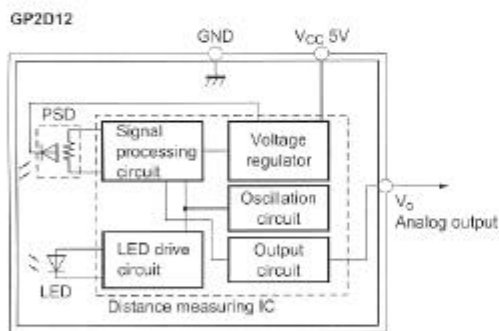


Fig.2 Internal Block Diagram

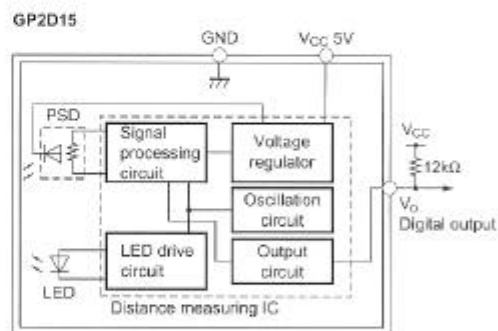
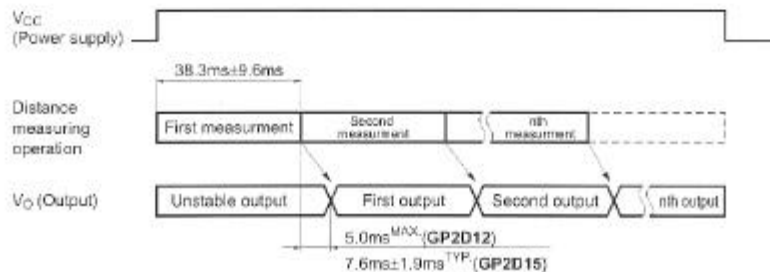


Fig.3 Timing Chart

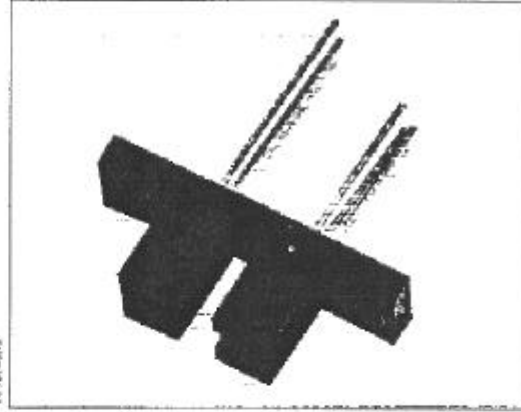


HOA2001

Transmissive Optoschmitt Sensor

FEATURES

- Direct TTL interface
- Buffer logic
- 0.060 in.(1.52 mm) dia. detector aperture
- 0.120 in.(3.05 mm) slot width
- 0.050 in.(1.27) offset pin circle detector leads



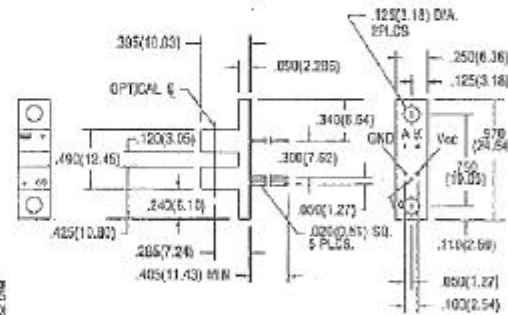
DESCRIPTION

The HOA2001 consists of an infrared emitting diode facing an Optoschmitt detector encased in a black thermoplastic housing. The photodetector consists of a photodiode, amplifier, voltage regulator, Schmitt trigger and an NPN output transistor with 10 KΩ (nominal) pull-up resistor. The buffer logic provides a high output when the optical path is clear, and a low output when the path is interrupted. The HOA2001 employs plastic molded components. For additional component information see SEP9506 and SDP8600.

Housing material is polyester. Housings are soluble in chlorinated hydrocarbons and ketones. Recommended cleaning agents are methanol and isopropanol.

OUTLINE DIMENSIONS in inches (mm)

Tolerance 3 plc decimals ±0.010(0.25)
2 plc decimals ±0.020(0.51)



HOA2001

Transmissive Optoschmitt Sensor

ELECTRICAL CHARACTERISTICS (25°C unless otherwise noted)

PARAMETER	SYMBOL	MIN	TYP	MAX	UNITS	TEST CONDITIONS
IR EMITTER						
Forward Voltage	V_F			1.6	V	$I_F=20\text{ mA}$
Reverse Leakage Current	I_R			10	μA	$V_R=3\text{ V}$
DETECTOR						
Operating Supply Voltage	V_{CC}	4.5		12	V	
Low Level Supply Current	I_{CCL}	4.0		12	mA	$V_{CC}=5\text{ V}$
		5.0		15		$V_{CC}=12\text{ V}$
High Level Supply Current	I_{CCH}	2.0		10	mA	$V_{CC}=5\text{ V}$
		3.0		12		$V_{CC}=12\text{ V}$
Low Level Output Voltage	V_{OL}			0.4	V	$I_{OL}=12.8\text{ mA}, I_F=0\text{ mA}$
High Level Output Voltage	V_{OH}	2.4			V	$I_{OH}=0, I_F=10\text{ mA}$
Propagation Delay, Low-High	t_{PLH}		5		μs	$V_{CC}=5\text{ V}, I_F=10\text{ mA}$
Propagation Delay, High-Low	t_{PHL}		5		μs	$V_{CC}=5\text{ V}, I_F=10\text{ mA}$
Rise Time	t_r		60		ns	$R_L=390\ \Omega, C_L=50\text{ pF}$
Fall Time	t_f		6		ns	$R_L=390\ \Omega, C_L=50\text{ pF}$
COUPLED CHARACTERISTICS						
IR LED Trigger Current	I_{FT}				mA	$V_{CC}=5\text{ V}$
HOA2001-001				10		

Notes

- It is recommended that a bypass capacitor, 0.1 μF typical, be added between V_{CC} and GND near the device in order to stabilize power supply line.

ABSOLUTE MAXIMUM RATINGS

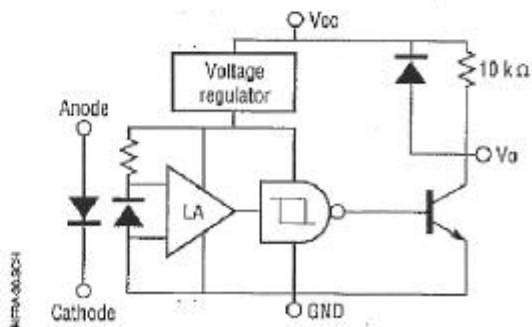
(25°C Free-Air Temperature unless otherwise noted)

Operating Temperature Range	-40°C to 70°C
Storage Temperature Range	-40°C to 85°C
Soldering Temperature (5 sec)	240°C
IR EMITTER	
Power Dissipation	100 mW ⁽¹⁾
Reverse Voltage	3 V
Continuous Forward Current	50 mA
DETECTOR	
Supply Voltage	12 V ⁽²⁾
Output Sink Current	18 mA
Duration of Output	
Short to V_{CC} or Ground	1.0 sec

Notes

- Derate linearly at 0.78 mW/°C 25°C.
- Derate linearly from 25°C to 5.5 V at 70°C.

SCHEMATIC



Honeywell reserves the right to make changes in order to improve design and supply the best products possible.

Honeywell

319

GLOSSARY

3DM	Microstrain 3DM solid-state 3-axis pitch, roll, and yaw sensor
'552	Philips S87C552-4A68 Microprocessor
Æ	Diameter
AC	Alternating Current
ADE	Address latch enable
BCD	Binary Coded Decimal
Bit	Binary value – 0 or 1
BSW	British Standard Whitworth thread
Byte	8-bits
CCA	Cold Cranking Amps
CCD	Charge Coupled Device
CPR	Counts Per Revolution
CW	Code Wheel
DAQ	Data Acquisition
DC	Direct Current
DGPS	Differential Global Positioning System
DPDT	Double Pole Double Throw
ECP	Extended Capabilities Port
Emf	Electro-magnetic field
GND	Ground
GPS	Global Positioning System
Gullet/ed	Recessed groove
I²C	Philips serial communication protocol
ID	Inner Diameter
I/O	Input/Output
IR	Infrared
LED	Light Emitting Diode

LSB	Least Significant Bit
M	Metric bolt diameter i.e. M10x1.5x20
M12	Motorola M12 Oncore global positioning unit
MOSFET	Metal-Oxide-Silicon Field-Effect Transistor
MSB	Most Significant Bit
OD	Outer Diameter
PID	Proportional, Integral, Differential
PWM	Pulse Width Modulation
RAM	Random Access Memory
RC	Reserve Capacity
RF	Radio Frequency
ROM	Read Only Memory
ROV	Remotely Operated Vehicle
RTC	Real Time Clock
SDO	Serial Data Output
SE	Shaft Encoder
SRAM	Static Random Access Memory
SPST	Single Pole Single Throw
TM	Track Modules
TMSP	Track Module Side Plates
TTF	Time to First Fix
UART	Universal Asynchronous Receiver/Transmitter
UHF	Ultra-High Frequency
UNC	United National Coarse
UNF	United National Fine thread
USB	Universal Serial Bus
VAC	Volts of Alternating Current
VDC	Volts of Direct Current
VI	Virtual Instruments
VX2	Vector VX2 electronic compass
YPS	Yaw and Pitch Sensor

BIBLIOGRAPHY

1. Bateson, R. N, 1996 *“Introduction to Control System Technology”*, 5th Edition, Prentice Hall.
2. Fowler, K. R, 1996 *“Electronic Instrument Design – Architecting for the Life Cycle”*, Oxford University Press.
3. Franklin, G. F, Powell, J. D, Emami-Naeini, A, 1994 *“Feedback Control of Dynamic Systems”*, 3rd Edition, Addison-Wesley Publishing Company.
4. Furuno Electric Company, 2000 *“Furuno Operator’s Manual – Colour GP-1650DF DGPS/Plotter/Sounder”*, Furuno Electric Company Limited.
5. Hibbeler, R. C, 1997 *“Mechanic of Materials”*, 3rd Edition (International Edition), Prentice Hall.
6. Horowitz, P, Hill, W, 1989 *“The Art of Electronics”*, 2nd edition, Cambridge University Press.
7. Hurd, S. A, 2001 *“laser Range Finding For AN Autonomous Mobile Security Device”*, MSc Thesis, Department of Physics and Electronic Engineering, University of Waikato.
8. Lawrence, S. M, 2000 *“Walking Robots: First Design”*, MSc Thesis, Department of Physics and Electronic Engineering, University of Waikato.
9. Loughnane, D. J, 2001 *“Design and Construction of an Autonomous Mobile Security Device”*, MSc Thesis, Department of Physics and Electronic Engineering, University of Waikato.

10. National Instruments, 1993 “*LabVIEW for Windows*”, National Instruments Corporation.
11. Philips Semiconductors, 1996 “*80C51-Based 8-bit Microcontrollers*”, Philips Electronics North America Corporation.
12. Shah, R. J, 1995 “*Simplifying Power Supply Technology*”, Prompt Publications.
13. Taberner, A. J, 1994 “*Design and Construction of a Microcat*”, MSc(Technology) Thesis, Department of Physics and Electronic Engineering, University of Waikato.
14. The Math Works, 1997 “*Simulink – Dynamic System Simulations for MATLAB*”, The Math Works Incorporated.

